

The Synthesis and Application of Polymer Immobilised Ionic Liquid Phase Catalysts

Ashley Reginald Clemmet

A thesis submitted for the degree of

Doctor of Philosophy in Chemistry



School of Chemistry

University of Newcastle upon Tyne

April 2016

“I have not failed. I’ve just found 10,000 ways that won’t work.

Thomas Edison

“Success is the ability to go from one failure to another with no loss of enthusiasm.”

Winston Churchill

'If you're committed enough, you can make any story work. I once told a woman I was Kevin Costner, and it worked because I believed it'

Saul Goodman

ABSTRACT OF THE THESIS

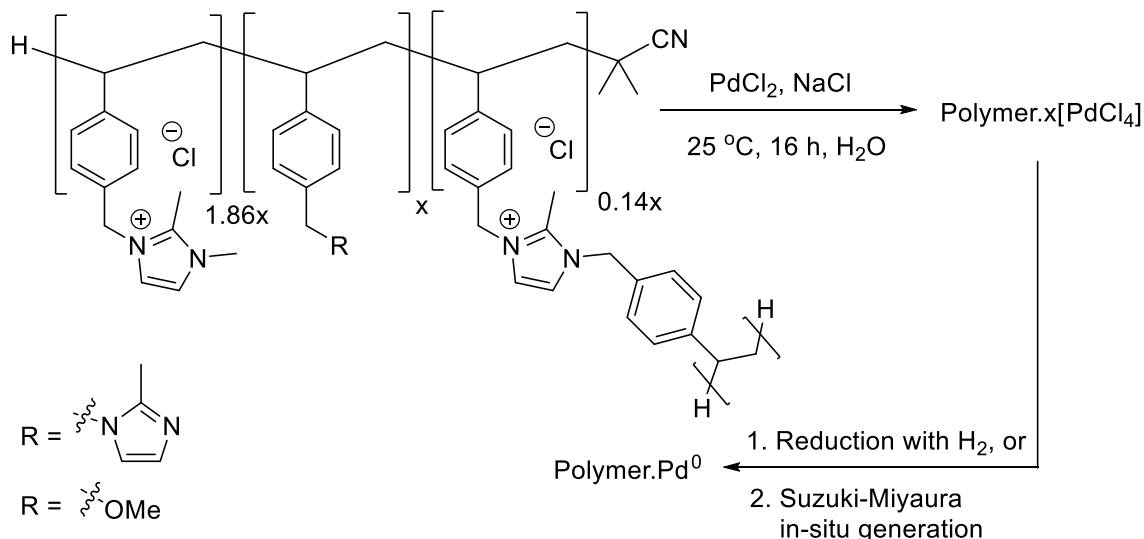
The Synthesis and Application of Polymer Immobilised Ionic Liquid Phase Catalysts

by

Ashley Reginald Clemmet

The utilisation of Ionic Liquids (ILs) and Supported Ionic Liquid Phase (SILP) materials in the support of transition metals has been an area of increasing interest in recent years. Drawing from existing literature the Knight-Doherty group has recently developed a range of Ring Opening Metathesis Polymerisation (ROMP) based Polymer Immobilised Ionic Liquid Phase (PIILP) materials for hydrogen peroxide mediated sulfide oxidation and asymmetric carbon-carbon bond formation. The aim of this project was to extend this range of materials incorporating novel functionalities via different polymerisation techniques and subsequently utilising these materials in new areas of catalysis.

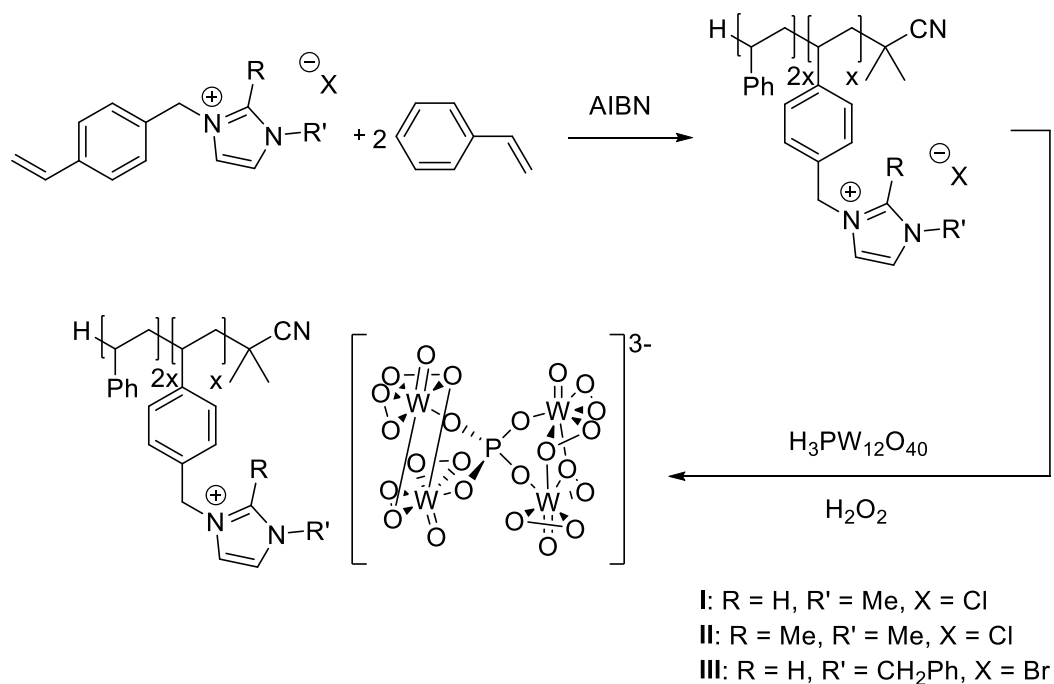
In Chapter 2 of the thesis radical polymerisation was utilised to synthesise two imidazolium-based cross-linked polymers incorporating different heteroatom donors, to support palladium nanoparticles (NPs) (**Scheme A**).



Scheme A Formation of palladium NPs from imidazolium-based cross-linked polymers.

Transmission Electron Microscopy (TEM) along with other techniques was used to determine the size of the NPs which were shown to be in the region of 1.5 nm in diameter. These supported materials were shown to be highly active in the Suzuki-Miyaura cross-coupling of a large range of aryl bromides with phenylboronic acid as part of an extensive catalytic investigation.

Chapter 3 of the thesis covers the synthesis and characterisation of a range of linear imidazolium-based polymeric supports for the immobilisation of the active Venturello peroxophosphotungstate species $[\text{PO}_4\{\text{WO}(\text{O}_2)_2\}_4]^{3-}$ (**Scheme B**).



Scheme B Reaction pathway to POM@PIILP materials.

These amorphous insoluble solid materials were synthesised in high yields requiring no chromatographic purification and fully characterised by a range of techniques. The benzylated imidazolium POM@PIILP **III** was shown to be highly efficient in the oxidation of a range of sulfides under mild reaction conditions utilising hydrogen peroxide as the oxidant in short reaction times. The kinetics of this system were studied and the relative rates of the first and second oxidations determined. A recycling study showed good promise and POM@PIILP **III** was transferred to a segmented flow process. High conversion and sulfoxide selectivity was achieved at a residence time of 4 min corresponding to a flow rate of just 1.1 mL min^{-1} in both ethanol and acetonitrile systems. A lifetime study showed the catalyst to be extremely robust in acetonitrile and a stable activity selectivity profile was achieved under continuous flow conditions over 8 h.

Chapter 4 builds upon the work carried out in the previous chapter via the application of POM@PIILP **III** to the oxidative desulfurisation of model oil. It was shown to be highly efficient and achieved 100 % removal of sulfur in the presence of MeOH after 140 min at 60°C . Promising recyclability results indicate this system also has future potential for transferral to a flow based system.

ACKNOWLEDGEMENTS

I would like to thank my supervisors Dr Julian Knight and Dr Simon Doherty for their excellent supervision and support throughout the course of my PhD. I have learnt so much from both of them, without whom my PhD would not have been possible. Many thanks also go to the technical support staff of the School of Chemistry, in particular, Dave Dunbar (ICP) & John Baron (CHN). Also thank you to our collaborator at York University, Professor Ian Fairlamb.

A special thanks to my friends and colleagues, both past and present, in Julian and Simon's group, including Dr Jack R. Ellison, Dr Nicholas Ward, Rua Alnoman & Daniel Perry to name but a few. Their friendship, advice and support will forever be appreciated.

My time at Newcastle University as both an undergraduate and a postgraduate has been amazing, not least because it is where I met my wonderful fiancée Rosi, who has believed in me and supported me completely since the day we met.

Finally, I would like to thank my entire family for all of their support. Most importantly of all my parents, for their unconditional love and unwavering support throughout everything I have ever endeavoured to achieve.

PREFACE

Declaration

All of the work described within this thesis was conducted in the chemical laboratories of the University of Newcastle upon Tyne during the period of September 2012 – September 2015 and is original except where acknowledged by reference.

ABBREVIATIONS

AIBN	Azobis(isobutyronitrile)
ATRP	Atom transfer radical polymerisation
CRP	Controlled/living radical polymerisation
DBT	Dibenzothiophene
DCPD	Dicyclopentadiene
DMF	<i>N,N</i> -Dimethyl formamide
DMSO	Dimethyl sulfoxide
DSC	Differential scanning calorimetry
FT-IR	Fourier transform infrared spectroscopy
GC	Gas chromatography
GPC	Gel permeation chromatography
HDS	Hydrodesulfurisation
ICP-OES	Inductively coupled plasma optical emission spectroscopy
IL	Ionic liquid
MHz	MegaHertz
NAIL	Non-aqueous ionic liquid
NHC	<i>N</i> -heterocyclic carbene
NMP	Nitroxide mediated polymerisation
NMR	Nuclear magnetic resonance
NP	Nanoparticle
PdNP	Palladium nanoparticle
PIILP	Polymer immobilised ionic liquid phase

POM	Polyoxometalate
ppm	Parts per million
RAFT	Reversible addition fragmentation chain transfer
ROMP	Ring opening metathesis polymerisation
RTIL	Room temperature ionic liquid
SCILL	Solid catalyst with ionic liquid layer
SEM	Scanning electron microscopy
SFRP	Stable free radical polymerisation
SILP	Supported ionic liquid phase
TEM	Transmission electron microscopy
TGA	Thermogravimetric analysis
THF	Tetrahydrofuran
TOF	Turnover frequency
TON	Turnover number
VOCs	Volatile organic compounds
XPS	X-ray photoelectron spectroscopy
XRD	X-ray diffraction

Ionic liquid cations:

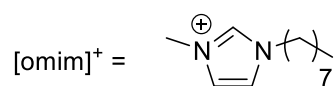
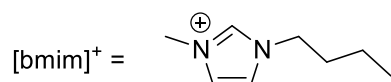
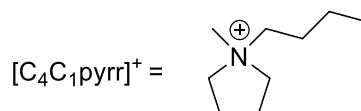
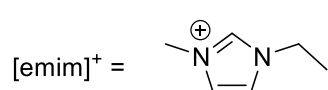


TABLE OF CONTENTS

Chapter 1. The Chemistry of Ionic Liquids, SILP, & PIILP	1
1.1 Ionic Liquids	1
1.2 Supported Ionic Liquid Phase	10
1.3 Polymer Immobilised Ionic Liquid Phase	13
1.4 Methods of Polymerisation	15
1.4.1 Radical	15
1.4.2 ATRP	17
1.4.3 ROMP	18
1.5 Project Aims	20
Chapter 2. Polymer Supported Palladium Nanoparticles: Synthesis & Catalysis	22
2.1 Introduction	22
2.2 Norbornene Based Monomer Synthesis	26
2.3 ROMP Polymer Development	27
2.4 Exo-Norbornene Based Polymer Synthesis	29
2.5 Styrene Based Monomer Synthesis	30
2.6 Cross-linked Styrene Radical Polymerisations	32
2.7 Formation of Polymer Immobilised Palladium Nanoparticles	36
2.7.1 XPS analysis	38
2.7.2 Powder XRD analysis	41
2.7.3 TEM analysis	42
2.8 Suzuki-Miyaura Coupling Reactions	45
2.8.1 Solvent optimisation	47
2.8.2 Water content optimisation	48
2.8.3 Base optimisation	48
2.8.4 Substrate screening	49
2.8.5 Kinetic study of cross-coupling	53
2.8.6 Ex-situ TEM analysis	54
2.8.7 Reaction dilution	56
2.8.8 Catalyst loading	57
2.8.9 Mercury poisoning	58
2.8.10 Boronic acid variation	59

2.8.11	Comparisons to commercially available catalysts.....	60
2.9	Conclusions	61
Chapter 3. Oxidation of Sulfides		63
3.1	Introduction.....	63
3.2	Synthesis of Styrene Based Monomers	65
3.3	Radical Polymerisations	66
3.4	Immobilisation of POM Species.....	69
3.5	Sulfide Oxidation System Optimisation.....	72
3.5.1	Solvent screening.....	73
3.5.2	Temperature optimisation.....	74
3.5.3	Peroxide concentration optimisation	74
3.6	Sulfide Substrate Screening.....	75
3.7	Kinetic Study of Oxidation of 4-Nitrothioanisole & Dibenzothiophene.....	78
3.8	Batch Recycling Study	81
3.8.1	Recycle in MeCN	81
3.8.2	Recycle in EtOH.....	82
3.8.3	Tandem recycling	83
3.9	Comparisons with Commercially Available Systems	84
3.10	Effects of Dilution on Polyphosphotungstate Loading.....	88
3.11	Sulfide Oxidation Under Flow Conditions.....	88
3.11.1	Segmented flow	90
3.11.2	Continuous flow	94
3.12	Conclusions	96
Chapter 4. Application of Imidazolium PIILP to Sulfide Removal from a Model Oil		98
4.1	Introduction.....	98
4.2	Model Oil Sulfide Removal System Optimisation	100
4.2.1	Reaction temperature optimisation.....	100
4.2.2	Catalyst loading optimisation	101
4.2.3	Peroxide concentration optimisation	102
4.3	Kinetic Study on Model Oil.....	103
4.4	Recyclability Study.....	103
4.5	Application to Sulfide Removal from Arab Light Crude Oil	104
4.6	Future Work.....	105
4.7	Conclusions	106

Chapter 5. Experimental	108
5.1 General Comments	108
5.2 Experimental Procedures Chapter 2	109
5.3 Experimental Procedures Chapter 3	131
5.4 Experimental Procedures Chapter 4	143
REFERENCES	145
APPENDICES	153

Chapter 1. The Chemistry of Ionic Liquids, SILP, & PIILP

1.1 Ionic Liquids

Ionic liquids (ILs) can be defined as organic salts in the liquid phase below 100 °C, or more loosely as low melting salts. They are liquids as a result of their low lattice energy and many of the lower melting ILs are commonly referred to as Room Temperature Ionic Liquids (RTILs) in the literature. ILs have attracted extensive interest in recent years for a range of applications and have become known as ‘neoteric solvents’ or ‘designer solvents’ due to their host of desirable properties such as high thermal stability, low volatility, non-flammable, ease of handling, immiscibility with many organic solvents and ease of reuse.^[1] In addition to these features, there is enormous scope for functionalisation via judicious choice of the anion and cation, through which it is possible to fine-tune properties such as polarity, stability, density, conductivity, viscosity and hydrophilicity/ hydrophobicity.^[2] Imidazolium based ILs formed the basis of much of the early work in the area but more recently an enormous range of anion and cation combinations have been developed. **Figure 1.1** shows the structures of typical cations and anions now being adopted for ILs.

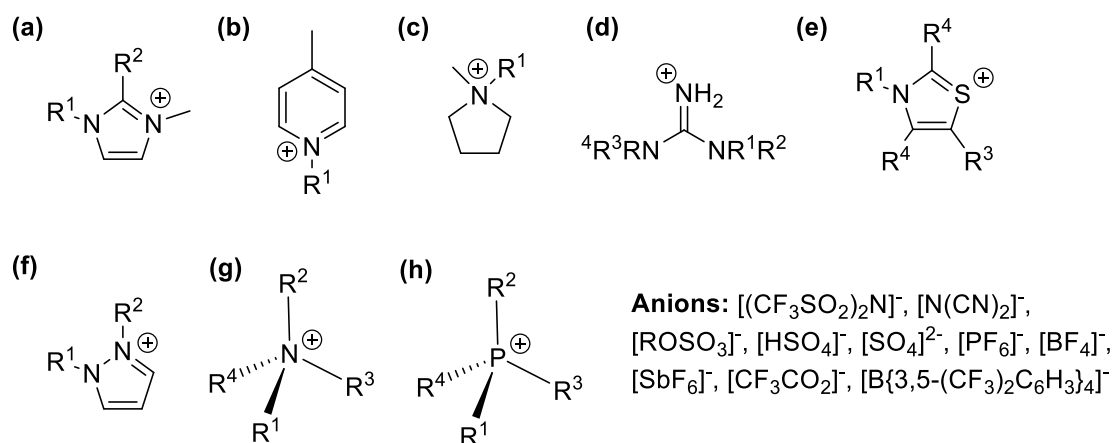
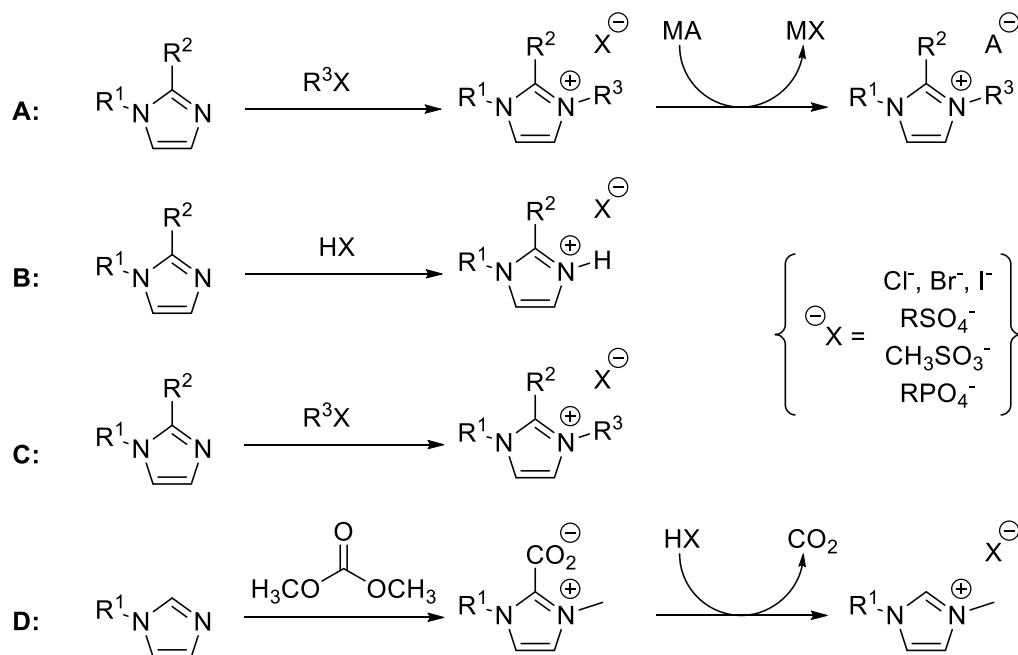


Figure 1.1 Typical IL cations and anions, (a) imidazolium, (b) pyridinium, (c) pyrrolidinium, (d) guanidinium, (e) thiazolium, (f) pyrazolium, (g) ammonium, (h) phosphonium.^[2]

Preparation of ionic liquids can be achieved through several routes, as summarised in **Scheme 1.1**, each with their own intrinsic advantages and disadvantages. IL synthesis has primarily been achieved via metathesis of the halide salt of an organic cation with a group 1 or ammonium salt containing the desired anion (route A).^[3] This route does however often lead to the production of unfavourable halide by-products which can prove difficult to remove. Alternatively, the presence of a halide can be avoided via an atom efficient neutralisation of base with Brønsted

acids (route B) or by direct alkylation of alkyimidazole (route C). In the case of route B it can be difficult to obtain ILs with a high degree of purity, as a result of trace amounts of the of alkyimidazole or acid remaining in the final ILs. Route C has been reported for the preparation of sulfate, phosphate or sulfonate based ILs.^[4] Route D is a relatively new route which also avoids the presence of halide and other by-products through the use of dimethylcarbonate (DMC) as a clean methylating agent to replace alkyl halides.^[5]



Scheme 1.1 Typical preparation routes for imidazolium-based ionic liquids: (route A) metathetic exchange of anion, (route B) neutralisation of base with Brønsted acids, (route C) direct alkylation of alkyimidazole, (route D) carbonate pathway.

Having emerged as ‘designer solvents’ ILs have increasingly been utilised in a range of applications from organic synthesis, catalysis, electrochemical devices and solvent extraction of a variety of compounds.^[6] The area that has garnered the most interest in the literature is catalysis in ionic liquids, which forms the basis of this review. Catalysis in ILs is in itself an extremely broad subject area and has come to include biocatalysis, catalytic conversion of biomass, homogeneous catalysis, heterogeneous catalysis, Supported Ionic Liquid Phase (SILP) and Solid Catalyst with Ionic Liquid Layer (SCILL) catalysis and electrocatalysis. A number of extremely informative reviews and influential papers are now available for each of these subject areas among many others.^[3, 7] It has been estimated that 10^{18} unique ILs are theoretically possible,^[8] presenting the opportunity for almost unlimited optimisation of catalytic systems. They can provide catalysts with a unique ionic micro environment that can play a positive role in the stabilisation of the reactive catalytic species or reaction intermediates. When compared to reactions carried out in traditional volatile organic solvents (VOCs), ILs

often show improved catalytic activities and unprecedented reactivities. A review by Kou *et al.* highlights many such examples and summarises the advantages of IL's over VOCs.^[3]

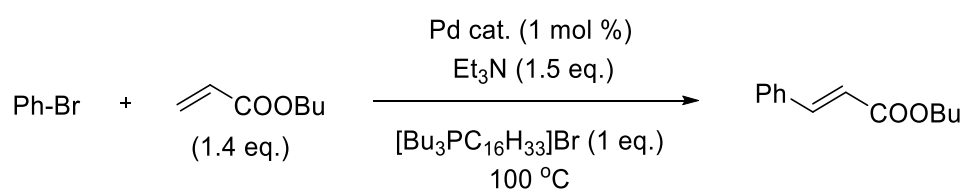
A review by S. Sugden and H. Wilkins in 1929 states that the development of ionic liquids dates back as far as 1914 when the synthesis of ethylammonium nitrate reported the salt to be a liquid at room temperature, however between 200 and 600 ppm of water was present.^[9] It was not until the mid-1980's that the use of ionic liquids as a new reaction media and catalysts for organic synthesis were first reported. Wilkes *et al.* reported the successful use of mixtures of 1-methyl-3-ethylimidazolium chloride and aluminium chloride (MeEtImCl-AlCl₃) as both the reaction medium and catalyst for Friedel-Crafts alkylations and acylations.^[10] This particular reaction continues to be an area of interest with a more recent publication demonstrating the use of pyridinium based ionic liquids as suitable media for Friedel-Crafts acylations. High conversions were obtained at relatively low temperature with the more environmentally favourable [EtPy]⁺[CF₃COO]⁻-FeCl₃, replacing the most commonly used AlCl₃.^[11] The same group have also carried out Friedel-Crafts alkylations of benzene utilising the same solvent-catalyst system and have successfully enhanced the green characteristics of the reaction through successful recycling and reuse of the ILs.^[12]

The use of ILs as solvents for homogeneous transition metal catalysis was first reported in 1990, again by Wilkes *et al.* and also by Chauvin *et al.* Chauvin dissolved nickel complexes in organochloroaluminate molten salts for the catalytic dimerisation of propene to hexane isomers,^[13] while Wilkes was successful in the polymerisation of ethylene via Ziegler-Natta catalysis in the RTIL AlCl₃.1-ethyl-3-methylimidazolium chloride, employing Cp₂TiCl₂ as the catalytic species with AlCl_{3-x}R_x (R= Me, Et) as a co-catalyst.^[14] The Wilkes group further established the potential for the application of a wide range of ILs, not limited to just chloroaluminate melts, with enhanced stability against hydrolysis, such as tetrafluoroborate melts.^[15]

Looking more closely now at transition metal-catalysed cross-coupling in ILs there are several reactions which have evolved in to powerful tools for C-C bond formation in ionic liquid media. Palladium catalysed reactions can have several drawbacks in conventional solvent systems such decomposition and leaching of the catalyst, difficulties isolating the product, low activities and selectivities, poor solubility and extremely difficult recycling procedures. Ligand free Pd-catalysed C-C bond formations have been reported but unfortunately they also have a number of associated drawbacks. Most notably the requirement for toxic solvents, high temperatures and extended reaction times.^[16] These drawbacks have led to the search for more efficient,

robust and cost effective catalysts that can overcome these limitations to existing systems.^[17] The importance of a catalytic system that is both recoverable and recyclable is also essential when the system is incorporating transition metals in order to limit the environmental impact of such a system and to enhance the economic viability. Water is the most obvious candidate as a potential replacement for conventional organic solvents as the cost is negligible, it is non-flammable and non-toxic. When water is utilised as a solvent it enables simple separation and subsequent recycling of hydrophilic metal catalysts. Unfortunately, in the case of neutral catalytic species, they will not be retained in water and are lost during product isolation, preventing recycling. Using metal complexes with charged groups to avoid catalyst leaching into the organic layer is one potential solution to this issue.^[18] ILs can provide solutions to many of these problems and are predominantly used in biphasic systems to immobilise the transition metal catalyst in the ionic phase.^[19]

The Heck reaction in particular is now a very important tool for formation of C-C bonds which has been applied to an extremely varied range of products and intermediates. The favourable properties of ILs such as their tunable polarity and low volatility, in addition to their ability to enhance catalyst stability and activity and provide simple catalyst separation and recycling, has led to the vinylation of aryl halides representing the most extensively studied Pd-catalysed process in ILs to date.^[20] One of the earlier well documented uses of ILs as the reaction media for the Heck reaction in the absence of additive ligands was carried out by Kaufmann *et al.*^[21] They successfully coupled *trans* cinnamic acid butylester with bromobenzene in both Pd(OAc)₂ and PdCl₂ based systems in [C₁₆PBu₃]Br (**Scheme 1.2**).



Scheme 1.2 Ligand-free Heck reaction in IL media.^[21]

They obtained a conversion of 81 % after 16 h with PdCl₂ and >99 % in the presence of Pd(OAc)₂ with the catalyst remaining in the IL following extraction with the latter enabling successful catalyst recovery via distillation and two further recycles were possible. This work provided a basis for other groups to develop ligand-free systems. The non-aqueous ionic liquid (NAIL) [NBu₄]Br has been shown to be an effective alternative solvent for the coupling of styrene with aryl bromides in the presence of NaOAc base and the phospho-palladacycle *trans*-di(μ-acetato)-bis[*o*-(di-*o*-tolylphosphino)benzyl] dipalladium(II) (**Figure 1.2**).^[22] As polar solvents such as DMF and NMP along with salt additives have been shown to stabilise the

palladacycle it was unsurprising to find that NAILs compared favourably with turnover numbers (TONs) as high as 1 000 000 mol product (mol Pd)⁻¹ being obtained with the activated aryl bromide 4-bromoacetophenone. Improvements in catalytic activity were also observed for deactivated aryl chlorides compared to reactions carried out in conventional solvents.

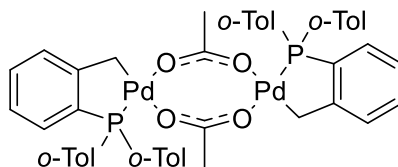
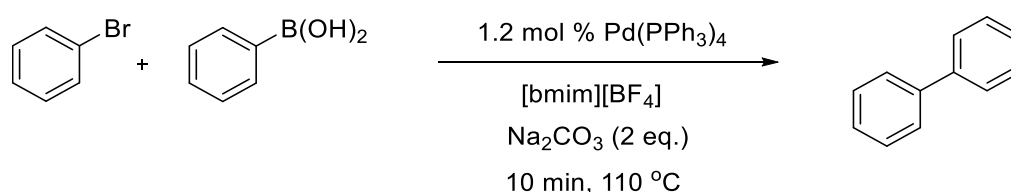


Figure 1.2 Palladacycle precatalyst, *trans*-di(μ -acetato)-bis[*o*-(di-*o*-tolylphosphino) benzyl] dipalladium(II).^[22]

More recent advances in the utilisation of ILs in Heck reactions include the incorporation of Pd nanoparticles in ligand-free systems. One such example which sits on the frontier between homogeneous and heterogeneous catalysis saw PdNPs with an average size distribution of 3 nm successfully prepared in-situ in a H₂O/ [bmim]PF₆ microemulsion.^[23] A microemulsion is a thermodynamically stable system formed by two or more immiscible liquids which are stabilised by a surfactant, sometimes referred to as ‘semi-homogeneous’ systems. In this particular case TX-100 served as the reductant and stabilised the PdNPs together with the ionic liquid [bmim]PF₆. The system proved to be an extremely efficient catalyst for the ligand free Heck cross-coupling of iodobenzene with a range of alkenes in reduced reaction times, when compared with conventional organic solvent systems. The IL microemulsion was recycled four times for the coupling of iodobenzene with butyl acrylate at 75 °C in the presence of Et₃N. However, by the fourth recycle a decrease in yield of 14 % was observed and the authors attributed this to TX-100 and [bmim]PF₆ entering the ethyl acetate extraction phase.

Although Heck reactions in ILs have been extensively studied in recent years, another class of C-C bond forming reactions that has not been as thoroughly investigated are the more complex Suzuki-Miyaura cross-couplings, employed most successfully for the synthesis of biaryls.^[24] The earliest examples of Suzuki-Miyaura cross-couplings in ILs were carried out in [bmim][BF₄], which successfully demonstrated a number of advantages when compared with conventional solvent systems. Firstly, a substantial rate increase was observed for non-activated electrophiles with a lower catalyst loading. Secondly, pure products were obtained, with no homo-coupled biaryls present. In addition to these advantages, recycling was performed in an experimentally straightforward manner and reactions performed in air did not see a decrease in yield. For example, the coupling of bromobenzene and phenylboronic acid under the original Suzuki conditions,^[25] afforded biphenyl with an 88 % yield in 6 h which corresponds to a TOF

of 5 (mol product)(mol cat.)⁻¹ h⁻¹. However, when Welton and co-workers carried out the same reaction in [bmim][BF₄] (**Figure 1.3**) a 93 % yield was achieved in just 10 min (TOF of 455 (mol product)(mol cat.)⁻¹ h⁻¹), which was over 90 times greater in reactivity. An even more marked improvement was observed when 4-methoxybiphenyl was afforded in a yield of 81 % in [bmim][BF₄] compared with just 40 % under the original Suzuki conditions. The clean IL catalytic solution was recovered, washed with water and reused three times without loss of activity for this reaction with reaction products isolated via a simple extraction in to diethyl ether.^[26]



Scheme 1.3 Suzuki-Miyaura cross coupling reaction of bromobenzene with phenylboronic acid.^[26]

In the context of Suzuki-Miyaura couplings in ILs there has been much discussion as to the role that Pd-NHC carbene complexes play in the reactions. Welton *et al.* have continued to study a wide range of ionic liquids in the presence of PPh₃. In doing so they found that with careful catalytic control recycling of the active solutions was possible in [C_nC₁im]⁺ (n = 2, 4, or 6) ILs, but not when [C₄C₁C₁²im]⁺ or [C₄C₁pyrr]⁺ ILs were used.^[27]

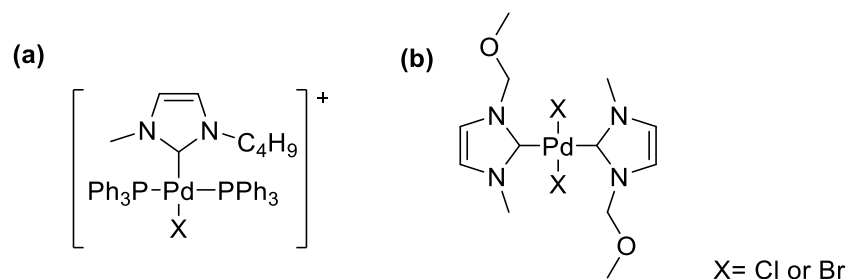
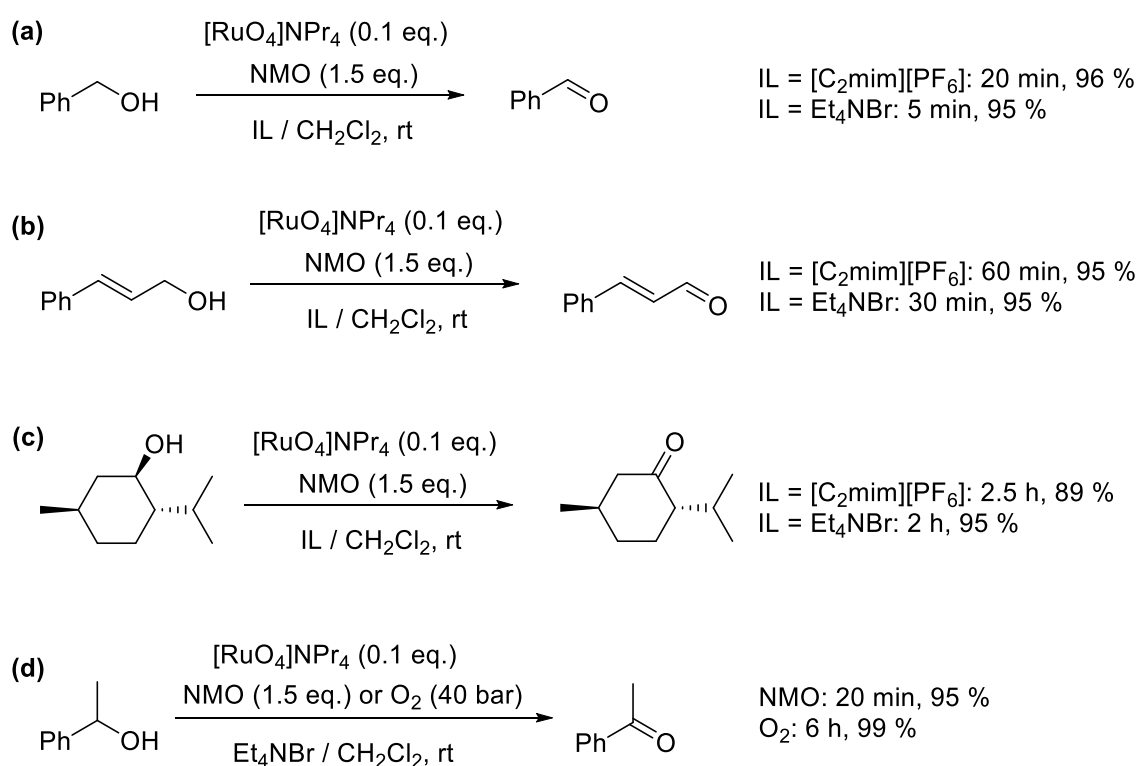


Figure 1.3 Phosphine-imidazolylidene palladium complex (a) [(bmimy)-(PPh₃)₂PdX]⁺ and (b) [(C₁OC₂)mimy]₂PdX₂.^[27]

Following further analysis of the catalytic solutions they were able to establish the presence of the mixed phosphine-imidazolylidene palladium complex (**Figure 1.3** (a)). Dyson *et al.* have carried out further studies on the cationic species of ILs in Suzuki coupling, looking in particular at ether functionalised ILs.^[28] They rationalised that the implementation of a task-specific ether-functionalised ILs in Suzuki reactions would facilitate and increase output due to the ether moiety stabilising the active catalytic species via weak interactions. They were able to obtain catalytically active solutions for ILs that were not capable of forming NHCs such as

$[(C_1OC_2)C_1^2pyr][NTf_2]$. When the imidazolylidene palladium complex (**Figure 1.3** (b)) was utilised, extremely poor yields were obtained and it was concluded that formation of Pd-NHCs was terminating the catalytic cycle in these ILs. It would be expected that the ether functionalities of Dyson's ILs would be less well coordinating to the palladium than PPh_3 . When the findings of both Welton and Dyson are combined it becomes clear that ether-functionalised ILs are providing palladium complexes which are of sufficient stability to form catalytically active and recyclable solutions. When the $[(C_1OC_2)C_1imy]_2PdCl_2$ complexes are added to these ILs, they are poor catalysts as a result of being so stable. However, upon addition of appropriate ligands, the mono-NHC complex $[(C_4C_1imy)(PPh_3)_2PdX]^+$ is formed and the solutions become catalytically active and recyclable.



Scheme 1.4 Oxidation of primary and secondary alcohols in ILs by Ley *et al.*^[29]

Homogeneous catalysis in ILs is by no means limited to transition metal cross-coupling. There are now a vast number of reactions which are carried out in IL media. One of particular interest which has attracted much attention is homogeneous oxidation. Since the first asymmetric epoxidation by a manganese(III) complex in IL was reported by Song *et al.* in 2000 a broad range of oxidation reactions in ILs have been reported.^[30] Oxidations have been carried out in IL media acting as the solvent, extractant or in some cases even the active catalytic species. The oxidation of alcohols initially received much attention with Ley *et al.* reporting the efficient oxidation of a variety of primary and secondary alcohols catalysed by tetra-*N*-propylammonium

perruthenate (TPAP) with *N*-methylmorpholine-*N*-oxide (NMO) in a biphasic mixture of either [emim][PF₆] or Et₄NBr with CH₂Cl₂. They also reported the successful use of oxygen in place of NMO for the oxidation of *sec*-phenylethyl alcohol (**Scheme 1.4** (d)). The reaction products were easily recovered by decanting and recycled with varying degrees of success depending on the nature of both the starting alcohol and the IL (**Scheme 1.4**).^[31]

Tandon *et al.* have also seen success in secondary alcohol oxidation with the imidazolium-based peroxophosphotungstate [bmim]₃[PO₄{WO(O₂)₂}]₄ catalyst in [bmim][BF₄] (**Figure 1.4**).^[32] The corresponding ketones were obtained in very good yield at 90 °C with reaction times between 2- 4 h. Recovery and recycling of the catalyst was possible and only a small decrease in activity was observed over a further three cycles.

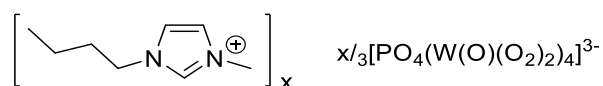
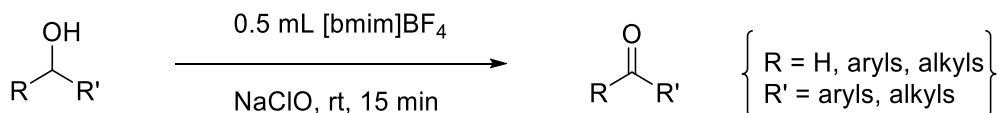


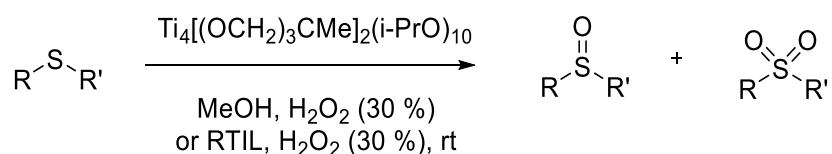
Figure 1.4 Imidazolium based phosphotungstate catalyst developed by Tandon *et al.*

More recently Han *et al.* have reported the dual functionality of [bmim]BF₄ as both the solvent and catalyst for the selective oxidation of primary and secondary alcohols using NaClO as the oxygen source (**Scheme 1.5**).^[33] The system was recovered and recycled up to five times without a significant decrease in catalyst activity.



Scheme 1.5 Oxidation of alcohols in [bmim]BF₄.

Another group of oxidation reactions which has received an increasing amount of interest is the oxidation of sulfides, which is of particular interest in relation to the removal of sulfur-containing compounds such as dibenzothiophene (DBT) from diesel fuels. The use of oxidation and extraction into ILs to remove these impurities presents a promising alternative to the current industrially adopted technique of hydrodesulfurisation (HDS) and will be discussed in more detail in Chapter 4. Biphasic homogeneous systems utilising hydrogen peroxide as the oxidant again have been developed by Reddy and Verkade who were able to oxidise a range of sulfides. They investigated the effect of carrying out the reaction in three different RTILs ([emim].BF₄, [bmim].BF₄ and [bmim].PF₆) and contrasted the results with those obtained in methanol (**Scheme 1.6**).^[34]



Scheme 1.6 Oxidation of sulfides with H₂O₂ in RTILs with Ti₄[(OCH₂)₃CMe]₂(i-PrO)₁₀ catalyst.^[34]

They found that oxidation was proceeding very rapidly with no sulfoxide being isolated. All three of the RTILs exhibited very similar levels of performance with reaction rates as much as 30% quicker when compared with those found in MeOH. In addition to this they were able to successfully recover the catalyst via a simple extraction in to diethyl ether which was subsequently recycled six times without a decrease in activity.

The group of Li *et al.* have carried out a wide variety of work focusing on sulfide oxidation. The authors studied the oxidation/desulfurisation (ODS) system for the removal of benzothiophene (BT), dibenzothiophene (DBT) and 4,6-dimethyldibenzothiophene (4,6-DMDBT) in several ILs. Notably their catalytic system containing Na₂MoO₄·2H₂O, H₂O₂, and [bmim].BF₄ achieved a 99 % removal of DBT from a model oil while the same reaction in the absence of IL achieved only 4 % desulfurisation due to decomposition of the hydrogen peroxide.^[35] This observation indicates that the IL was acting in the capacity of both solvent, extractant and also providing stabilisation effects. **Table 1.1** shows the results they obtained in various IL systems. Li *et al.* also investigated the extent of leaching occurring in the system and found that 0.9 % of the catalyst was leaching in 1000 mL of the substrate phase. However, the Mo-content in the substrate phase could be removed via a simple extraction with water.

Entry ^a	IL	IL alone ^b	IL + H ₂ O ₂ ^b	IL + Na ₂ MoO ₄ + H ₂ O ₂ ^b
1	[bmim].BF ₄	16	32	99
2	[omim].BF ₄	21	35	68
3	[bmim].PF ₆	15	39	70
4	[omim].PF ₆	20	45	78
5	[bmim].TA	15	31	49
6	[omim].TA	21	32	37

Table 1.1 IL systems investigated by Li *et al.* for oxidative desulfurisation.^[36] ^a Model oil prepared by dissolving DBT in *n*-octane (S-content = 1000 ppm). Reaction Conditions: T = 70 °C, t = 3 h, model oil = 5 mL, IL = 1 mL, 5 mol % catalyst. ^b % Yield.

1.2 Supported Ionic Liquid Phase

Despite the ongoing progress being made in the utilisation of ILs in homogeneous catalysis, such systems possess a number of intrinsic disadvantages. Most significantly is the difficulties of recovery and recyclability of such systems as they frequently require purification of the IL in between each reuse, typically via energy intensive distillation which often prevents their implementation on an industrial scale. Added to this, the cost of ILs remains high in comparison to conventional organic solvents, hence alternative methods to the conventional biphasic systems which aim to minimise the quantities required are extremely desirable. Such biphasic systems also suffer from mass transfer limitations as a result of the often high viscosity of ILs.^[37]

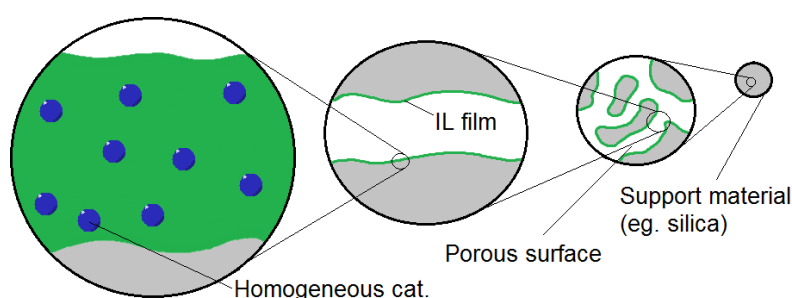


Figure 1.5 Supported Ionic Liquid Phase (SILP) system.

One such method which has received considerable interest is that of Supported Ionic Liquid Phase (SILP) (**Figure 1.5**). This technique aims to retain the excellent benefits of IL systems such as the improvements in yield and selectivities which have been exhibited, whilst simultaneously addressing the drawbacks of homogeneous catalysis. It does so by immobilising a thin film of metal catalyst-containing IL on an inert support material, the preparation of which is extremely straightforward. The IL solution is typically dissolved in an organic solvent along with the catalytic metal complex before addition of the support material followed by removal of the organic solvent under reduced pressure, resulting in a film of the IL adhered to the support material. Ideally the support material is porous in order to increase surface area.

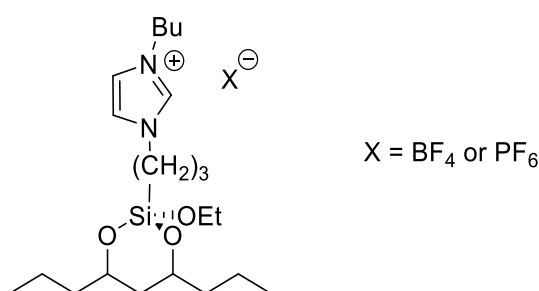


Figure 1.6 First example of SILP: a surface modified silica with an immobilised IL fragment.

The technique was first introduced by Mehnert and co-workers in 2002 for the hydroformylation reaction of 1-hexene to form *n,i*-heptanal.^[38] They prepared two surface modified silica gels with a covalently anchored ionic liquid fragment (**Figure 1.6**). The support material was then loaded with a pre-prepared active rhodium catalyst species $[\text{HRh}(\text{CO})\{\text{tri}(m\text{-sulfonyl})\text{triphenyl phosphine trisodium}\}_3]$ or $[\text{HRh}(\text{CO})\{\text{tri}(m\text{-sulfonyl})\text{triphenyl phosphine tris}(1\text{-butyl-3-methyl-imidazolium})\}_3]$ to afford the SILP material as a free-flowing powder. Following a comparative study of the SILP catalyst and the analogous biphasic IL system, it was found that the supported system demonstrated slightly enhanced activity and comparative selectivity with the added advantage of simple catalyst recovery. However, both systems were found to exhibit very similar metal leaching levels which was attributed to IL becoming partially dissolved in the organic phase at high aldehyde concentrations.

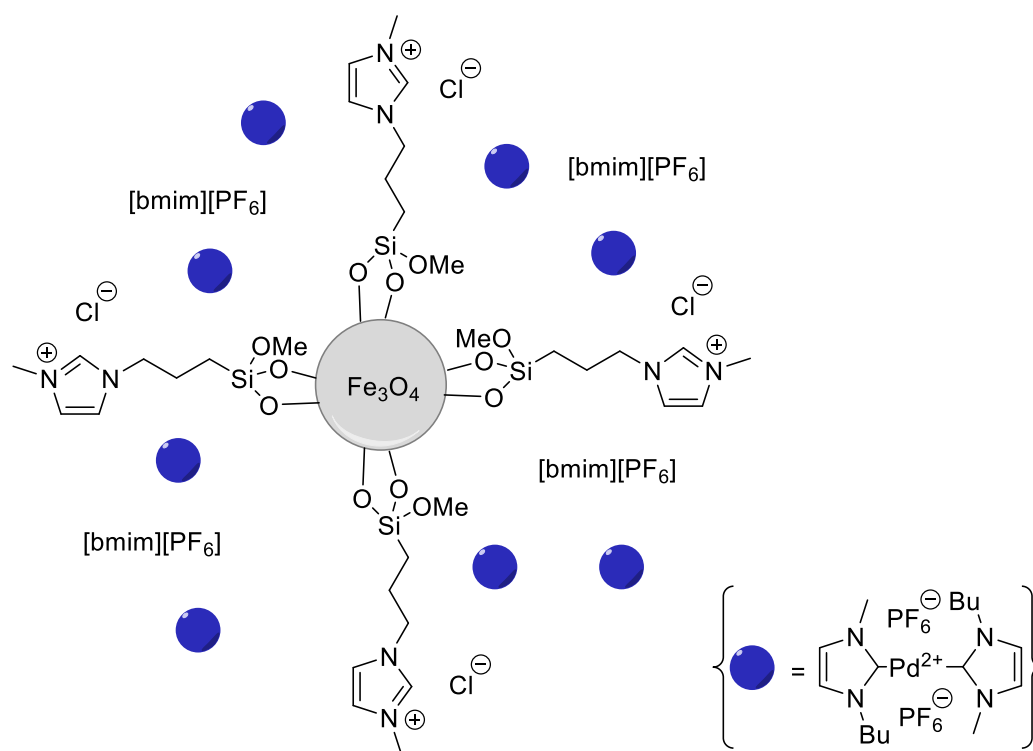


Figure 1.7 Pd-NHC catalyst immobilised on a nanoparticle-IL matrix.

This concept has been built on extensively in recent years with highly specialised ionic liquid frameworks being supported by a number of different materials such as zeolites,^[39] nanosilica dendrimers,^[40] magnetic nanoparticles,^[41] and carbon nanotubes among many others.^[42] The highly active and magnetically recoverable Pd-NHC catalyst immobilised on a Fe_3O_4 -IL matrix developed by Jin *et al.* is shown in **Figure 1.7**. It was successfully utilised in Suzuki cross-coupling reactions in aqueous media and demonstrates the complexity of current research in to SILP materials.

Despite the vast number of alternative support materials available, silica remains the most widely used support for IL materials. There now exist two types of SILP@SiO₂ materials which can be prepared via covalent grafting of a preformed IL-based silane or by co-condensation. As shown in **Figure 1.8 (a)** the IL can be placed on the outer surface of the silica support as has become the conventional approach or alternatively ILs can be encapsulated within a silica sphere (**Figure 1.8 (b)**).^[42]

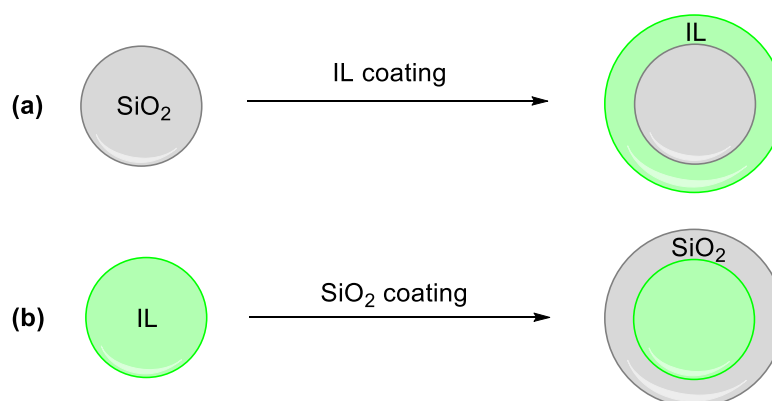
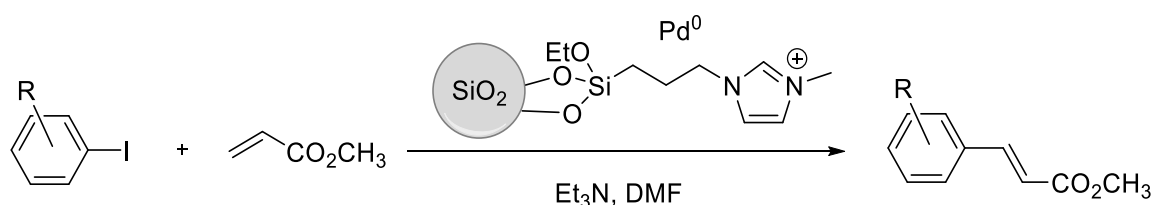


Figure 1.8 SILP@SiO₂ materials prepared with (a) IL surface coating and (b) IL encapsulation in silica.

This simple grafting approach was used to obtain Pd@cSILP materials for the Heck reaction of aryl iodides and methyl acrylate (**Scheme 1.7**).^[43] The catalysts were prepared from chloropropylated silica and 1-methylimidazole, followed by impregnation with a solution of Pd(OAc)₂ in IL.



Scheme 1.7 Pd@cSILP catalyzed Heck reaction of aryl iodide with methyl acrylate.

A range of catalysts was obtained with varying ionic liquid loadings and stable performances were achieved for several hours in continuous flow Heck coupling reactions between aryl iodides and methyl acrylate. A similar system of particular interest was synthesised by Shi *et al.* for the selective oxidation of sulfides to sulfoxides. They immobilised the peroxotungstate [W₂O₃(O₂)₄]²⁻ on a multilayer imidazolium modified silica (**Figure 1.9**).

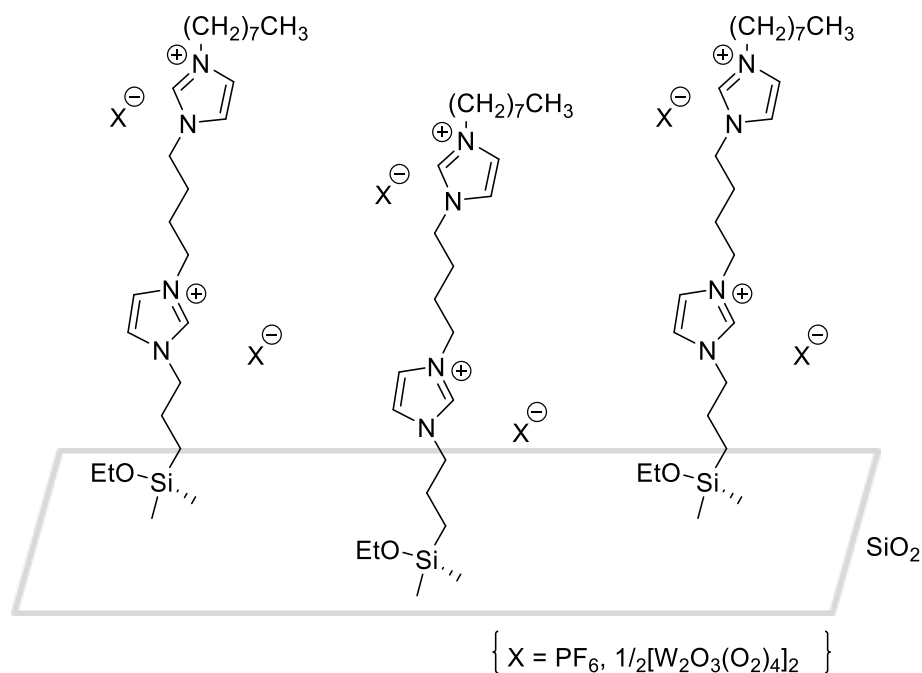


Figure 1.9 Peroxotungstate immobilised on multilayer IL-modified silica.

This proved to be a more efficient catalyst than the corresponding monolayer imidazolium and pyridinium IL systems, affording yields in excess of 90 % in a reduced reaction time in the presence of only 1.5 mol % of the catalyst. The authors attributed this enhanced catalytic activity to the multilayer providing a system which closely resembles the liquid phase which would be present in a biphasic system containing IL. The system provided a straightforward catalyst recovery and recycling was possible for a further seven reactions with only a slight decrease in efficiency observed.

1.3 Polymer Immobilised Ionic Liquid Phase

The concept of Polymer Immobilised Ionic Liquid Phase materials (PIILP) is one which is beginning to attract much interest among research groups desiring a SILP like system which aids catalyst recovery and recycling, whilst addressing the issue of leaching of the IL from the support material. The system does so by incorporating IL-like fragments within a polymer structure, thereby preventing them from being lost via leaching into the surrounding conventional solvent whilst having the added advantage of being able to design cross-linked polymer networks to encapsulate the active species. **Figure 1.10** shows a visual representation of the concept.

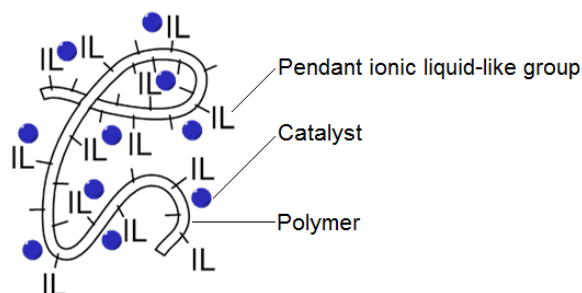
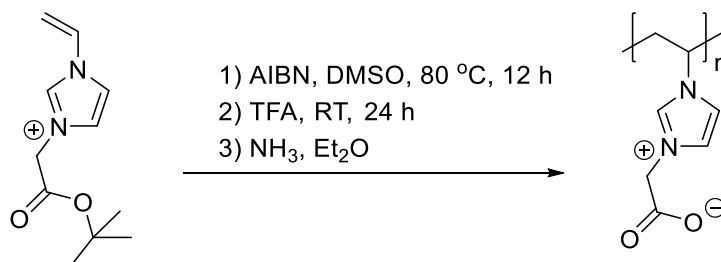


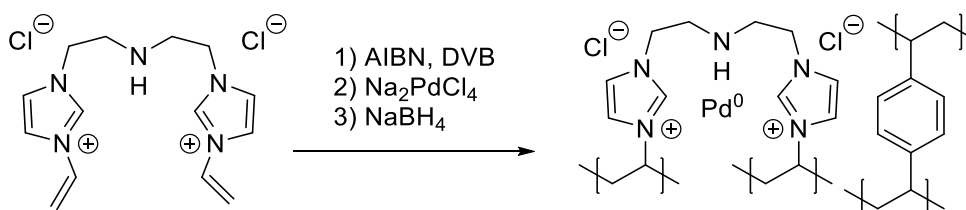
Figure 1.10 Polymer Immobilised Ionic Liquid Phase (PIILP).

Incorporation of imidazolium pendants into a homopolymer was recently reported. This was prepared via radical polymerisation followed by deprotection and precipitation to afford the charged polymer species (**Scheme 1.8**).^[44] The homopolymer was utilised in the formation of cyclic carbonates from various epoxides with CO₂ in high yields and selectivity between 87-98 %. Most importantly the system was reused for a total of 4 times.



Scheme 1.8 Zwitterionic imidazolium containing homopolymer.

Cross-linked polymeric materials have also been prepared via radical polymerisation for the immobilisation of PdNPs. **Scheme 1.9** shows the preparation of such a system developed by Liu *et al.* via copolymerisation of a imidazolium monomer with DVB for the Suzuki coupling of aryl iodides to aryl boronic acids.^[45]



Scheme 1.9 Cross-linked PIILP materials for PdNP catalysed Suzuki cross-coupling.

Following immobilisation of the Pd^{II} species reduction to the active Pd⁰ species was achieved with NaBH₄. Excellent yields were obtained for the Suzuki coupling of a range of substrates and hot filtration and mercury poisoning tests revealed that the palladium species which had leached from the polymer into the solvent during the reaction was subsequently redeposited

into the polymer network after the reaction was complete. Recycling of the system was possible up to a maximum of 5 cycles however a small decrease in activity was observed. The authors attributed this to a combination of leaching of Pd from the PIILP support and a small amount of aggregation of the PdNPs.

Aside from radical polymerisation other polymerisation techniques have been used to generate PIILP support materials. Work carried out within the Knight-Doherty group has already demonstrated the successful utilisation of a peroxophosphotungstate-based PIILP catalyst for the epoxidation of allylic alcohols.^[46] **Figure 1.11** shows the PIILP catalyst which was synthesised via Ring-Opening Metathesis Polymerisation (ROMP) of *cis*-cyclooctene and a pyrrolidinium functionalised norbornene monomer, catalysed by Grubbs 1st generation catalyst.

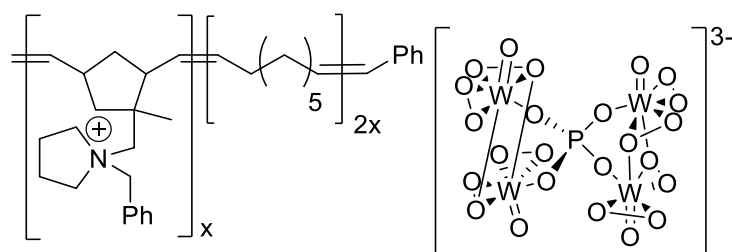


Figure 1.11 POM@PIILP catalyst of the Knight-Doherty group for the epoxidation of allylic alcohols.

The PIILP catalyst was shown to be an efficient system for the epoxidation of allylic alcohols and alkenes and most encouragingly it was possible to recover and reuse the catalyst in a straightforward manner with only a minor decrease in performance observed.

1.4 Methods of Polymerisation

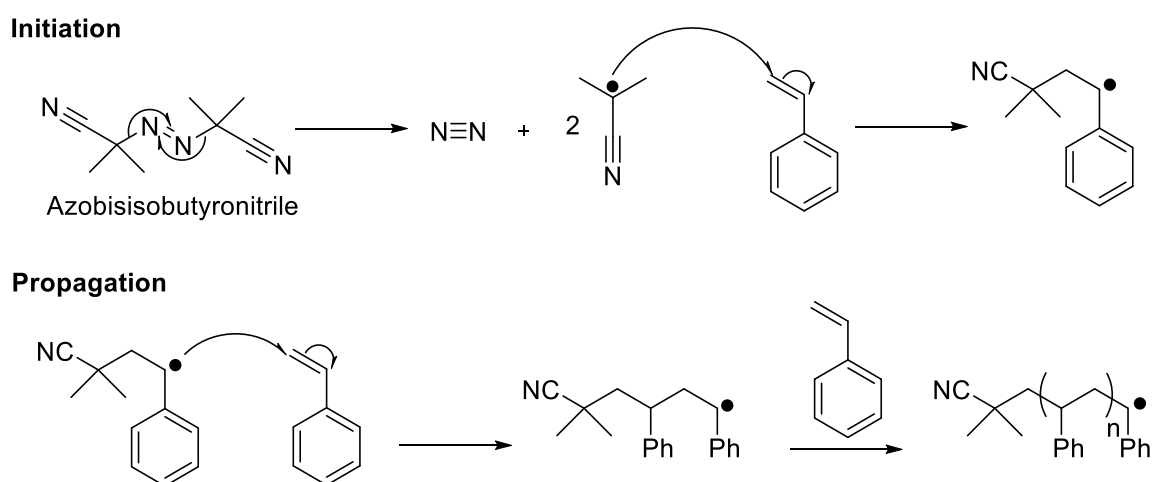
In order to synthesise PIILP materials a range of different polymerisation techniques have to be considered. As well as being synthetically straightforward, the chosen technique would also provide a high degree of functionalisation to enable the surface properties, microstructure, ionic microenvironment, stability and porosity to be modified in a rational and systematic manner, which would enable catalyst–surface interactions, substrate accessibility and efficiency to be optimised, property–function relationships to be elucidated and new activity–selectivity relationships to be established.

1.4.1 Radical

Since the 1980's around 50 % of all synthetic polymers produced worldwide (ca. 100 million tons) have been obtained via a free radical polymerisation process. These commercial processes typically lead to high molecular weight polymers which are cheap to produce and can tolerate

a wide variety of monomers. The use of the term ‘free-radical polymerisation’ as a general description of all free-radical propagating polymerisations has now become less appropriate since the introduction of reversible-deactivation radical polymerisation systems. As such the abbreviated ‘radical polymerisation’ is more appropriate.

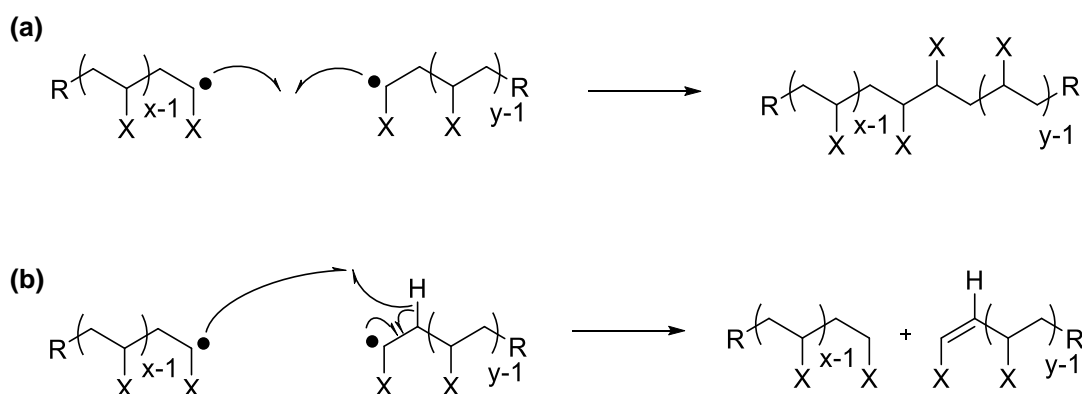
Radical polymerisation proceeds via sequential addition of unsaturated monomers to a terminal radical, referred to as the active centre. This active centre can then attack the π -bond of a molecule of monomer causing it to break homolytically. Experimentally this can be achieved extremely simply due to the high degree of tolerance towards water and protic solvents. The only requirement of such systems is the complete removal of oxygen from the system prior to activation to prevent the polymerisation being inhibited. This is typically achieved in the laboratory via several cycles of a freeze / pump / thaw process.



Scheme 1.10 Initiation and propagation of radical polymerisation of styrene initiated by AIBN.

Formation of free-radicals can occur in one of two ways, (i) *homolytic scission*, which sees the two bonding electrons of a bond transferred to the associated atoms creating two free radical species, and (ii) *single-electron transfer*, which involves the transfer of a single electron to or from an ion or molecule.^[47] **Scheme 1.10** shows the general mechanism of radical polymerisation initiated by azobisisobutyronitrile (AIBN) which undergoes homolysis via thermolysis at relatively low temperatures and produces N_2 which provides the driving force for the reaction. Other potential thermal initiators include benzoyl peroxide, and *t*-butyl hydroperoxide. Homolysis may also be achieved via photolysis with UV radiation of an appropriate photochemical initiator such as benzophenone. This also provides the added advantage of instantaneous formation of free radicals when the light source is applied, which will also cease when the source is removed.

The termination of radical polymerisation occurs most frequently via one of two irreversible bimolecular reactions of the propagating chains (**Scheme 1.11**). The first is combination of two growing chains to form a single polymer strand while the second is a disproportionation where a proton is abstracted from the penultimate carbon of one chain by another active centre, resulting in two deactivated polymer molecules, one with a saturated terminus and the other with an unsaturated terminus.



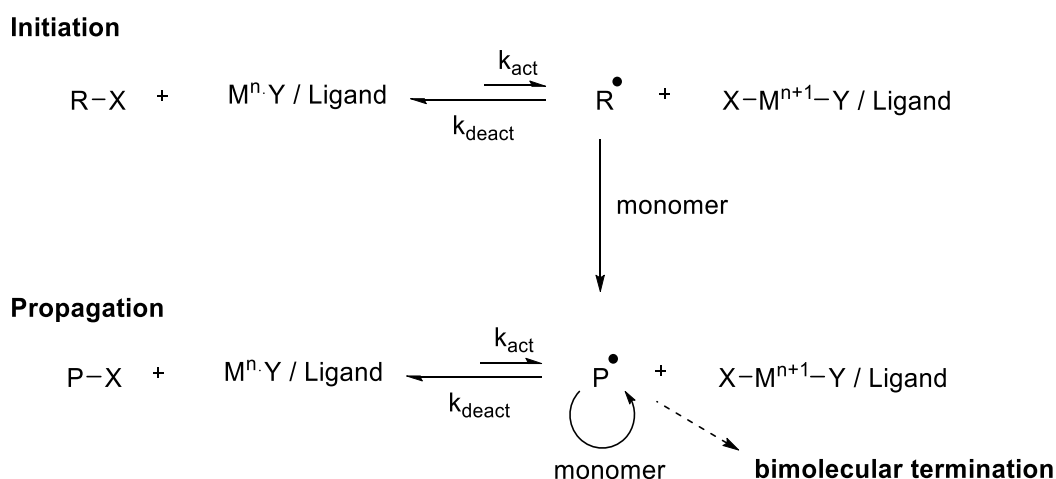
Scheme 1.11 Mechanisms of (a) combination and (b) disproportionation termination.

There are however several notable disadvantages to radical polymerisation. Most significantly is the uncontrolled nature of the process leading to poor molecular weight distributions. In addition to this, the lack of control also prevents formation of the often desirable block copolymers and architectural control is typically very limited via this technique.

1.4.2 ATRP

The development of controlled/living radical polymerisation (CRP) methods has been a long-standing goal in polymer chemistry, as a radical process is more tolerant of functional groups and impurities and is the leading industrial method to produce polymers.^[48] Living polymerisation can be defined as one which proceeds without chain transfer or termination. All the chains are initiated at the start of the reaction, grow at equal rates and remain active or 'living' after the consumption of all the monomer present. In this way, materials with very narrow molecular weight distributions can be afforded. Recently a large amount of progress has been made in the development of several methods of CRP including atom-transfer radical polymerisation (ATRP),^[49] reversible addition fragmentation chain transfer (RAFT),^[50] nitroxide mediated polymerisation (NMP)^[51] and stable free radical polymerisation (SFRP).^[52]

ATRP in particular has proved promising having first been introduced by Sawamoto^[53] and Matyjaszewski^[54] in 1995. It is a means of forming a carbon-carbon bond through a transition metal catalyst. **Scheme 1.12** shows the general mechanism of ATRP.



Scheme 1.12 General mechanism of ATRP.

Here the catalyst or ‘activator’ is in the form of a metal salt which initiates the reaction via a single electron transfer to the organic halide resulting in homolysis and the generation of the radical species and an increase in the transition metal oxidation state which will subsequently pick up the free halogen. It is the equilibrium which exists between the propagating radicals (R^\bullet) and the dormant species in the form of $R-X$ which ultimately controls the ATRP. The dormant species (RX or PX , **Scheme 1.12**) intermittently reacts with the transition metal complex when it is in its lowest oxidation state, which acts as the initiation to form a propagating radical and a deactivator- TM^{n+1} complex with the coordinated halide. This species can then react with the propagating radical to proceed in the reverse reaction. The chain continues to grow through a series of activation-propagation-deactivation cycles and as such the equilibrium must be forced to lie close to the left to ensure rapid exchange for each monomer.

1.4.3 ROMP

Living ring-opening metathesis polymerisation (ROMP) is a variation of the olefin metathesis reaction which has emerged as a particularly powerful method for synthesising polymers with tunable sizes, shapes, and functions.^[55] ROMP utilises transition metal metathesis catalysts such as molybdenum and tungsten (Schrock type catalysts) or ruthenium to generate polymers from cyclic alkenes. The most important catalysts for ROMP are now widely accepted to be those based on ruthenium as developed by Grubbs and co-workers (**Figure 1.12**). These catalysts are air stable, functional group tolerant and effective at moderate temperatures between 25- 50 °C.^[47]

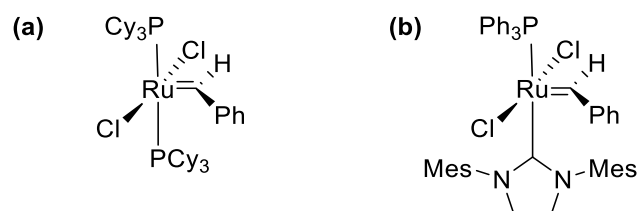
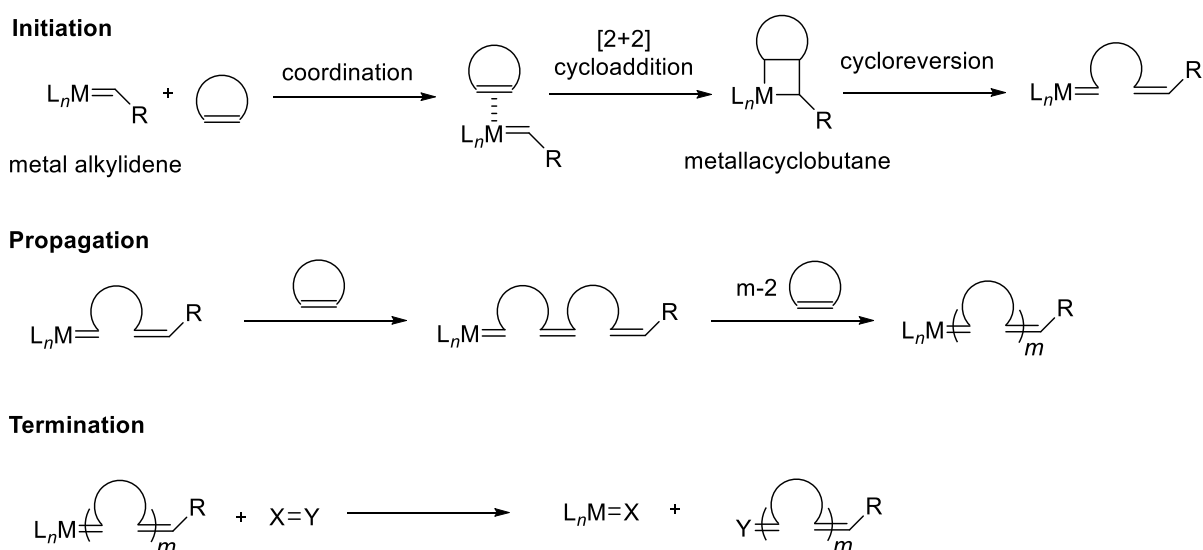


Figure 1.12 Two of the ruthenium catalysts developed by Grubbs *et al.* (a) first generation catalyst, (b) second generation catalyst.

The process is most effective where the cyclic alkene is a strained system. The relief of ring strain will therefore provide the major driving force for the reaction whilst at the same time a decrease in entropy is occurring. Common monomers utilised for ROMP are cyclic olefins which exhibit considerable ring strain ($>5 \text{ kcal mol}^{-1}$), such as cyclobutene, cyclopentene, *cis*-cyclooctene and norbornene.^[56] The mechanism itself is based on olefin metathesis, a metal-mediated C-C double bond exchange process.^[57] A general mechanism for ROMP, based on the original proposal by Chauvin *et al.*,^[58] is shown in **Scheme 1.13**.



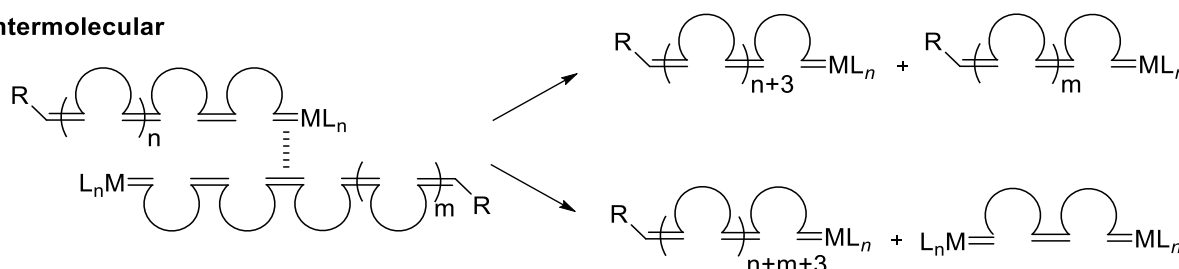
Scheme 1.13 General mechanism of ring opening metathesis polymerisation (ROMP).^[58]

Initiation proceeds with coordination of the transition metal alkylidene to a cyclic olefin followed by a [2+2] cycloaddition to afford a metallacyclobutane intermediate. This intermediate is the start of the polymer chain and cycloreversion will afford a new metal alkylidene. Propagation of the intermediate will eventually result in the incorporation of all of the monomer and the polymerisation will cease at this point or if an equilibrium is reached. The metallocarbene end groups remain active in a living polymerisation and propagation will continue in the event of more monomer being added. The normal practise is to remove these groups via addition of an appropriate chain-terminating reagent. Typically, ethyl vinyl ether is used to displace the chain and afford an inactive ruthenium complex. Alternatively, the

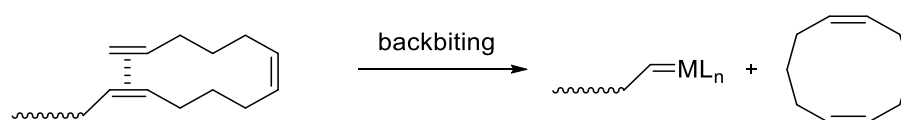
ruthenium may also be displaced via the addition of a specialised chain transfer agent such as *cis*-1,4-diacetoxy-2-butene which can be easily deprotected to give hydroxyl groups that can be further reacted to create ABA block polymers if so desired.

In addition to the general mechanism other secondary metathetical pathways can take place depending upon the reaction conditions. **Scheme 1.14** shows both intermolecular and intramolecular chain-transfer reactions which can also occur.

Intermolecular



Intramolecular

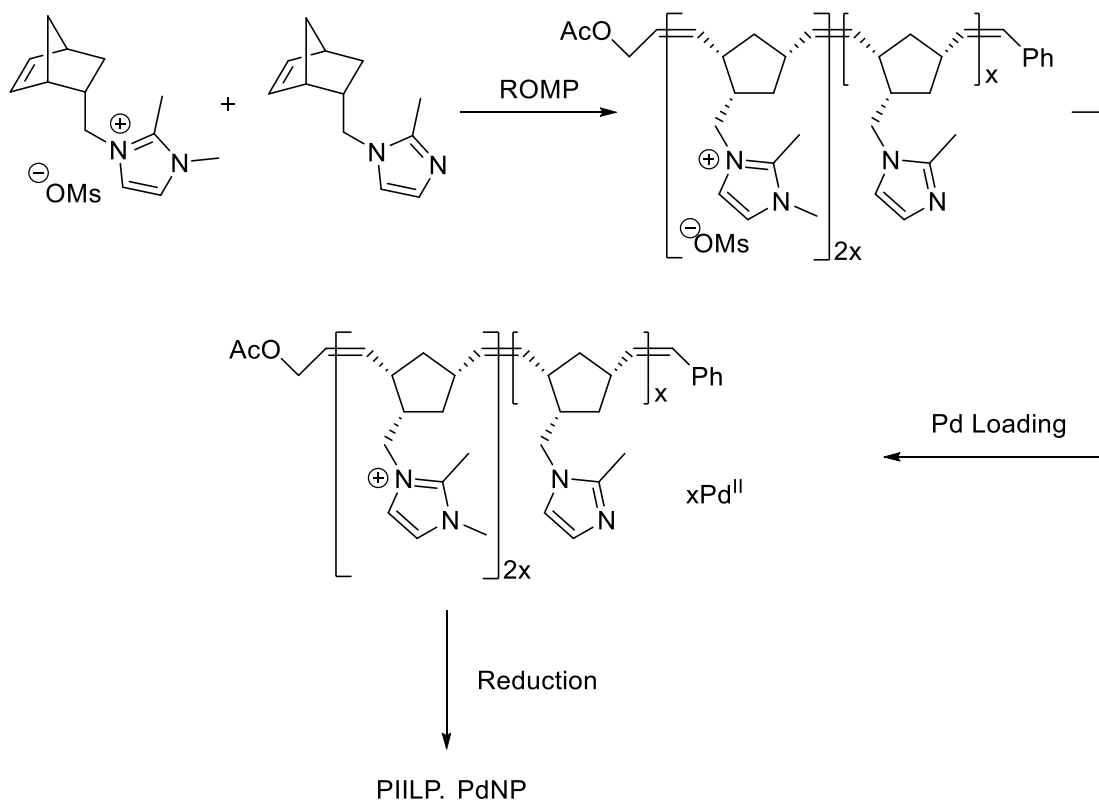


Scheme 1.14 Intermolecular and intramolecular secondary metathetical pathways.^[55]

In an intermolecular chain-transfer, one polymer chain containing an active metal alkylidene terminus can react with the backbone of another polymer chain resulting in a broader molar mass distribution. In the case of an intramolecular chain transfer or ‘backbiting’, the active metal alkylidene terminus of the polymer reacts with itself to afford a cyclic chain and a linear polymer chain of reduced length. The net effect of these secondary reactions is a broadening of the polydispersity of the system. As with all chain polymerisations however the effect of chain transfer to polymer can be minimised through the use of lower reaction temperatures.

1.5 Project Aims

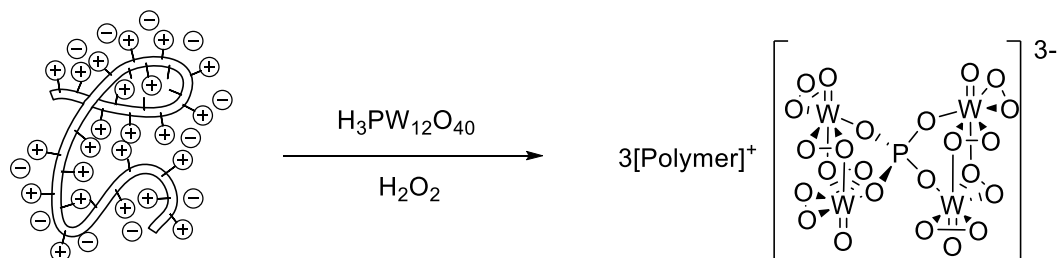
Drawing from the existing literature the aim of this project was to initially investigate ROMP to develop a range of tunable polymeric support materials featuring C-2 methylated imidazolium and imidazole pendants. ROMP was chosen based upon its functional group tolerance and ability to ultimately produce polymers of tunable sizes, shapes, and functions. These materials would then be used to support palladium as PdCl_4^{2-} which could subsequently be reduced via hydrogenation or in-situ to afford PdNPs. The hope was that these NPs would be encapsulated within the polymeric material preventing leaching of the active species and enabling straightforward and effective catalyst recovery and recycling.



Scheme 1.15 Proposed route to PdNP@PIILP materials.

Scheme 1.15 shows the proposed synthetic route to the desired materials. The aim was for these materials to be fully characterised to better understand how the ionic microenvironment effects nanoparticle size distribution and for them to be extensively studied for the Suzuki-Miyaura cross-coupling of a range of aryl bromides with phenylboronic acid.

In addition to studying PIILP immobilised PdNPs this project also aimed to demonstrate the scope of PIILP materials in catalysis. The immobilisation of a polyoxometalate (POM) species on a range of polymeric support materials is described in Chapter 3 with the goal of achieving highly efficient sulfide oxidations.



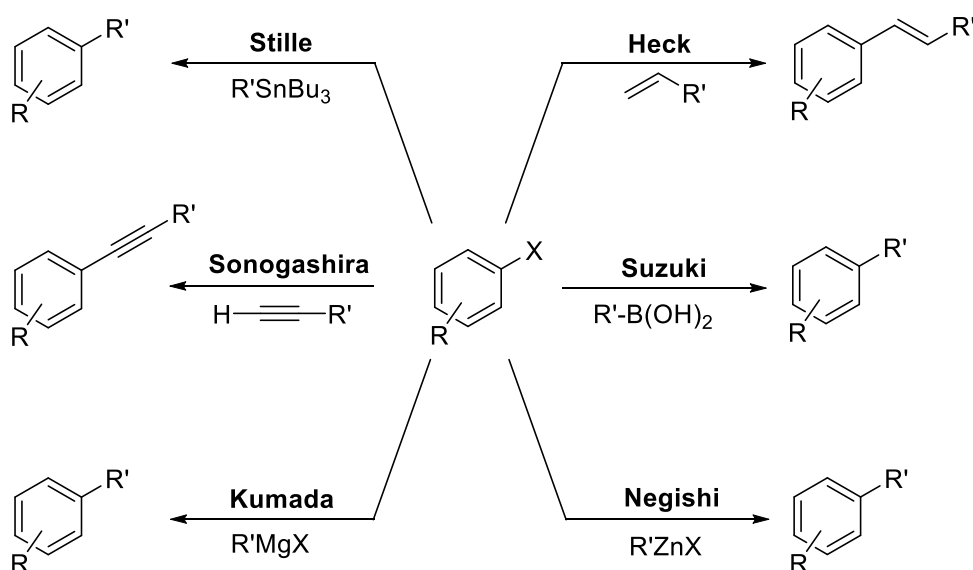
Scheme 1.16 Proposed POM@PIILP catalyst for sulfide oxidation.

Scheme 1.16 shows the proposed POM species generated from hydrogen peroxide mediated decompositions of phosphotungstic acid which will be immobilised on the polymer via simple anion exchange. The ultimate goal for this system was its application in crude oil desulfurisation which is discussed in Chapter 4.

Chapter 2. Polymer Supported Palladium Nanoparticles: Synthesis & Catalysis

2.1 Introduction

The use of palladium catalysts in carbon-carbon cross-coupling reactions has had a profound effect on synthetic organic chemistry, which was acknowledged by the 2010 Nobel Prize for R. F. Heck, E-I. Negishi and A. Suzuki for their work in this area. Their work, along with other chemists has resulted in a range of cross-coupling reactions (**Scheme 2.1**) with applications in fields such as polymer production and the synthesis of agrochemicals and pharmaceutical intermediates.^[59]



Scheme 2.1 Pd-Catalysed C-C bond-forming cross-coupling reactions (X = halide, pseudohalide, OTf etc.).^[60]

Despite the availability of more cost-effective catalysts such as nickel,^[61] copper^[62] and iron,^[63] palladium possesses several notable advantages such as higher activity which can enable the conversion of less reactive substrates, performance at relatively low temperatures and high catalyst turnover numbers (TONs).^[64] Suzuki cross-coupling reactions have become the most widely used protocol for the formation of biaryl compounds, with extensive applications in pharmaceuticals and natural product synthesis. The factors which have contributed to the success of this reaction are primarily the tolerance for a wide range of functional groups as a result of the mild reaction conditions and the availability, stability and sustainability of the boronic acid starting materials.^[65] These transformations have typically been catalysed by soluble Pd^{II}/Pd⁰ complexes in the presence of phosphines or other ligands in organic solvents and aqueous media exhibiting the high activity and catalyst TONs associated with palladium.^[66]

However, sustainability issues have arisen due to difficulties in separation of the catalyst from the reaction product. Heterogenisation of the process has overcome this issue to a degree, in particular the use of palladium nanoparticles (PdNPs) supported on a variety of conventional and non-conventional solid supports has proved particularly promising for Suzuki cross-couplings, enabling recovery/recycling of the catalyst in a ‘ligand free’ synthesis.

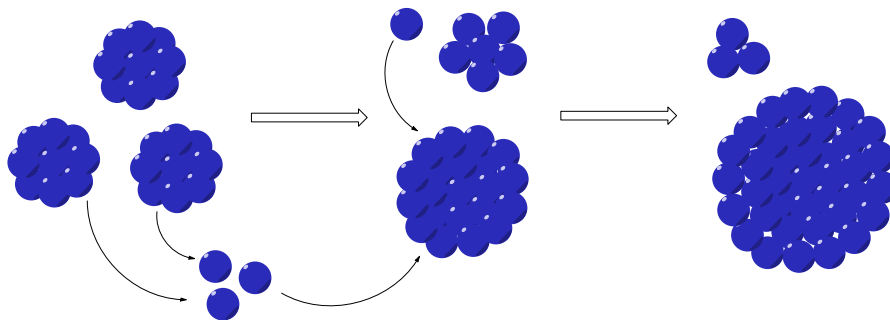


Figure 2.1 Schematic representation of Ostwald ripening.

Nanoparticles are defined as particles between 1 and 100 nm in size and metal NPs achieve high catalytic activity as a result of their high surface area to volume ratio. Highly active small NPs, though kinetically stable, will however agglomerate unless a stabilising agent or capping ligand is present, as larger particles are more thermodynamically favourable. This process is described by the principle of Ostwald ripening,^[67] whereby coordinatively unsaturated atoms at the surface of small particles are substantially less energetically stable than those which are fully coordinated and well-ordered in the bulk material. Therefore, larger particles which possess a lower surface to volume ratio have a lower surface energy. The system will try to reduce its overall energy via detachment of atoms or molecules from the surface of smaller particles and their subsequent attachment to the surface of larger particles, resulting in a decrease in the number of smaller particles (**Figure 2.1**).

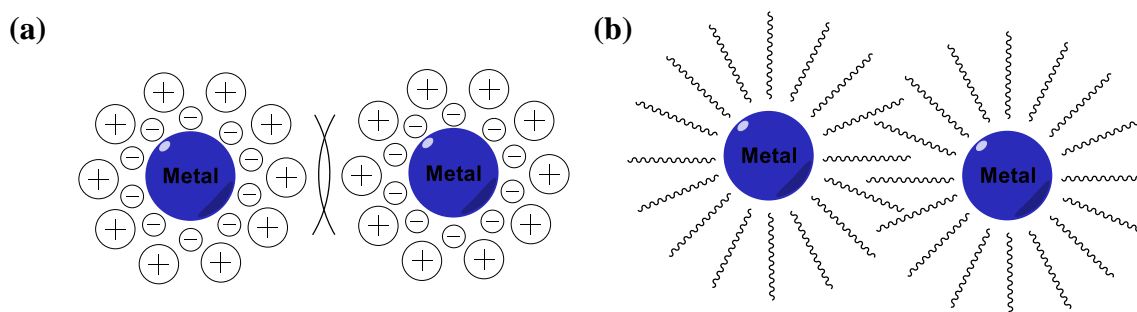
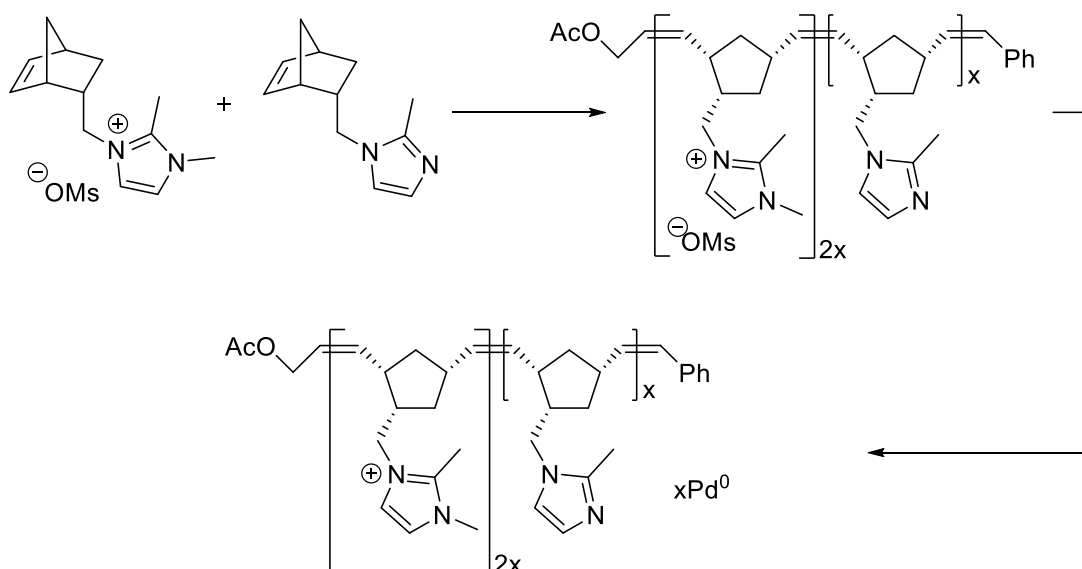


Figure 2.2 Schematic representation of (a) electrostatic stabilisation of metal NPs, (b) steric stabilisation of metal NPs.

Stabilisation of metal NPs has typically involved electrostatic and/or steric protection (**Figure 2.2**), for example using water soluble polymers,^[68] quaternary ammonium salts,^[69] surfactants^[70] or polyoxoanions.^[71] Ionic liquids (ILs) have proven to be extremely effective for both the generation and stabilisation of small metal NPs as they act as both the solvent and stabiliser. Derjaguin-Landau-Verwey-Overbeek (DLVO) theory states that ILs form a 'protective shell' around metal-NPs providing electrostatic stabilisation. It predicts that the inner shell will be anionic and this initial shell will provide the primary source of stabilisation to the metal nanocluster.^[72]

Building upon the literature precedent for NP stabilisation in both ILs and polymer supported systems, a heteroatom-modified PIILP would be expected to provide both electrostatic and steric stabilisation of PdNPs against agglomeration, known as electrosteric stabilisation.^[73] Utilisation of the polymerisation techniques described in Chapter 1 could enable the system to be effectively tuned to control NP size distribution via variation of the heteroatom, charge density and the amount of cross-linkage in the system. In addition, through variation of comonomers it could be possible to enhance catalyst activity and selectivity. The use of a PIILP based system would also enable easy and efficient recovery and reuse of the catalyst and as such this practise is becoming increasingly popular across a range of catalysis. Utilising a styrene-based imidazolium chloride homopolymer Dyson has reported that a range of transition metal NPs including Pd were stabilised through electrostatic effects and it was possible to transfer the NPs from the aqueous phase to an IL without aggregation occurring through anion exchange of the polymer.^[74] Similarly Dyson *et al.* have recently had success utilising ROMP to generate a water soluble methyl-imidazolium-based ionic homopolymer which was successfully used to prepare aqueous solutions of small well defined and stable NPs which were shown to exhibit excellent activity for the reduction of *p*-nitrophenol and the hydrogenation of cinnamaldehyde.^[75] Suzuki-Miyaura coupling has also been efficiently performed by polymer supported PdNPs under air in water at 100 °C which was active for 5 recycles.^[76] The group of Garcia-Verdugo have synthesised a range of cross-linked PIILP like materials which they refer to as gel-supported ionic liquid-like phases (g-SILLPs) featuring imidazolium moieties which act as a PdNP reservoir for the efficient catalysis of Heck, Sonogashira and Suzuki reactions.^[77] As there exists an increasingly large literature precedent for the effects of IL moieties contained within polymeric materials this would suggest that the concept of PIILP as described in Chapter 1 would be an obvious candidate for the preparation and stabilisation of metal NPs with the goal of successfully achieving cross-coupling reactions.

As discussed in the previous chapter ring opening metathesis polymerisation was identified here as the optimum method of polymerisation to generate the cross linked cationic polymer support owing to the ease and scope for functionalisation that this living polymerisation technique allows. The proposed synthetic pathway is shown in **Scheme 2.2** which would result in the generation of PdNPs on a methyl imidazolium co-polymer which would be the active catalytic species.



Scheme 2.2 Overview of synthetic pathway to PIILP catalyst materials.

Imidazolium was selected as a result of the extensive literature on its use in ILs as a nanoparticle stabiliser by way of the strong interactions between M-NPs and the imidazolium ring.^[78] The imidazolium moiety is methylated at the C2 position as it has been suggested that Pd-*N*-heterocyclic carbene complexes (**Figure 2.3**) may precede the formation of PdNPs through deprotonation at this position or via oxidative addition.

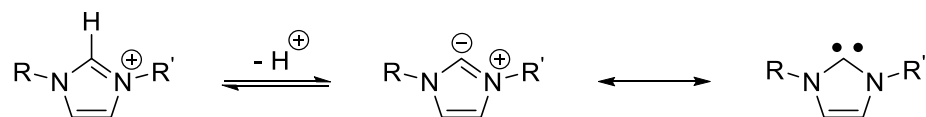


Figure 2.3 Formation of *N*-heterocyclic carbene at the imidazolium C-2 position.

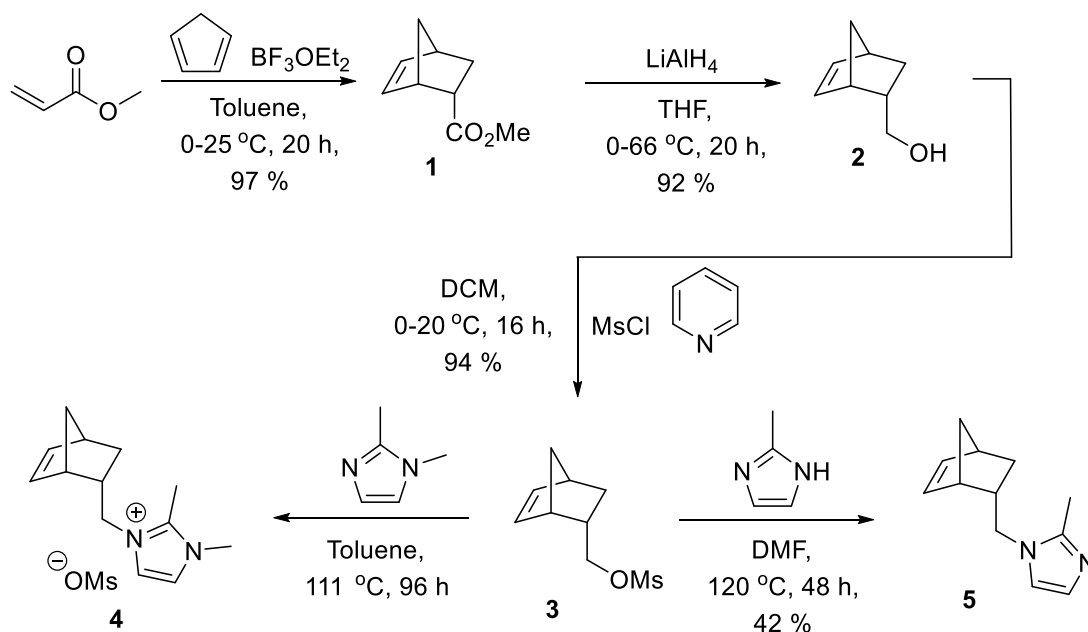
Although Pd-*N*-heterocyclic carbene complexes can prove to be the source of positive IL effects in some systems,^[17b] there are several reports where this effect has led to deactivation of the catalyst.^[79] In order to avoid this possibility, the synthesis of polymers incorporating a 2-substituted imidazolium ion was envisaged. An imidazole co-monomer was also incorporated in the hope of achieving extra stabilisation through coordination to the metal surface with the

intention being that this heteroatom-functionalised moiety could be varied by the introduction of N-, O- or P- containing functionalities to achieve potential improvements in catalytic activity.

It is also essential to note a key issue in PdNP-catalysed cross-coupling reactions in relation to the mechanistic nature of these processes. There remains debate as to whether PdNP catalysis is a direct result of the NPs themselves or potentially from leached metal within the systems. This mechanistic uncertainty has been the subject of intense debate in the past decade, and several conflicting theories have arisen. Rothenburg and co-workers utilised a special membrane reactor which showed that Pd atoms were in fact leaching in both Heck and Suzuki coupling reactions^[80] which would support work by de Vries^[81] and Schmidt^[82] who have proposed that NPs are acting as a reservoir of Pd atoms which ultimately catalyse the reaction. Both ionic liquids and solid supports have been shown to minimise the apparent NP leaching and as such we hoped to see a predominantly heterogeneous process when the system was applied to cross-coupling reactions, which would be addressed as part of the investigation.

2.2 Norbornene Based Monomer Synthesis

The synthesis of both norbornene-based monomers **4** and **5** (**Scheme 2.3**) was achieved via a modular synthesis. The Diels Alder cycloaddition of methyl acrylate to cyclopentadiene, in the



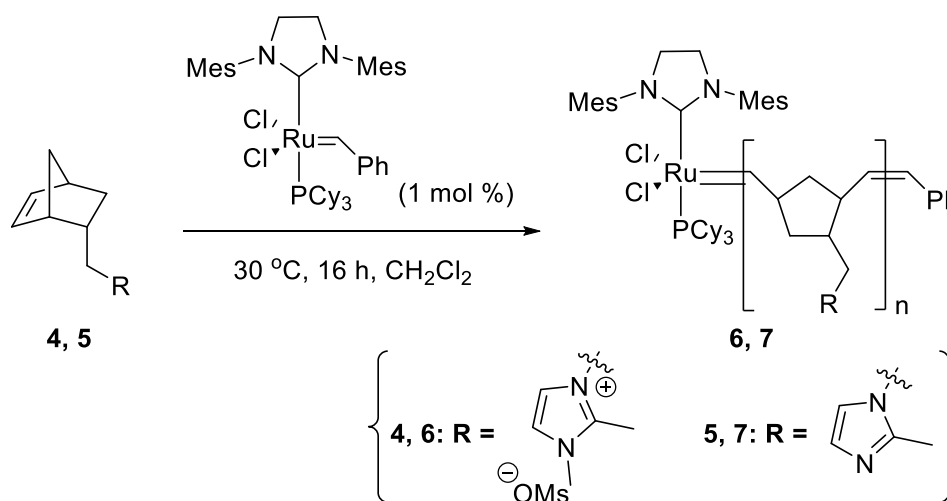
Scheme 2.3 Synthesis of *endo* norbornene-based monomers.

presence of the Lewis acid boron trifluoride diethyl etherate, afforded the norbornene methyl ester **1** with an *endo*: *exo* ratio in excess of 99: 1. This was followed by the reduction of the ester using lithium aluminium hydride in THF under reflux to afford the alcohol **2** which was

subsequently mesylated to **3** with mesyl chloride in the presence of pyridine. Nucleophilic substitution by 1,2-dimethylimidazole in toluene under reflux or 2-methylimidazole in DMF at 120 °C afforded the desired monomers **4** and **5** respectively.

2.3 ROMP Polymer Development

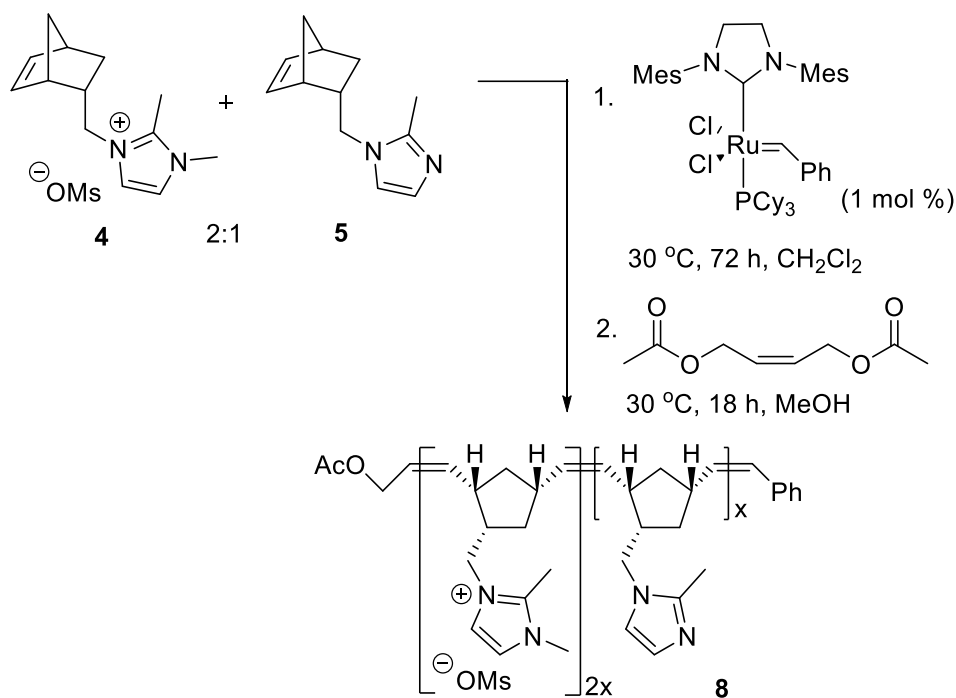
In order to determine the feasibility of synthesising our proposed co-polymer, both homo polymers of the respective monomers **4** and **5** were first synthesised. Following the literature preparation from Dyson *et al.*^[75] poly-**6** and poly-**7** were synthesised in the presence of 2nd generation Grubbs catalyst (**Scheme 2.4**).



Scheme 2.4 Synthesis of norbornene-based homo polymers **6** and **7** from **4** and **5**.

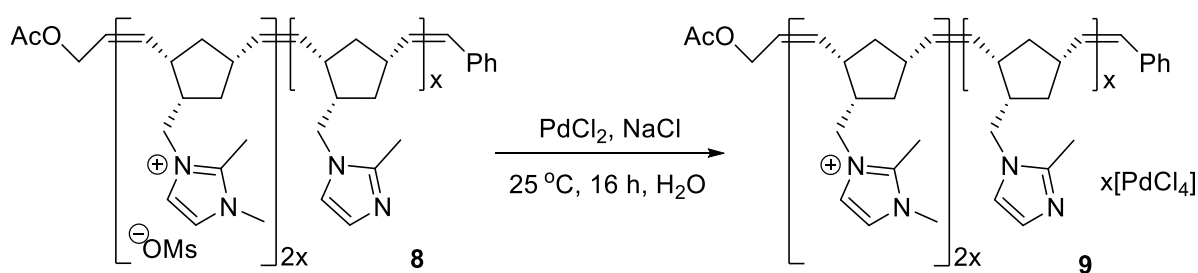
Both polymerisations were carried out in the presence of 1,3-dinitrobenzene which acted as an NMR standard, chosen as a result of its ¹H NMR chemical shifts not interfering with those of interest. The NMR data showed no sharp peaks associated with unincorporated monomer confirming that both polymerisations had successfully incorporated all of the monomer and the NMR data for poly-**6** agreed with the existing literature data.^[75] As no utilisation of these polymers was required for loading or catalysis there was no need to remove the Ru from the ends of the chains. Formation of the desired co-polymer incorporating an intended 2: 1 ratio of monomers **4**: **5** respectively was attempted, again using Grubbs 2nd generation catalyst in dry dichloromethane (**Scheme 2.5**). The reaction was left for 72 h to allow time for incorporation of both monomers. NMR monitoring of the reaction revealed equal incorporation of the monomers had taken place however the reaction proceeded extremely slowly and complete polymerisation was not achieved. After 72 h with no further reduction in monomer taking place the reaction was ceased and the ruthenium was removed with *cis*-1,4-diacetoxy-2-butene. The polymer required dialysis in distilled water to remove the presence of residual monomer. This

afforded the polymer as a glassy brown solid which was not a tractable material for its desired purpose as a support material.



Scheme 2.5 Synthesis of norbornene-based *endo*-co-polymer **8**.

The stereochemistry of the polymer structure as drawn represents the relative stereochemistry within a single monomer unit only, as the monomers are racemic it would be impossible to represent the absolute stereochemistry for the entire polymer. As the material was water soluble it was possible to attempt to load the palladium on to the polymer in the hope that this would induce precipitation of the Pd-loaded species **9** as a granular solid (**Scheme 2.6**).



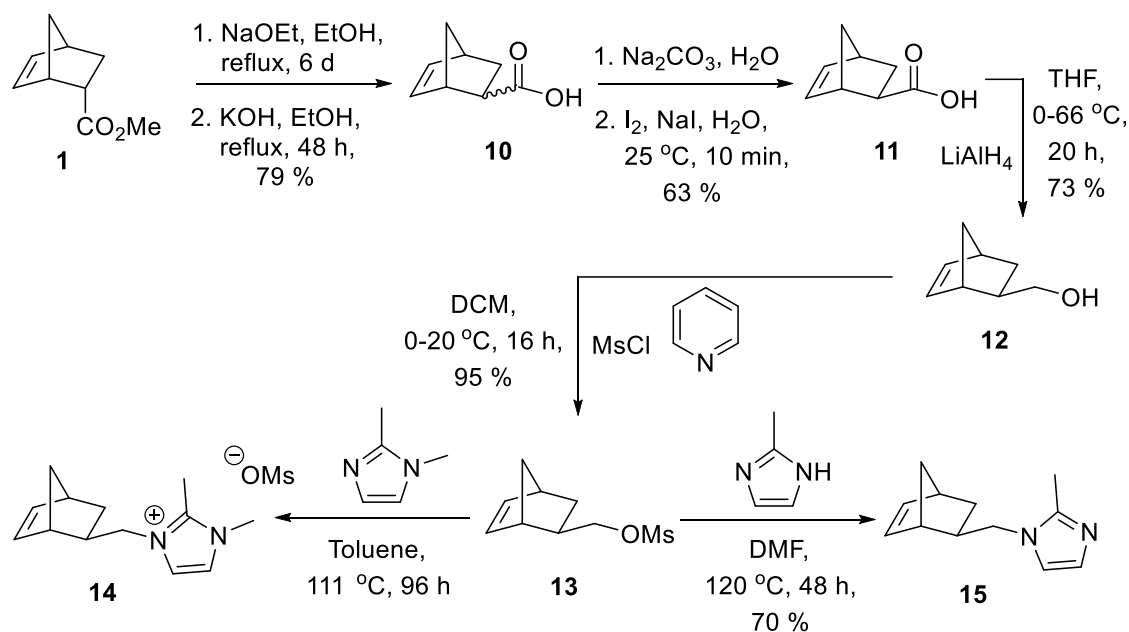
Scheme 2.6 Palladium loading of norbornene-based *endo*-co-polymer **8**.

Unfortunately, the Pd-loaded species failed to precipitate out of solution to afford anything which would prove to be a tractable material for catalysis. The poor polymerisation performance of this particular system was thought to be caused by coordination of both the imidazolium and imidazole rings to the Ru metal introduced from the Grubbs 2nd generation catalyst. A study by Nishihara on the comparative reactivity of *endo*- and *exo*-isomers in the Ru-initiated ROMP of doubly functionalised norbornenes suggested that as the *endo*- monomer

is capable of coordinating to the Ru centre as a bi- or tridentate ligand this may be suppressing its polymerisation.^[83] Propagation of the *exo*- monomer however, proceeds by the less hindered end of the catalyst to produce larger molecular weights and molecular weight distributions than for the *endo*- monomer. This indicated that a possible solution to this issue was to prepare the *exo*-isomer rather than the *endo*- form which had resulted from the initial Diels Alder reaction.

2.4 Exo-Norbornene Based Polymer Synthesis

The synthesis of the *exo*- isomers **14** and **15** (Scheme 2.7) was achieved via a modular synthesis starting from the *endo*-ester **1**. Following epimerisation with sodium ethoxide in EtOH and hydrolysis with KOH the carboxylic acid **10** was afforded as a diastereomeric mixture and subsequent isolation of the *exo*- isomer **11** was achieved by selective removal of the *endo*- isomer by iodolactonisation. Under the same reaction conditions as used for the *endo*- monomer synthesis the carboxylic acid was reduced, mesylated and reacted with the appropriate imidazole to afford the *exo*- monomers **14** and **15**.



Scheme 2.7 Synthesis of *exo*-norbornene-based monomers.

Under the same conditions as the *endo*- polymerisation the *exo*- monomer polymerisation again proceeded with equal incorporation of both monomer **14** and **15**, as indicated by the equal consumption of the remaining monomer in the ¹H NMR spectrum however, an extremely slow rate of reaction was once again observed and did not result in complete incorporation of the monomer material.

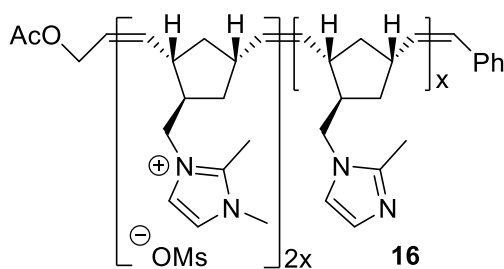


Figure 2.4 *Exo*-norbornene based co-polymer **16** which was afforded as a glassy brown solid.

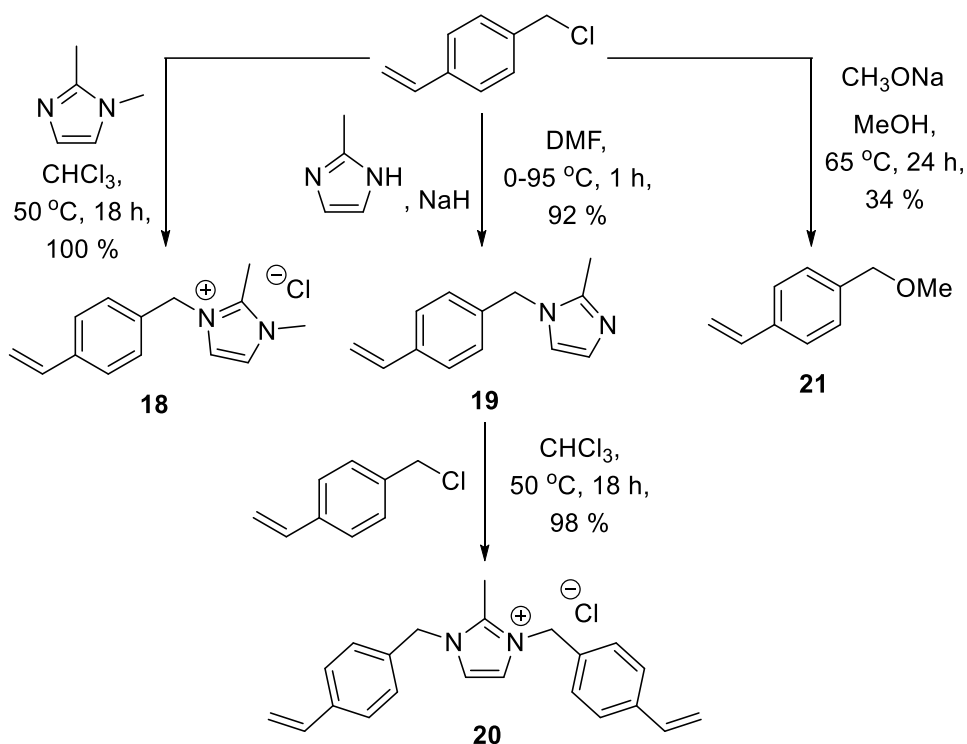
The resulting co-polymer **16** (Figure 2.4) was once again afforded as a glassy solid following dialysis. Palladium loading of this material failed to induce precipitation once more and the resulting material, **17**, was abandoned.

Although the intention of using ROMP was to allow for a greater degree of design and functionality potential for PIILP materials, this particular system requires extensive further development in order for it to yield tractable material appropriate for catalysis. Taking in to account the poor incorporation of monomers during the polymerisation process and the difficulties which arise in handling the highly hygroscopic charged monomer species **4** and **14**, the decision was taken to utilise an alternative and more simplistic method of polymerisation, rather than carry out the extensive polymer development required by this particular system. This alternative approach to the polymerisation would instead allow for the implementation of the PIILP concept in the preparation of PdNPs to be investigated as a proof of principle exercise, rather than optimising and extending the ROMP system.

2.5 Styrene Based Monomer Synthesis

Previous work carried out within the group had shown that polystyrene-based PIILP materials behaved similarly to norbornene-based ROMP materials. In addition to this, the synthetic pathway to analogous styrene-based materials was considerably shorter and does not require chromatographic purification, resulting in increased yields. The styrene-based imidazolium analogue **18** was prepared as a white powder in an operationally straightforward single step via reaction of 4-vinylbenzyl chloride with 1,2-dimethylimidazole in chloroform at 50 °C. The neutral imidazole analogue, **19**, was afforded as a pale yellow oil from the deprotonation of 2-methylimidazole with sodium hydride followed by reaction with 4-vinylbenzyl chloride. In order to increase the likelihood of attaining tractable materials the decision was taken to cross-link the final polymer materials. The ionic cross-linker **20**, was prepared by reacting monomer **19** with a further equivalent of 4-vinylbenzyl chloride to yield the cross-linker as a pure white powder. Owing to the simplicity of the monomer synthesis an alternative heteroatom-modified

neutral monomer unit, **21**, was prepared by reaction of 4-vinylbenzyl chloride with sodium methoxide to afford the monomer as a colourless oil.

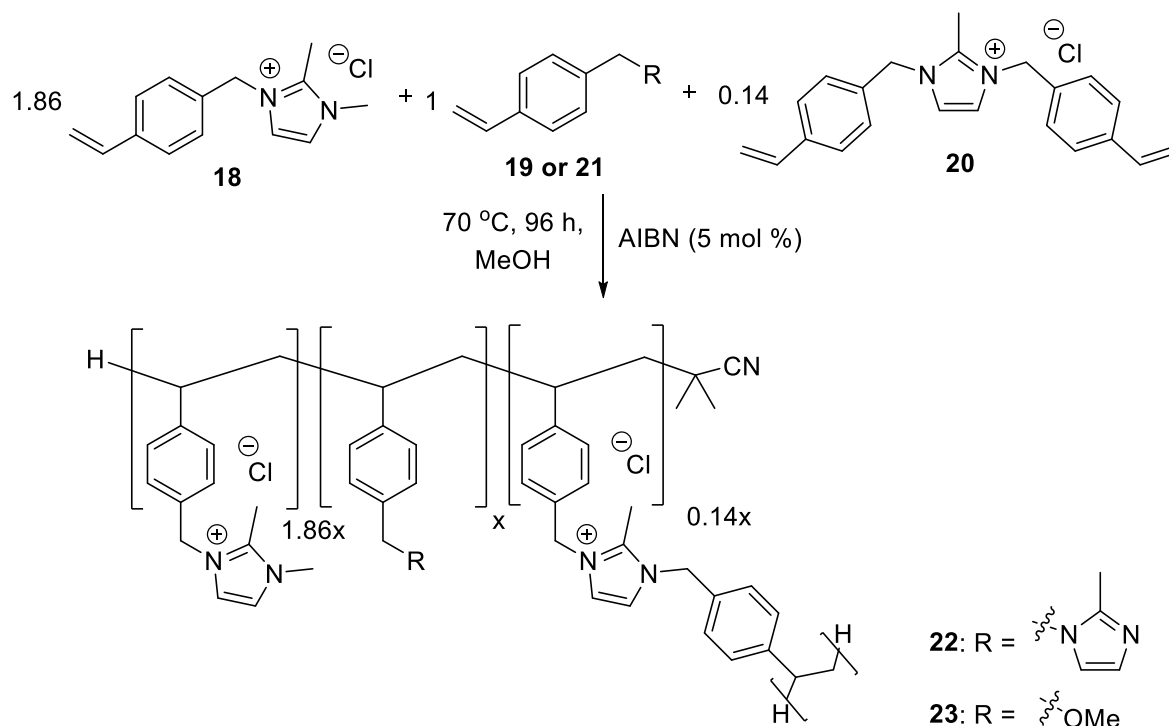


Scheme 2.8 Synthesis of styrene-based monomers **18**, **19** and **21** and cross-linker **20** from 4-vinylbenzyl chloride.

In addition to each of these monomer units being obtained via an experimentally simple route in high yield as stable solids or oils unlike their hygroscopic norbornene based analogues, they also avoid having to account for any potential complications arising from the *endo/exo* monomer isomers of the norbornene-based PIILP materials.

2.6 Cross-linked Styrene Radical Polymerisations

Two cross-linked imidazolium based PIILP supports were prepared via free-radical initiated polymerisation to investigate the effects of the different functionalities on nanoparticle size distribution and their catalytic activity (**Scheme 2.9**).



Scheme 2.9 AIBN initiated synthesis of cross-linked styrene-based co-polymers **22** and **23**.

The polymerisations were initiated by 5 mol % AIBN with a desired overall charge ratio of 2: 1 imidazolium fragments: neutral co-monomer respectively. This monomer ratio would provide a total of two imidazolium and 1 heteroatom donor groups per Pd atom in the final catalyst. Initial polymerisations were carried out for 40 h at 70 °C, however large amounts of monomer still remained so the reaction time was subsequently extended to 96 h.

Following this increase in reaction time the amount of monomer remaining had significantly decreased, however a further equivalent of AIBN was required along with a further 19 h stir to achieve complete reaction of the monomer affording both polymers **22** and **23** as fine white powders following precipitation into diethyl ether. The ^1H NMR spectra of both polymers (**Figure 2.5**) shows how all monomer material had been fully incorporated.

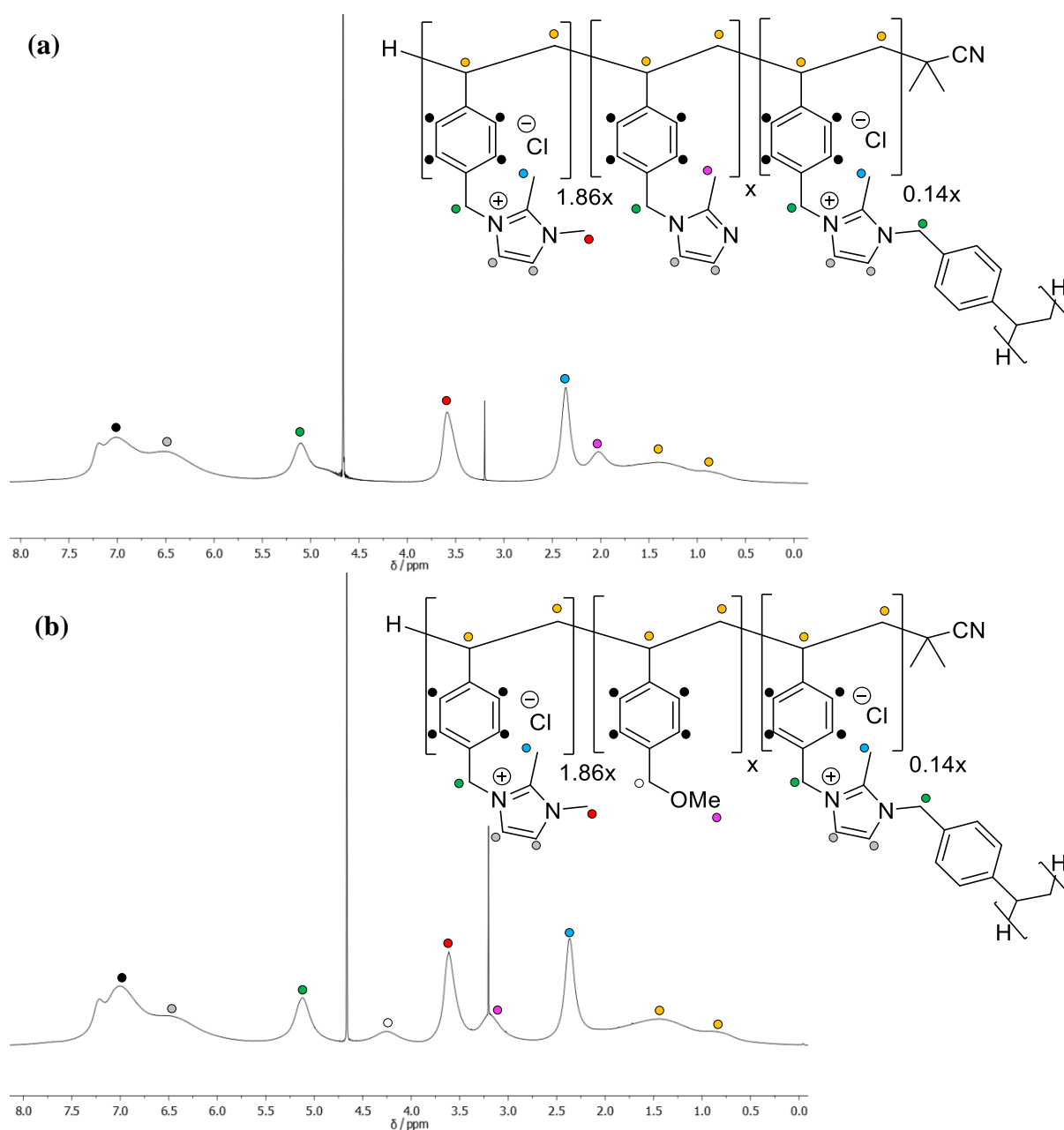


Figure 2.5 ^1H NMR spectra of polymers; (a) **22** and (b) **23** in D_2O . The broad signals associated with polymeric materials and lack of any sharp peaks associated with the monomer units confirm the full incorporation of the monomers. Colour coded assignments are shown.

Unfortunately, due to the cross-linked nature of these particular PIILP materials it proved impossible to completely remove all residual solvent meaning elemental analysis could not be used as a reliable technique to determine the composition of the materials. This residual solvent was thought to be occurring as a result of it becoming trapped within the polymer structure. This theory was supported by the appearance of ‘pores’ in the SEM images of both **22** and **23** (Figure 2.6).

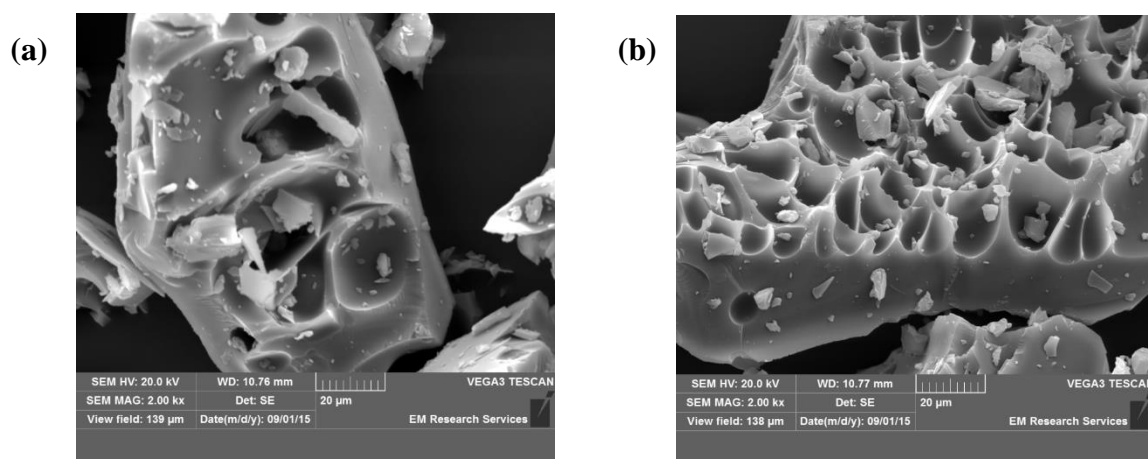


Figure 2.6 SEM images of polymers; (a) **22**, (b), **23** showing micro scale pores in cross sections of polymer which appears to have been broken apart as a result of processing of the material.

Solid state ^{13}C NMR spectroscopy was used to confirm the differences in the polymer structures as a result of the variation of the heteroatom monomer. The short-recycle, direct-excitation spectra (**Figure 2.7**) revealed peaks at 11 and 36 ppm which were consistent with the methyl imidazolium groups present in both systems. Polymer **23** also showed a peak at 58 ppm corresponding to the methyl group of the methyl ether and another signal at 74 ppm which is likely to be the $\text{CH}_2\text{-O}$. There were also relatively narrow lines at 26 and 49 ppm which do not correspond to the polymer structures but support the theory of solvent being trapped within the polymers.

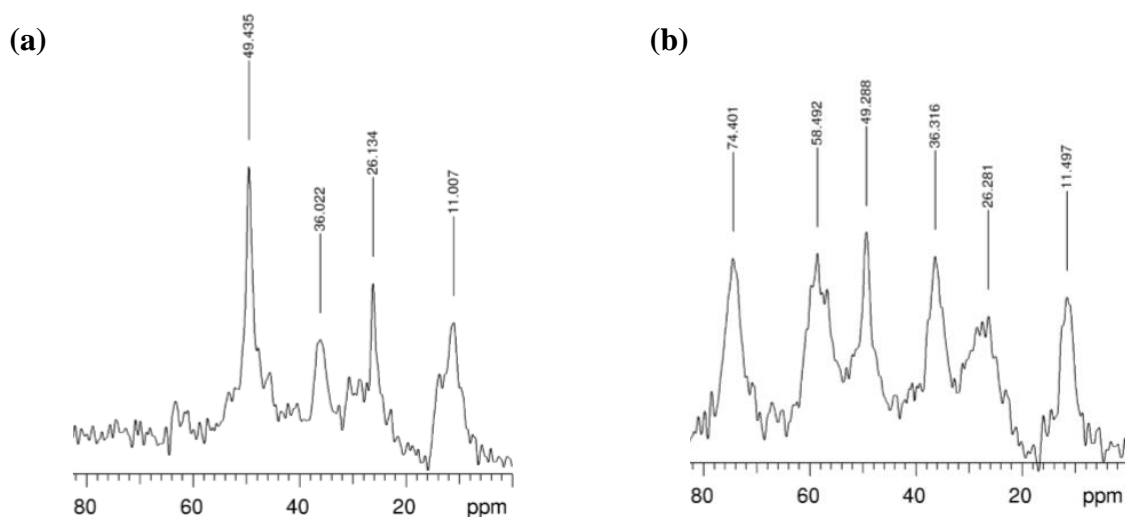


Figure 2.7 Solid state ^{13}C NMR direct-excitation spectra; (a) **22**, (b), **23**.

The thermal stability of each of the polymers was evaluated by thermogravimetric analysis (TGA) and differential scanning calorimetry (DSC). **Figure 2.8** shows the TGA/ DSC traces for polymer **22** which show a small initial weight loss ($\sim 5\%$) which was attributed to the evaporation of water or residual reaction solvent.

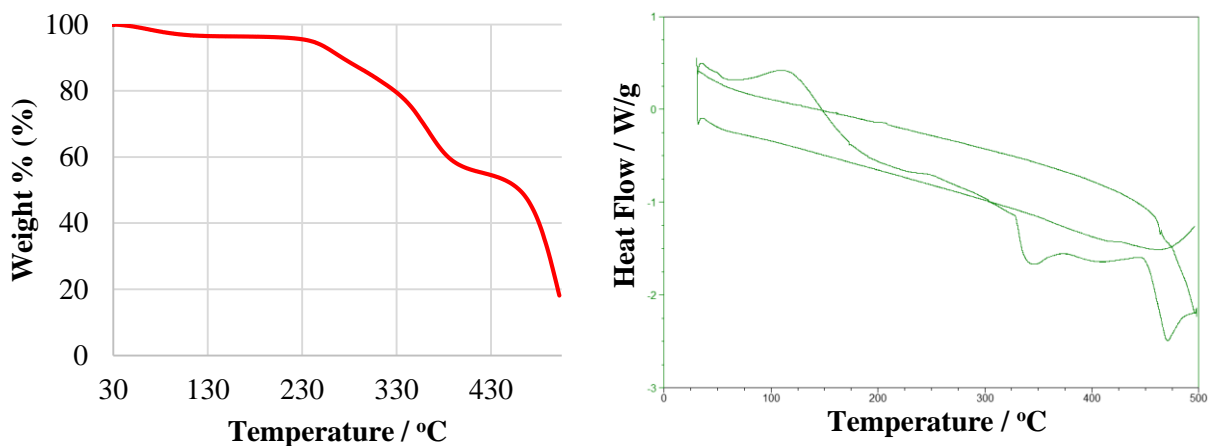
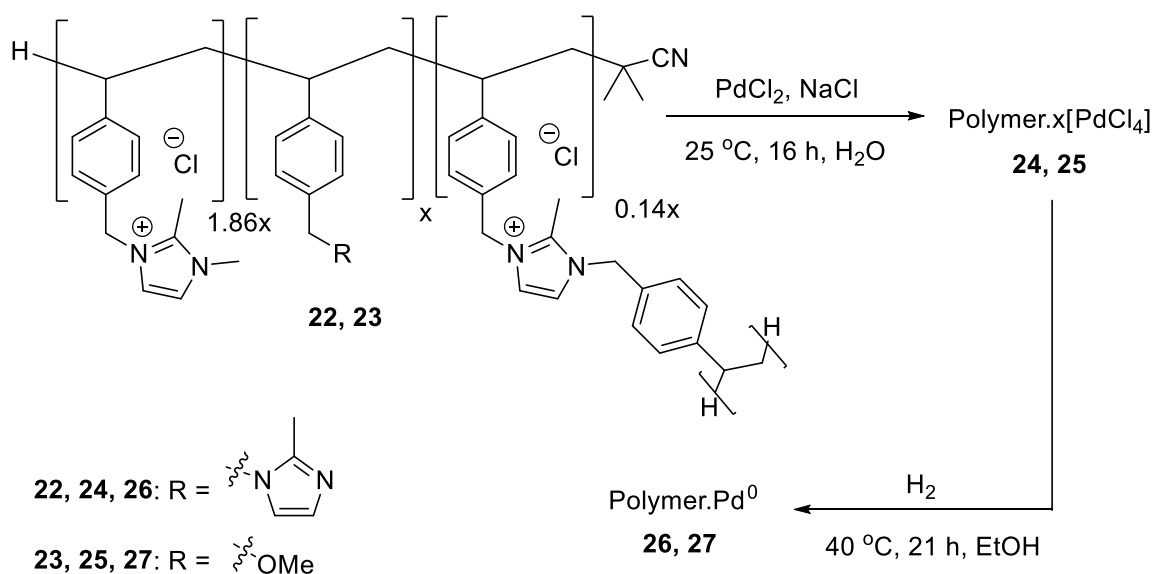


Figure 2.8 TGA/ DSC traces for polymer **22** showing an initial weight loss (~5 %) followed by degradation events at ~250 °C, then ~330 °C and a large step decomposition just above 450 °C.

This was followed by three separate degradation stages, the first at ~250 °C, then ~330 °C which was associated with the degradation of the imidazole pendants. The large step decomposition just above 450 °C corresponds to the main chain decomposition which conforms to that found in the literature and by 500 °C less than 20 % by weight of the material remains.^[80] The heat flow plot also shows an exotherm at 100 °C which could correspond to Hoffmann elimination with no loss in mass. These features were present in both of the polymers. See **Appendix 1** for TGA/DSC traces.

2.7 Formation of Polymer Immobilised Palladium Nanoparticles

Following the successful synthesis and characterisation of the cross-linked polymers **22** and **23**, they were to be loaded with Pd^{II} which would act as a precursor to nanoparticle formation and subsequently reduced to form the active Pd⁰ species (**Scheme 2.10**). Following recent literature precedent,^[84] for anion exchange, a solution of PdCl₂ and NaCl in water was added to the polymers in water. Immediate precipitation of the palladium loaded species occurred which were isolated via filtration to afford PdCl₄@Imid-PIILP **24** and PdCl₄@OMe-PIILP **25** as orange and pink solids respectively.



Scheme 2.10 Synthesis of palladium loaded cross-linked styrene-based co-polymers.

It was envisaged that the active Pd⁰ nanoparticles could be generated in two ways. They could be formed in-situ from the Pd^{II} species during catalysis in a Suzuki-Miyaura cross-coupling or alternatively pre-formed via reduction. The reduction of the Pd^{II} loaded species was achieved under 70 psi of hydrogen in EtOH at 40 °C to afford both Pd⁰@Imid-PIILP **26** and Pd⁰@OMe-PIILP **27** as black solids which were indicative of successful reduction.

Scanning Electron Microscopy (SEM) was again used to visualise the surfaces of each of the Pd loaded materials (**Figure 2.9**). This revealed that the surface of each of the materials had become uneven and granular in nature with small ‘deposits’ distributed throughout. These ‘deposits’ are likely to be a result of the extra processing of the materials resulting in damage and fragmentation.

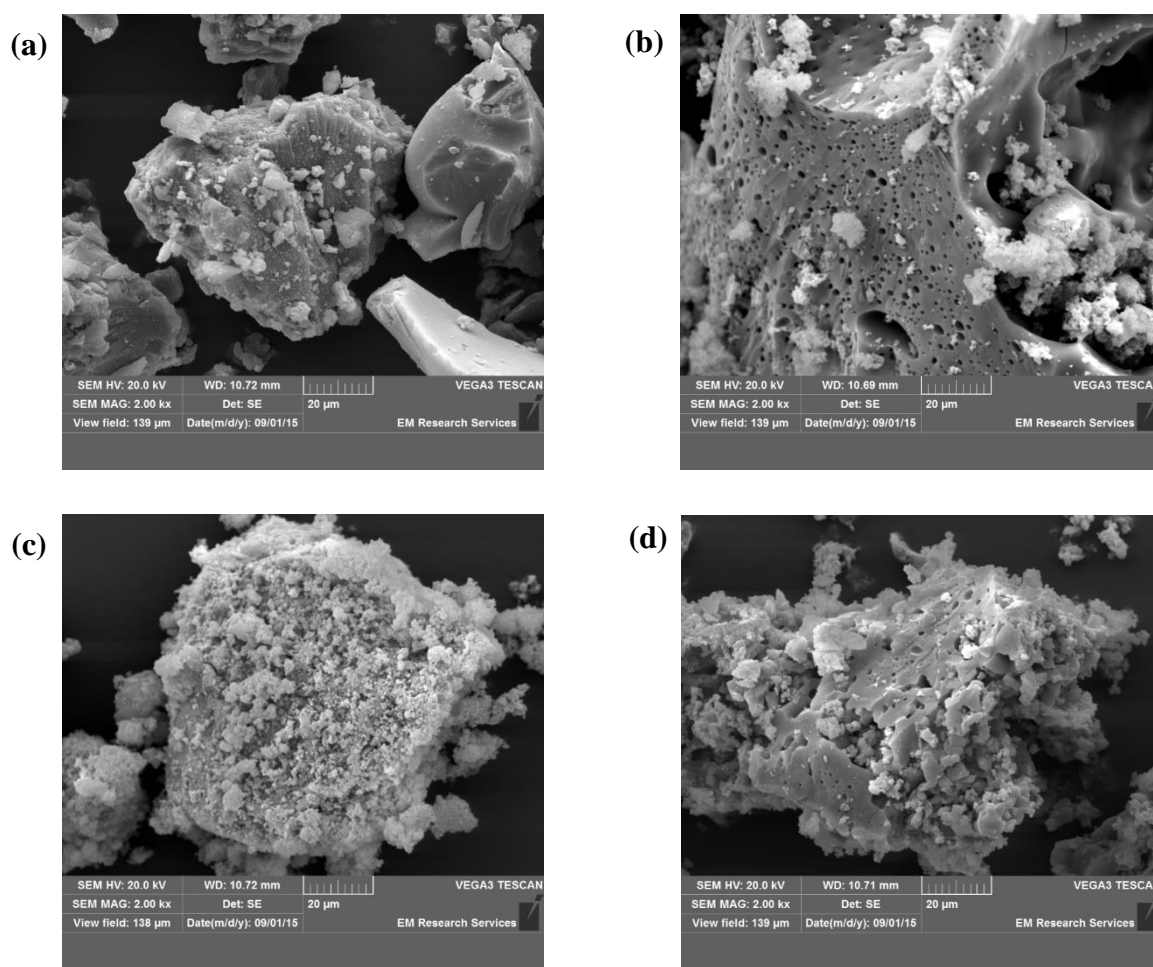


Figure 2.9 SEM images of Pd@PIILP materials; (a) **24**, (b), **26**, (c) **25**, (d) **27** showing the uneven surface of the polymer materials following POM loading.

ICP-OES analysis of PdCl₄@Imid-PIILP **24** and PdCl₄@OMe-PIILP **25** revealed that 91 % and 99 % respectively of the desired Pd had been incorporated, indicating extremely efficient anion exchange had taken place. Analysis of Pd⁰@Imid-PIILP **26** and Pd⁰@OMe-PIILP **27** showed that 79 % and 96 % respectively of the Pd remained incorporated in to the materials which suggests that a small amount of leaching has taken place during the process of reduction. The presence of the OMe functionality also appeared to have a positive effect on the extent of Pd incorporation compared with the imidazole species.

The thermal stability of each Pd loaded species was evaluated via TGA/ DSC. **Figure 2.10** shows the TGA curves for PdCl₄@Imid-PIILP **24** and PdCl₄@OMe-PIILP **25**. Here both materials show broadly similar traces with degradation occurring at around 250 °C and 400 °C. The traces for both Pd⁰@Imid-PIILP **26** and Pd⁰@OMe-PIILP **27** show little variation in their traces and can be found in **Appendix 1**.

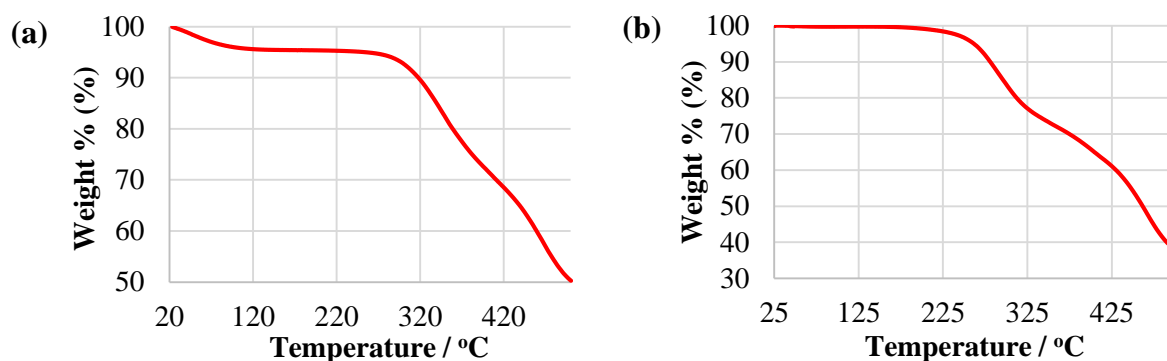


Figure 2.10 TGA traces: (a) PdCl₄@Imid-PIILP **24**, (b) PdCl₄@OMe-PIILP **25** showing similar degradation events at ~250 °C and ~400 °C.

In order to determine the composition of the Pd contained within each of the materials both X-ray Photoelectron Spectroscopy (XPS) and Powder X-ray Diffraction (XRD) were utilised.

2.7.1 XPS analysis

Although a surface technique XPS was used to give an indication of the oxidation state of the palladium content of both the reduced and pre-reduced materials. **Figure 2.11** shows the XPS spectra for both the pre-reduction and reduced imidazole catalysts which have undergone peak fitting for the 3d_{5/2} and 3d_{3/2} binding energy regions.

The spectrum for PdCl₄@Imid-PIILP **24** reveals the palladium is in the +2 oxidation state as expected with Pd 3d_{5/2} at 338 eV and Pd 3d_{3/2} at 343 eV as reported in the literature.^[85] The spectrum for Pd⁰@Imid-PIILP **26** however reveals a combination of palladium in both the +2 and 0 oxidation states with the appearance of two additional peaks corresponding to Pd⁰ 3d_{5/2} at 341 eV and Pd 3d_{3/2} at 336 eV. The area of the fitted peaks reveal the surface composition of the material to be 40.5 % Pd^{II} to 59.5 % Pd⁰ which suggests that incomplete reduction of the palladium has taken place.

The spectrum for PdCl₄@OMe-PIILP **25** (**Figure 2.12**) again shows the peaks corresponding to Pd^{II} of Pd 3d_{5/2} at 338 eV and Pd 3d_{3/2} at 343 eV and the spectrum of the reduced material Pd⁰@OMe-PIILP **27** again shows a further two peaks corresponding to Pd⁰ with Pd 3d_{5/2} at 341 eV and Pd 3d_{3/2} at 336 eV. Unfortunately however the surface composition in this case is 86.9 % Pd^{II} to only 13.1 % Pd⁰. This observation would indicate that the presence of the methyl ether is having a negative effect on the reduction process whilst also inferring that that methyl ether is interacting with the Pd nanoparticle. It is worth noting however that there is evidence to suggest that the surface of metal NPs are more susceptible to oxidation in air than the bulk metal

which may explain the large percentage of Pd^{II} observed for both systems. This oxide layer may even be a source of stabilisation of the metal.^[86]

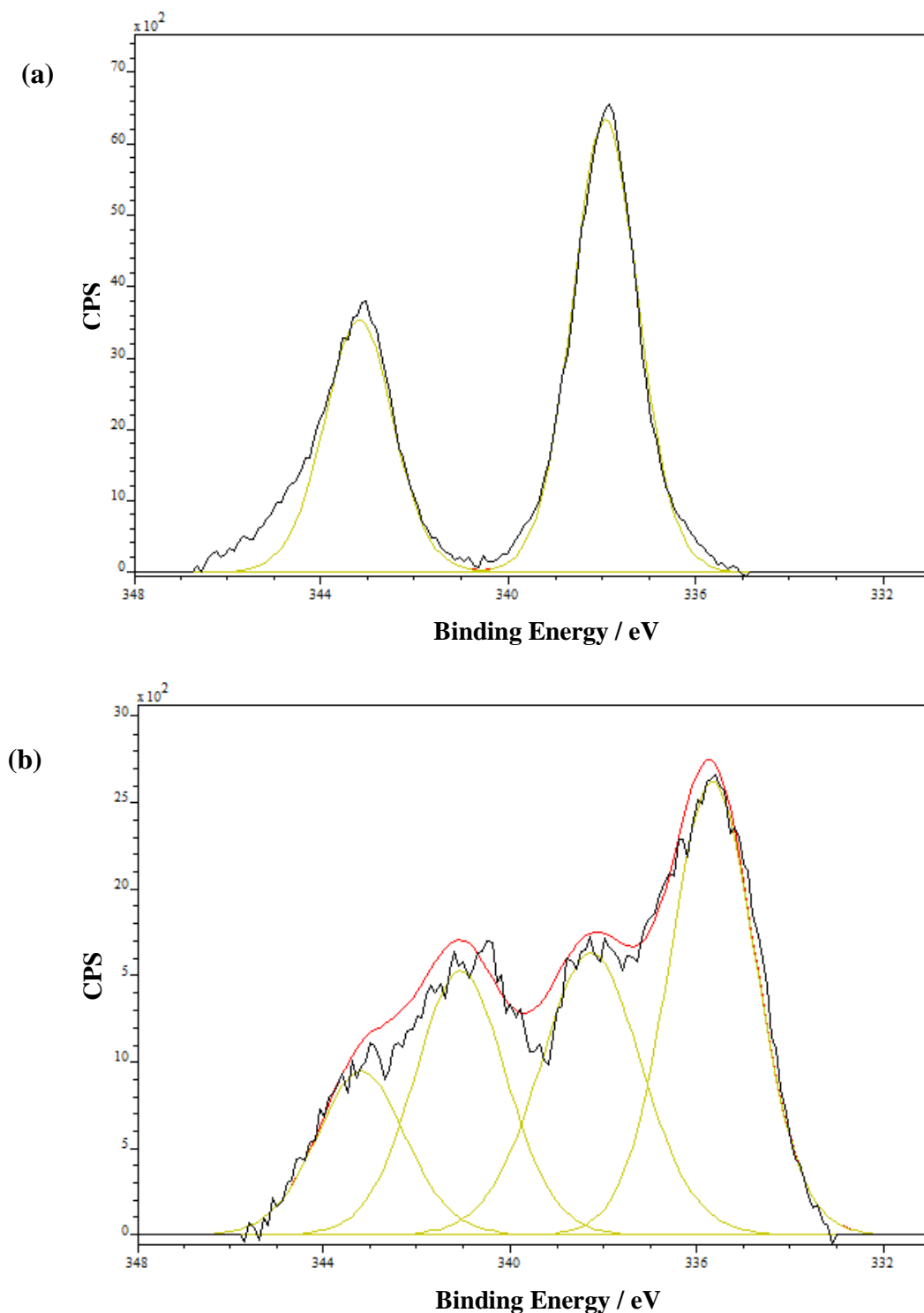


Figure 2.11 XPS Spectra and peak fits; (a) PdCl₄@Imid-PIILP **24** showing Pd 3d_{5/2} at 338 eV and Pd 3d_{3/2} at 343 eV corresponding to Pd^{II}, and (b) Pd⁰@Imid-PIILP **26** showing two additional peaks corresponding to Pd⁰ 3d_{5/2} at 341 eV and Pd 3d_{3/2} at 336 eV indicating a combination of palladium in both the +2 and 0 oxidation states.

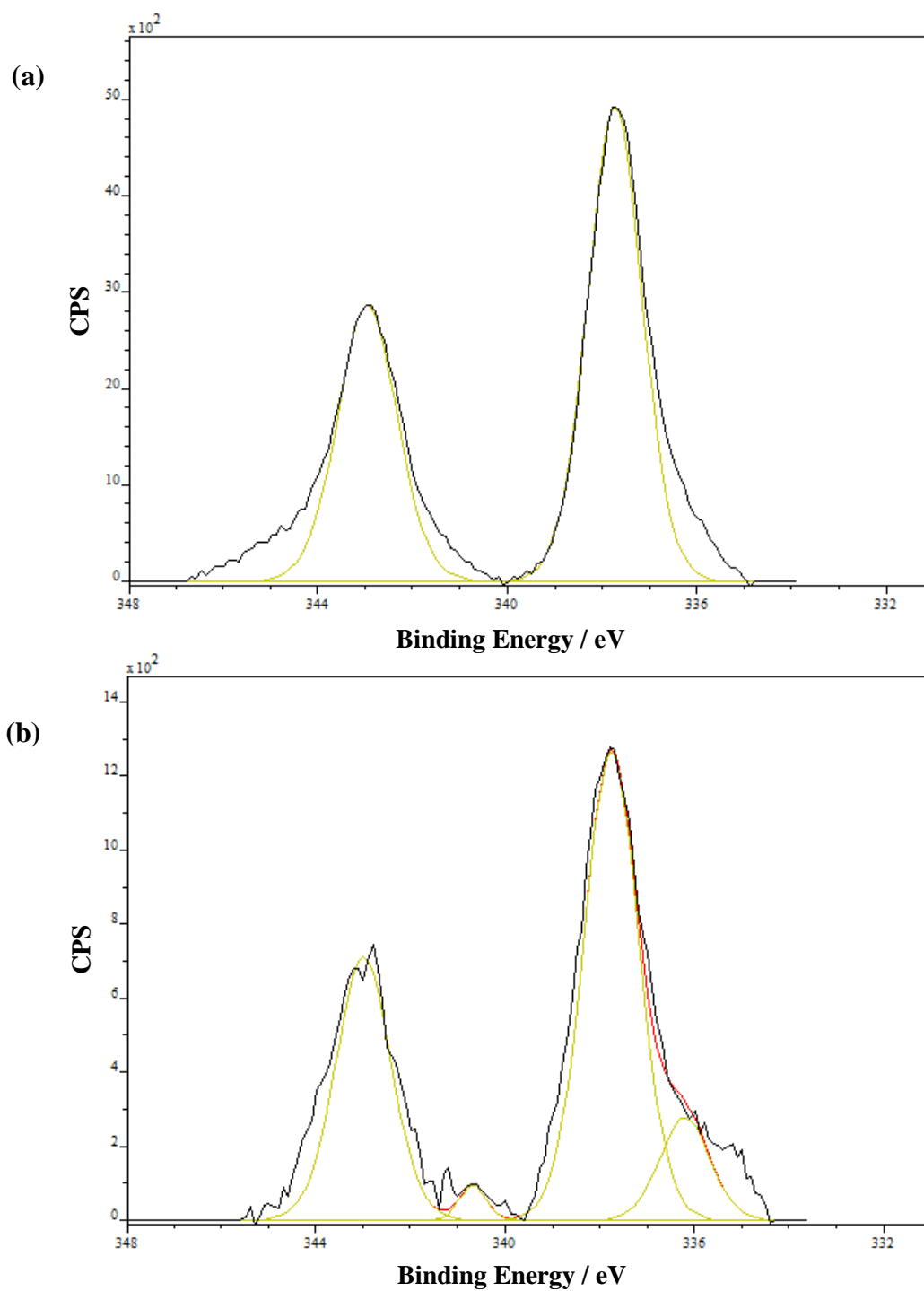


Figure 2.12 XPS Spectra and peak fits; (a) PdCl₄@OMe-PIILP **25** showing Pd 3d_{5/2} at 338 eV and Pd 3d_{3/2} at 343 eV corresponding to Pd^{II}, and (b) Pd⁰@OMe-PIILP **27** showing two additional peaks corresponding to Pd⁰ with Pd 3d_{5/2} at 341 eV and Pd 3d_{3/2} at 336 eV indicating a combination of palladium in both the +2 and 0 oxidation states.

2.7.2 Powder XRD analysis

Powder XRD analysis was used to analyse the pre-formed nanoparticles. **Figure 2.13** shows the XRD patterns for Pd⁰@Imid-PIILP **26** and Pd⁰@OMe-PIILP **27** which provide information on both the purity and on the crystallinity of the Pd⁰ nanoparticles following analysis.

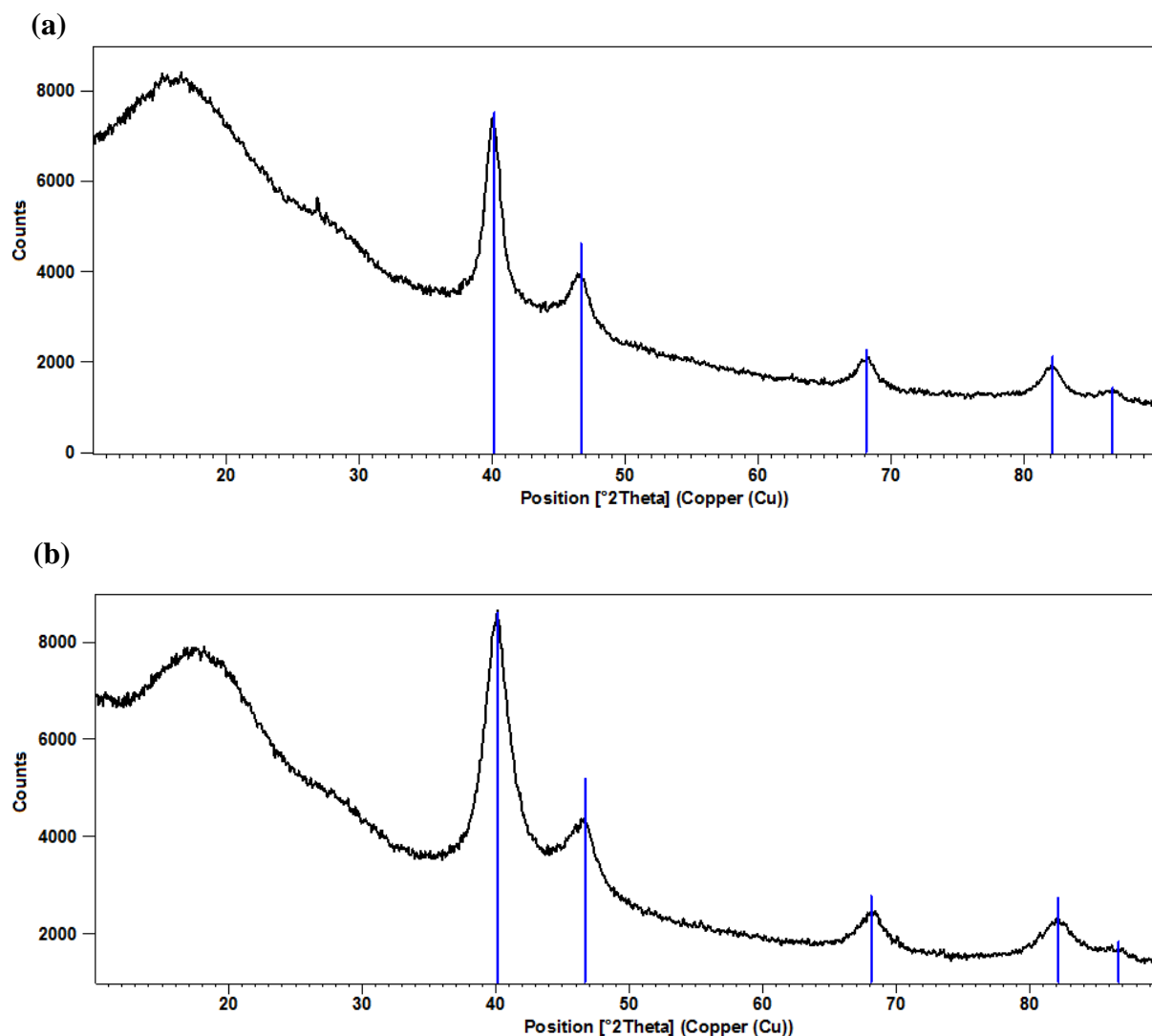


Figure 2.13 Powder XRD patterns; (a) Pd⁰@Imid-PIILP **26**, (b) Pd⁰@OMe-PIILP **27** showing diffraction peaks at Bragg angles of 40.1, 46.7, 68.2, 82.0 and 86.2 correspond to the 111, 200, 220, 311 and 331 facets of elemental palladium.

The results reveal the Pd NPs to have Fm-3m face centered cubic structure and the strong diffraction peaks at Bragg angles of 40.1, 46.7, 68.2, 82.0 and 86.2 correspond to the 111, 200, 220, 311 and 331 facets of elemental palladium. The particle sizes were determined by the X-ray line broadening method using the Scherrer equation (**Figure 2.14**).^[87]

$$D = \frac{k \lambda}{\beta_s \cos \theta}$$

Where: D = Crystallite size (Å)
 $\beta_s = \beta_{\text{structural}} = \beta_{\text{observed}} - \beta_{\text{standard}}$ (where β is the FWHM in radians)
 λ = X-ray wavelength (Å)
 θ = theta (half the Bragg angle in radians)
 k = shape factor (a value of 0.9 assumes spherical crystallites)

$$D = \frac{0.9(1.541874)}{\left(\left(\frac{(1.61) * \pi}{180}\right)\right) * \left(\cos\left(\left(\frac{40.114}{2}\right) * \pi\right) / 180\right)}$$

$$= 52.56 \text{ \AA} = \mathbf{5.26 \text{ nm}}$$

Figure 2.14 Calculation of Pd⁰@OMe-PIILP **27** NP size using the Scherrer equation.

Thus the average particle size for Pd⁰@OMe-PIILP **27** was determined to be 5.26 nm via XRD analysis. The same technique was applied to Pd⁰@Imid-PIILP **26** which afforded an average NP size of 7.53 nm.

2.7.3 TEM analysis

Transmission Electron Microscopy (TEM) images were obtained to determine the size distribution of the pre-formed NPs Pd⁰@Imid-PIILP **26** and Pd⁰@OMe-PIILP **27** (**Figure 2.15**). The NPs appear as dark contrasting circles which are surrounded by a more poorly contrasting area of polymeric material. For both pre-formed species the NPs appear to be agglomerating in to small clusters, which is particularly evident in the images of Pd⁰@Imid-PIILP **26**, making accurate analysis more challenging. This effect could potentially be a result of the uncontrolled nature of the polymerisation leading to areas of varying charge density throughout the polymer network. The particle size distribution for both species is relatively large with particles ranging from 3 – 14 nm upwards for **26** and from 2 – 11 nm and above for **27**.

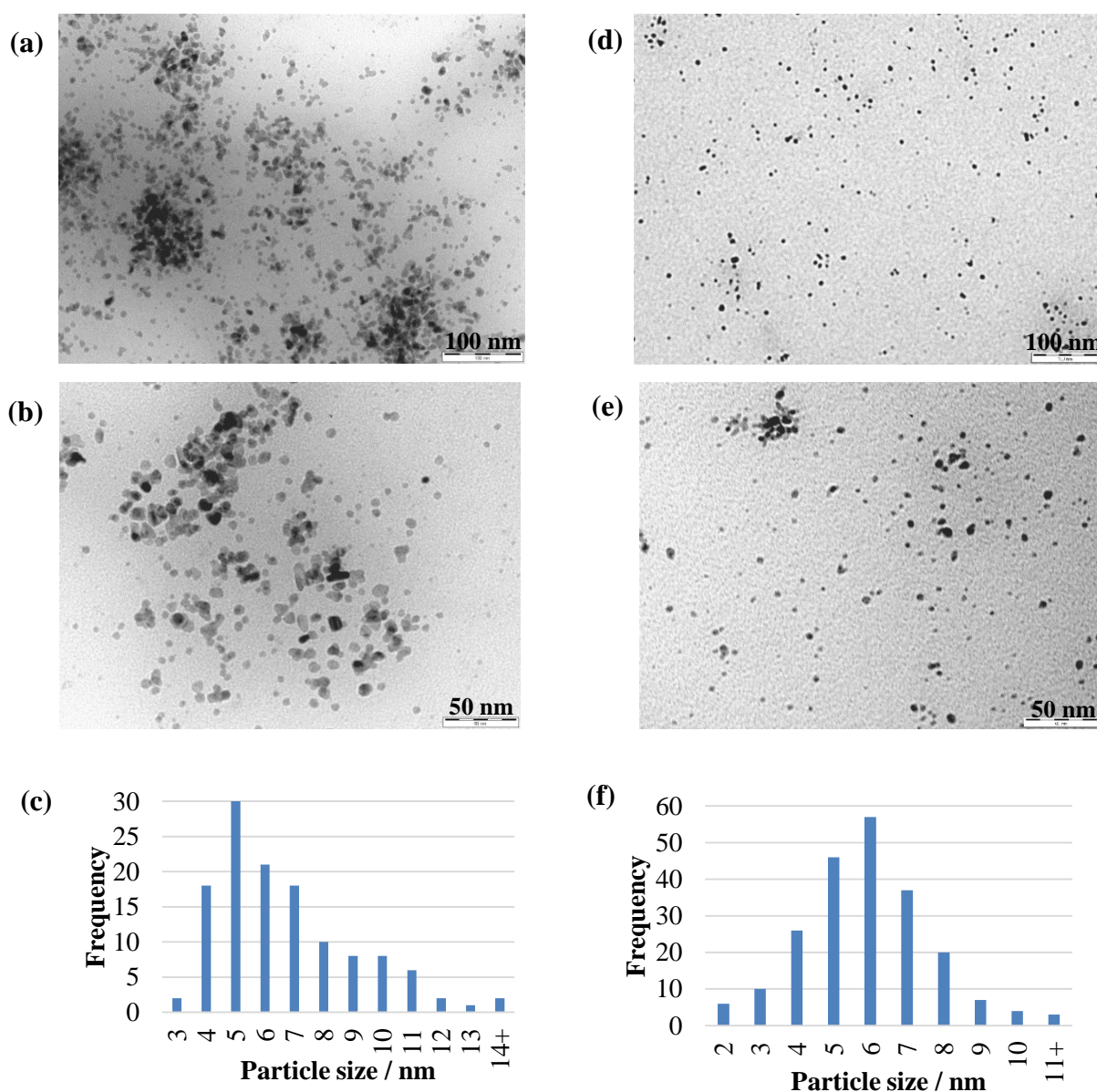
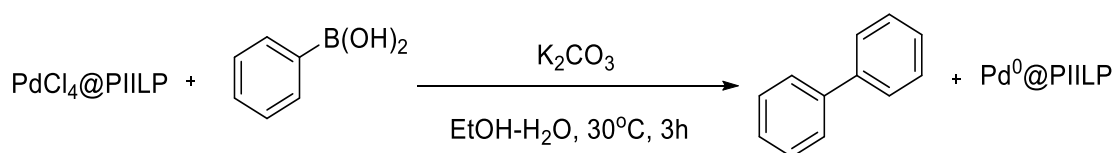


Figure 2.15 TEM images and particle size distributions of pre-formed NPs; (a)(b)(c) Pd⁰@Imid-PIILP **26**, (d)(e)(f) Pd⁰@OMe-PIILP **27**.

The most abundant particles for Pd⁰@OMe-PIILP **27** are in the region of 4-6 nm which gratifyingly is in agreement with the value of 5.26 nm calculated from the XRD analysis. Pd⁰@Imid-PIILP **26** shows more abundance in the region of 5-7 nm which is also in agreement with the prediction of a larger 7.53 nm particle from the XRD analysis. These particle sizes are also typical of other pre-formed Pd NPs reported in the literature.^[87-88]

In addition to the pre-formed NPs generated via reduction with H₂, NPs were also generated in-situ during Suzuki-Miyaura cross-coupling reactions from their Pd^{II} precursors. In order to make it possible to utilise TEM to evaluate the size distribution of such particles, they were generated under the conditions shown in **Scheme 2.11**.



Scheme 2.11 In-situ generation of Pd NPs for TEM imaging.

Here the particles are generated under standard Suzuki conditions in the presence of the boronic acid and the absence of the electrophile to prevent the formation of products which would obscure the imaging of the NPs under TEM. The images obtained for particles formed from PdCl₄@Imid-PIILP **24** and PdCl₄@OMe-PIILP **25** in this manner are shown along with their particle size distributions in **Figure 2.16**.

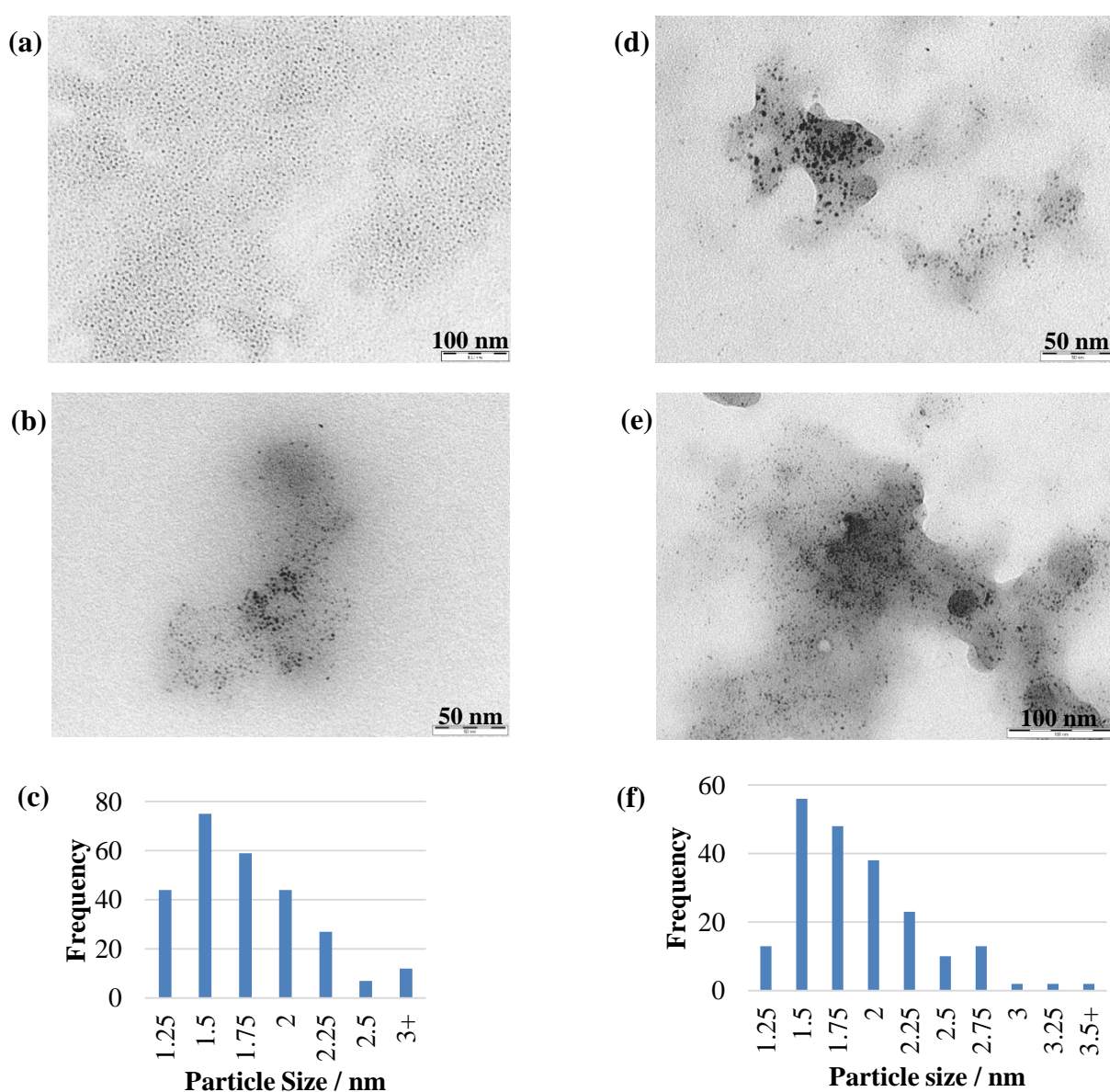
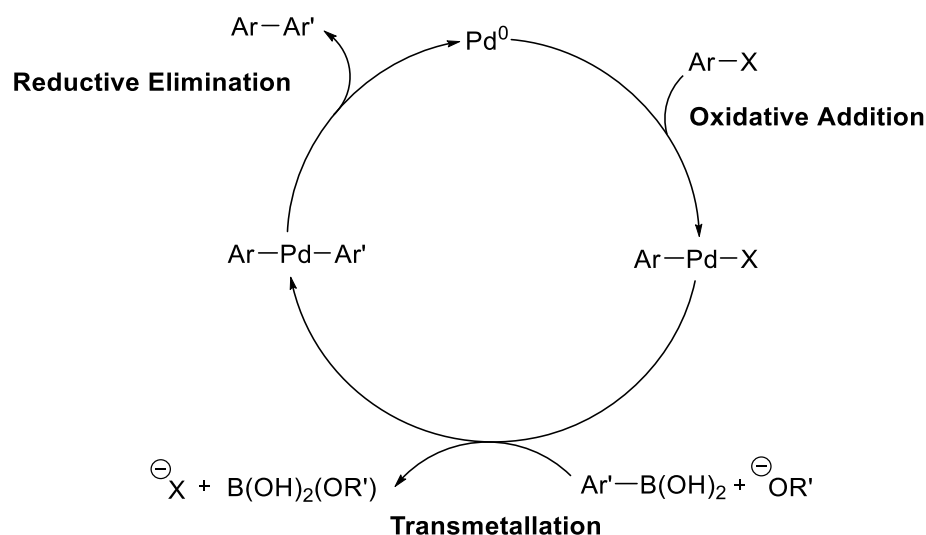


Figure 2.16 TEM images and particle size distributions of NPs generated in-situ from; (a)(b)(c) PdCl₄@Imid-PIILP **24**, (d)(e)(f) PdCl₄@OMe-PIILP **25**.

The TEM images show that both species formed in-situ have resulted in much smaller NPs which appear evenly distributed throughout the encapsulating polymer. The size distributions are much smaller with the most abundant particle size being 1.5 nm for both species. The group of Han *et al.* have successfully generated highly active palladium NPs in-situ with an average diameter of 2.6 nm which effectively catalysed the Suzuki coupling of aryl chlorides and aryl boronic acids at room temperature in polyethylene glycol. The group of Liu *et al.* have also succeeded in generating cationic imidazole based ionic liquids for the support of similarly sized Pd NPs.^[45] They were shown to successfully catalyse carbonylative Suzuki couplings whilst proving to be recyclable over 5 consecutive cycles with little decrease in activity.

2.8 Suzuki-Miyaura Coupling Reactions

To determine the activity of the four Pd@PIILP catalysts they were utilised in Suzuki-Miyaura coupling reactions. As previously discussed, these reactions have been shown to be an extremely useful class of carbon-carbon bond formations with Pd NPs proving to be successful catalysts when immobilised on a range of ionic support materials. As such they provide an ideal reaction to evaluate the novel Pd@PIILP systems and provide a literature basis to evaluate their success against.



Scheme 2.12 Catalytic cycle for the Pd-catalysed Suzuki-Miyaura cross-coupling reaction.

The catalytic cycle for the Pd catalysed Suzuki-Miyaura reaction is well established (**Scheme 2.12**), following an oxidative addition, transmetalation, reductive elimination catalytic cycle that benefits from the use of electron-donating, sterically demanding ligands which promote the first and last steps.^[89] In the presence of the preformed nanoparticles the initial generation step will not be required, however in the presence of the PdCl_2 @PIILP species an initial reduction

will generate the required Pd(0) species. Oxidative addition occurs via the insertion of the palladium species into the C-X bond of the electrophile. Oxidative addition is often the rate determining step of the catalytic cycle and as such the electronic effects of the substituents on the aryl group will facilitate or hinder this step of the catalytic cycle. The next step is transmetallation, during which the base-mediated exchange of the R group on the boron species with the X group of the intermediate takes place. Although the exact mechanism of this step is yet to be determined, it is believed that the base activates the organoboron compound. The final step of reductive elimination then occurs to liberate the product and regenerate the Pd(0) species which can continue the cycle.

The exact mechanism for PdNP-catalysed cross-couplings, and the true nature of the catalytic species remains widely debated, as such, the aim of increasing our understanding of the mechanistic process of the Pd@PIILP catalysts will also be addressed later in this chapter.

Figure 2.17 summarises the current prevailing homogeneous and heterogeneous proposed mechanisms which will be addressed. Catalysis might be mediated by a soluble Pd species or alternatively a heterogeneous process may be involved. In the case of a heterogeneous process, both the aryl halide and the boronic acid would come into contact on the nanoparticle surface and not within the solution.

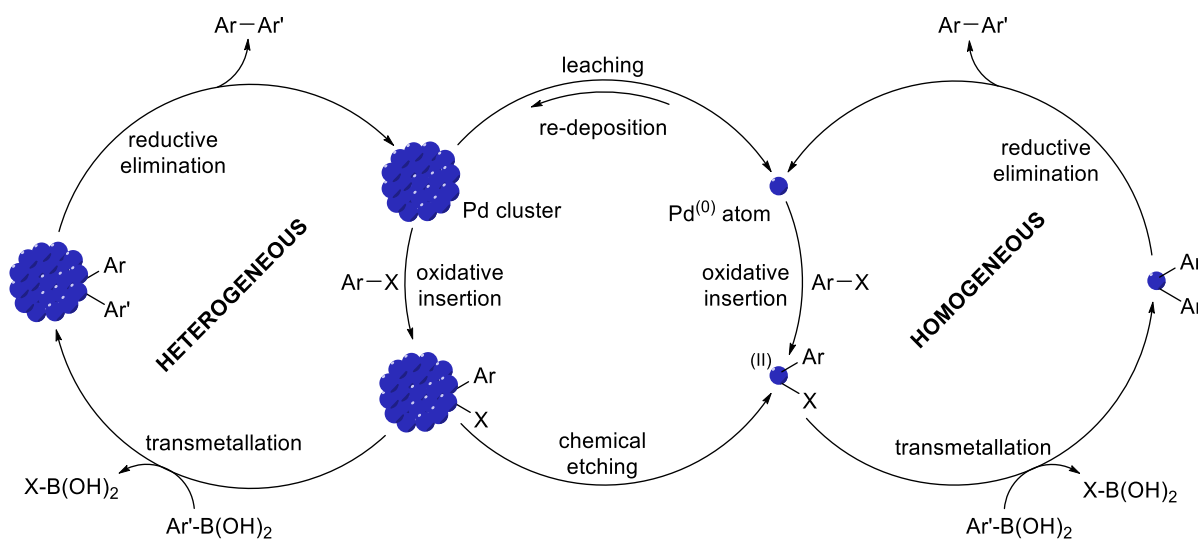
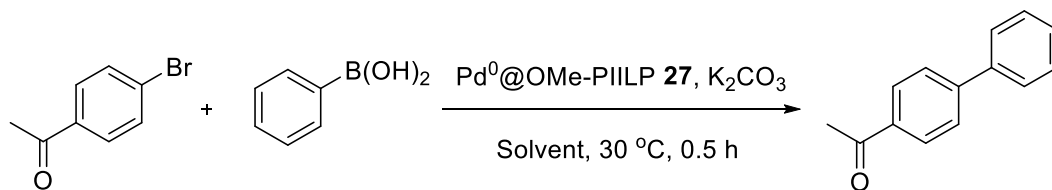


Figure 2.17 Proposed homogeneous and heterogeneous PdNP-catalysed Suzuki mechanisms.^[60]

A series of optimisation reactions were carried out on the Pd@PIILP system. Initial catalyst optimisation employed 4-bromoacetophenone and phenylboronic acid due to their high conversion in a relatively short reaction time, along with a small excess of base in the presence of the pre-formed Pd⁰@OMe-PIILP **27** catalyst.

2.8.1 Solvent optimisation

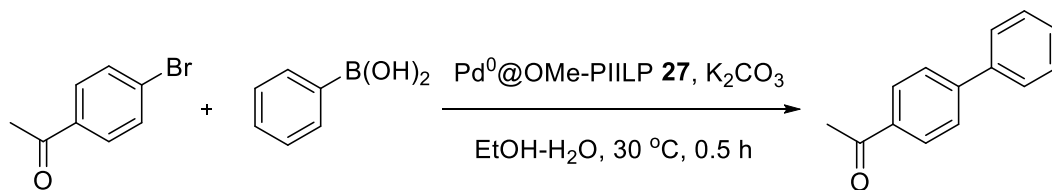


Entry ^a	Solvent	Conversion ^b / %
1	EtOH	24
2	H ₂ O	14
3	toluene	2
4	THF	5
5	DMF	13
6	EtOH-H ₂ O ^c	84
7	toluene-H ₂ O ^c	3
8	THF-H ₂ O ^c	17

Table 2.1 Optimisation of reaction solvent using Pd⁰@OMe-PIILP **27**. ^a Reaction Conditions: 0.1 mol % Pd⁰@OMe-PIILP **27** based on repeat unit and assumed complete Pd loading, 1 mmol aryl halide, 1.13 mmol phenylboronic acid, 1.2 mmol K₂CO₃, 2.4 mL solvent, 30 °C, 0.5 h. ^b Determined by GC with 1 mmol decane std, average of 2 runs. ^c 50 : 50 mixture.

A range of reaction solvents were screened in order to obtain optimum performance in a system which would also ideally exhibit green credentials. The conversions obtained in single solvent systems ranged from being extremely poor in both non-polar and polar aprotic solvents with conversions in toluene, THF and DMF of just 2, 5 and 13 % respectively. In the presence of polar protic solvents the conversions improved slightly in the case of water to 14 % and quite considerably in EtOH to 24 %, however these conversions were still relatively poor. Interestingly, upon the addition of water to create a mixed solvent system the conversions increased in each case. In particular, the combination of EtOH and water resulted in a dramatic increase to 84 % conversion in just 30 min which may be attributed to the ability of water to dissolve the inorganic base more efficiently leading to increased activity. There are several reports citing the use of water as a co-solvent and in particular the importance of the ratio of water to the co-solvent on the amount of cross-coupling achieved and the overall reaction time.^[90]

2.8.2 Water content optimisation

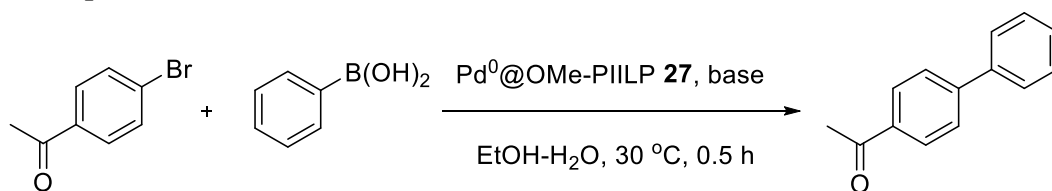


Entry ^a	EtOH : H ₂ O	Conversion ^b / %
1	100 : 0	24
2	75 : 25	71
3	50 : 50	84
4	25 : 75	82
5	0 : 100	14

Table 2.2 Optimisation of solvent water content using Pd⁰@OMe-PIILP **27**. ^a Reaction Conditions: 0.1 mol% Pd⁰@OMe-PIILP **27** based on repeat unit and assumed complete Pd loading, 1 mmol aryl halide, 1.13 mmol phenylboronic acid, 1.2 mmol K₂CO₃, 2.4 mL solvent, 30 °C, 0.5 h. ^b Determined by GC with 1 mmol decane std, average of 2 runs.

In order to determine the optimum ratio of ethanol: water in the mixed solvent system, a series of reactions were carried out again utilising 4-bromoacetophenone and phenylboronic acid (**Table 2.2**). Although a purely water system results in a very poor conversion of 14 %, it is clear that the presence of water in the mixed solvent system has an extremely positive effect on catalyst performance. With just a 75: 25 ratio of EtOH: H₂O a conversion of 71 % was achieved. A further increase to 84 % was achieved in the 50: 50 mixture, however when the amount of water was increased further the catalyst activity began to decrease, hence a 50: 50 EtOH: H₂O mixture was deemed to be optimum ratio.

2.8.3 Base optimisation



Entry ^a	Base	Conversion ^b / %
1	NaOAc	14
2	CsOAc	15
3	NBu ₃	5
4	K ₃ PO ₄	76
5	CsF	32

Entry ^a	Base	Conversion ^b / %
6	NaHCO ₃	39
7	NaCO ₃	67
8	K ₂ CO ₃	84
9	Cs ₂ CO ₃	96

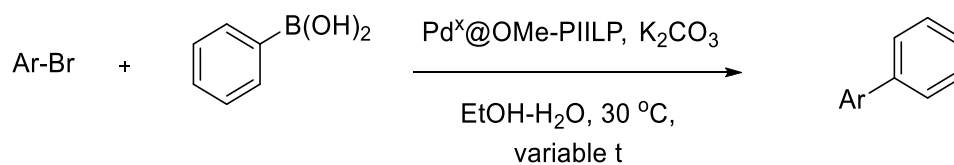
Table 2.3 Optimisation of base using Pd⁰@OMe-PIILP **27**. ^a Reaction Conditions: 0.1 mol% Pd⁰@OMe-PIILP **27** based on repeat unit and assumed complete Pd loading, 1 mmol aryl halide, 1.13 mmol phenylboronic acid, 1.2 mmol base, 1.2 mL EtOH, 1.2 mL H₂O, 30 °C, 0.5 h. ^b Determined by GC with 1 mmol decane std, average of 2 runs.

The initial catalyst optimisations were carried out with potassium carbonate present as the base. This base was initially chosen due to the large literature precedence for this particular base. Having achieved a conversion of 84 % with 4-bromoacetophenone in a 50: 50 EtOH: H₂O mixture, a range of other bases were screened to determine if another base may be more suitable to the system. The best results were obtained with potassium phosphate, 76 % and caesium carbonate, 96 %. Although Cs₂CO₃ provided an increase in conversion of 12 %, this increase in conversion was not deemed significant enough to outweigh the extra cost of this particular base for use in a large substrate screening. Hence optimum reaction conditions were deemed to be 50: 50 EtOH: H₂O with K₂CO₃.

2.8.4 Substrate screening

Following optimisation of the reaction conditions, catalyst testing was carried out on a full range of electrophiles for both of the pre-formed Pd⁰ catalysts Pd⁰@Imid-PIILP **26** and Pd⁰@OMe-PIILP **27** and both of the Pd^{II} species PdCl₄@Imid-PIILP **24** and PdCl₄@OMe-PIILP **25**. The results of which are summarised in **Table 2.4**. The mild reaction conditions of 30 °C and a catalyst loading of only 0.1 mol % resulted in a wide range of results for the varied selection of electrophiles from extremely high conversion to extremely low.

Looking initially at Pd⁰@OMe-PIILP **27** it is clear that performance is extremely efficient with electron deficient *para*- substituted aryl halides such as 4-bromoacetophenone and 4-bromobenzonitrile with conversions of 84 % and 96 % respectively achieved in just 30 min (entries 8 and 16). Conversion of 98 % was also achieved with 4-bromobenzaldehyde in just 10 min (entry 13). However, in the case of the *meta*- substituted derivatives 3-bromoacetophenone, 3-bromobenzaldehyde and 3-bromobenzonitrile, conversions of 89 %, 83 % and 32 % were achieved in increased reaction times of 19, 16 and 1 h respectively (entries 7, 12 and 15).



Entry a	Electrophile	Time (h)	Pd ⁰ @ OMe- PIILP b / %	PdCl ₄ @OMe -PIILP b / %	Pd ⁰ @ Imid- PIILP b / %	PdCl ₄ @Imid -PIILP b / %
1		16	80	71	8	70
2		6	85	84	57	65
3		6	83	86	34	66
4		19	52	52	3	34
5		19	61	65	0	42
6		16	5	8	0	0
7		19	89	8 ^c	0	28
8		0.5	84	99	9	46
9		19	71	78	31	70
10		6	79	86	60	79
11		5	85	81	65	82

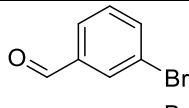
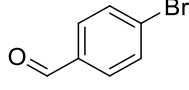
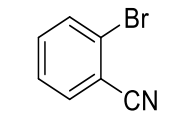
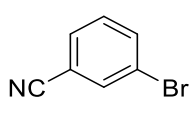
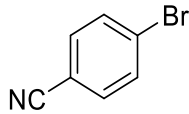
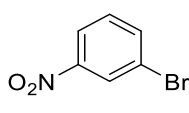
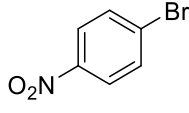
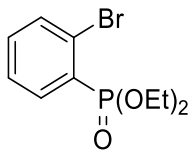
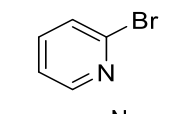
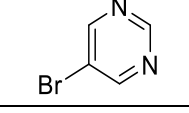
Entry ^a	Electrophile	Time (h)	Pd ⁰ @ OMe- PIILP ^b / %	PdCl ₄ @OMe -PIILP ^b / %	Pd ⁰ @ Imid- PIILP ^b / %	PdCl ₄ @Imid -PIILP ^b / %
12		16	83	96	0	72
13		0.5	98 ^d	99 ^d	90	99
14		5	84	99 ^e	53	97
15		5	32 ^f	52 ^f	0	18 ^f
16		0.5	96	71 ^g	3	27
17		4	84	92 ^h	1 ⁱ	98 ^e
18		4	72 ⁱ	62 ^e	85	97
19		6	72	71	64	63
20		19	10	18	4	18
21		19	18	29	12	17

Table 2.4 Suzuki-Miyaura substrate screening. ^a Reaction Conditions: 0.1 mol % cat. based on repeat unit and assumed complete Pd loading, 1 mmol aryl halide, 1.13 mmol phenylboronic acid, 1.2 mmol K₂CO₃, 1.2 mL EtOH, 1.2 mL H₂O 30 °C. ^b Determined by GC with 1 mmol decane std and confirmed by ¹H NMR, average of 2 runs. ^c 16 h. ^d 10 min. ^e 2 h. ^f 1 h. ^g 2 min. ^h 30 min. ⁱ 3 h.

This extremely large reduction in activity indicates that the *meta*-substituents are resulting in a decreased positive charge on the *ipso*-carbon which results in a stronger C-Br bond and an increase in the rate of oxidative addition.

In the case of all *ortho*-substituted electrophiles such as 2-bromotoluene, 2-methoxy bromobenzene and 2-bromobenzonitrile the increased steric hindrance has resulted in increased reaction times being required compared to their *para*-substituted derivatives to achieve

conversions of 80 %, 71 % and 84 % respectively (entries 1, 9 and 14). 2-Bromoacetophenone in particular achieves only a negligible conversion of 5 % after 16 h (entry 6). This high degree of steric intolerance is again demonstrated with electron rich electrophiles with bulky substituents such as 3,5-dimethylbromobenzene and 4-*tert*-butylbromobenzene which achieved conversions of just 52 % and 61 % respectively after much prolonged reaction times of 19 h (entries 4 and 5).

When compared with catalysis conducted with PdCl₄@OMe-PIILP **25** the results are extremely similar, following the same trends in catalytic activity depending upon electronic and steric effects. There are however, certain substrate specific differences between the two species, most notably in the case of 3-bromoacetophenone which only achieved an 8 % conversion in the presence of PdCl₄@OMe-PIILP **25** compared to the 89 % conversion achieved with Pd⁰@OMe-PIILP **27**. Conversely **25** has outperformed **27** for several substrates in particular the CN- substituted electrophiles (entries 14-16) with 99% conversion being achieved with 2-bromobenzonitrile in just 2 h, 52 % with 3-bromobenzonitrile in 2 h and 71 % conversion with 4-bromobenzonitrile in just 2 min.

The catalysis performed in the presence of the PdCl₄@Imid-PIILP **24** showed a similar but slightly decreased level of activity compared to the OMe- catalysts without exception. The pre-formed Pd⁰@Imid-PIILP **26** species however, revealed a dramatic decrease in catalytic activity when compared with all three of the other catalysts. In particular this lack of activity is evident with the sterically hindered substrates with zero or very little conversion being achieved for 2-bromotoluene, 1-bromo-3,5-dimethylbenzene, 4-*tert*-butylbromobenzene and 2-bromoacetophenone. The catalyst has performed most poorly for each substrate suggesting that the imidazole functionality may have hindered the pre-formation reduction via hydrogenation. However, the nature of the catalytic performance does appear to be somewhat substrate specific so it would be unwise to attribute too much influence to the nature of the support material. In order to provide a clearer indication as to the effects of the supports a more in depth study of the reaction mechanism and the nature of the support-nanoparticle interaction would be required on a wider range of polymeric support materials.

The performance of the methyl ether functionalised catalysts under the mild reaction conditions compares favourably with the current literature. A recent communication from J. Huang *et al* has reported the successful utilisation of PdNPs immobilised on a polymer formed from the coupling of tris(4-bromophenyl)amine and benzene-1,4-diboronic acid in the presence of an immobilised triphenylphosphine, for the Suzuki coupling of a range of aryl bromides to

phenylboronic acids at 70 °C.^[91] The group of R. Fareghi-Alamdari also employed immobilised Pd(0) NPs on a phosphine functionalised graphene for Heck, Suzuki and N-arylation reactions.^[92] High temperatures were again required along with an increased catalyst loading of 1.2 mol % to achieve comparable conversion to the Pd@OMe-PIILP systems. It is of note however, that in both of these literature examples a wide range of substrates were successfully coupled, including those that are more sterically demanding.

2.8.5 Kinetic study of cross-coupling

Several of the substrates in the screening required very long reaction times and even so, 100 % conversion still could not be achieved. The suspicion was that the reactions were plateauing and a kinetic study would confirm this.

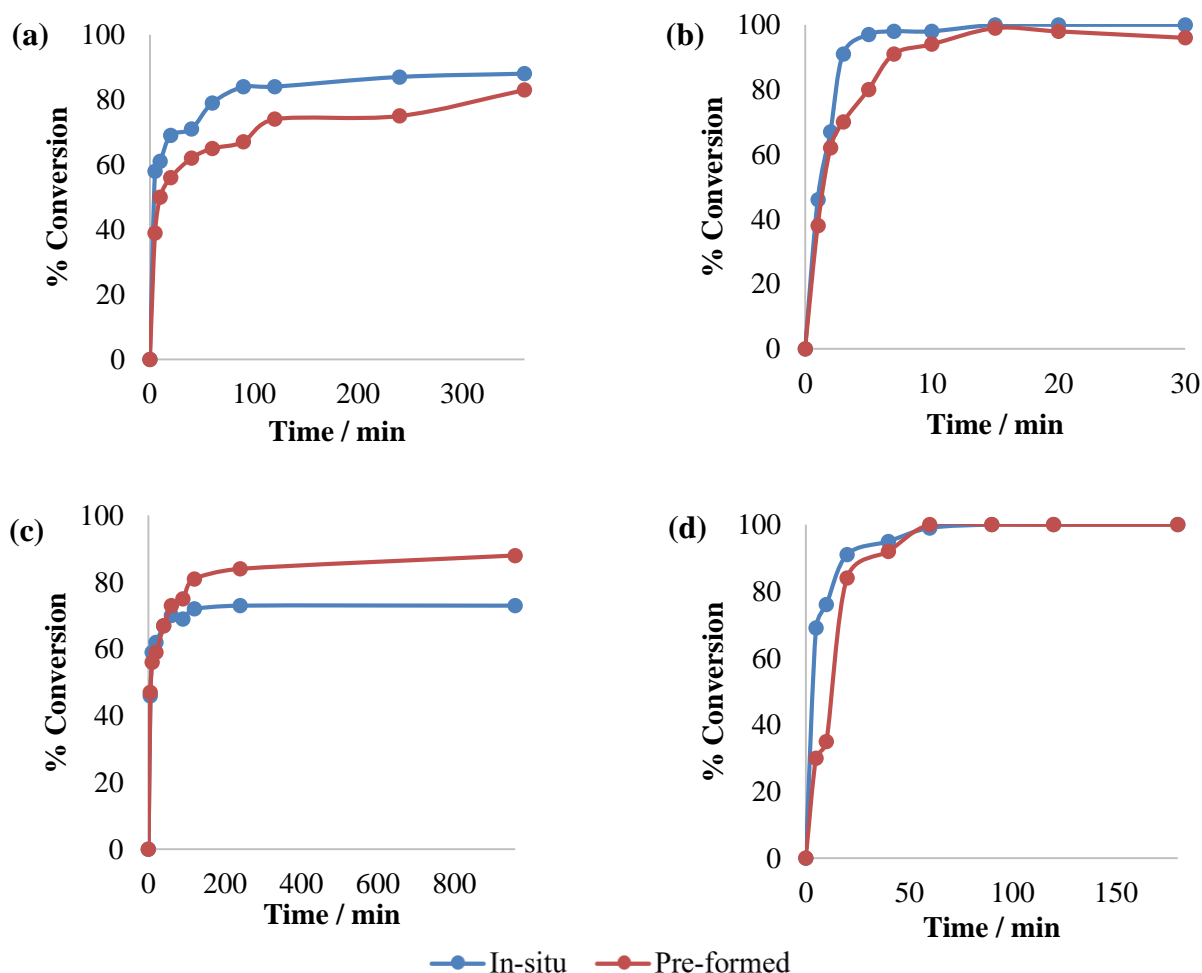


Figure 2.18 Kinetic profiles of Suzuki-Miyaura reactions catalysed by PdCl₄@OMe-PIILP **25** & Pd⁰@OMe-PIILP **27** using; (a) 4-bromotoluene, (b) 4-bromobenzonitrile, (c) 2-bromotoluene, (d) 1-bromo-3-nitro benzene. Reaction Conditions: 0.1 mol% catalyst based on repeat unit and assumed complete Pd loading, 1 mmol aryl halide, 1.13 mmol phenylboronic acid, 1.2 mmol K₂CO₃, 2.4 mL solvent, 30 °C.

Following substrate screening the kinetics of 4-bromotoluene, 4-bromobenzonitrile, 2-bromotoluene and 1-bromo-3-nitro benzene, chosen due to their favourable reaction times, were monitored in the presence of the best performing methyl ether functionalised catalysts PdCl₄@OMe-PIILP **25** and Pd⁰@OMe-PIILP **27**. **Figure 2.18** shows the kinetic profiles obtained for each of the four substrates in the presence of both the pre-formed and in-situ formed PdNP catalysts. As each of the substrates indicates a fast rate of initial reaction with no activation period visible, a plot of time vs ln(Conversion_{max} - Conversion) was made which enabled the initial rate constants to be determined for each of the substrates. These *k*_{obs} values are summarised in **Table 2.5**. Intriguingly the initial rate constants were consistently faster for the NPs formed in-situ. It was also evident that in the case of 4-bromotoluene and 2-bromotoluene, the reactions were plateauing and 100 % conversion was not achievable irrespective of the reaction time. This could be an effect of a number of factors, including the possibility that the NPs are undergoing Ostwald Ripening and aggregating, leading to a loss in activity. In order to shed light on this question an ex-situ study of nanoparticle size distribution was performed.

Electrophile	<i>k</i> _{obs} (s ⁻¹)	
	PdCl ₄ @OMe-PIILP 25	Pd ⁰ @OMe-PIILP 27
4-bromotoluene	1.2	0.6
4-bromobenzonitrile	45.0	16.8
2-bromotoluene	2.4	1.2
1-bromo-3-nitrobenzene	3.8	3.8

Table 2.5 Initial rate constants (*k*_{obs}) for Suzuki cross-couplings.

2.8.6 Ex-situ TEM analysis

Ex-situ TEM analysis was carried out by isolating a sample of the reaction mixture of 1-bromo-3-nitrobenzene with phenylboronic acid in the presence of Pd⁰@OMe-PIILP **27** after 3 h. This particular electrophile was chosen due to the relatively short reaction time and the solubility of both the reagent and products in EtOH-H₂O, enabling clearer visualisation of the NPs during TEM imaging. **Figure 2.19** shows the image obtained post catalysis along with the particle size distribution.

The post catalysis particle size distribution reveals the NPs are primarily in the region of 1.5-1.75 nm in diameter, indicating that no significant aggregation has taken place following catalysis.

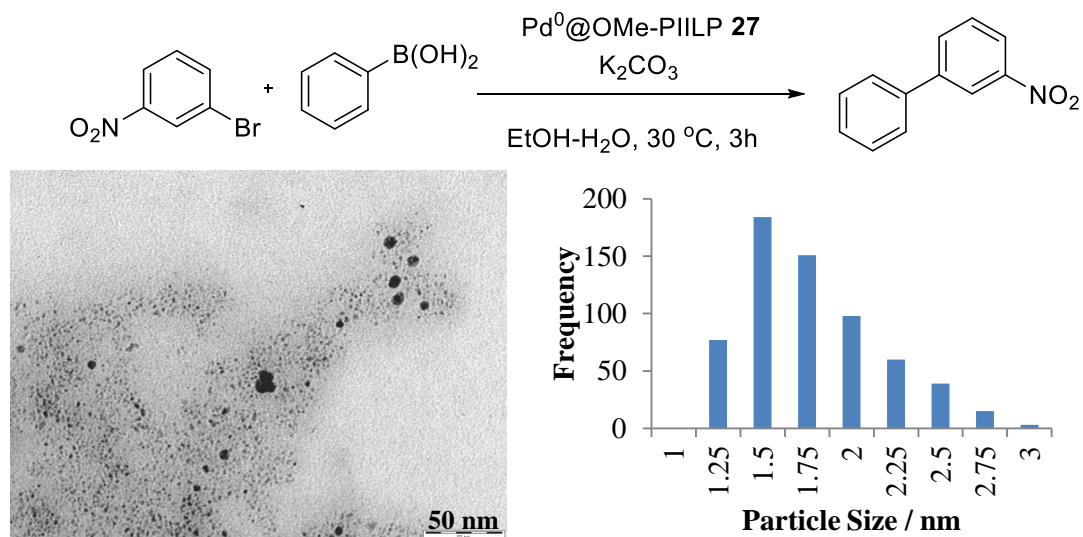


Figure 2.19 TEM & particle size distribution of in-situ NPs generated from Pd⁰@OMe-PIILP **27**.

In order to further confirm that no variation in NP size was occurring during catalysis the reaction of 2-bromotoluene with phenylboronic acid in the presence of PdCl₄@OMe-PIILP **25** was intercepted after both 10 min and 5 h. 2-Bromotoluene was chosen due to its longer reaction time and evidence of the reaction plateau. After 10 min, catalysis was still actively taking place and after 5 h, the plateau had been reached. **Figure 2.20** shows the TEM images and size distributions obtained at both time points.

The size distribution remained constant throughout the course of the reaction, indicating that aggregation was not taking place during the reaction and the reaction plateau must be attributed to another factor. One possible explanation was that the boronic acid was simply being used up during the course of the extended reaction times preventing formation of further product. In order to establish if this was the case, the reaction of 2-bromotoluene was carried out in the presence 2 equivalents of phenylboronic acid and also with 1 equivalent followed by a further equivalent after 5 h. Unfortunately, in the presence of 2 equivalents no improvement in conversion was observed and when the reaction was reactivated after 5 h, only a negligible improvement was obtained. This again highlights the complex nature of the system and the mechanism taking place.

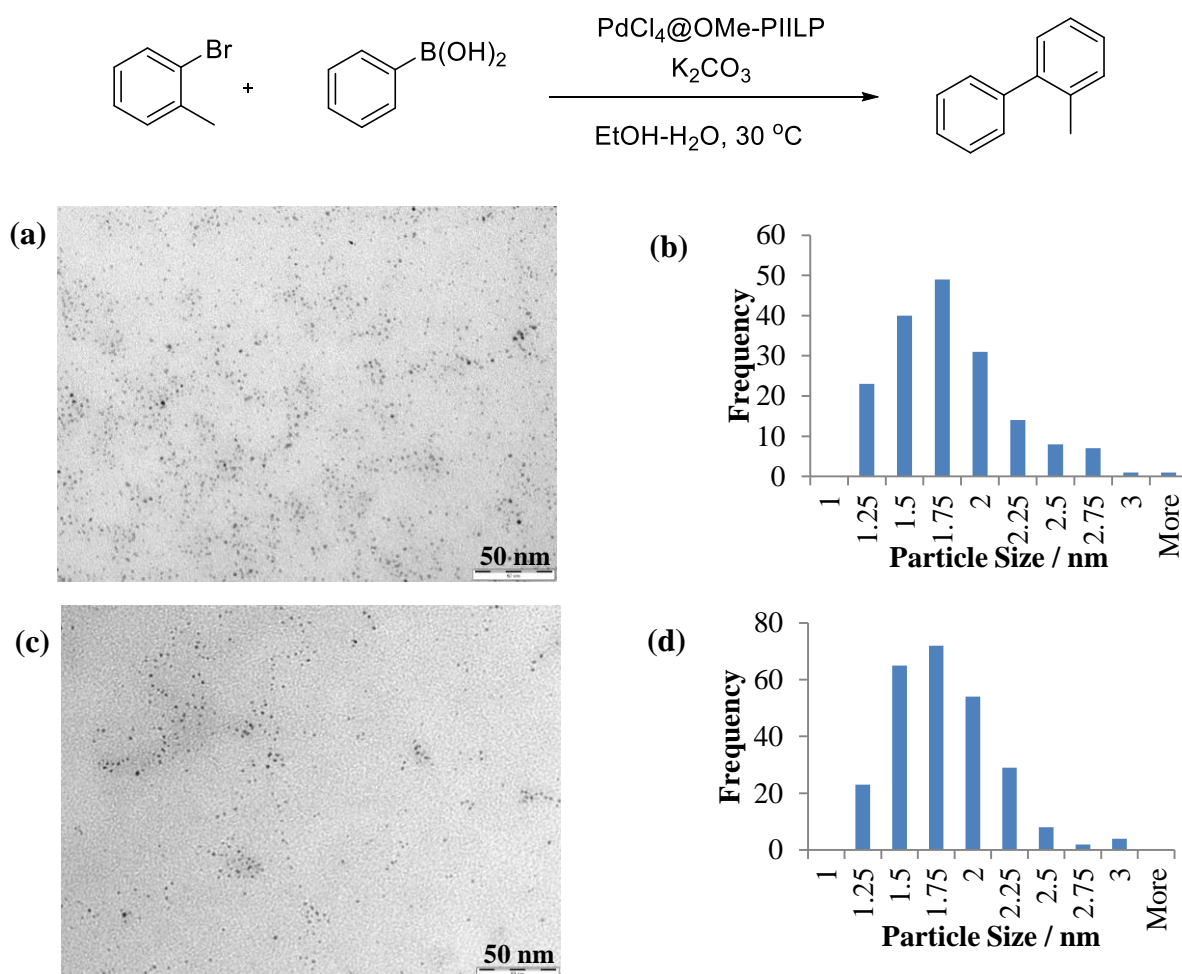


Figure 2.20 Ex-situ TEM analysis and particle size distribution of the Suzuki-Miyaura coupling of 2-bromotoluene with phenylboronic acid catalysed by PdCl₄@OMe-PIILP **25** after; (a)(b) 10 min, (c)(d) 5 h.

2.8.7 Reaction dilution

Through increasing the reaction dilution it may be expected that the rate of reaction would decrease in a near linear manner if the system were homogeneous in nature. If however the system were heterogeneous, the opposite effect may be exhibited, potentially as a result of the increased dilution resulting in less agglomeration of the nanoparticles. Conversely a heterogeneous system may show a decrease in activity under more concentrated conditions as a result of increased nanoparticle agglomeration resulting in catalyst deactivation. In order to determine the effect that reaction dilution plays in this system, the Suzuki coupling of 4-bromotoluene was carried out at a range of dilutions with both PdCl₄@OMe-PIILP **25** and Pd⁰@OMe-PIILP **27** (**Figure 2.21**).

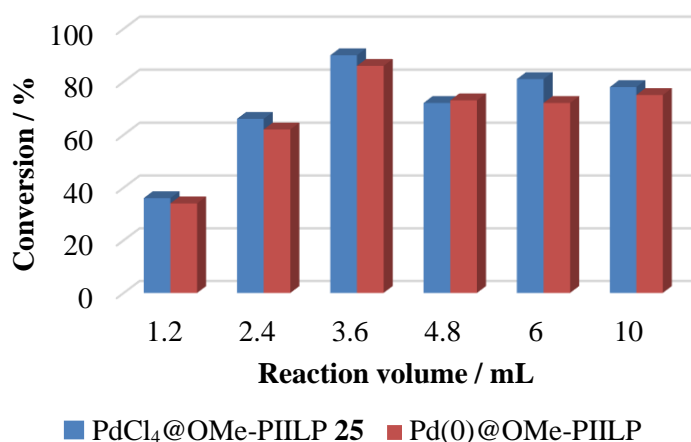
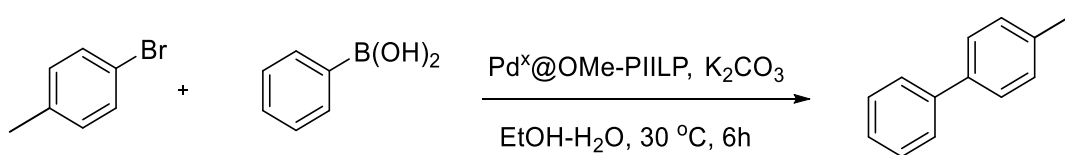


Figure 2.21 Effect of reaction dilution on the Suzuki-Miyaura coupling of 4-bromotoluene with phenylboronic acid catalysed by PdCl₄@OMe-PIILP **25** & Pd⁰@OMe-PIILP **27**. Reaction Conditions: 0.1 mol% catalyst based on repeat unit and assumed complete Pd loading, 1 mmol 4-bromotoluene, 1.13 mmol phenylboronic acid, 1.2 mmol base, EtOH, H₂O, 30 °C, 6 h.

A noticeable decrease in performance was observed in low volumes of solvent for both catalysts with optimum conversions in excess of 80 % observed at a reaction volume of 3.6 mL. In excess of this volume the catalyst activity appeared to decrease, however, rather than continuing to decrease as might be expected, the conversion appears to stabilise at around 70 %. The results of both the Pd(II) and Pd(0) systems were extremely similar and the overall trend would suggest a heterogeneous process is occurring in both cases, potentially as a result of the more dilute conditions preventing NP agglomeration. However, a more in depth study of the reaction dilution would be required to determine the effects of extremely dilute systems to determine when a further decrease in activity would be observed.

2.8.8 Catalyst loading

The outcome of the couplings in the presence of both -OMe catalysts in the same 4-bromotoluene / phenylboronic acid system was studied at a range of catalyst loadings from 0.05 to 3.0 mol % of catalyst (**Figure 2.22**).

As expected there appears to be an overall increase in conversion as the catalyst loadings increase for both systems. The optimum catalyst loading for the NPs generated in-situ was achieved at 2 mol % while the pre-formed NPs perform best at a loading of 0.5 mol %. The overall similarity in the level of performance of both catalyst systems is notable.

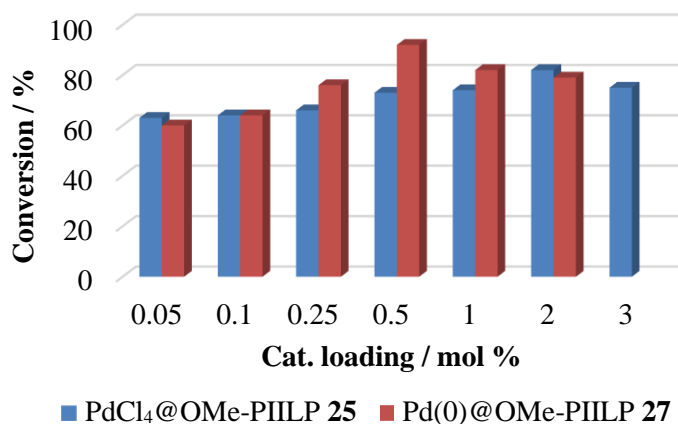
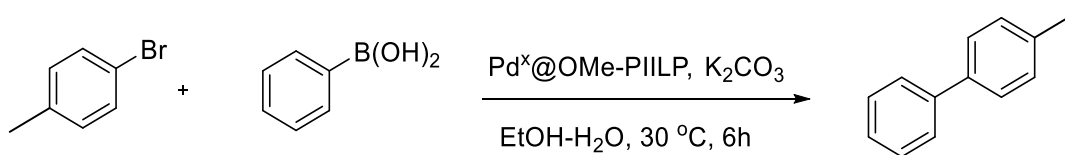


Figure 2.22 Effect of catalyst loading on the Suzuki-Miyaura coupling of 4-bromotoluene with phenylboronic acid catalysed by $\text{PdCl}_4\text{@OMe-PIILP 25}$ & $\text{Pd}^0\text{@OMe-PIILP 27}$. Reaction Conditions: $\text{Pd}^x\text{@OMe-PIILP}$, 1 mmol 4-bromotoluene, 1.13 mmol phenylboronic acid, 1.2 mmol base, 1.2 mL EtOH, 1.2 mL H_2O , $30\text{ }^\circ\text{C}$, 6 h.

The conversion appears not to scale in proportion to the catalyst loading, as might have been expected. It is possible that the overall conversion, after 6 h of reaction, is determined by catalyst deactivation. A more detailed study of the conversion-time profile for each catalyst loading would be required to shed light on this. It is clear from **Figure 2.18 (a)** that at 0.1 mol % loading, the conversion reaches its maximum after approximately 2 h.

2.8.9 Mercury poisoning

Mercury poisoning experiments are used to investigate the heterogeneity or homogeneity of a system.^[45] The poisoning itself is a surface effect and as such if nanoparticles are present then it would be expected that the mercury would block the surface of these particles resulting in a deactivation of the catalyst and a reduction in conversion would be observed. If however a system is homogeneous in nature then the mercury would have no effect on free palladium and no effect would be seen in the resulting conversions. The reaction of 4-bromotoluene was chosen due to the favourability of the reaction time and solubility of the reaction products. The reactions were carried out in the presence of both the preformed and in-situ $-\text{OMe}$ catalysts. The catalyst, base, phenylboronic acid and solvents were charged and stirred in the presence of a large excess of mercury for increasing lengths of time prior to initiation of the reaction via addition of the aryl halide. The boronic acid was present from the beginning to ensure the NPs formed in-situ were formed prior to poisoning. **Figure 2.23** shows the results obtained from mercury poisoning along with the results obtained when no poisoning had taken place.

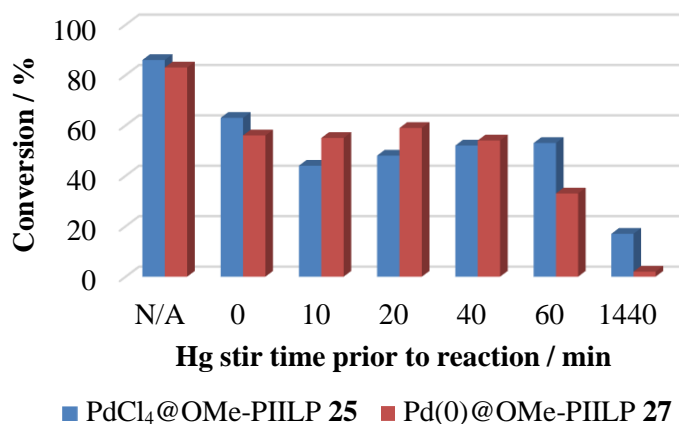
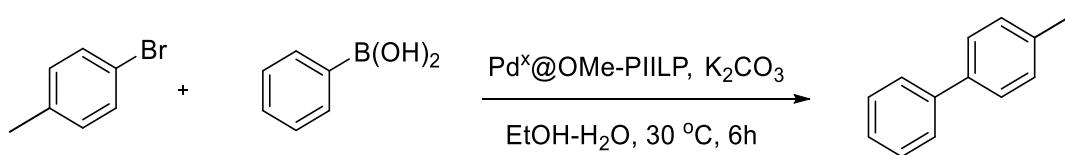
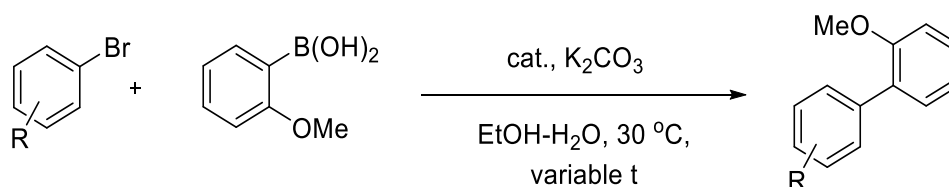


Figure 2.23 Effect of mercury poisoning on the Suzuki-Miyaura coupling of 4-bromotoluene with phenylboronic acid catalysed by $\text{PdCl}_4\text{@OMe-PIILP 25}$ & $\text{Pd}^0\text{@OMe-PIILP 27}$. Reaction Conditions: 0.1 mol% catalyst based on repeat unit and assumed complete Pd loading, mercury (200 eq. to catalyst), 1 mmol 4-bromotoluene, 1.13 mmol phenylboronic acid, 1.2 mmol base, 1.2 mL EtOH, 1.2 mL H_2O , $30\text{ }^\circ\text{C}$, 6 h.

When no mercury is present the conversions achieved with $\text{PdCl}_4\text{@OMe-PIILP 25}$ & $\text{Pd}^0\text{@OMe-PIILP 27}$ are 86 % and 83 % respectively. Upon addition of mercury along with the other reagents the conversions instantly decrease by over 20 % for both catalysts. Following an extended stir of up to 1 h in the presence of mercury, reasonable conversion was still achieved with both catalysts. This may suggest that the Suzuki couplings proceed, at least to some degree, via leaching of active Pd species from the support. In order confirm or disprove this hypothesis a further reaction was carried out following a poisoning period of 24 h. This resulted in low conversions of just 2 % for $\text{Pd}^0\text{@OMe-PIILP 27}$ and 17 % for $\text{PdCl}_4\text{@OMe-PIILP 25}$. This observation would appear to confirm that the mechanism is heterogeneous in nature for the pre-formed NPs with the Hg almost entirely blocking the active Pd. The NPs formed in situ however, may be undergoing a combination of both homogeneous and heterogeneous pathways.

2.8.10 Boronic acid variation

In order to evaluate the scope of the system for transferral to the coupling of aryl halides with other boronic acids a small substrate screening was carried out with 2-methoxyphenylboronic acid. (Table 2.6).



Entry ^a	R	Time / h	Conversion ^b / %	
			PdCl ₄ @OMe-PIILP	Pd ⁰ @OMe-PIILP
1	4-C(O)Me	0.5	55	50
2	3-Me	6	8	10
3	3-CN	1	17	6
4	2-OMe	19	0	0
5	3-CHO	16	0	1

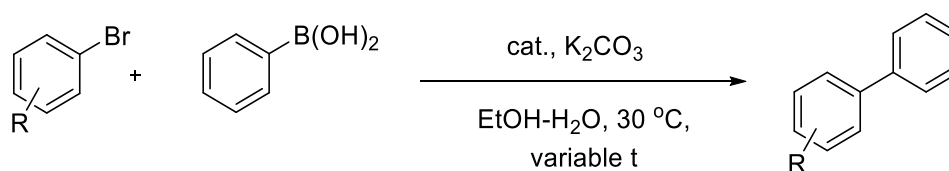
Table 2.6 Suzuki-Miyaura couplings of aryl bromides with 2-methoxyphenylboronic acid catalysed by PdCl₄@OMe-PIILP **25** & Pd⁰@OMe-PIILP **27**. ^a Reaction Conditions: 0.1 mol % cat. based on repeat unit and assumed complete Pd loading, 1 mmol aryl halide, 1.13 mmol 2-methoxyphenylboronic acid, 1.2 mmol K₂CO₃, 1.2 mL EtOH, 1.2 mL H₂O 30 °C. ^b Determined by GC with 1 mmol decane std and confirmed by ¹H NMR, average of 2 runs.

Unfortunately, very poor conversions were observed for all electrophiles, in particular the coupling with 2-methoxy bromobenzene and 3-bromobenzaldehyde performed extremely poorly. These results further highlight the complexity of the system and the importance of optimisation of each component of the reaction.

2.8.11 Comparisons to commercially available catalysts

To determine the viability of the system a range of commercially available Pd/C catalysts were screened to determine the relative merits of our PdNP@PIILP system. **Table 2.7** shows the conversions obtained for the Pd/C catalysts along with the comparable results obtained with both the –OMe and –Imid preformed catalysts Pd⁰@Imid-PIILP **26** and Pd⁰@OMe-PIILP **27**.

Gratifyingly the PdNP@PIILP catalysts consistently outperform the commercially available systems, with 4-bromoacetophenone in particular showing a dramatic difference in the catalytic activities. It is evident that there are also large variations in the performance of commercial catalysts sourced from different suppliers, particularly evident in the case of 2-methoxy bromobenzene with 5 % Pd/C which showed a variation of 31 % between suppliers. The results indicate potential for the PdNP@PIILP system for substrates where commercially available alternatives perform poorly.



R	Time / h	Catalyst - Conversion ^b / %				
		Pd/C 10% (Sigma)	Pd/C 5% (Sigma)	Pd/C 5% (Alfa)	Pd ⁰ @OMe-PIILP 27	PdCl ₄ @OMe-PIILP 25
4-C(O)Me	0.5	6	9	1	84	99
3-Me	6	53	61	74	85	84
2-OMe	19	51	39	70	70	78

Table 2.7 Comparison of Suzuki-Miyaura couplings of aryl bromides with phenylboronic acid catalysed by commercially available catalysts. ^a Reaction Conditions: 0.1 mol % cat. based on repeat unit and assumed complete Pd loading, 1 mmol aryl halide, 1.13 mmol phenylboronic acid, 1.2 mmol K₂CO₃, 1.2 mL EtOH, 1.2 mL H₂O 30 °C. ^b Determined by GC with 1 mmol decane std and confirmed by ¹H NMR, average of 2 runs.

2.9 Conclusions

Imidazolium functionalised norbornene monomers were synthesised in both their *endo*- and *exo*- forms, and subsequent ring opening metathesis polymerisation with Grubbs 2nd generation catalyst resulted in polymeric materials that proved to be unsuitable for palladium loading and catalysis. Subsequently, styrene based analogues of the monomers were successfully synthesised and radical polymerisation was adopted to produce two cross-linked imidazolium based PIILP supports, one with an imidazole pendant, the other with a methyl ether functionality. Both were obtained as amorphous insoluble solids in high yields that were subsequently loaded with a Pd^{II} precursor via simple anion exchange with PdCl₄. Subsequent reduction to the active Pd⁰ species was achieved via simple hydrogenation and also via in-situ generation under Suzuki coupling conditions. The resulting PIILP stabilised PdNPs were fully characterised via a range of techniques.

The size distribution of the pre-formed NPs was shown to be relatively broad with particles primarily in the region of 5-7 nm in diameter. In-situ generation afforded much smaller particles in the region of 1.5 nm in diameter with narrower size distributions which compare very favourably to many Pd NP systems in the literature which commonly report mean particle diameters in the region of 2 – 4 nm.^[93] The variation in the heteroatom donor moiety showed

little to no impact upon nanoparticle formation however and as such further investigation in to a broader range of heteroatom donors may be informative.

Following a series of optimisation reactions, promising performance was demonstrated by the in-situ generated imidazole catalyst and both of the –OMe functionalised catalysts for a range of substrates in a Suzuki-Miyaura cross-coupling screening, with a slight increase in activity for NPs formed in-situ being observed. Other immobilised PdNP systems in the literature have reported similarly high conversions for the coupling of aryl bromides with phenylboronic acid however such systems often require much increased reaction temperatures in excess of 70 °C.^[91]

Kinetic analysis revealed a tendency for the reactions to reach a plateau in the level of conversion. Ex-situ monitoring of NP size revealed no change in particle size distribution during the course of the reactions and hence the reaction plateau was not attributed to this. To shed more light on this effect a series of reactions were carried out to probe the homogeneity or heterogeneity of the reaction mechanism. A mercury poisoning study indicated that the pre-formed Pd⁰@OMe-PIILP **27** was probably catalysing the reaction in a solely heterogeneous manner while the results obtained for NPs generated in-situ from PdCl₄@OMe-PIILP **25** were less clear cut and suggest a certain amount of leaching of molecular Pd may be taking place. A more in-depth study would be required to determine the precise nature of the reaction mechanism.

A batch scale recycling study was not deemed suitable due to the difficulties which would be encountered in isolating the catalyst from the solid reaction products. Recycling of other immobilised PdNP systems have been reported, however they frequently exhibit catalyst deactivation in under five recycles, as a result of loss of catalyst during the recycling process.^[91] To overcome this possible issue, the potential for scaling the reaction up to a continuous flow process remains a possibility. Building upon this work, other members of the research group are continuing an ongoing investigation in to analogous styrene based PIILP materials featuring nitrile, phosphine, amino and styrene functionalities.

Chapter 3. Oxidation of Sulfides

3.1 Introduction

The selective oxidation of sulfides to their corresponding sulfoxides and sulfones is an area that has seen considerable interest in recent years due primarily to the importance of sulfoxides as intermediates in the chemical and pharmaceutical industries.^[94] The process of sulfide oxidation also forms the basis of catalytic desulfurisation of crude oil which will be discussed in Chapter 4. The synthesis of sulfoxides was first reported in 1865 by Marcker and subsequently a number of methods were developed for sulfoxidation.^[95] Unfortunately these methods frequently incorporated stoichiometric quantities of strong oxidants such as nitric acid which created large quantities of waste,^[96] harsh reaction conditions and expensive catalysts and the issue of over-oxidation to sulfone remained.^[97] As sulfoxides are used for C-C bond formation and functional group transformations the search for new methods of selective oxidation have continued.^[95] Acceptable processes utilising hydrogen peroxide as the oxidant in the presence of a catalyst are particularly attractive from both an environmental and economic standpoint and it is also relatively atom efficient. Many different catalyst systems have been developed including organocatalysts,^[98] and numerous transition metal catalysts based on molybdenum,^[99] vanadium,^[100] titanium,^[101] ruthenium,^[102] and tungsten etc.^[103] Although such catalysts have been successful in achieving a number of advances such as high selectivity, simple preparation and long term stability, there remain drawbacks such as issues with catalyst isolation and recovery, long reaction times and their suitability for transferral to continuous flow and industrial processes.

The use of polyoxometalates (POMs) has received considerable attention in a variety of oxidation reactions owing to their special intrinsic metal-oxo cage structure.^[104]

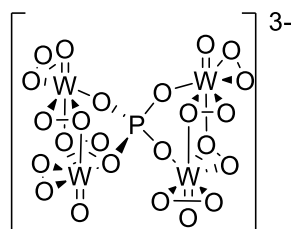


Figure 3.1 Molecular structure of the Venturello POM species $[\text{PO}_4\{\text{WO}(\text{O}_2)_2\}_4]^{3-}$ formed from the H_2O_2 mediated degradation of the Keggin dodecatungstophosphate ion $[\text{PW}_{12}\text{O}_{40}]^{3-}$.^[105]

The commercially available Keggin heteropolyacid (HPA), phosphotungstic acid, is of particular interest. This species degrades in the presence of excess hydrogen peroxide to form the peroxo species $[\text{PO}_4\{\text{WO}(\text{O}_2)_2\}_4]^{3-}$ as reported by Venturello and co-workers, which is the

true catalytically active intermediate (**Figure 3.1**).^[105] Here, one of the peroxy oxygens is activated towards electrophilic transfer by the non-bonded interaction with an adjacent metal centre.^[106]

Such POMs have recently been successfully incorporated into ionic liquid based systems. Ionic liquids and their excellent properties, as discussed in Chapter 1, are a class of compounds which have become very popular as both ‘green’ solvents or in supported (SILP) systems to immobilise catalysts and promote enhanced performance, traditionally through functionalisation of the cationic moiety. Recently ionic liquids incorporating functionalised anions have been explored and the first POM-based ionic liquid (POM-IL) was reported by Bourlinos *et al.*^[107] They reported that the partial exchange of the protons of the POM by a polyethylene glycol (PEG)-containing quaternary ammonium afforded a liquid derivative of the POM. An alternative and more simplistic route to obtaining POM-ILs, was adopted by Rickert *et al.*,^[108] which involved pairing a Keggin POM anion with a tetraalkylphosphonium cation. Many similar species have since proven to be promising electrolytes for use in both fuel cells and supercapacitors.^[107-109]

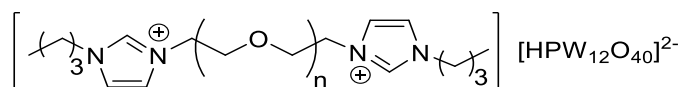
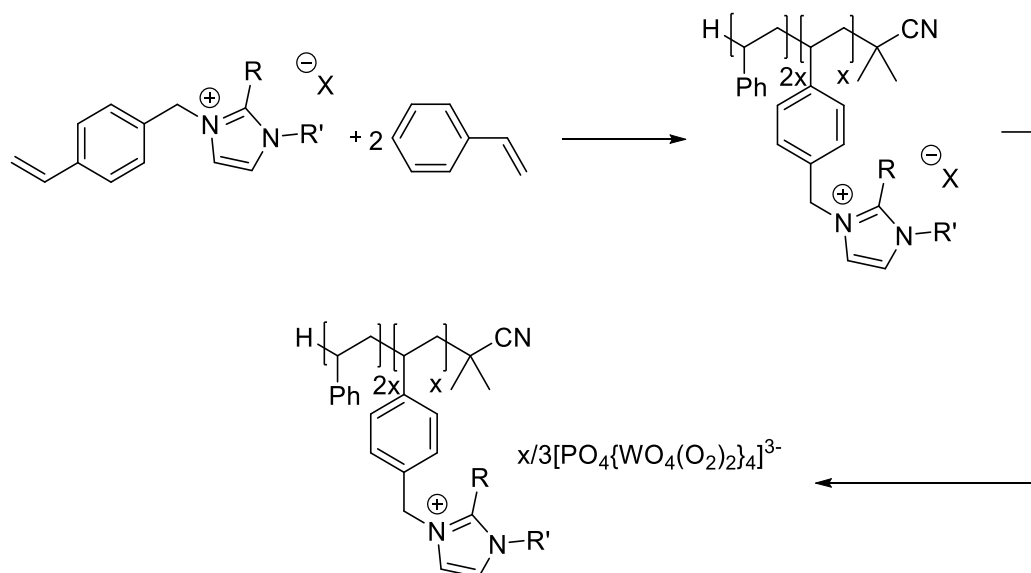


Figure 3.2 PEG-2000 based POM-IL incorporating the Keggin POM.

As well as tetraalkylammonium and tetraalkylphosphonium cations, imidazolium and pyridinium derivatives have been employed for the synthesis of these POM-ILs. One such imidazolium based system incorporated the Keggin POM by partial exchange of the POM protons with a PEG-2000 chain-functionalised alkylimidazolium chloride (**Figure 3.2**).^[110]

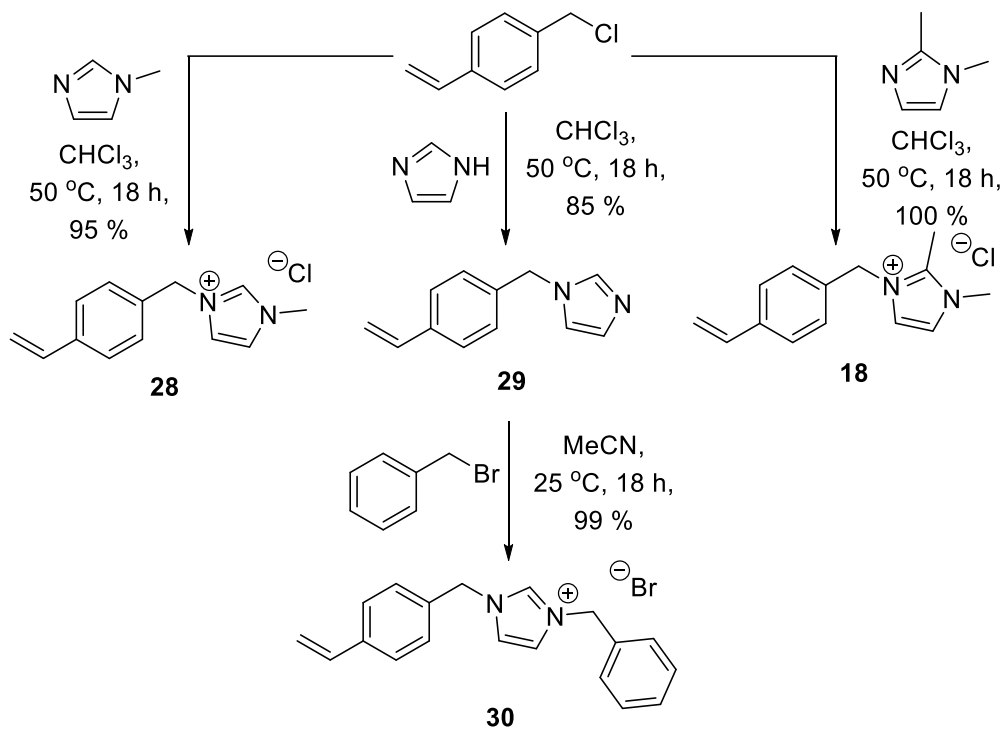
Taking this information into account the active Venturello POM, $[\text{PO}_4\{\text{WO}_4(\text{O}_2)_2\}_4]^{3-}$, was deemed to be an ideal candidate to incorporate into a new PIILP system to determine its effectiveness in the oxidation of sulfides. As discussed in the previous chapter radical polymerisation was identified here as the optimum method of polymerisation to generate the cationic support, owing to the same factors of experimental simplicity. The proposed synthetic pathway is shown in **Scheme 3.1** which would result in the generation of three POM loaded styrene based imidazolium PIILP catalysts.



Scheme 3.1 Overview of synthetic pathway to PIILP catalyst materials.

3.2 Synthesis of Styrene Based Monomers

Three styrene based imidazolium monomers were synthesised, featuring variations in what would become the ionic liquid like pendants of the final polymers. All three monomers were derived from 4-vinylbenzyl chloride in a simple one or two step synthesis requiring no chromatographic purification as shown in **Scheme 3.2**.

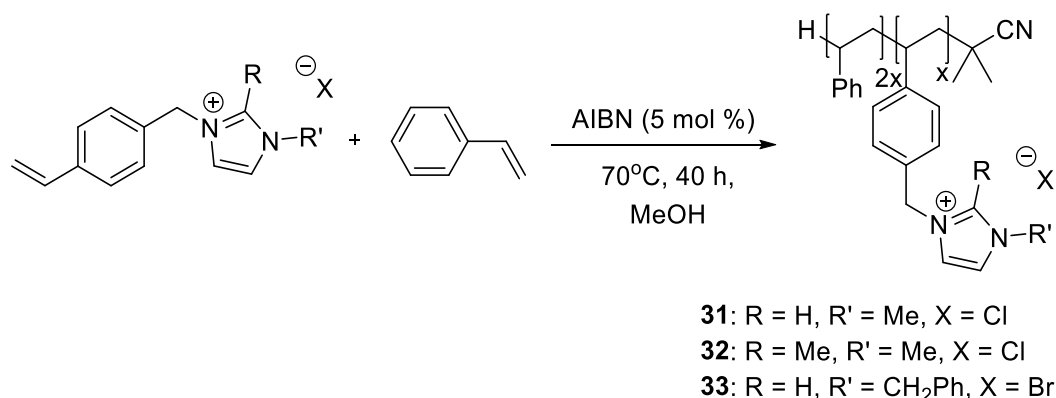


Scheme 3.2 Synthesis of styrene-base imidazolium monomers **28**, **30** and **18** from 4-vinylbenzyl chloride.

Monomer **28** was prepared in 95 % yield in a single step via reaction of 4-vinylbenzyl chloride with 1-methyl imidazole in CHCl_3 for 18 h at 50 °C. Monomer **30** was prepared in an overall yield of 84 % through the initial reaction of 4-vinylbenzyl chloride with 5 equivalents of imidazole in CHCl_3 at 50 °C to afford the 4-vinylbenzyl imidazole **29** which was converted to the desired product **30** via a quaternisation reaction with benzyl bromide in MeCN. The final monomer **18** was prepared under the same conditions as stated in Chapter 2.

3.3 Radical Polymerisations

The three functional styrenic imidazolium monomers **28**, **30** and **18** were used to prepare three linear co-polymers incorporating the desired functionality. As discussed in Chapters 1 and 2, radical polymerisation was chosen as the polymerisation method for the generation of these linear PIILP materials **31**, **32** and **33** due to the experimental simplicity, low cost synthetic route and ease of analysis of the resulting materials. The resulting amorphous white solids were characterised by a combination of ^1H NMR and solid state ^{13}C NMR spectroscopy, elemental analysis, IR, TGA/DSC, GPC and SEM imaging.



Scheme 3.3 AIBN initiated synthesis of linear styrene based co-polymers **31**, **32** and **33**.

The polymers were prepared via an AIBN initiated radical polymerisation in the presence of styrene which acted as a co-monomer (**Scheme 3.3**). This co-monomer was required due to the charged nature of the material which would likely have resulted in a homopolymer being water soluble, which as a result would not have been appropriate as an insoluble support. The desired imidazolium monomer: styrene monomer ratio was 1: 2. ^1H NMR spectroscopic data of the polymers suggested that the ratio of imidazolium monomer: styrene monomer was exactly that of the 1: 2 monomer feed ratio as expected. This ratio was determined via comparison of the integration of the N- CH_2 signals (δ 5.49 - 5.36) with the total integration for the aromatic protons (δ 7.89 – 6.48) (**Figure 3.3**).

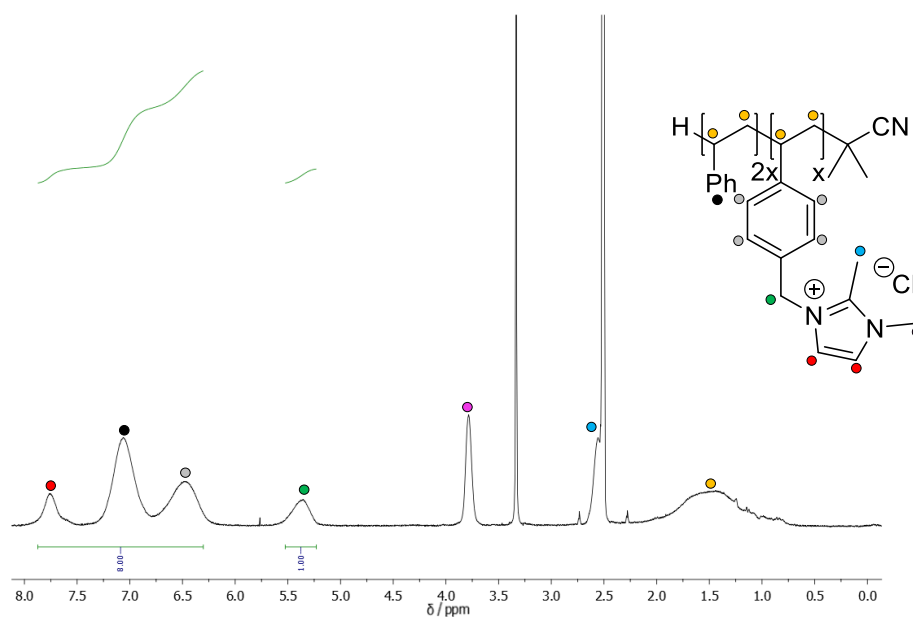


Figure 3.3 ^1H NMR spectrum of polymer **32** in D_2O showing the relative integrals of the aromatic protons at δ 7.75 - 6.48 to the N- CH_2 protons at δ 5.37. The ratio of 8:1 corresponds to an imidazolium monomer: styrene monomer ratio of 1: 2. Colour coded assignments are shown.

Calculation of this ratio was also possible from the elemental (CHN) analysis. The calculation for the 2-methyl imidazole polymer **31** can be found in **Appendix 2** and corresponded to an imidazolium monomer: styrene monomer ratio of 1:1.9 respectively. Dimethyl imidazolium polymer **32** was shown to have a ratio of 1: 1.5 and benzylated imidazolium polymer **33** was calculated to be 1: 1.8.

Solid state ^{13}C NMR spectroscopy further confirmed the structural dissimilarities between polymers **31** and **32**. The presence of the *N*-methyl of **31** was confirmed by a signal at 37 ppm and the presence of a signal at 11 ppm corresponding to the extra methyl group in **32** was shown in the dipolar dephasing solid state ^{13}C NMR spectra (**Figure 3.4**).

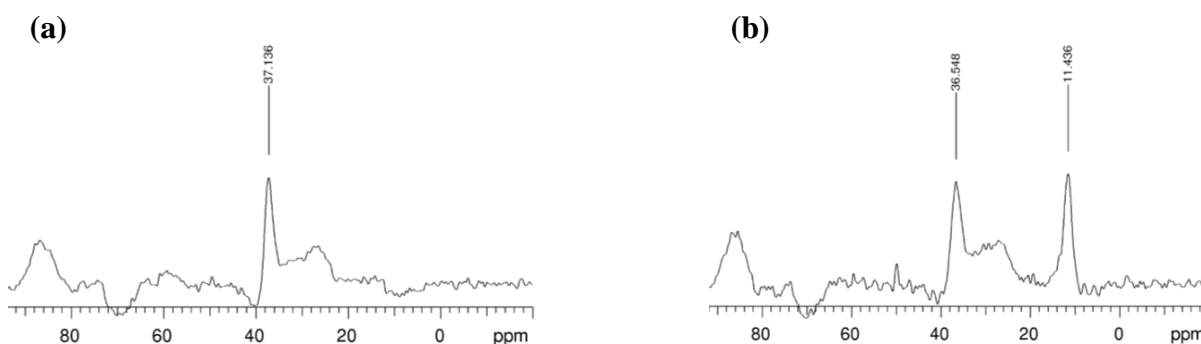


Figure 3.4 Solid state ^{13}C dipolar dephasing NMR spectra; (a) **31**, (b) **32**.

The extra components present in the benzylated imidazolium polymer **33** overlap with signals from the rest of the polymer so it is difficult to definitively prove their existence with ^{13}C NMR spectroscopy.

Gel permeation chromatography (GPC) was utilised to give some indication about the molecular weights of the polymers (**Table 3.1**). As radical polymerisation is an uncontrolled technique the PDI was expected to be quite high, potentially in the region of 2.00, and as the polymers are charged then some degree of contraction would be expected.

Polymer	M_w	M_n	PDI
31	27800	23800	1.17
32	26100	22000	1.19
33	31700	23900	1.33

Table 3.1 GPC results for linear styrene polymer; eluent: DMF/LiBr, flow rate: 1.00 ml/min.

These values correspond to degrees of polymerisation of approximately 63, 57 and 56 repeat units for polymers **31**, **32** and **33** respectively, each exhibiting a pleasingly low PDI, of between 1.17 and 1.33, for an uncontrolled polymerisation.

The thermal stability of each of the polymers was evaluated by thermogravimetric analysis (TGA) and differential scanning calorimetry (DSC). **Figure 3.5** shows the TGA/ DSC traces for polymer **32**. The TGA shows a small initial weight loss (~5 %) which was attributed to the evaporation of water or residual reaction solvent. This loss was followed by two main degradation stages; the first at ~320 °C was associated with the degradation of the imidazole pendant and suggests thermal stability up to this point. The large step decomposition just above 420 °C corresponds to the main chain decomposition which conforms to that found in the literature and by 500 °C less than 20 % by weight of the material remains.^[111] The heat flow plot also shows an exotherm at 100 °C which could correspond to Hoffmann elimination with no loss in mass. These features were present in all three of the polymers (See **Appendix 1** for TGA/DSC traces).

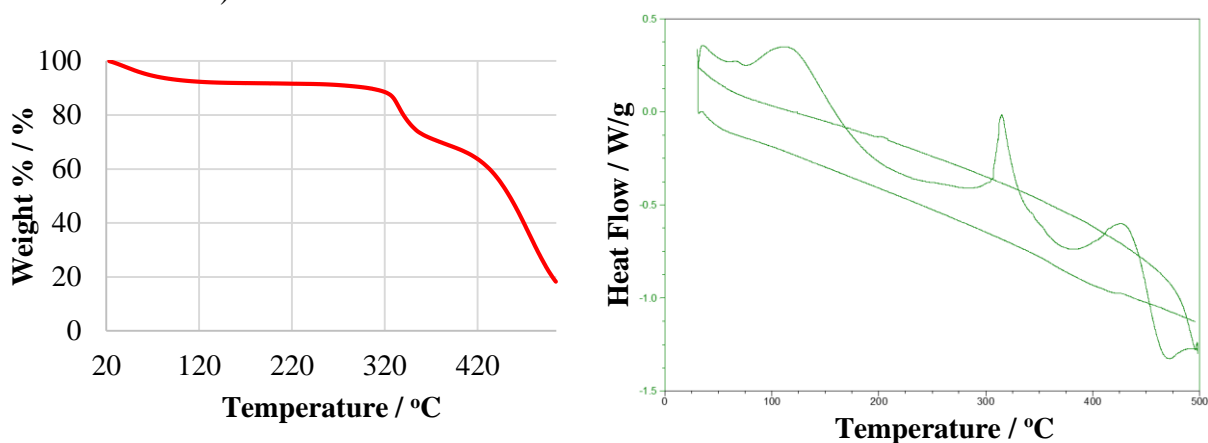
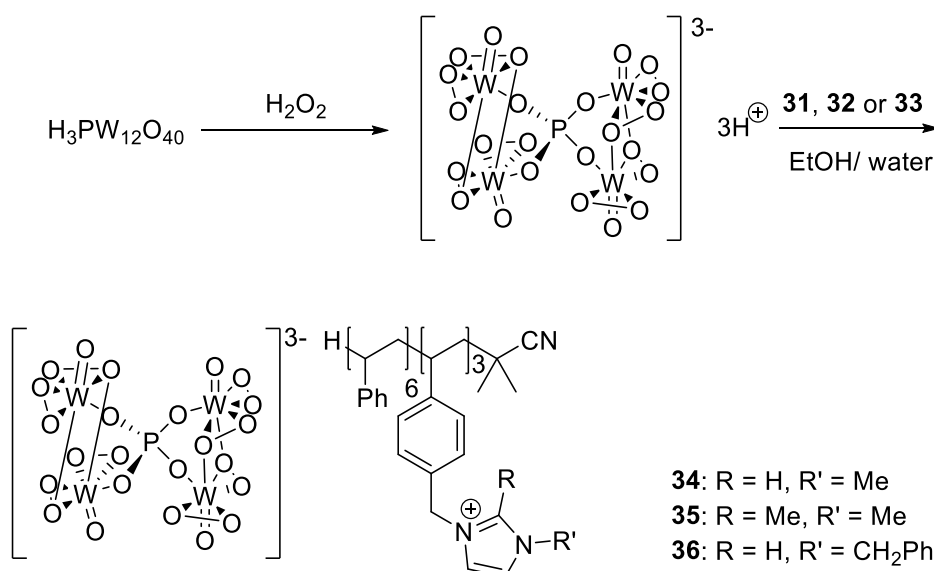


Figure 3.5 TGA/ DSC traces for polymer **32** showing an initial weight loss (~5 %) followed by degradation events at ~320 °C, then a large step decomposition just above 420 °C.

3.4 Immobilisation of POM Species

The peroxophosphotungstate-based PIILP catalysts **34**, **35** and **36** were prepared via stoichiometric exchange of the halide counterions of polymers **31**, **32** and **33** with the Venturello anion $[\text{PO}_4\{\text{WO}(\text{O}_2)_2\}_4]^{3-}$ (**Scheme 3.4**), as discussed previously. It was decided to generate the active POM anion before immobilisation on the PIILP materials by ion exchange. This generation of the active species was achieved by reacting phosphotungstic acid with 200 equivalents of hydrogen peroxide and then adding the resulting solution to the polymer materials in EtOH whilst stirring rapidly to induce precipitation. The resulting amorphous white solids were isolated by filtration and dried under high-vacuum to afford the POM@PIILP catalysts **34-36**.



Scheme 3.4 Generation of Venturello anion $[\text{PO}_4\{\text{WO}(\text{O}_2)_2\}_4]^{3-}$ from phosphotungstic acid and subsequent immobilisation of this POM species on polymers **31-33**.

The POM@PIILP catalysts were characterised utilising the same techniques as their corresponding polymers, along with solid state ^{31}P NMR spectroscopy. Solid state ^{31}P NMR spectroscopy of the PIILP materials confirmed the decomposition of HPA $\text{H}_3\text{PW}_{12}\text{O}_{40}$ into $[\text{PO}_4\{\text{WO}(\text{O}_2)_2\}_4]^{3-}$ by a large sharp signal between δ 2.8 and 6.4 ppm (**Figure 3.6**). POM@PIILPs **34** and **36** also showed the presence of several unidentified phosphorus-containing species previously observed by Hill and co-workers during their study on the formation, reactivity and stability of $[\text{PO}_4\{\text{WO}(\text{O}_2)_2\}_4]^{3-}$.^[112]

The NMR spectroscopic data was also supported by the IR data which saw the appearance of characteristic bands at $\sim 1079 \text{ cm}^{-1}$ $\nu(\text{P-O})$ and 956 cm^{-1} $\nu(\text{W=O})$ which are consistent with those reported in the literature for supported peroxometalates.^[113]

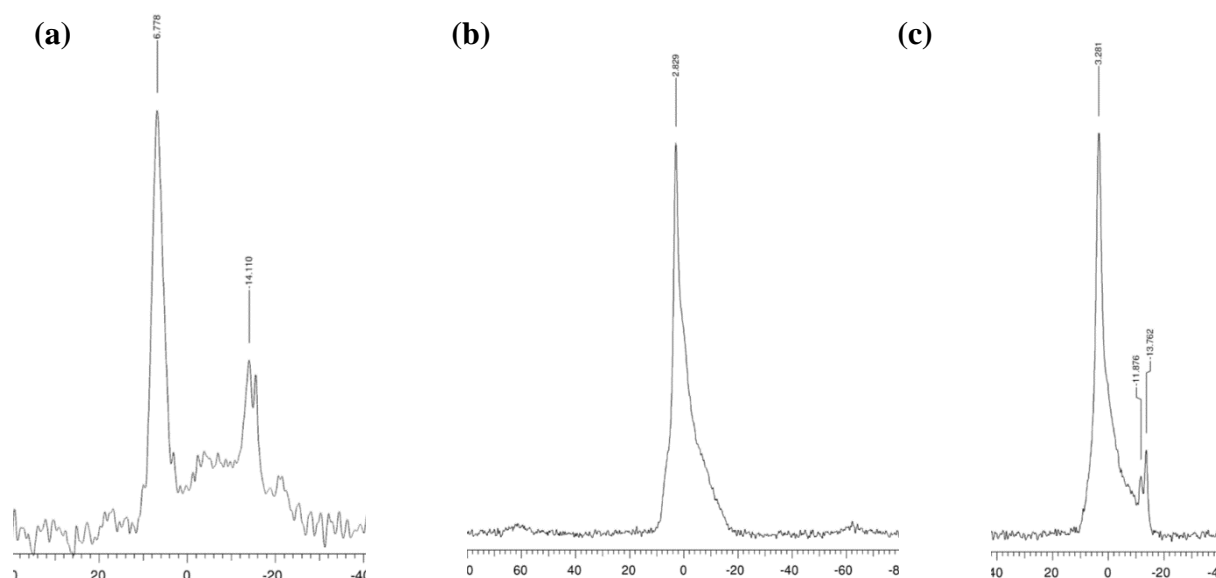


Figure 3.6 Solid state ^{31}P NMR spectra of POM@PIILP catalysts (a) **34**, (b) **35** and (c) **36**.

The thermal stability of each PIILP catalyst was again evaluated via TGA/ DSC. **Figure 3.7** shows the TGA/ DSC curves for POM@PIILP **35**. Unlike the polymers which showed only two main degradation stages, there are three present for each of the PIILP materials, the first at ~ 150 $^{\circ}\text{C}$, then ~ 300 $^{\circ}\text{C}$ and ~ 425 $^{\circ}\text{C}$. In contrast to the corresponding polymer material which resulted in less than 20 % of material remaining by 500 $^{\circ}\text{C}$, here PIILP **35** still retained around 60 % of its weight, suggesting that the POM species is extremely thermally robust and remains beyond this point, which is supported by a calculated POM loading of 53.4 % for PIILP **35** from CHN analysis. Very similar results were obtained for the other two POM@PIILP species. See **Appendix 1** for TGA/DSC traces.

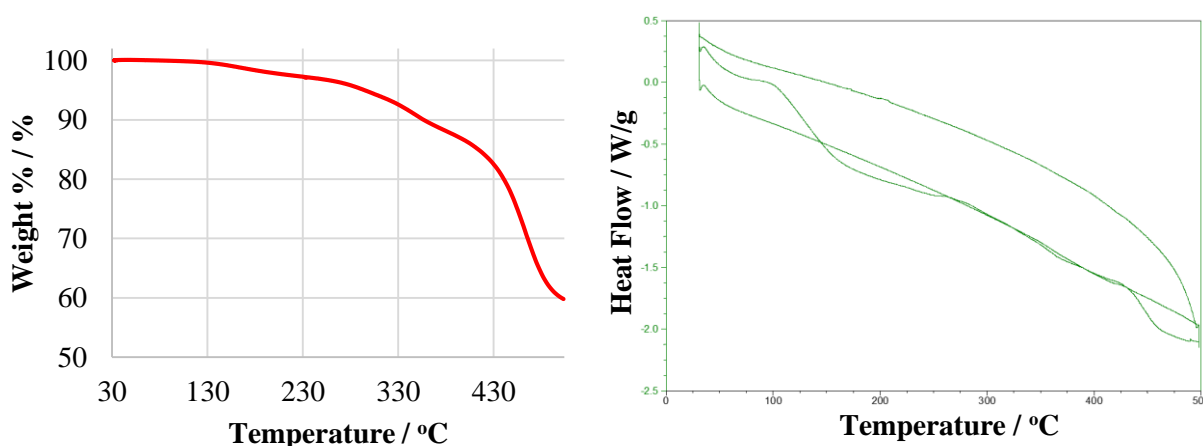


Figure 3.7 TGA/ DSC traces for PIILP **35** showing three degradation events at ~ 150 $^{\circ}\text{C}$, ~ 300 $^{\circ}\text{C}$ and a large step decomposition just above ~ 425 $^{\circ}\text{C}$.

Further investigation in to the morphology of both the polymers and POM@PIILP catalyst materials by scanning electron microscopy (SEM) (**Figure 3.8**) revealed that each of the

polymers was granular in nature with smooth surfaces and no visible evidence of pores or surface deposition. The POM@PIILP catalysts however showed an uneven surface suggesting that this was either the peroxophosphotungstate which was aggregating and becoming visible on the surface or perhaps was simply as a result of the further processing leading to an 'uneven' polymer surface.

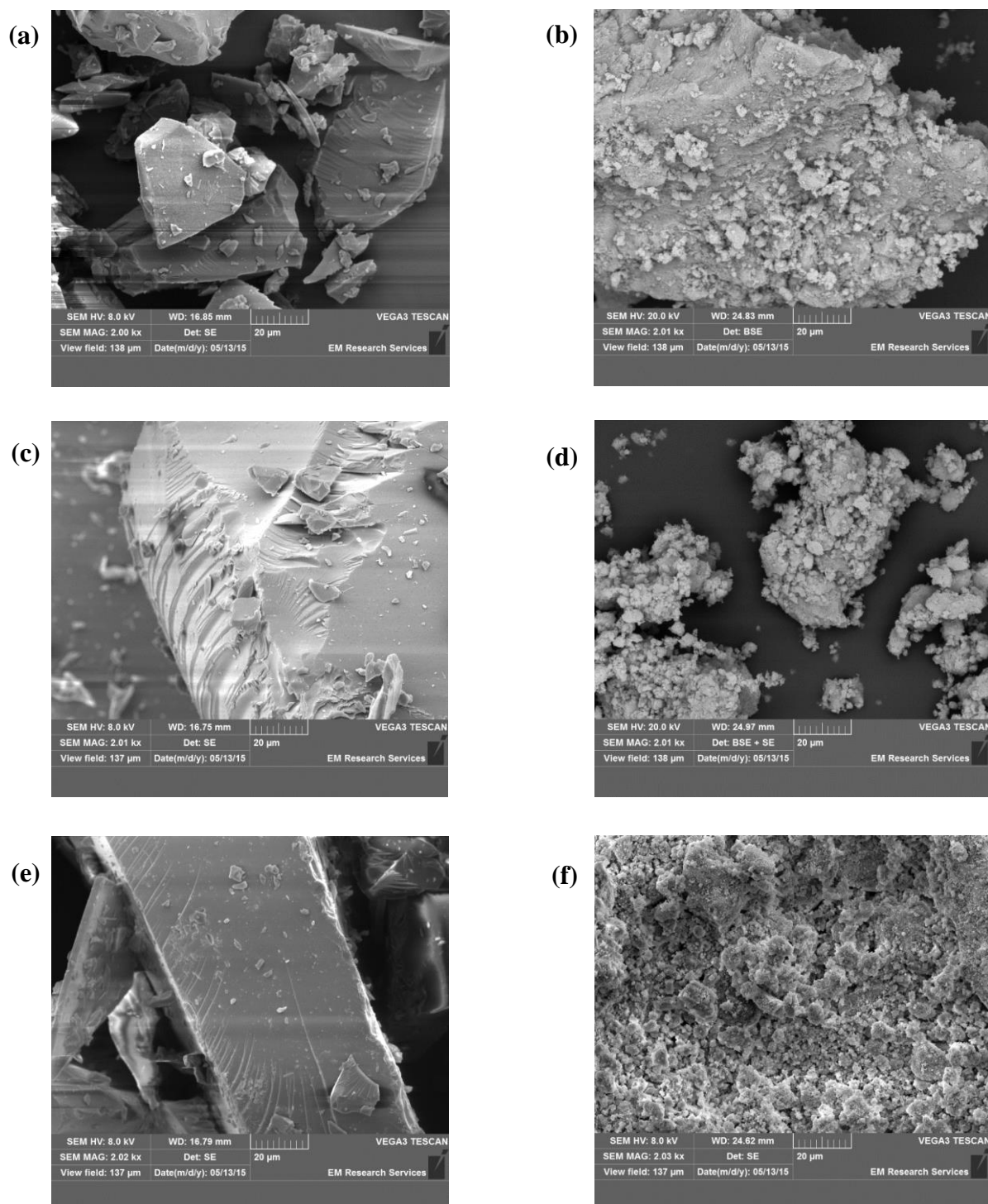


Figure 3.8 SEM images of polymers and POM@PIILP materials; (a) **31**, (b), **34**, (c) **32**, (d) **35**, (e) **33**, (f) **36** showing smooth surfaced granular polymer material and the uneven surface of the POM@PIILP materials.

Due to difficulties in digestion of the peroxophosphotungstate species it was not possible to obtain a tungsten content via conventional ICP-OES. It was possible however to determine a W content of the materials via calculation from the elemental analysis. An example calculation for PIILP **34** is shown in **Figure 3.9**. The calculations for all other PIILPs can be found in **Appendix 3**.

CHN Anal. Calc. for C₈₇H₉₃N₆O₂₄PW₄ (2373.041) C, 44.03; H, 3.95; N, 3.54 %.
Found: C, 41.04; H, 3.99; N, 3.14 %.

Therefore: 1 g of PIILP contains 0.0314 g N = 2.241×10^{-3} moles N
(Polymer alone has 4.490×10^{-3} moles N per g from CHN analysis)

Therefore, 1g polymer contains (4.490×10^{-3} moles N)

So if 1g of PIILP has 2.241×10^{-3} moles N then 2.00 g of PIILP contains 4.482×10^{-3} moles N which corresponds to 1g of polymer

1.00 g extra mass is from $-3\text{Cl}^- + \text{POM} = (3 \times (-35.453)) + 1150.31 = 1043.951$

$1.00/1043.951 = 0.958$ mmol of POM = 1.102 g POM

Therefore 1 g of PIILP contains $(1/2.00) \times 1.102 = 0.551$ g POM = 0.479 mmol POM

This corresponds to $(0.479 \text{ mmol} \times 4) = 1.916$ mmol W
= 0.35 g W = **35 %**

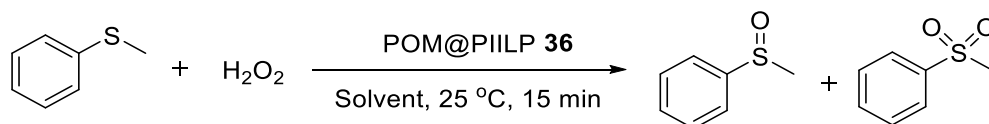
Figure 3.9 Calculation of tungsten loading for PIILP **34** from the CHN elemental analysis.

This calculation utilises the CHN data of both the POM@PIILP catalyst and its corresponding polymer. The value of POM loading of 0.479 mmol g⁻¹ for **34** was extremely close to a theoretical 100 % loading of 0.451 mmol g⁻¹ indicating complete anion exchange with the polymer chloride had occurred and also the proposed formulation was correct, as was the case for PIILP **35**. The calculated POM loading for PIILP **35** was 0.464 mmol g⁻¹ and the theoretical value was 0.447 mmol g⁻¹. PIILP **36** however contained a slightly increased 0.441 mmol g⁻¹ POM compared to a theoretical value of 0.358 mmol g⁻¹ which may suggest that some free POM could be present in this material.

3.5 Sulfide Oxidation System Optimisation

Initial catalyst optimisation and evaluation employed thioanisole as the benchmark substrate as this oxidation has recently been catalysed by a range of supported and immobilised systems including on the surface of ionic liquid modified silica,^[114] ionic liquid-based polyoxometalate salts,^[115] and as tungstate ions embedded in mesochannels of SBA-15 and poly(ionic) liquid entrapped magnetic nanoparticles.^[73]

3.5.1 Solvent screening

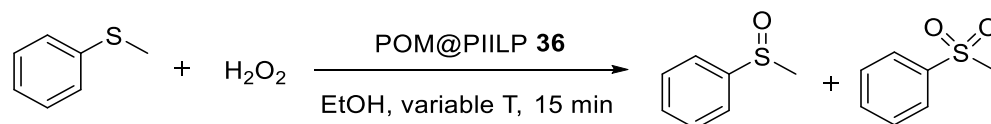


Entry ^a	Solvent	Sulfide / %	Sulfoxide / %	Sulfone / %	Conversion ^b / %	Sulfoxide Selectivity ^c / %
1	MeOH	1	95	4	99	96
2	EtOH	6	91	3	94	96
3	iPrOH	8	88	4	92	96
4	Ethylene glycol ^d	4	90	6	96	93
5	2-Me THF ^d	0	0	100	100	0
6	MeCN	19	78	3	81	97

Table 3.2 Optimisation of reaction solvent using POM@PIILP 36. ^a POM@PIILP 36 (13 mg, 0.5 mol%), thioanisole (1 mmol), solvent (3 mL), 35% H₂O₂ (2.5 mmol), 25 °C, 15 min. ^b Conversion measured by ¹H NMR (average of 2 runs). ^c Sulfoxide selectivity = [%sulfoxide / (%sulfoxide + %sulfone)]. ^d Carried out at 50 °C.

In order to investigate the effect of the reaction solvent on sulfide oxidation and sulfoxide selectivity a range of reactions were performed using POM@PIILP 36 as the catalyst. Initial reaction conditions were derived from previous work carried out in the group on a norbornene based pyrrolidinium species.^[116] This work was carried out in MeOH and MeCN which were chosen as the initial solvents to investigate. MeOH resulted in a 99 % conversion with 96 % selectivity for the sulfoxide while MeCN didn't perform quite as well with 81 % conversion however, the selectivity was equally as high at 97 %. With a view to reducing the environmental impact of our work over time, a range of more 'green' solvents were investigated. Of these, EtOH proved to be most promising with a conversion of 94 % and selectivity of 96 %. At 25 °C both ethylene glycol and 2-Me THF could only achieve conversions of 34 % and 46 % respectively. An increased temperature of 50 °C was required for these solvents to achieve higher conversions in line with the other solvents, at which point no sulfoxide selectivity was observed for 2-Me THF. MeCN and EtOH were chosen as the reaction solvents which would enable comparisons to previous systems with the increased 'green' credentials of EtOH over MeOH.

3.5.2 Temperature optimisation

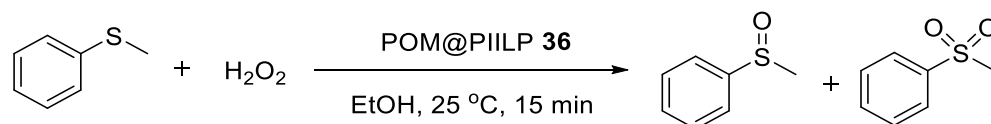


Entry	Temp	Sulfide	Sulfoxide	Sulfone	Conversion	Sulfoxide Selectivity
1	25	6	91	4	94	96
2	30	0	91	8	100	92
3	35	0	70	30	100	70
4	40	0	56	44	100	56
5	45	0	42	58	100	42
6	55	0	8	92	100	8

Table 3.3 Optimisation of reaction temperature using POM@PIILP 36. ^a POM@PIILP 36 (13 mg, 0.5 mol%), thioanisole (1 mmol), EtOH (3 mL), 35% H₂O₂ (2.5 mmol), 15 min. ^b Conversion measured by ¹H NMR (average of 2 runs). ^c Sulfoxide selectivity = [%sulfoxide / (%sulfoxide + %sulfone)].

A range of temperatures from room temperature up to 55 °C were carried out in EtOH. As expected an increase in temperature afforded a 100 % conversion and the sulfoxide selectivity reduced as the reaction was pushed to completion of the second oxidation to sulfone. In order to maximise the selectivity for sulfoxide the chosen reaction temperature was 25 °C which afforded a conversion of 94 % and selectivity of 96 %.

3.5.3 Peroxide concentration optimisation



Entry	H ₂ O ₂ Conc. / eq.	Sulfide / %	Sulfoxide / %	Sulfone / %	Conversion ^b / %	Sulfoxide Selectivity ^c / %
1	2	25	74	2	76	98
2	2.5	6	91	3	94	96
3	3	5	91	3	95	96
4	4	0	91	9	100	91
5	5	0	83	17	100	83

Table 3.4 Optimisation of peroxide concentration using POM@PIILP 36. ^a POM@PIILP 36 (13 mg, 0.5 mol%), thioanisole (1 mmol), EtOH (3 mL), 35% H₂O₂ (x mmol), 15 min. ^b Conversion measured by ¹H NMR (average of 2 runs). ^c Sulfoxide selectivity = [%sulfoxide / (%sulfoxide + %sulfone)].

The final aspect of the reaction to be optimised was the concentration of the oxidant hydrogen peroxide. Molar equivalents of between 2 and 5 to the substrate were investigated. It was shown that 2.5 equivalents resulted in a conversion of 94 % with a selectivity of 96 %. Any increase

in concentration above this level did not yield significant improvements. Thus, the optimised set of conditions for sulfide oxidation reactions using the POM@PIILP catalyst were MeCN or EtOH, 25 °C and 2.5 equivalents of H₂O₂.

3.6 Sulfide Substrate Screening

The encouraging optimisation results for the selective oxidation of thioanisole with POM@PIILP **36** lead to catalyst testing being extended to a full range of alkyl and aryl alkyl

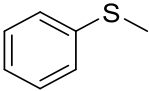
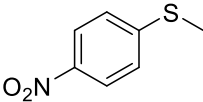
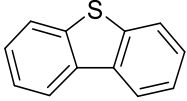
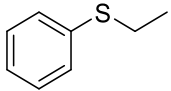
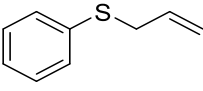
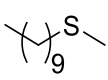
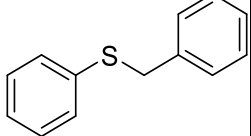
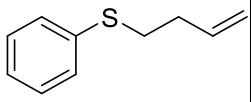
Substrate ^a	PIILP 34		PIILP 35		PIILP 36	
	Conv. ^b (selectivity) / % ^c	TOF ^f	Conv. ^b (selectivity) / % ^c	TOF ^f	Conv. ^b (selectivity) / % ^c	TOF ^f
	52 (98)	359	49 (98)	337	76 (97)	533
	36 (97)	248	24 (98)	167	54 (94)	376
	19 (71) ^e	63	3 (100) ^e	12	41 (79) ^e	143
	64 (96)	437	49 (97)	342	77 (95)	539
	40 (96) ^d	272	38 (96) ^d	261	69 (97) ^d	482
	75 (99)	512	89 (98)	619	97 (97)	675
	33 (99)	222	48 (97)	336	63 (97)	437
	40 (97)	277	65 (96)	450	72 (96)	500

Table 3.5 Substrate screening in MeCN. ^a Reaction Conds: 0.5 mol % cat. based on repeat unit and assumed complete POM loading, 1 mmol sulfide, 2.5 mmol 35% H₂O₂, 3.0 mL MeCN, 25 °C, 15 min.

^b % conversion determined by ¹H NMR with 0.5 mmol 1,3-dinitrobenzene std, average 2 runs. ^c Sulfoxide selectivity = [%sulfoxide / (%sulfoxide + %sulfone)]. ^d % conversion determined by ¹³C NMR with 0.5 mmol 1,3-dinitro benzene std, average 2 runs. ^e Reaction Conds: 0.5 mol % cat. based on repeat unit and assumed complete POM loading, 1 mmol sulfide, 2.5 mmol 35% H₂O₂, 4.0 mL MeCN, 25 °C, 30 min. ^f TOF = moles sulfide consumed per mole catalyst per h.

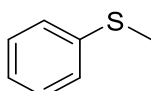
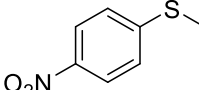
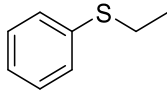
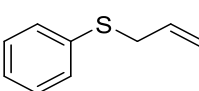
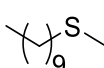
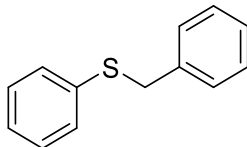
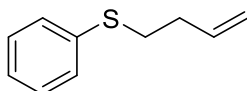
Substrate ^a	PIILP 34		PIILP 35		PIILP 36	
	Conv. ^b (selectivity) / % ^c	TOF ^e	Conv. ^b (selectivity) / % ^c	TOF ^e	Conv. ^b (selectivity) / % ^c	TOF ^e
	34 (99)	234	25 (100)	173	89 (97)	622
	8 (100)	52	5 (100)	37	37 (96)	258
	27 (97)	183	19 (97)	135	85 (96)	595
	15 (100) ^d	103	11 (100) ^d	76	75 (97) ^d	526
	69 (100)	473	55 (100)	380	100 (95)	698
	16 (100)	108	11 (100)	78	68 (97)	475
	16 (97)	112	13 (96)	91	66 (98)	459

Table 3.6 Substrate screening in EtOH. ^a Reaction Conds: 0.5 mol % cat. based on repeat unit and assumed complete POM loading, 1 mmol sulfide, 2.5 mmol 35% H₂O₂, 3.0 mL EtOH, 25 °C, 15 min. ^b % conversion determined by ¹H NMR with 0.5 mmol 1,3-dinitrobenzene std, average 2 runs. ^c Sulfoxide selectivity = [%sulfoxide / (%sulfoxide + %sulfone)]. ^d % conversion determined by ¹³C NMR with 0.5 mmol 1,3-dinitro benzene std, average 2 runs. ^e TOF = moles sulfide consumed per mole catalyst per h.

Sulfides in both MeCN and EtOH under optimum conditions for all three POM@PIILP catalysts as summarised in **Table 3.5** and **Table 3.6** respectively. High turnover frequencies were obtained across the range of substrates examined and the selectivity for sulfoxide was

comparable or higher in ethanol than in acetonitrile. Oxidation of allyl phenyl sulfide and homoallyl phenyl sulfide occurred with complete chemoselectivity for sulfoxide and sulfone with no evidence for epoxidation of the double bond, presumably due to the mild conditions and short reaction times.

As expected the TOF was considerably higher with the simple alkyl substrate *n*-decyl methyl sulfide. The poor performance of all PIILPs in the oxidation of dibenzothiophene (DBT) is in keeping with the proposed electrophilic pathway, in agreement with previous reports that the rate of oxidation increases with increasing nucleophilicity of the sulfide.^[117] Unfortunately, it was not possible to exploit the slightly increased preference for sulfoxide selectivity observed in EtOH for DBT due to its limited solubility in in this particular solvent.

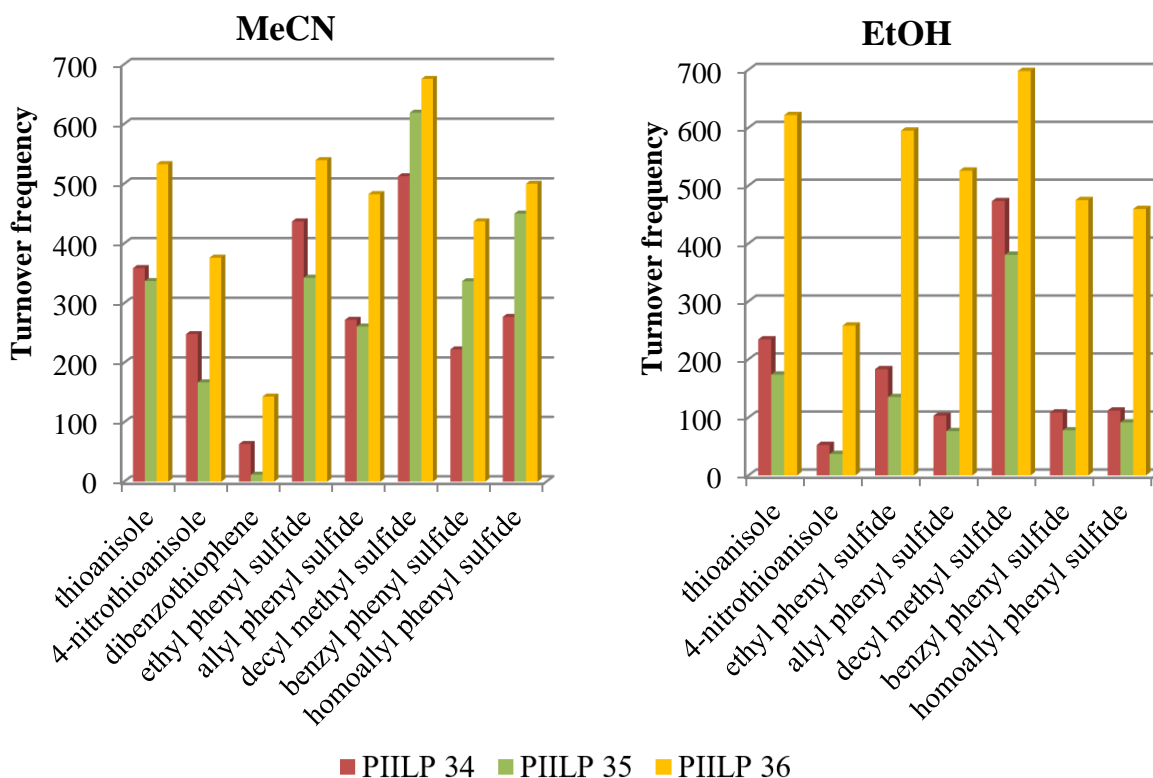


Figure 3.10 Turnover frequency profiles for the oxidation of various sulfides under the conditions outlined in **Tables 3.5** and **3.6** respectively. TOF = moles sulfide consumed per mole catalyst per h.

The visual comparison of turnover frequencies for each catalyst in both reaction solvents is shown in **Figure 3.10**. In MeCN this visual comparison highlights that catalyst **36** has outperformed catalysts **34** and **35** for each sulfide in both solvents, yielding much higher turnover frequencies whilst retaining equally high sulfoxide selectivity. Catalyst **35** performed particularly poorly in EtOH and almost as poorly in MeCN. The greater activity of catalyst **36** could be a result of an increased affinity of the substrate for the support material as a result of the increased hydrophobicity of the cation. The benzyl side chain could potentially be creating

more hydrophobic regions which are effectively retaining the substrates in closer proximity to the active POM. There is also a likelihood that the microstructure of these materials contains pores which could be limiting the accessibility of larger substrates to the active sites.

Another possible explanation for the variation in catalyst activity is the electrophilic nature of the oxidation mechanism itself, which would suggest that the presence of the positive charge of the imidazolium fragment could be facilitating oxidation via stabilisation of the forming partial charges in the transition state. This hypothesis would explain the poor activity of catalyst **35**, as electron donation of the C-2 methyl would reduce the overall positive charge of the imidazolium fragment of this particular functionality compared with both **34** and **36** which are not methylated at the C2 position.

Whilst the results obtained do suggest the catalyst performance is dependent upon the IL support, as demonstrated by the significant increase in turnover frequency achieved with the benzylated IL functionality, it would perhaps be an oversimplification to attribute these differences solely to the nature of the cationic support. It is worth noting that each of the loaded polymer catalysts will have its own unique morphology which will inevitably play a significant role in the catalyst activity. The results, while promising in terms of turnover frequency and sulfoxide selectivity do highlight the complex interactions between the cationic support, POM and the substrate.

3.7 Kinetic Study of Oxidation of 4-Nitrothioanisole & Dibenzothiophene

As both sulfoxides and sulfones are useful classes of compounds, the kinetics of reactions of dinitrobenzene and 4-nitrothioanisole, chosen due to their favourable reaction times, were monitored in the presence of the best performing catalyst, POM@PIILP **36**. The previously established optimum reaction conditions were used in scaled up reactions which were sampled at the desired time points.

The experimental data for each kinetic profile is an average of two runs which have been fitted to 3 different equations (**Figure 3.11**). One expresses the reduction in sulfide, the second the increase and subsequent decrease in sulfoxide and the final equation expresses the increase in sulfone.

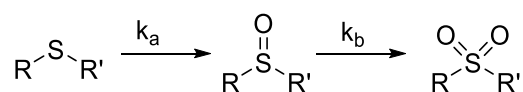
$$\text{Sulfide: } 100 \times e^{(-k_a t)}$$

$$\text{Sulfoxide: } \left(\frac{100 \times k_a}{k_a - k_b} \right) \times (e^{(-k_a t)} - e^{(-k_b t)})$$

$$\text{Sulfone: } 100 \times \left\{ 1 + \left(\frac{1}{k_a - k_b} \right) \times \left[\left(k_b e^{(-k_a t)} \right) - \left(k_a e^{(-k_b t)} \right) \right] \right\}$$

Figure 3.11 Equations used to fit sulfide oxidation experimental data.

These equations describe the proposed reaction pathway (**Scheme 3.5**) with two separate rate constants for the oxidation of sulfide to sulfoxide and sulfoxide to sulfone, k_a and k_b respectively.



Scheme 3.5 Reaction pathways for two step sulfide oxidation

The GnuPlot fitted data for each of the kinetic profiles is shown in **Figures 3.12 – 3.14**. The red line represents the sulfide, the green the sulfoxide and the blue the sulfone.

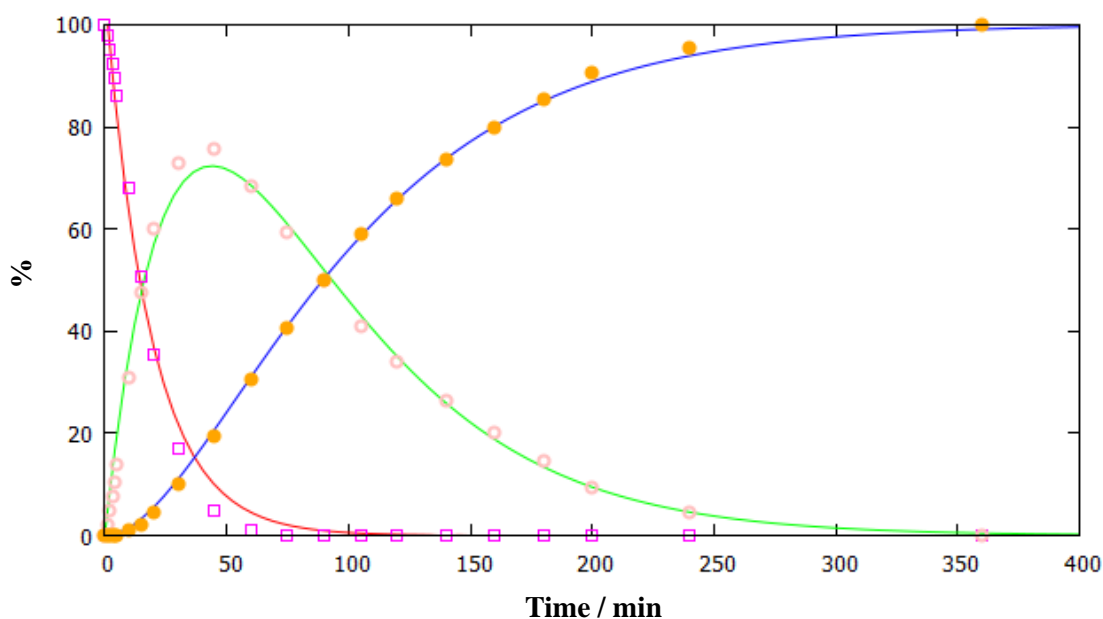


Figure 3.12 Kinetic profile for the oxidation of 4-nitrothioanisole with POM@PIILP **36** in MeCN. Experimental data points are an average of two results. Lines represent fitted data.

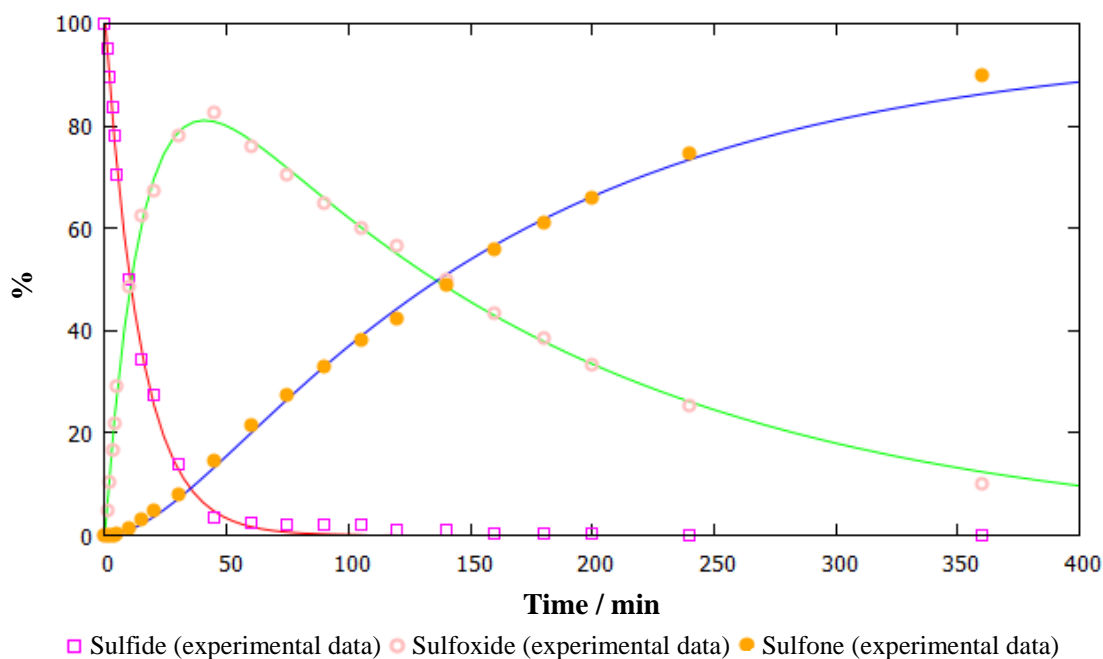


Figure 3.13 Kinetic profile for the oxidation of 4-nitrothioanisole with POM@PIILP **36** in EtOH. Experimental data points are an average of two results. Lines represent fitted data.

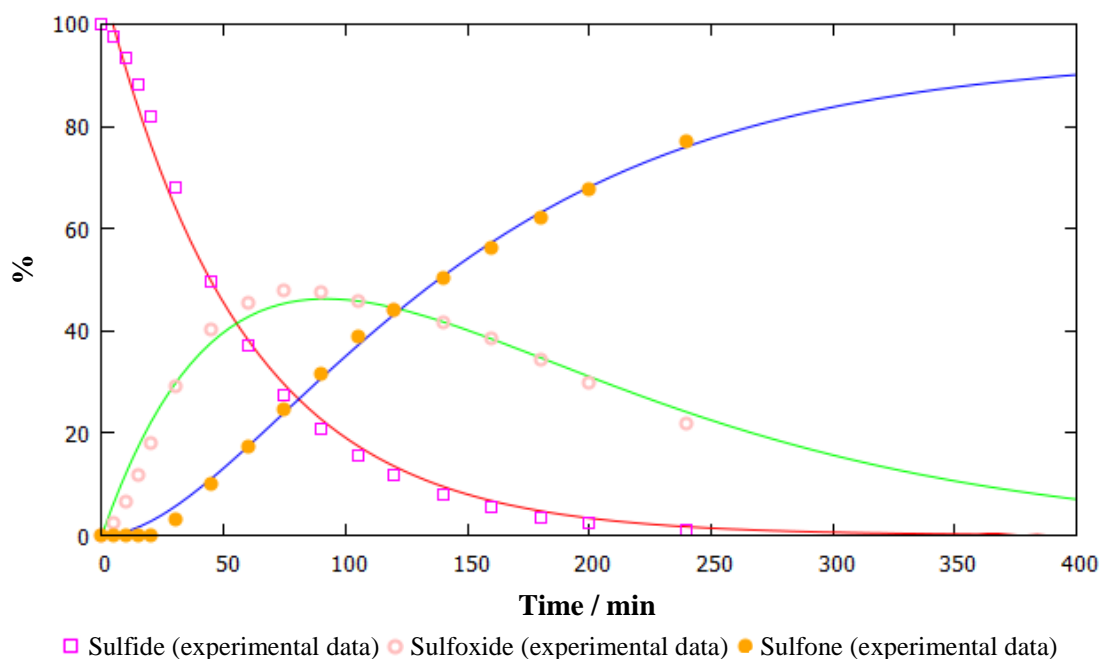


Figure 3.14 Kinetic profile for the oxidation of dibenzothiophene with POM@PIILP **36** in MeCN. Experimental data points are an average of two results. Lines represent fitted data.

It is clear from a visual comparison that the experimental data is closely associated to that of the fitted data, indicating that the results are consistent with the anticipated reaction pathway. From the fitted data it was possible to extract both a k_a and k_b value along with the associated error as summarised in **Table 3.7**.

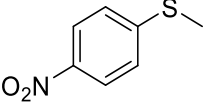
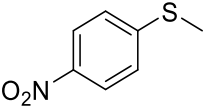
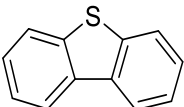
Sulfide	Solvent	k_a	Asymptotic Standard Error / %	k_b	Asymptotic Standard Error / %
	MeCN	0.053	4.4	0.022	150.3
	EtOH	0.068	1.9	0.0062	3.8
	MeCN	0.017	3.9	0.010	82.6

Table 3.7 Rate constants for oxidation of sulfide and sulfoxide with POM@PIILP **36**.

The rate constant for the first oxidation (k_a) from sulfide to sulfoxide is higher than the second oxidation from sulfoxide to sulfone (k_b) for both substrates in both solvents. In MeCN the second oxidation is 1.7 times slower than the first for DBT and 2.4 times slower for 4-nitrothioanisole. In EtOH however there is a greater than tenfold decrease in the rate of the second oxidation. This observation suggests that the EtOH is having a stabilising effect on the sulfoxide, potentially via hydrogen bonding, leading to a dramatic decrease in the rate of the second oxidation to the sulfone.

3.8 Batch Recycling Study

As the peroxometalate is retained by the PIILP support it was reasoned that effective recycling of the system should be possible. Hence catalyst recycles were performed on POM@PIILP **36** on the sulfoxidation of thioanisole in both MeCN and EtOH to assess the robustness of the system and its potential for transferral to segmented and continuous flow processes. The recycling required the catalyst to be isolated via centrifugation, washed with the reaction solvent and reused without being replenished.

3.8.1 Recycle in MeCN

Eleven catalyst recycles were carried out in MeCN (**Figure 3.15**), the first ten involved no reconditioning of the catalyst taking place. The 11th recycle was carried out following an 18 h stir with an extra equivalent of hydrogen peroxide to investigate the possible effect of catalyst reactivation.

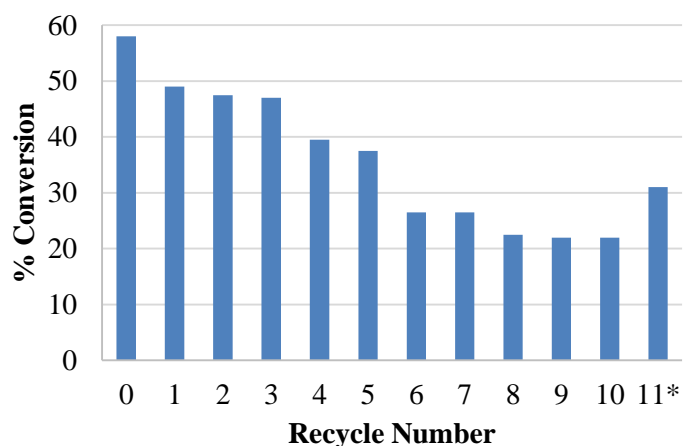


Figure 3.15 Recycling of POM@PIILP 36 in MeCN. *Catalyst re-activated with H₂O₂.

The data clearly shows a relatively large initial decrease of 9 % conversion after the first recycle. The next two recycles show only a slight decrease of 2 % and a further drop to 38 % by the fifth recycle. It was at this point that the catalyst was stored overnight under N₂, however it is evident that during this time the conversion has dropped significantly by the 6th recycle. Recycle 11 shows a large increase in conversion suggesting that the catalyst has been reactivated by the presence of hydrogen peroxide.

2.8.2 Recycle in EtOH

The same conditions were followed for the eleven recycles in EtOH (**Figure 3.16**) as in MeCN. Here it was evident that the initial decrease seen in MeCN was not occurring with no decrease in conversion after the first recycle. A gradual decrease in conversion of only 11 % was observed up to the 4th recycle. Again it was clear that the catalyst had deactivated slightly following storage overnight after the 5th recycle, however a less dramatic increase in conversion was observed following reactivation with H₂O₂.

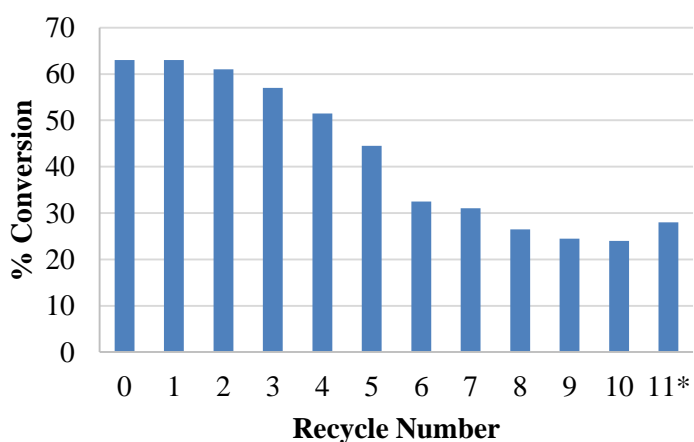


Figure 3.16 Recycling of POM@PIILP 36 in EtOH. *Catalyst re-activated with H₂O₂

Thus overall the decrease in conversion was similar in both solvent systems, however the EtOH performed much better at the initial stages of recycling.

3.8.3 Tandem recycling

A tandem recycle was carried out in both solvents to determine the potential for catalyst **36** to catalyse more than one sulfoxidation following recycling. The procedure followed that of the standard recycling however after the initial reaction with 4-nitrothioanisole the catalyst was washed and the second recycle carried out with thioanisole, followed by a final recycle with ethyl phenyl sulfide.

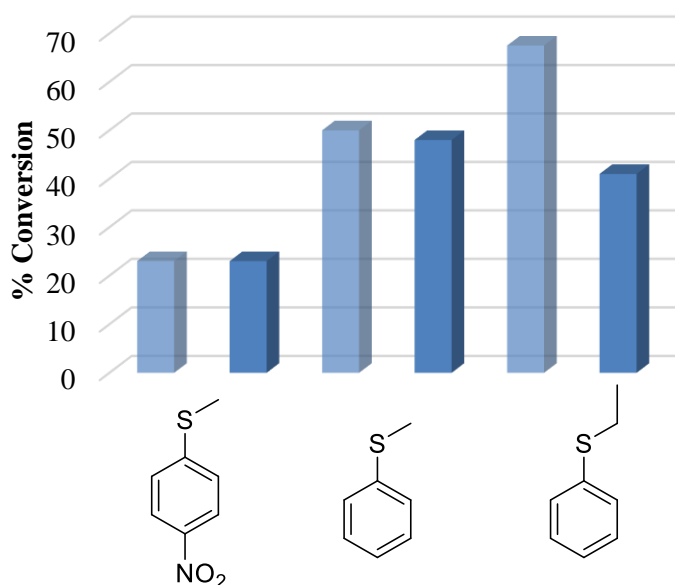


Figure 3.17 Tandem recycling of POM@PIILP **36** in MeCN with 4-nitrothioanisole followed by thioanisole and ethyl phenyl sulfide; Transparent = Ref. value from single batch reaction in substrate screening.

Tandem recycling in MeCN (**Figure 3.17**) showed an initial conversion of 23 % with 4-nitrothioanisole which was slightly lower than the result achieved under normal batch conditions (**Table 3.5**). Following centrifugation and washing a recycle was carried out with thioanisole. This resulted in a conversion of 48 % which was a decrease of only 2 % on the result found previously under the same conditions. Finally the sulfide was replaced with ethyl phenyl sulfide. This time a decrease in activity of 27 % was observed compared to an experiment carried out under the same conditions, suggesting there is very little potential for tandem recycling in MeCN.

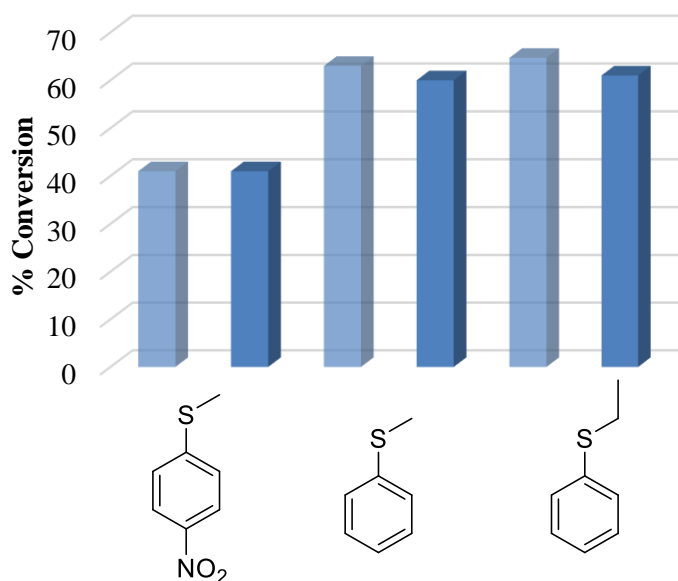
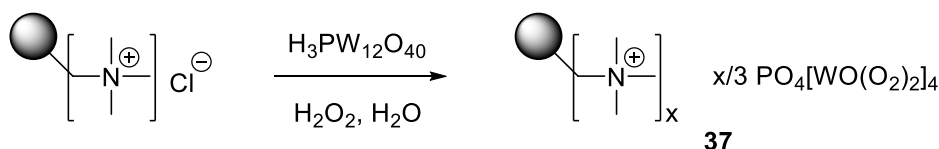


Figure 3.18 Tandem recycling of POM@PIILP **36** in EtOH with 4-nitrothioanisole followed by thioanisole and ethyl phenyl sulfide; Transparent = Ref. value from single batch reaction in substrate screening.

The tandem recycle in EtOH (**Figure 3.18**) showed an initial conversion of 41 % which is in agreement with the result achieved for 4-nitrothioanisole under normal batch conditions (**Table 3.6**). This time the tandem recycle with thioanisole resulted in a conversion of 60 % which was a decrease of only 3 % on the result found previously under the same conditions, comparable to the decrease seen with MeCN. However when the sulfide was replaced with ethyl phenyl sulfide a decrease in activity of only 4 % was observed compared to an experiment carried out under the same conditions. This result was extremely promising and suggested a greater potential for recycling in an EtOH based system over MeCN.

3.9 Comparisons with Commercially Available Systems

In order to determine the validity of the results found with the POM@PIILP systems **34**, **35** and **36**, two more catalysts, **37** and **40**, were synthesised from commercially available resins.



Scheme 3.6 Synthesis of functionalised Amberlite **37** via loading of Amberlite IRA 900 chloride form with Venturrello POM species.

Scheme 3.6 shows the peroxometalate loading of the ion exchange resin Amberlite which afforded the functionalised Amberlite species **37**. This was prepared in water with hydrogen peroxide using an excess of the POM species and washed with water and diethyl ether. Silver

nitrate was used to check for the presence of chloride in the filtrate and a signal at 6.9 ppm in the solid state ^{31}P NMR spectra confirmed the presence of $[\text{PO}_4\{\text{WO}(\text{O}_2)_2\}_4]^{3-}$.

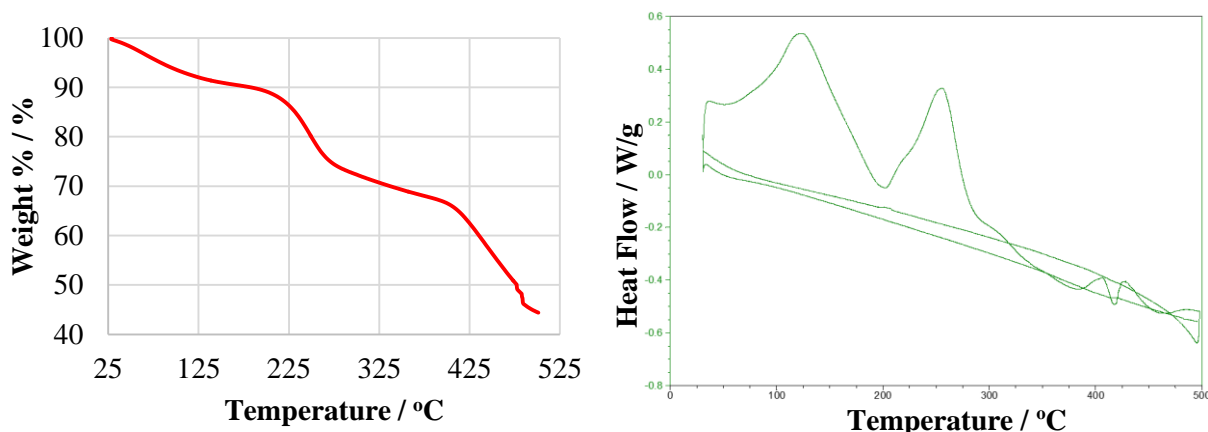
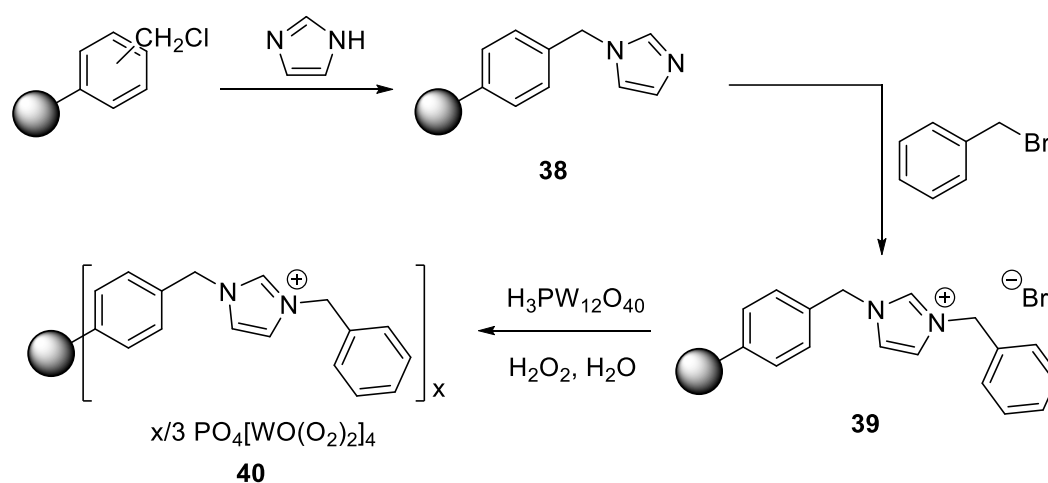


Figure 3.19 TGA/ DSC traces for functionalised Amberlite **37** showing two large decomposition events at ~ 200 °C and also ~ 400 °C.

The TGA/DSC of the functionalised Amberlite (**Figure 3.19**) showed a decomposition event at ~ 200 °C and also ~ 400 °C. The final weight % for PIILP **37** was 44 %, and assuming this remaining material is that of the POM this would suggest a lower POM loading than the previously synthesised PIILP materials which contained in the region of 60 % above 500 °C. A POM loading of $0.223 \text{ mmol g}^{-1}$ as calculated from the elemental analysis supports this observation.

Scheme 3.7 shows the two-step synthesis of POM@PIILP **40** from Merrifield resin **38**. Following quaternisation with benzyl bromide the functionalised Merrifield species **39** was loaded with POM to afford PIILP **40** as a fine white powder.



Scheme 3.7 Synthesis and loading of POM@ functionalised Merrifield resin.

As with the Amberlite, the TGA (**Figure 3.20**) showed a low final weight percentage of 24 %, however the elemental analysis didn't fully support this observation with a POM loading of $0.413 \text{ mmol g}^{-1}$. This calculated loading could be slightly higher than expected as a result of solvent/ water trapped within the cross-linked Merrifield network.

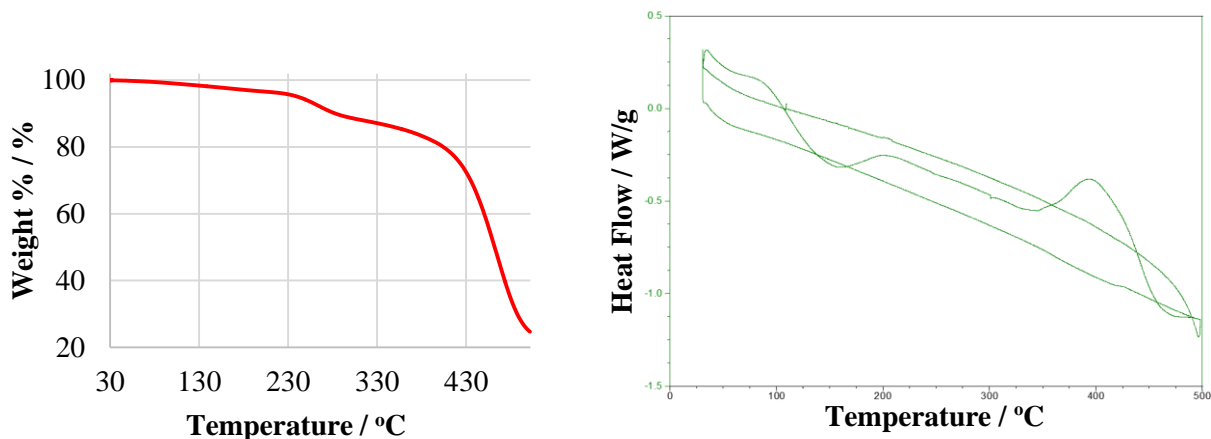


Figure 3.20 TGA/ DSC traces for functionalised Merrifield resin **40** showing a decomposition event at $\sim 250 \text{ }^\circ\text{C}$ followed by a large step decomposition just above $\sim 400 \text{ }^\circ\text{C}$.

SEM imaging of the Merrifield resin before and after functionalisation (**Figure 3.21**) demonstrates the dramatic effect that the processing has had on the polymer morphology. The spherical beads have been largely destroyed resulting in a catalyst which is predominantly granular.

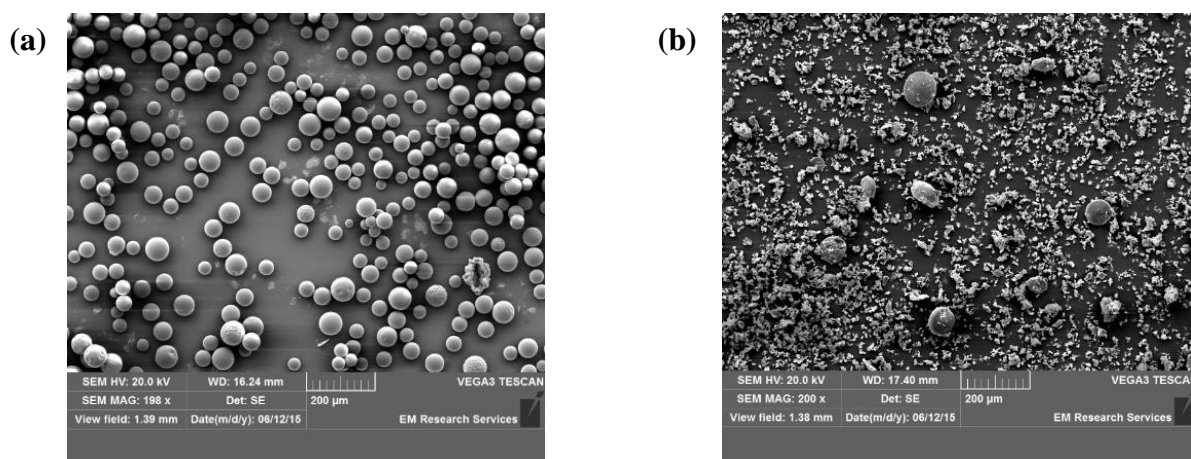
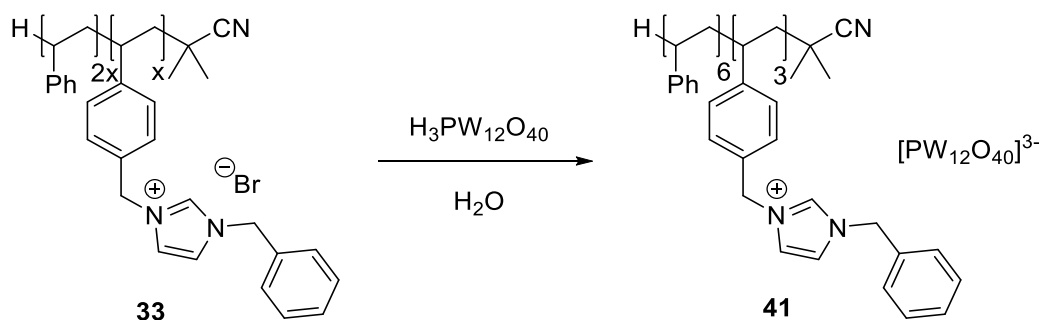


Figure 3.21 SEM images of (a) Merrifield resin showing spherical beads and (b) POM@Merrifield resin **40** revealing largely granular material as a result of destruction of the beads.

The final catalyst synthesised for the purpose of comparison was the phosphotungstic acid loaded PIILP **41**. Polymer **33** was loaded with phosphotungstic acid in the absence of hydrogen peroxide to determine the importance of pre-forming the active Venturello POM species (**Scheme 3.8**).



Scheme 3.8 Loading of Keggin POM on to polymer **33** in the absence of hydrogen peroxide to afford the phosphotungstic acid loaded polymer **41**.

The solid state ^{31}P NMR spectra showed a single peak at -15.1 ppm, characteristic of the Keggin POM species. The IR spectrum also shows the appearance of characteristic bands at 1077 cm^{-1} $\nu(\text{P-O})$, 974 cm^{-1} $\nu(\text{W=O}_{\text{terminal}})$, 894 cm^{-1} $\nu(\text{W-O}_a\text{-W, octahedral edge-sharing})$ and 799 cm^{-1} $\nu(\text{W-O}_b\text{-W, octahedral edge-sharing})$. From the elemental analysis a Keggin POM loading of 0.251 mmol g^{-1} was calculated for POM@PIILP **41**.

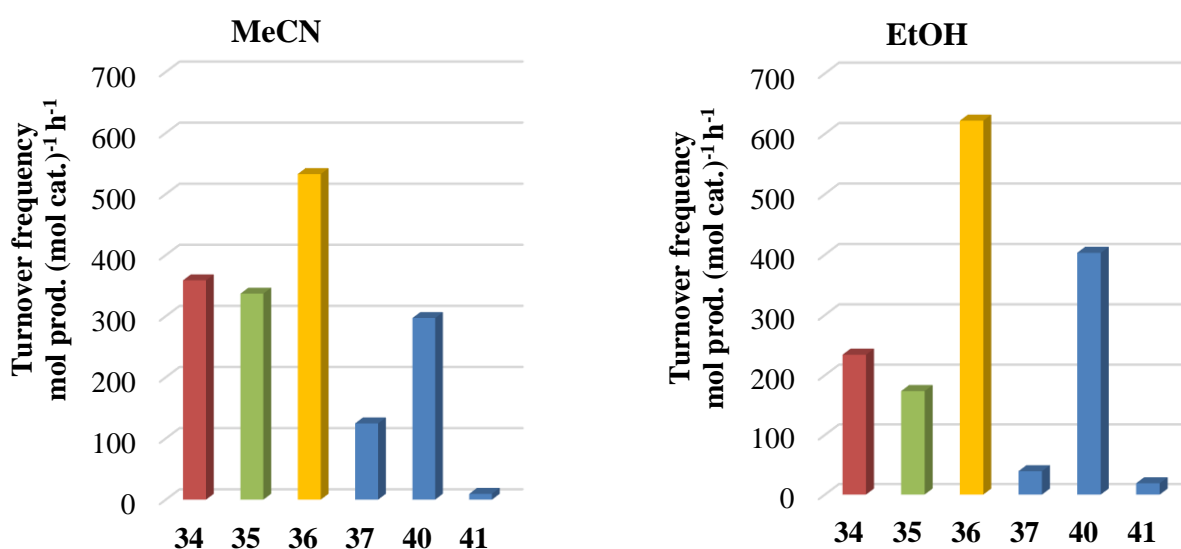


Figure 3.22 Catalyst comparison of turnover frequencies obtained with thioanisole in both MeCN and EtOH.

Catalyst testing was carried out on thioanisole under the standard reaction conditions. A comparison of the turnover frequencies achieved with the commercial resin-based catalysts to POM@PIILPs **34-36** is shown in **Figure 3.22**. Pleasingly it is clear that the polymer loaded with the Keggin POM@PIILP **41** has achieved minimal turnover frequency indicating that the activated Venturello anion is essential for catalytic activity. The POM@ functionalised Amberlite PIILP **37** also performed relatively poorly in both solvents compared to even the poorest performing imidazolium PIILP system. The functionalised Merrifield resin performed comparatively to catalysts **34** and **35** in MeCN and even outperformed them in EtOH. As the

structure of these catalysts is predominantly polystyrene based this wasn't a completely unexpected result as there will be similarities in the polymer morphologies. The benzylated imidazole POM@PIILP **36** performed substantially better than both commercially available materials and subsequently was selected for further investigation and application.

3.10 Effects of Dilution on Polyphosphotungstate Loading

As the Venturello POM species is prepared before it is loaded on to the polymer material in solution, there was a question of whether the dilution of the polymer at the loading stage would have an effect on PIILP material, due to a variation in the number of inter- and intramolecular polymer interactions, and its catalytic performance. Two further POM@PIILP **36** analogues were synthesised, loading the same polymer, **33**, with the activated POM species under more dilute and more concentrated conditions. PIILP **42** was loaded in a tenfold increase in polymer dilution, while PIILP **43** was loaded under doubly concentrated conditions which was the highest achievable concentration as a result of reaching the solubility limit of polymer **33** in EtOH.

The characterisation data for both of these catalysts was consistent with that found for catalyst **36** and can be found in **Appendix 4**. From the elemental analysis a POM loading of 0.464 mmol g⁻¹ for POM@PIILP **42** and 0.895 mmol g⁻¹ for POM@PIILP **43** was calculated.

Table 3.8 summarises the turnover frequencies achieved at the varied POM loading dilutions in both MeCN and EtOH.

Catalyst	TOF / mol prod. (mol cat.) ⁻¹ h ⁻¹	
	MeCN	EtOH
36	533	622
42	527	577
43	189	172

Table 3.8 Turnover frequencies at varying polymer dilutions with thioanisole in MeCN and EtOH.

Increasing the dilution appears to have little to no effect on the performance of the catalyst in MeCN or EtOH while under more concentrated conditions a dramatic drop in catalytic activity is evident. This effect could be a result of the POM being unevenly distributed throughout the polymer network resulting in less 'active sites' for catalysis to take place.

3.11 Sulfide Oxidation Under Flow Conditions

This extensive evaluation of the POM@ polystyrene based imidazolium supported catalysts demonstrates them to be both highly active and selective for sulfoxide under mild reaction

conditions while also being recyclable, this makes them ideal candidates for use in scaled up, heterogeneous synthesis. In recent years, continuous flow chemistry has been extensively studied as a means of achieving effective scale up of reactions, acting as an intermediary between laboratory scale chemistry and industrial scale plant manufacturing.

Reactions performed in flow reactors have some key advantages over batch scale work, in particular superior heat and mass transfer, mixing control, increased process safety, ease of scale-up and the possibility to include automated product purification and analysis.^[118]

Flow chemistry is best described by the principles of microfluidics. This term is used to define any flow device with dimensions ranging from millimetres to micrometres that has a volume capacity of fluid in the range of nano- to microliters (10^{-9} – 10^{-6} L). It is an area of particular interest, not only in high-throughput synthesis but also in analytical chemistry, microbiological analysis and any application where portability and the ‘lab on chip’ concept is an advantage.^[119]

Under microfluidic conditions the narrow channels in which the reaction occurs significantly increase the surface area to volume ratio. This high ratio greatly assists heat transfer, allowing for more rapid, efficient and uniform heating to occur in the reaction media.^[120] Mixing is critical in the effectiveness of microfluidic flow systems and there are two types of flow which may be occurring in such systems, laminar and turbulent. Such flow patterns are typically defined in terms of their Reynolds number (Re). This can be defined as the ratio of momentum forces to viscous forces and as a result quantifies their relative importance in given flow conditions. Given that we employ a packed bed column the Reynolds number can be defined as:^[121]

$$\text{Re} = \frac{\rho v_s D}{\mu}$$

where: ρ = density of fluid (kg/m^3)

v_s = superficial velocity (m/s)

D = diameter of particles (m)

μ = dynamic viscosity of fluid (kg/m.s)

Under our reaction conditions flow was carried out in both MeCN and EtOH and this would equate to Reynolds numbers of between 0.007 and 0.221 in MeCN and 0.003 to 0.076 in EtOH. Given that laminar flow conditions apply up to $\text{Re} = 10$ and fully turbulent conditions in excess of $\text{Re} = 2000$ we would expect laminar flow to be predominant in our system and as such the component streams will mix only by diffusion while present on the column reactor.^[122]

3.11.1 Segmented flow

In order to achieve rapid reaction screening without the need to establish the steady state of a continuous flow process, segmented flow conditions were utilised in which a particular volume of reaction solution is passed through the flow system by a carrier solvent, requiring considerably less reagent. As such the initial optimisations were carried out under segmented flow conditions by Jack R. Ellison as part of a study into sulfide oxidation utilising ROMP based pyrrolidinium PIILP catalysts, which was used as the basis for the proof of principle of our styrene based system.^[116]

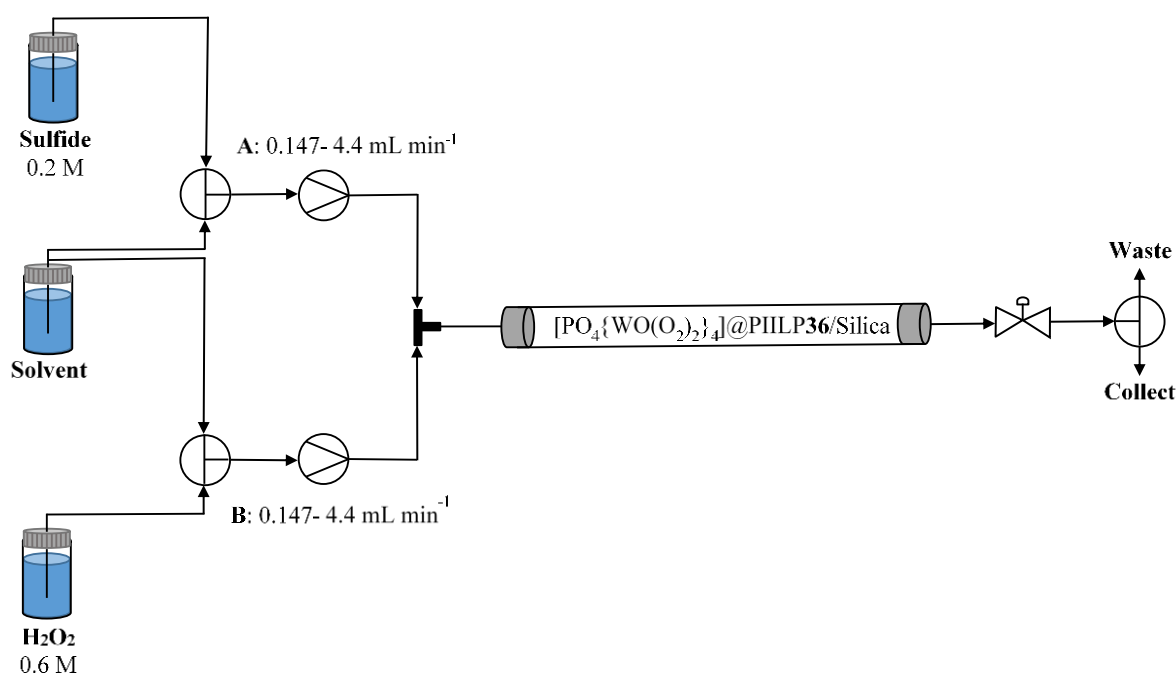


Figure 3.23 Schematic of the segmented flow sulfoxidation carried out on the Uniqsis FlowSyn reactor at 30 °C.

The optimised process was carried out on a Uniqsis FlowSyn reactor (**Figure 3.23**) using two reagent reservoirs of sulfide (0.2 M) and 35 % hydrogen peroxide (0.6 M) which were simultaneously pumped through separate selection valves which can select a central solvent reservoir to act as the mobile phase. Mixing of the two streams occurred at a T-piece before the combined mixture was passed through a column reactor packed with the heterogeneous catalyst contained in a heating jacket. As POM@PIILP **36** had proved to be highly active under very mild batch conditions it was decided that the amount of catalyst could be reduced by using a mixture of PIILP catalyst (0.1 g) and silica (2.0 g of Geduran® Si60 43 – 60 μm), which would also provide an increased reactor bed length to give appropriate residence times. The process was carried out at 30 °C as this had been shown to provide the optimum balance between conversion and sulfoxide selectivity during the previous study.^[116] As the stoichiometry of the reaction was controlled through the concentration of the reagent solutions, each pump could be

set at the same flow rate and the residence times could then be calculated based on the combined flow rates to minimise the error in the system which could arise from varying flow rates. 2 mL aliquots of the product stream were collected in duplicate and subjected to the standard sulfoxidation aqueous workup used for the batch reactions and the product analysed by ^1H NMR.

Using the optimum flow conditions, the influence of residence time on the conversion-selectivity profile was explored for the sulfoxidation of thioanisole in acetonitrile and ethanol (**Figure 3.24**).

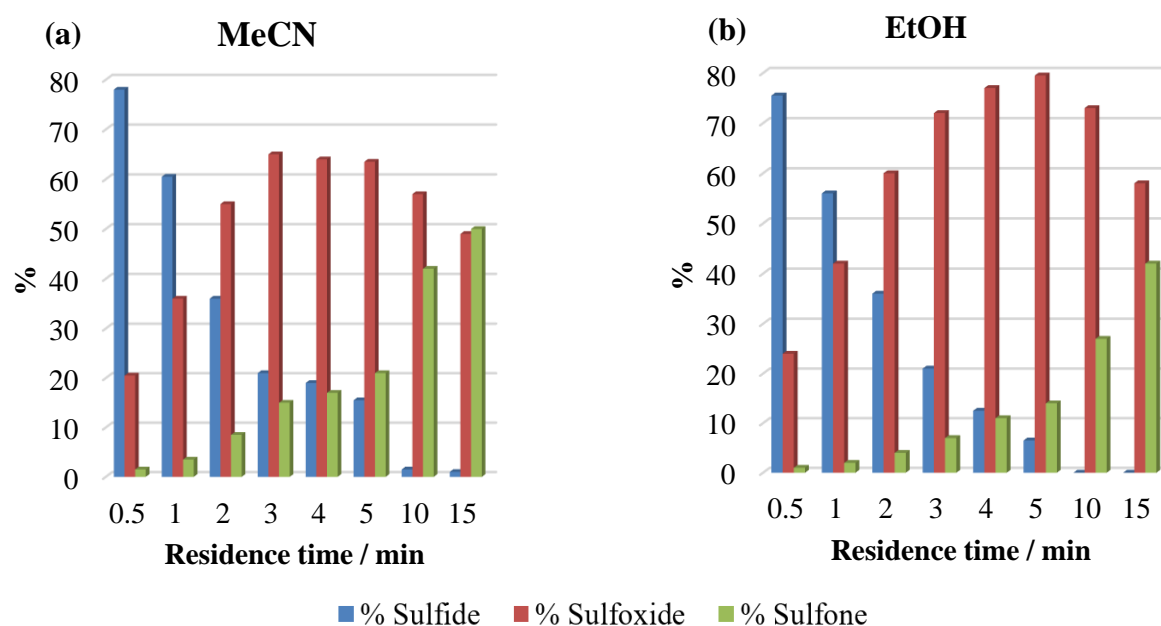


Figure 3.24 Segmented flow with thioanisole catalysed by POM@PIILP **36** at 30 °C in (a) MeCN, (b) EtOH. Residence time (min) = column volume (4.4 mL) / flow rate (x mL min⁻¹).

The results with thioanisole employing acetonitrile as the mobile phase showed that conversions increased incrementally with increasing residence time from 23 % for a residence time of 0.5 min to 81 % for a 4 min residence time. It was also shown that high selectivity for sulfoxide was maintained for residence times of between 3 and 5 min, however selectivity decreased quite dramatically at longer residence times with the eventual effect being that sulfone was obtained as the major product with a 15 min residence time. In comparison the conversion-selectivity profile in ethanol was broadly similar and interestingly the optimum compromise between conversion and sulfoxide selectivity of 87 % and 88 % respectively was also obtained at a residence time of 4 min which was a significant improvement on that in acetonitrile. Therefore, the data in **Figure 3.24** clearly indicates that a high selectivity for sulfoxide can be obtained under continuous flow processing at the optimum reaction conditions with a prudent choice of residence time and solvent.

To put these results in to context a comparison can be drawn to the pyrrolidinium based ROMP system previously investigated within the research group and as discussed in Chapter 1 (**Figure 3.25**). This species was prepared as part of a much larger investigation into ROMP based PIILP materials and their utilisation in flow based epoxidation and sulfoxidation.^[116]

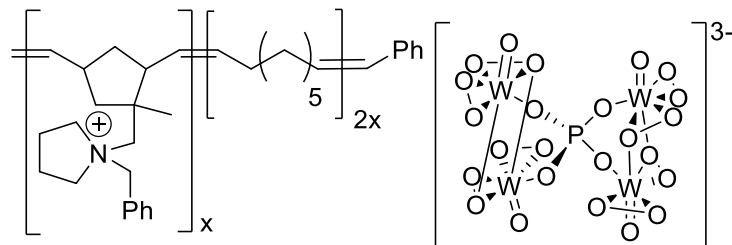


Figure 3.25 Pyrrolidinium-POM species synthesised via ROMP by J. R. Ellison.

The structural similarities between catalyst **36** and the pyrrolidinium species are the ionic pendant which features a benzylated pyrrolidinium analogue to the imidazolium of **36** and the immobilisation of the same Venturello POM species. The results obtained with this catalyst under the same segmented flow conditions with thioanisole are shown (**Figure 3.26**).

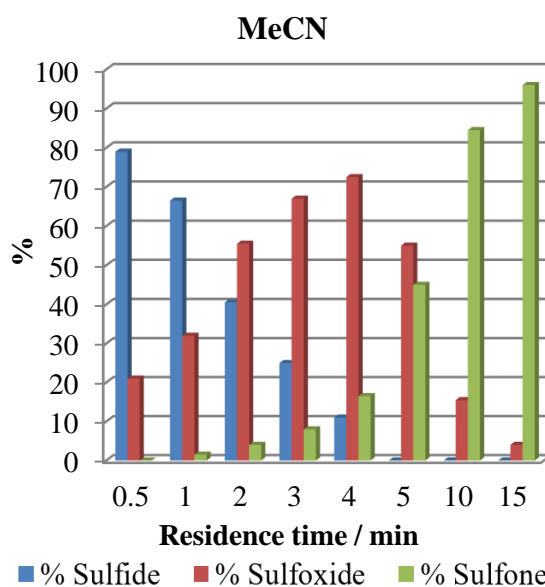


Figure 3.26 Segmented flow with thioanisole catalysed by pyrrolidinium PIILP at 30 °C in MeCN. Residence time (min) = column volume (4.4 mL) / flow rate (x mL min⁻¹).

The results with the pyrrolidinium catalyst showed a slight increase in conversion and selectivity for a 4 minute residence of 90 % and 96 % respectively. It was also shown that after 15 min the sulfone was being obtained as the major product in 96 % selectivity, indicating potential for obtaining both compounds under flow conditions. Given that the synthetic route to the pyrrolidinium catalyst involves 6 steps and incorporates the use of Grubbs 1st generation catalyst and results in poor yield, these increases in conversion and selectivity were deemed to be minimal. As previously discussed in Chapter 2, the experimental simplicity of the styrene

based PIILP materials enables them to be synthesised in large quantities which is ideal for study on the flow system.

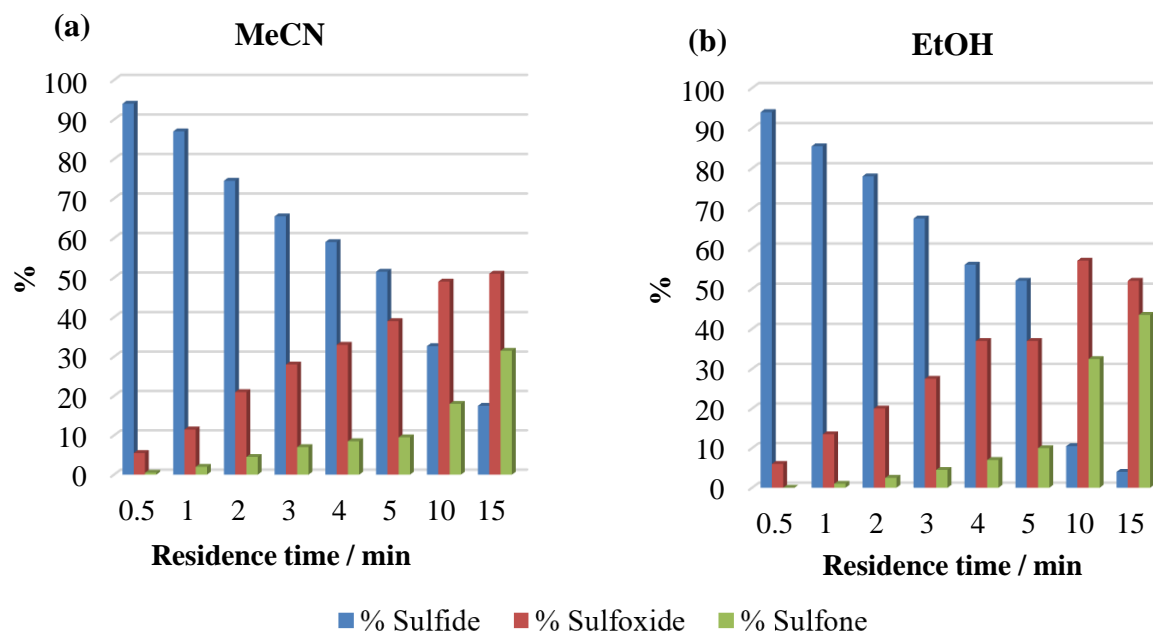


Figure 3.27 Segmented flow with 4-nitrothioanisole catalysed by POM@PIILP **36** at 30 °C in (a) MeCN, (b) EtOH. Residence time (min) = column volume (4.4 mL) / flow rate ($\times \text{mL min}^{-1}$).

Still utilising the optimised conditions, the substrate range was extended to establish the scope and efficiency of this system. **Figure 3.27** shows the segmented flow profiles achieved with 4-nitrothioanisole in both acetonitrile and ethanol. Slightly longer residence times were required in order to achieve sulfoxide selectivity along with reasonable conversions in both solvents with the optimum appearing to peak at a flow rate of 0.44 mL min^{-1} ($R_t = 10 \text{ min}$).

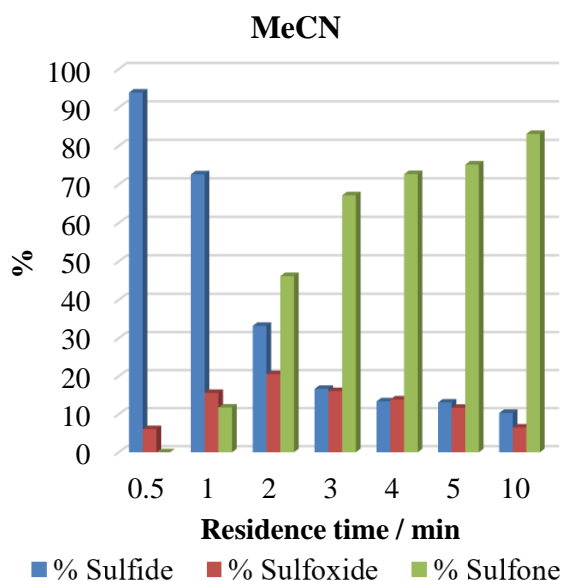


Figure 3.28 Segmented flow with dibenzothiophene catalysed by POM@PIILP **36** in MeCN at 90 °C. Residence time (min) = column volume (4.4 mL) / flow rate ($\times \text{mL min}^{-1}$).

In order to establish the potential for the application of this system to the sulfoxidation of crude oil impurities, an initial investigation utilising dibenzothiophene, a more challenging sulfide typically contained in crude oil, was carried out (**Figure 3.28**). Preliminary runs under our standard reaction conditions indicated that sufficient conversion could not be achieved at 30 °C so the temperature was increased to 90 °C. Under these conditions sulfone was obtained as the major product with a conversion of 90 % and in 93 % selectivity at a flow rate of 0.44 mL min⁻¹ (Rt = 10 min). This result proved promising for the scope of this particular study and for future applications of this system.

3.11.2 Continuous flow

The encouraging performance of PIILP **36** under segmented flow conditions and its potential for recyclability lead to a scaled-up continuous flow study conducted in both acetonitrile and ethanol.

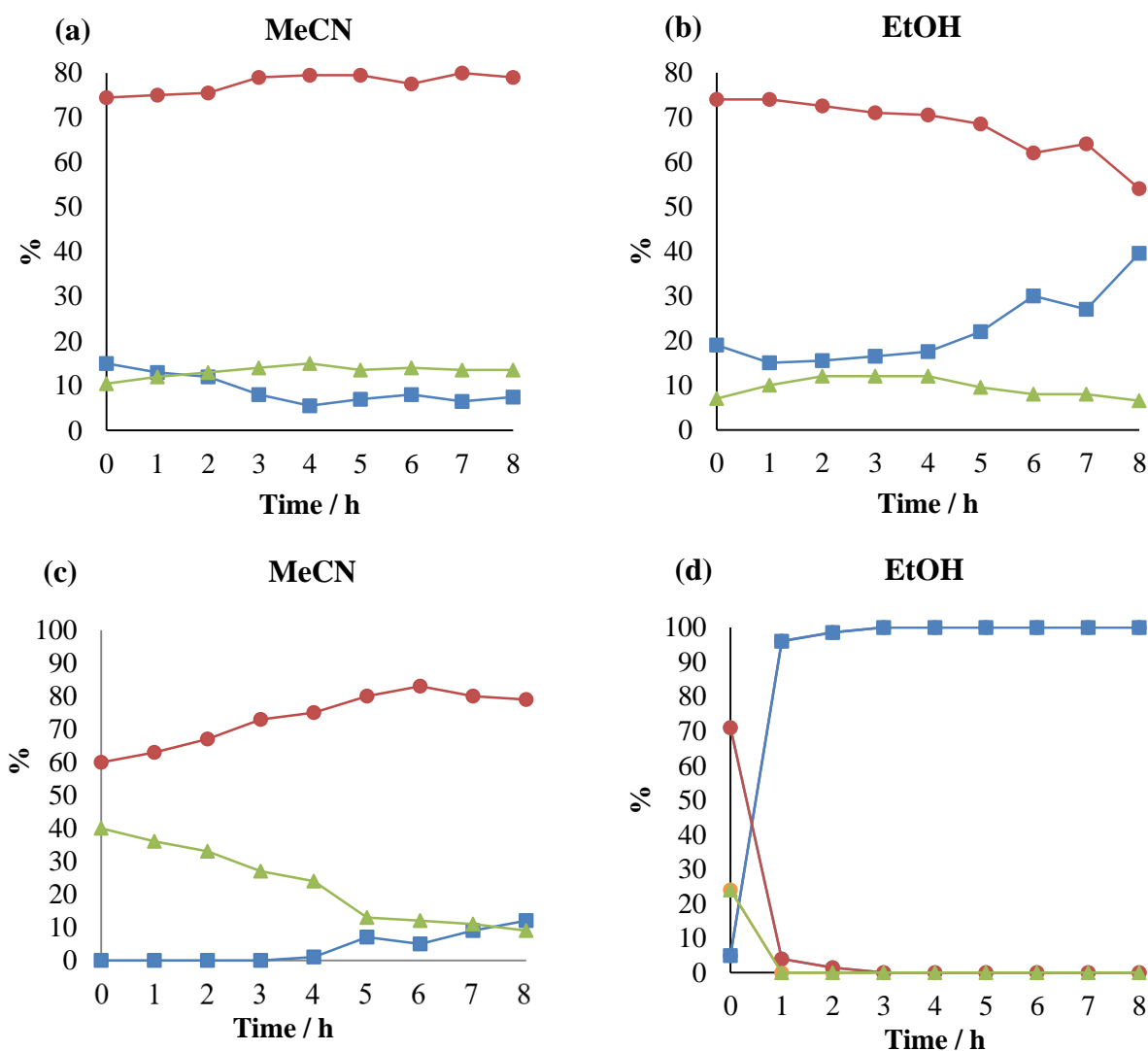


Figure 3.29 Continuous flow profiles with thioanisole at 30 °C with a residence time of 4 min in (a) MeCN catalysed by POM@PIILP **36**, (b) EtOH catalysed by POM@PIILP **36**, (c) MeCN catalysed by POM@TBA, (d) EtOH with POM@TBA. H₂O₂ replenished after 4 h. ■ Sulfide, ● Sulfoxide, ▲ Sulfone.

A flow rate of 1.1 ml min^{-1} corresponding to a residence time of 4 min was selected and monitored over 8 h. In order to assess the merits of the PIILP based system a comparative lifetime study was also carried out on POM@TBA which consisted of a mixture of $[\text{NBu}_4]_3[\text{PO}_4\{\text{WO}(\text{O}_2)_2\}_4]$ and silica containing a W content representative of that in the flow reactor column, to assess the robustness and longevity of the PIILP based system.

Figure 3.29 shows the time-performance profiles of POM@PIILP **36** and the POM@TBA in both acetonitrile and ethanol. In both systems the hydrogen peroxide reagent stream was replenished after 4 h to ensure that peroxide decomposition was not having an effect on the system. In acetonitrile PIILP **36** showed virtually no decrease in activity as evidenced by the conversion remaining at 92 % after 8 h. In ethanol the catalytic activity remained relatively constant up to 4 h then decreased gradually throughout the final 4 h. This loss of activity could be a result of leaching of the POM species being facilitated by the more polar mobile phase. Under the same conditions the POM@TBA did initially exhibit higher activity than catalyst **36** in both solvents, encouragingly however a dramatic decrease in conversion and an increase in sulfoxide selectivity was observed in acetonitrile, while in ethanol the catalytic activity had almost completely ceased after just 1 h. This result suggests that the POM species is simply being stripped from the silica as soon as it comes in to contact with the mobile phase.

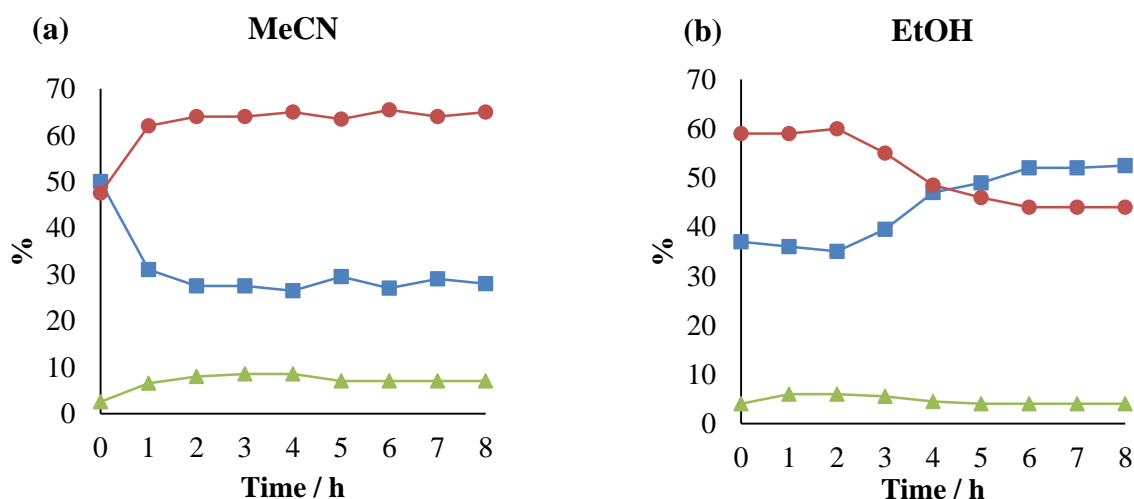


Figure 3.30 Continuous flow profiles with thioanisole at $30 \text{ }^\circ\text{C}$ with a residence time of 4 min in (a) MeCN catalysed by POM@Merrifield **40**, (b) EtOH catalysed by POM@Merrifield **40**. H_2O_2 replenished after 4 h. ■ Sulfide, ● Sulfoxide, ▲ Sulfone.

These results indicated promising long term stability of $[\text{PO}_4\{\text{WO}(\text{O}_2)_2\}_4]$ @PIILP **36** for the continuous flow oxidation of thioanisole in acetonitrile and clearly demonstrate the merits of the PIILP based system as opposed to the SILP methodology.

In order to quantify the effectiveness of our particular PIILP system, the POM@PIILP **40** based on the commercially available Merrifield resin was subjected to the same continuous flow conditions in both acetonitrile and ethanol (**Figure 3.30**). Although the system shows good promise for sustained catalytic activity in MeCN, when compared to our POM@PIILP **36** system, the conversion after 8 h is 20 % lower. In EtOH the reduced catalytic activity is even more evident, performing poorly from time zero and decreasing throughout unlike catalyst **36** which sustained performance over the initial 4 h.

3.12 Conclusions

Via a simple three or four step synthesis requiring no purification it was possible to produce three styrene based imidazolium pendant decorated $[\text{PO}_4\{\text{WO}(\text{O}_2)_2\}_4]\text{@PIILP}$ catalysts as amorphous insoluble solids in high yields, which were fully characterised by a range of techniques. The benzylated imidazolium POM@PIILP **36** has been shown to be highly efficient in the oxidation of a range of sulfides under mild reaction conditions utilising hydrogen peroxide as the oxidant in short reaction times. High selectivity for sulfoxide was achieved at room temperature in both acetonitrile and the more ‘green’ ethanol, outperforming PIILP systems synthesised from commercially available resins. The effect on catalysis of the nature of the cationic polymer support suggested that a more cationic imidazolium moiety was facilitating oxidation and the addition of the benzyl group was potentially increasing the hydrophobicity of the system leading to increased activity. However, it may be an oversimplification to attribute these effects purely to the nature of the polymeric support due to the multisite nature of the active catalyst anion.

A full kinetic profile of the oxidation of 4-nitrothioanisole and dibenzothiophene was obtained and showed relative rates of the first and second oxidations. A promising recycling study in both solvents was achieved via simple centrifugation of the catalyst achieving good conversion over several runs which lead to the extension of POM@PIILP **36** to application in flow processes. A segmented flow process utilising a column reactor packed with a mixture of PIILP **36** and silica achieved high conversion and sulfoxide selectivity at a short residence time of 4 min corresponding to a flow rate of just 1.1 mL min^{-1} in both ethanol and acetonitrile. A lifetime study showed the catalyst to be extremely robust in acetonitrile and a stable activity selectivity profile was achieved under continuous flow conditions for 8 h, highlighted both by its outperformance of the PIILP system based on commercially available resin and the extremely poor performance of the analogous POM@TBA SILP system which demonstrated a dramatic reduction in catalyst performance with time. There is still room for future improvement

however as the continuous flow process still requires an aqueous work up which leaves scope for future optimisation of this particular system.

Given that the optimisation of the system was carried out one variable at a time in a straightforward manner it is possible that the true optimum performance of the system has not been achieved but rather a local optimum. With this in mind it may be valuable to explore avenues such as design of experiments to achieve a more definitive set of optimum conditions both in batch and under flow conditions. The success of this system, given its relatively high degree of cost in comparison to more experimentally simplistic systems will ultimately be determined by its activity and recyclability under continuous flow conditions.

Ultimately the POM@PIILP **36** system has proven its potential for scale up and transferral of PIILP systems to industrial processes and also for the oxidative desulfurisation of crude oil as will be discussed in Chapter 4.

Chapter 4. Application of Imidazolium PIILP to Sulfide Removal from a Model Oil

4.1 Introduction

The refining of crude oil requires it to undergo desulfurisation as sulfur is the most abundant heteroatom impurity, and its price is dependant, among several factors, upon its sulfur content. Over recent years the desulfurisation of fuels has become an area of increasing interest due in part to legislation aimed at reducing the sulfur content of diesel and gasoline to less than 10 ppm by 2010 with a view to producing sulfur free fuels in subsequent years.^[123] These sulfur impurities are converted to SO_x by combustion and are a major contributing factor in air pollution and acid rain formation. The total amount of sulfur in crude oil is typically in the region of 0.1 – 5.0 % depending upon the particular type of crude.^[124] The nature of sulfur compounds varies with distillation range and the general trend shows that sulfur content increases with boiling point as demonstrated by Heinrich and Kasztelaan (**Table 4.1**).^[125]

Distillation range / °C	Sulfur content / %	Sulfur compound distribution / %			
		Thiols	Sulfides	Thiophenes	Other*
70-180	0.02	50	50	trace	-
160-240	0.2	25	25	35	15
230-350	0.9	15	15	35	35
350-550	1.8	5	5	30	60
>550	2.9	trace	trace	10	90

Table 4.1 Distribution of sulfur compounds over the distillation range of a crude oil with total sulfur content of 1.2%. * = Benzothiophenes, dibenzothiophenes and heavy sulfides.

The most prominent current industrial method for the removal of these impurities is a catalytic hydrodesulfurisation (HDS). This process involves passing a feed of oil and hydrogen through a fixed-bed reactor packed with the HDS catalyst. This catalyst is typically NiMo/ Al₂O₃ with hydrotreating conditions ranging from 200 to 425 °C and 1- 18 MPa, depending on the degree of desulfurisation required and the nature of the sulfur compounds within the crude.^[126] During this process the sulfur of the organosulfur compounds is converted to H₂S which can then subsequently be converted into elemental sulfur or sulfuric acid (H₂SO₄). Although it is possible to fully remove aliphatic sulfur via this process, thiophenes and in particular dibenzothiophene are much more difficult to remove. This is a result of the lone pair of electrons on sulfur participating in the π -electron structure of the aromatic system. This resonance stabilisation is

typically around $120\text{--}130\text{ kJ mol}^{-1}$,^[127] sufficient enough to make HDS energetically demanding in terms of both high hydrogen pressure and operating temperatures which are both costly and environmentally undesirable. Resonance stabilisation of thiophenes also prevents cracking and as a result most thiophenic sulfur compounds form coke during fluid catalytic cracking.^[128]

Recently several alternative methods to HDS have been investigated. These include extraction with ionic liquids,^[129] selective absorption,^[130] bioprocesses^[131] and oxidative desulfurisation (ODS).^[132] The most promising of these has so far proven to be a combination of ODS and extraction into ionic liquids to remove sulfur containing compounds such as dibenzothiophene (DBT) and its alkyl substituted derivatives from fuel.^[133] This technique incorporates a suitable oxidation catalyst such as a peroxophosphomolybdate^[134] or tungstate^[133] species in an ionic liquid. The sulfide species is then extracted into the ionic liquid layer where it will remain following oxidation to its corresponding sulfone, due to the increase in polarity. The oil can then be isolated via a simple separation (**Figure 4.1**).

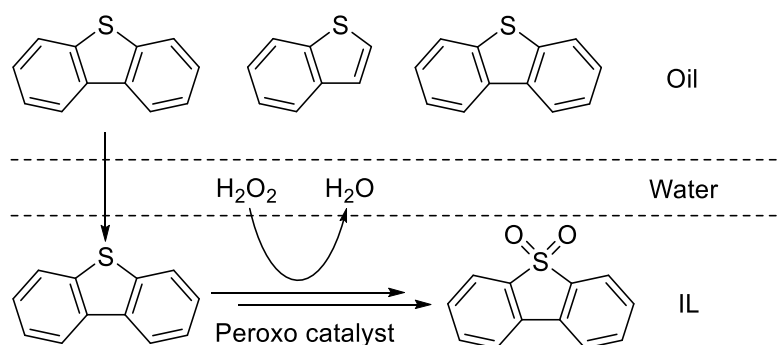


Figure 4.1 Concept of ODS with ionic liquid extraction.

The oxidant used has been the subject of several studies however hydrogen peroxide has proven to be the most desirable oxidant due to its low cost, availability and environmental compatibility as water is the only by-product.^[135] Li and Lu *et al.* have successfully utilised extraction and catalytic oxidative desulfurisation (ECODS) on a model oil containing 1000 ppm sulfur in *n*-octane with 1 mol % phosphotungstic acid and 3 equivalents of H_2O_2 . They screened a range of ionic liquids and found that after 1 h at $30\text{ }^\circ\text{C}$ [bmim][BF_4] removed 98.2 % of dibenzothiophene, 74.6 % of 4,6-dimethylbenzothiophene and 65.7 % of benzothiophene at $30\text{ }^\circ\text{C}$ after 1 h. After 3 h with an increased temperature of $70\text{ }^\circ\text{C}$ complete removal of each substrate was achieved. The ionic liquid-catalyst mixture recycled five times, showing a drop in efficiency from 98.2 to 96.1%.

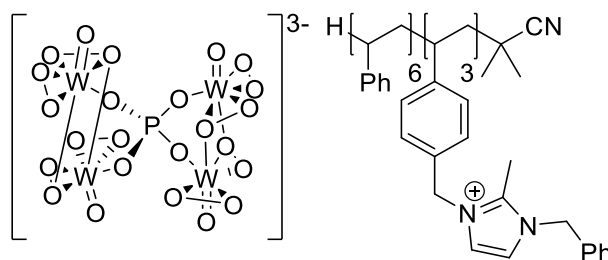


Figure 4.2 Peroxophosphotungstate loaded benzylated imidazolium POM@PIILP **36**.

Although effective this technique does require large quantities of ionic liquid which remains prohibitively expensive for industrial application. With this in mind this work was used as the basis for which the POM@PIILP **36** catalyst (**Figure 4.2**) could be evaluated to determine its effectiveness in the oxidative desulfurisation of model crude oil.

4.2 Model Oil Sulfide Removal System Optimisation

Initial system optimisation was carried out on a model oil which was prepared by dissolving DBT in *n*-octane to give a corresponding sulfur content of 1000 ppm, representative of that contained in diesel fuel. Due to the miscibility of EtOH in octane, MeOH was chosen as the conventional solvent layer to facilitate extraction. Following reaction with vigorous mixing to ensure efficient extraction both the octane and MeOH were subjected to an aqueous work up. Determination of the sulfide removal percentage was calculated by ^1H NMR analysis of both the octane and MeOH layers relative to a 1,3-dinitrobenzene NMR standard to establish mass balance.

4.2.1 Reaction temperature optimisation

A range of temperatures from room temperature up to 80 °C were carried out with MeOH as the extraction solvent for a 30 min reaction time and it was shown that the percentage of sulfur extracted increased with increasing temperature (**Figure 4.3**). Between room temperature and 45 °C a gradual small increase in removal was observed from 22 – 27 %. By 60 °C a very promising 48 % of the sulfur had been removed in the relatively short reaction time. Upon a further 20 °C increase the sulfur extracted only increased to 61 %. In order to limit the environmental impact of the final process, an optimum temperature of 60 °C was established.

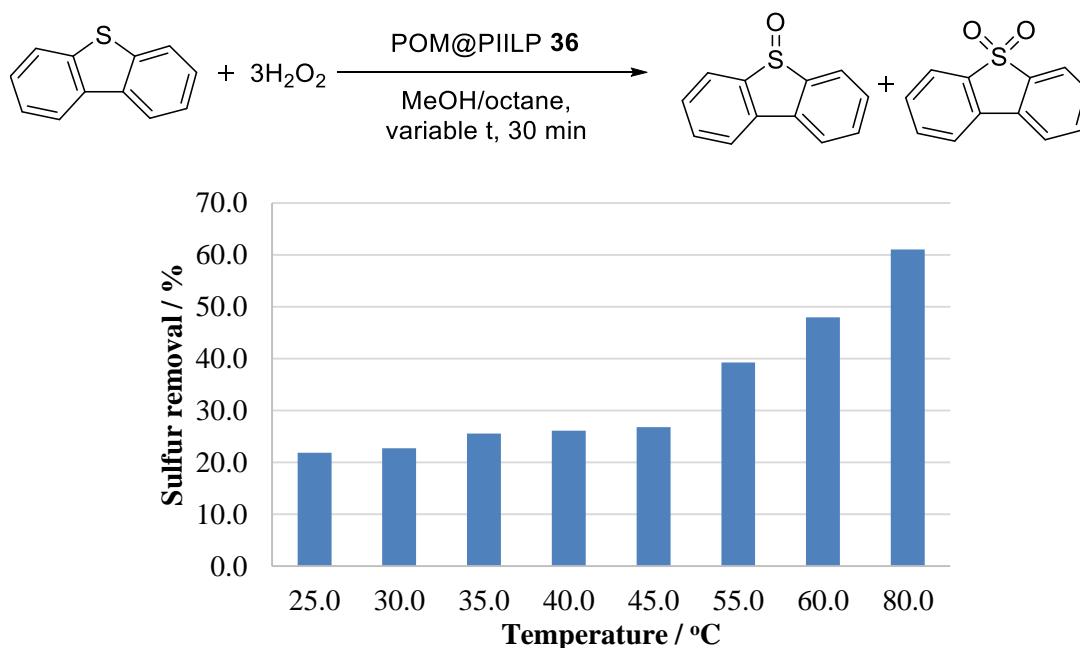


Figure 4.3 Sulfur removal temperature optimisation. ^a POM@PIILP 36 (8.7 mg, 1.0 mol %), dibenzothiophene (0.33 mmol), MeOH (4 mL), octane (10 mL), 35% H₂O₂ (1.0 mmol), 30 min. ^b Conversion measured by ¹H NMR (average of 2 runs).

4.2.2 Catalyst loading optimisation

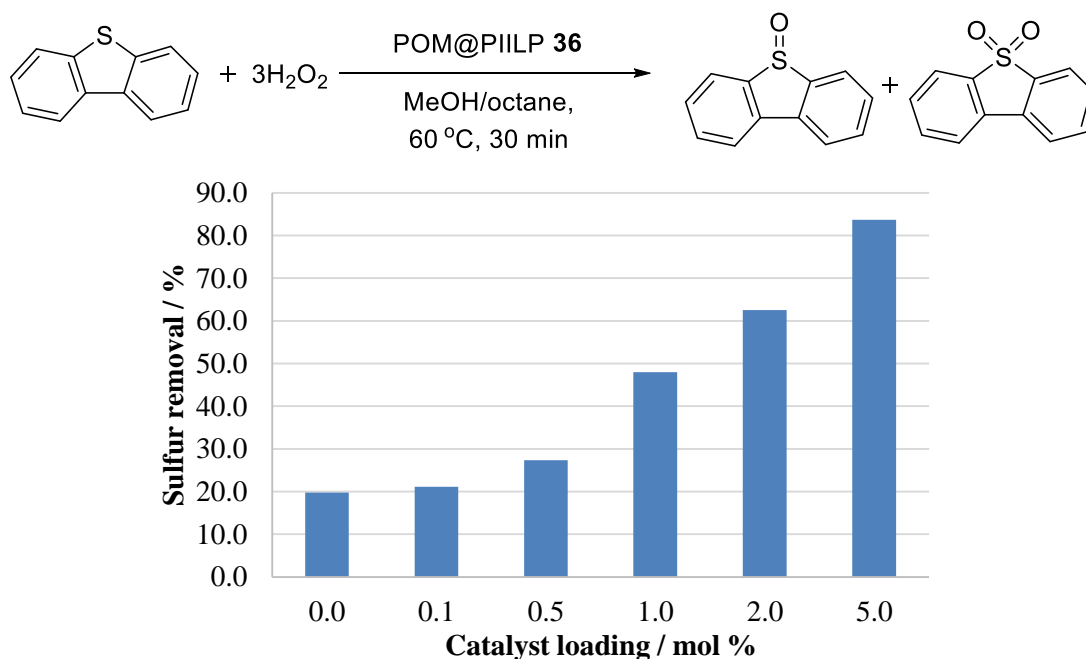


Figure 4.4 Sulfur removal catalyst loading optimisation. ^a POM@PIILP 36, dibenzothiophene (0.33 mmol), MeOH (4 mL), octane (10 mL), 35% H₂O₂ (1.0 mmol), 60 °C, 30 min. ^b Conversion measured by ¹H NMR (average of 2 runs).

In order to establish the influence of the DBT/ catalyst loading, reactions were carried out at 60 °C in the presence of POM@PIILP 36 catalyst loadings ranging from 0 – 5.0 mol %. Gratifyingly the sulfur removal was limited to less than 20 % when no catalyst was present in the system, indicating that this is essential if sulfur removal is to exceed the amount possible

via simple phase transfer in the presence of hydrogen peroxide. The results clearly indicate the catalyst dosage is a key factor in reaction activity and a maximum 84 % removal was achieved with 5 mol % catalyst, however, due to the large amount of material required it was deemed unsuitable for the system. The 48 % sulfur removal as previously demonstrated with 1 mol % catalyst was determined to be the optimum balance between removal and catalyst loading.

4.2.3 Peroxide concentration optimisation

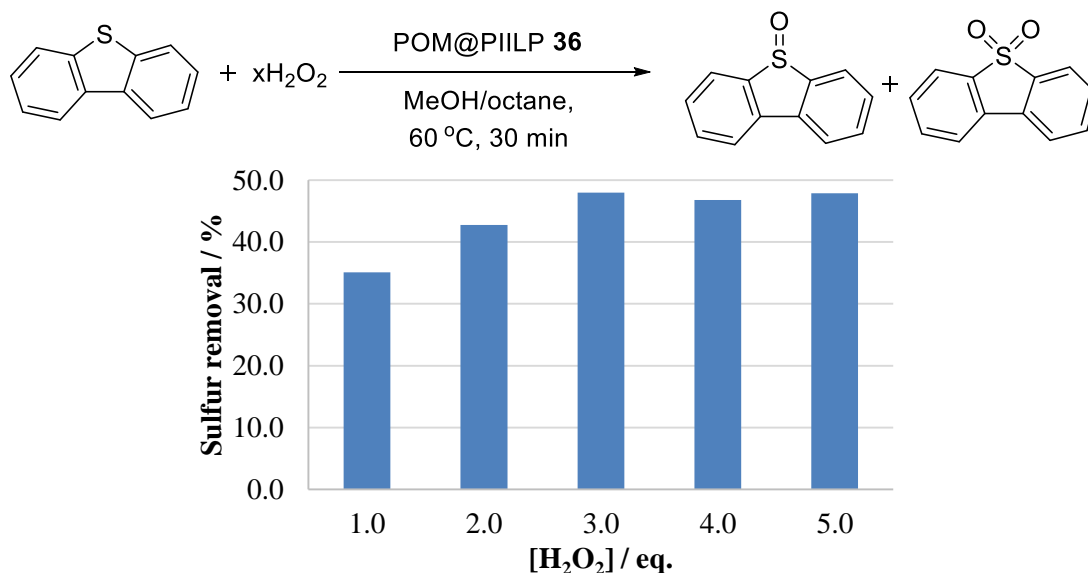


Figure 4.5 Sulfur removal peroxide concentration optimisation. ^a POM@PIILP **36** (8.7 mg, 1.0 mol %), dibenzothiophene (0.33 mmol), MeOH (4 mL), octane (10 mL), 35% H₂O₂, 60 °C, 30 min. ^b Conversion measured by ¹H NMR (average of 2 runs).

The final aspect of the desulfurisation system to undergo optimisation was the determination of the effect of the amount of oxidation agent. Reactions were carried out at 60 °C for 30 min under varying H₂O₂/ sulfur molar ratios. The stoichiometry of the reaction indicates that 2 equivalents of oxidant are required for 1 equivalent of sulfur. **Figure 4.5** shows that the ratio had a strong influence on the reaction and with a deficiency of oxidant present at 1.0 equivalents the sulfur removal could only proceed to 35 %. However, upon increasing this to 3.0 equivalents of hydrogen peroxide, 48 % removal was achieved. Further increase in peroxide concentration did not afford improvements in reaction activity hence 3.0 equivalents of peroxide was determined to be the optimum amount. Thus, the optimised set of conditions for sulfur removal from model oil reactions were 1.0 mol % of POM@PIILP **36** catalyst in MeOH, 60 °C and 3.0 equivalents of H₂O₂.

4.3 Kinetic Study on Model Oil

Under the optimised reaction conditions, the progress of sulfur removal from model oil was monitored as a function of time. The batch reaction conditions were scaled up and the reaction sampled at regular intervals. **Figure 4.6** shows the plot obtained as an average of two kinetic runs.

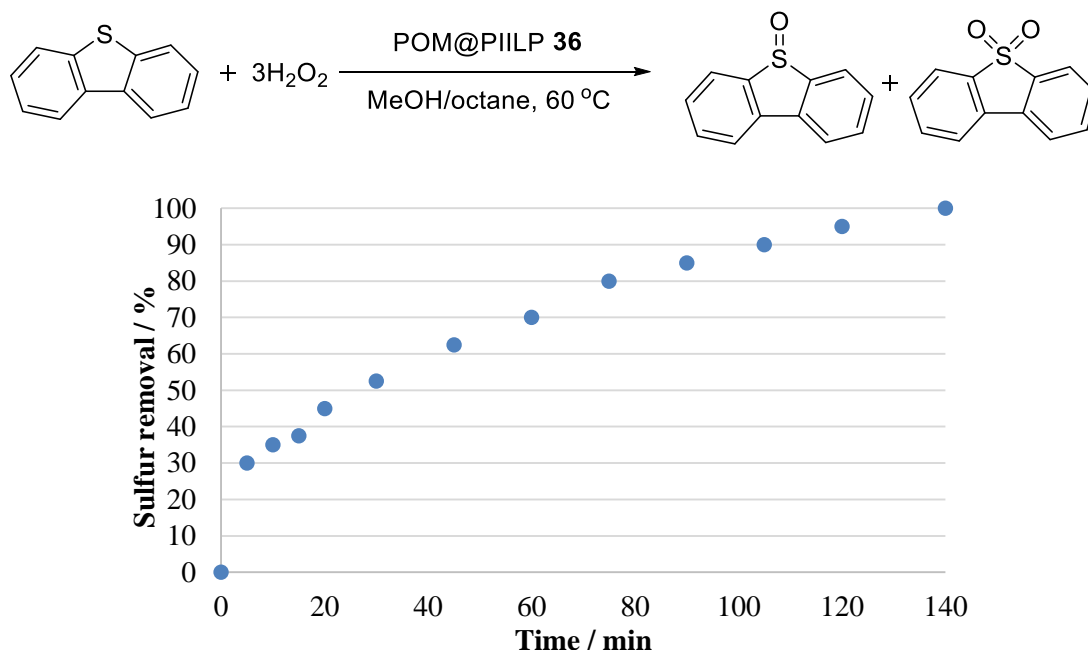


Figure 4.6 Kinetic study of sulfur removal from model oil. ^a POM@PIILP **36** (8.7 mg, 1.0 mol %), dibenzothiophene (0.33 mmol), MeOH (4 mL), octane (10 mL), 35% H₂O₂ (1.0 mmol), 60 °C. ^b Conversion measured by ¹H NMR (average of 2 runs).

The results showed a continuous increase in the removal of DBT in *n*-octane with increasing time. The initially fast rate of removal and subsequent slowdown could be a result of a reduction in mixing efficiency as the reaction proceeds and the catalyst becomes deposited on the walls of the reaction vessel. Gratifyingly the results showed that 100 % removal was achieved by 140 min at 60 °C. This result shows a similar level of performance to two separate biphasic ionic liquid based systems developed by Li *et al.* utilising phosphotungstic acid in [bmim]BF₄ and also decatungstate complexes in [bmim]PF₆.^[132-133] They were able to achieve 100 % DBT removal in 3 h at 70 °C with their phosphotungstic acid based system and 98.2 % DBT removal in 1 h at 50 °C with their decatungstate based system.

4.4 Recyclability Study

To assess the robustness and potential merits for this system to be transferred to continuous flow, catalyst recycles were performed with POM@PIILP **36** on the extraction of dibenzothiophene from model oil in MeOH (**Figure 4.7**). Utilising the same system as was

implemented for sulfur oxidation in the previous chapter, the catalyst was isolated via centrifugation, washed with the reaction solvent and reused without being replenished. The results show a decrease in performance of just over 10 % upon 1 recycle followed by a stabilisation in performance and a subsequent dramatic decrease following the third recycle.

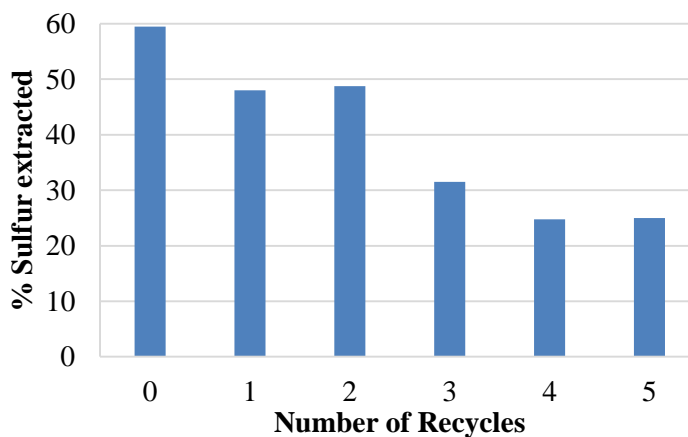


Figure 4.7 Recycling of POM@PIILP **36** for the extraction of sulfur from model oil. ^a POM@PIILP **36** (4.4 mg, 1.0 mol %), dibenzothiophene (0.17 mmol), MeOH (2 mL), octane (5 mL), 35% H₂O₂ (0.5 mmol), 60 °C. ^b Conversion measured by ¹H NMR (average of 2 runs).

This reduction in performance has initially been attributed to a loss of material upon separation of the model oil from the MeOH. As the reaction was carried out on a small scale to facilitate isolation of the catalyst via filtration, small losses in catalyst material have equated to large decreases in sulfur removal. Further investigation including working at a much increased scale will be required to determine the true recyclability of the system. Compared with the current literature however, this approach does appear to be an avenue worth exploring as very little processing of the catalyst is required, unlike biphasic ionic liquid based systems, which require the IL phase to be distilled typically for around 10 h at 70 °C before further recycles can be performed, so clearly there is potential for this system to afford a ‘greener’ process.^[132]

4.5 Application to Sulfide Removal from Arab Light Crude Oil

In order to further establish the potential for application of this system to an industrial clean-up of crude oil some initial screening experiments were carried out on crude oil. The crude oil chosen was Arab Light crude which is sourced from Saudi Arabia and has a sulfur content of 1.97 % by mass and American Petroleum Institute (API) gravity of 32.8°. These figures indicate that the oil is ‘sour’ as it has a sulfur content of > 1.0 % weight and consists of primarily short hydrocarbon chains as indicated by a high API value. Two reactions were carried out in parallel, one in the presence of POM@PIILP **36** and the other with no catalyst present. In order to determine the sulfur content of the samples they were submitted for CHNS elemental analysis

before and after the desulfurisation had taken place. The reaction conditions and results obtained are shown in **Table 4.2**.

Entry ^a	Sulfur content / % mass ^b
1	2.05
2	1.79
3	1.52

Table 4.2 Sulfur removal from Arab Light crude oil; Entry 1 – Arab light crude oil before processing, Entry 2 – following reaction with no catalyst present, Entry 3 – following reaction in the presence of POM@PIILP **36**. ^a Reaction conditions based upon optimisations: POM@PIILP **36** (4.4 mg, 1.0 mol %), crude oil (5 mL), MeOH (2 mL), 35% H₂O₂ (0.5 mmol), 60 °C, 140 min. ^b Conversion measured by elemental analysis.

The results of this initial screening experiment showed a 26 % reduction in sulfur content of the crude oil in the presence of catalyst **36** while only 13 % of sulfur was removed when the catalyst was not present indicating that the success of the process is dependent upon the presence of the catalyst.

4.6 Future Work

Although many of the results obtained in this oxidative desulfurisation investigation were very promising there are areas that can be extended to achieve a more comprehensive investigation by other members of the research group to enable more satisfactory conclusions to be established.

As previously mentioned, an increase in the scale of a recycling study may reduce the error associated with loss of material following centrifugation and separation of the phases. An extension of the kinetic study at different temperatures would enable a more thorough comparison to the systems currently in the literature and may lead to further optimisation of the system. It would also be prudent to carry out the desulfurisation on a model oil containing other sulfides and a mixed sulfide system. In particular, benzothiophene is another impurity which often proves particularly resistant to deep desulfurisation of crude oil via HDS and with further investigation in to this substrate this could lead to a greater percentage of sulfur removal from the Arab Light crude oil.

As the ultimate goal of this investigation is its transferral to a continuous flow desulfurisation process this remains the focus of future work. Following on from some initial screening work on the Flowsyn it is apparent that with some simple modifications made to the flow setup

described in Chapter 3, an operationally straightforward and environmentally benign oxidative desulfurisation system for model oil may be achievable (**Figure 4.8**).

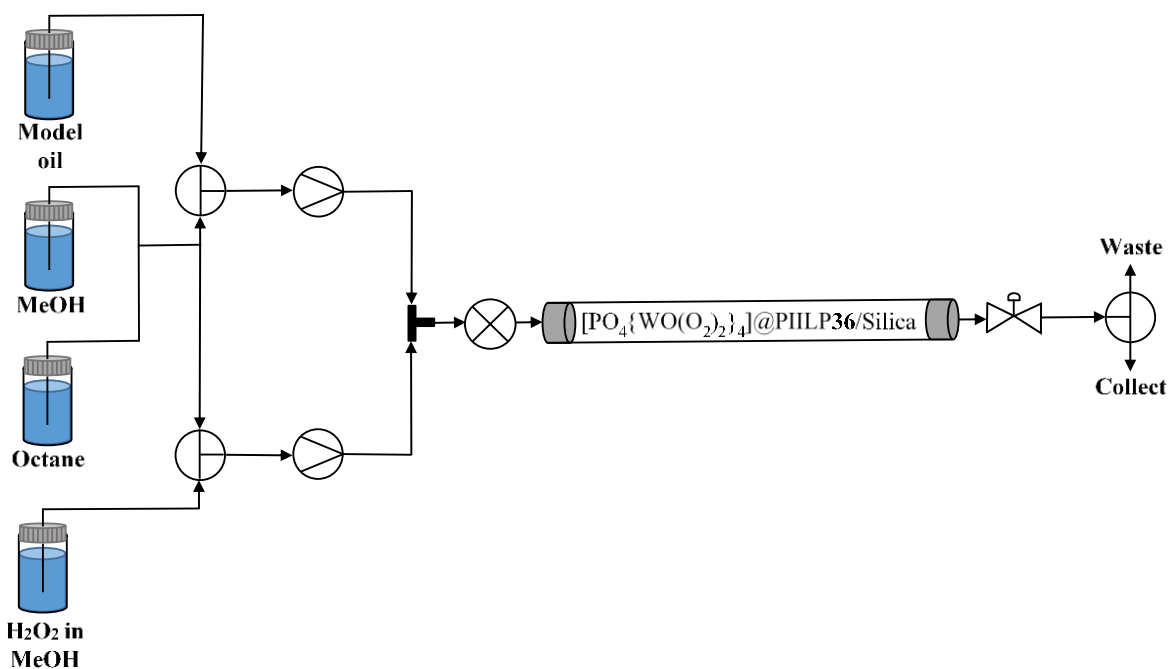


Figure 4.8 Schematic of proposed Uniqsis FlowSyn setup for model oil oxidative desulfurisation.

The key modifications of such a system would be the introduction of reservoirs of both MeOH and octane to act as carrier solvents along with the presence of a mixer chip before the catalyst column to ensure effective mixing within the system.

4.7 Conclusions

Utilising the styrene based benzylated imidazolium pendant decorated $[\text{PO}_4\{\text{WO}(\text{O}_2)_2\}_4]@\text{PIILP}$ catalyst **36** prepared as described in Chapter 3 it was possible to apply this system to the oxidative desulfurisation of model oil. PIILP catalyst **36** was shown to be highly efficient and achieved 100 % removal of sulfur in the form of DBT in the presence of MeOH after 140 min at 60 °C. Current literature shows comparable results were obtained with peroxotungstate catalysts in biphasic systems exhibiting 100 % removal at temperatures between 50 °C and 70 °C in under 3 hours.^[132-133] However, a system utilising the acidic ionic liquid $[\text{bmim}]\text{HSO}_4$ as both the extractant and catalyst was reported to exceed these results with a 100 % DBT removal at 60 °C in 30 min.^[135]

A recyclability study showed promise for the system to be recycled under more environmentally benign conditions than the current method employed with biphasic ionic liquid based systems which also report up to 5 cycles at best.^[133] Initial screening reactions of the oxidative

desulfurisation of Arab Light crude oil also afforded promising results and a 26 % reduction in sulfur content.

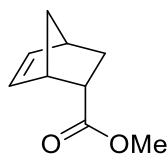
Although this study has acted as an initial proof of principle there is still much scope for further optimisation and development of the system. As in Chapter 3 it may be wise to optimise the system more extensively by utilising a design of experiments approach to find the systems true optimum at a range of temperatures in a systematic and efficient manner. Ultimately the success or failure of this particular system will be determined by its effectiveness as a desulfurisation method under continuous flow conditions.

Chapter 5. Experimental

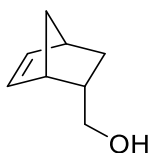
5.1 General Comments

All manipulations involving air-sensitive materials were carried out using standard Schlenk line techniques under an atmosphere of nitrogen in flame-dried glassware. All dry solvents were distilled under an atmosphere of nitrogen with; CHCl_3 and CH_2Cl_2 from CaH_2 ; MeOH and EtOH from magnesium; THF and Et_2O from Na / benzophenone; toluene from sodium; CH_3CN from K_2CO_3 ; DMF from vacuum distillation. All chemicals were bought from commercial suppliers and used as received without further purification. ^1H and $^{13}\text{C}\{^1\text{H}\}$ NMR spectra were recorded on either a Bruker Avance III HD 500, JEOL ECS-400 or a Bruker Avance III 300 spectrometer. All ^1H / ^{13}C NMR were referenced relative to CDCl_3 ($\delta_{\text{H}} = 7.26$, $\delta_{\text{C}} = 77.16$) or d_6 -DMSO ($\delta_{\text{H}} = 2.50$, $\delta_{\text{C}} = 39.52$). FT-IR spectroscopy was performed on a Varian 800 FT-IR instrument (Varian Inc.). CHN analysis was performed on a Carlo Erba 1108 Elemental Analyser and controlled with Carlo Erba Eager 200 software. Thermogravimetric analysis (TGA) performed using a PerkinElmer Thermogravimetric Analyser with a heating rate of $10\text{ }^\circ\text{C min}^{-1}$. Gas chromatography was performed using a Shimadzu 2010 series gas chromatograph with a Supelco Beta DEX column. Total flow 92.5 mL/min; column flow 1.76 mL/min; pressure 21.2 psi; makeup flow 30 mL/min; H_2 flow 40 mL/min; air flow 400 mL/min. TEM images were obtained on a FEI Tecnai 12 G2 transmission electron microscope fitted with a CCD camera. SEM images were obtained on a Tescan Vega 3LMU scanning electron microscope with digital image collection. XPS was conducted using a Theta Probe from Thermo Scientific. Mass spectra were recorded on a Micromass LCT Premier Mass Spectrometer. Gel permeation chromatography (GPC) was conducted on a Varian ProStar instrument (Varian Inc.) equipped with a Varian 325 UV-vis dual wavelength detector (254 nm), a Viscotek 3580 differential RI detector, and a pair of PL gel $5\text{ }\mu\text{m}$ Mixed D 300×7.5 mm columns with guard column (Polymer Laboratories Inc.) in series. Near monodisperse polystyrene standards (Polymer Laboratories) were used for calibration. Data collection was performed with Galaxie software (Varian Inc.) and chromatograms analysed with the Cirrus software (Varian Inc.). Thin layered chromatography was carried out on aluminium sheets pre-coated with silica gel 60F 254 and column chromatography was performed using Merck Kieselgel 60. Melting points were obtained on a Stuart SMP3 instrument. All new compounds were fully characterised. Full characterisation for known compounds can be found from the literature references. See **Appendix 5** for representative GC, GPC, FTIR and MS traces.

5.2 Experimental Procedures Chapter 2

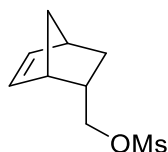
**Endo-bicyclo[2.2.1]hept-5-en-2-carboxylic acid methyl ester (1).**^[136]

A flame dried, 3-neck 250 mL round-bottomed flask under N₂ was charged with methyl acrylate (10.5 mL, 116 mmol) in toluene (25 mL). The resulting solution was stirred and cooled to 0 °C. Boron trifluoride diethyl etherate (1.43 mL, 11.6 mmol, 10 mol %) was added to the solution followed by freshly cracked cyclopentadiene (19.5 mL, 232 mmol) which was added to the cold solution drop-wise. After the addition was complete the reaction mixture was stirred for 3 h. The crude reaction mixture was poured onto 10 % sulfuric acid (100 mL) and ice. The organic layer was washed with sodium carbonate solution (100 mL) until basic and then washed with saturated brine (50 mL). The organic layer was then dried (MgSO₄), filtered and the solvent removed under reduced pressure to afford the crude product. The crude product was dissolved in CH₂Cl₂ (20 mL) and silica was added to the solution and the solvent was removed under reduced pressure to afford a free flowing powder. The mixture was applied to a silica column and the product was eluted with 10: 90 ethyl acetate: petrol. This afforded the *endo*-norbornene ester **1** as an orange oil (17.21 g, 97 %). ¹H NMR (400 MHz, CDCl₃, δ): 6.17 (dd, *J* = 5.6, 3.0 Hz, 1H, *H*-C=C-*H*), 5.91 (dd, *J* = 5.6, 2.8 Hz, 1H, *H*-C=C-*H*), 3.61 (s, 3H, O-CH₃), 3.18 (br s, 1H, *CH*-CH=CH-*CH*), 2.93 (dt, *J* = 9.3, 3.9 Hz, 1H, *CH*(CO₂Me)), 2.89 (br s, 1H, *CH*-CH=CH-*CH*), 1.89 (m, 1H), 1.40 (m, 2H), 1.26 (d, *J* = 8.1 Hz, 1H); ¹³C NMR (100 MHz, CDCl₃, δ): 175.0, 137.6, 132.3, 51.3, 49.5, 45.6, 43.1, 42.5, 29.17; FT-IR (neat, cm⁻¹): $\tilde{\nu}$ = 3062, 2975, 2951, 2877, 1733, 1435, 1336, 1271, 1196, 1175, 1031, 900, 849, 839, 776, 710. This is consistent with data reported in the literature.^[137]

**Endo-5-hydroxymethylbicyclo[2.2.1]hept-2-ene (2).**^[138]

A flame dried, 3-neck 1 L round-bottomed flask under N₂ was charged with lithium aluminium hydride (6.53 g, 172 mmol) in dry THF (100 mL). The mixture was stirred and cooled to 0 °C in an ice bath. *Endo*-bicyclo[2.2.1]hept-5-en-2-carboxylic acid methyl ester **1** (11.9 g, 78.2

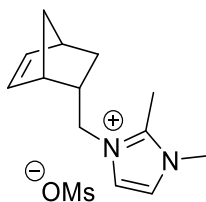
mmol) was dissolved in dry THF (50 mL) and added drop-wise to the reaction mixture. The mixture was allowed to warm to room temperature and stirred for 18 h. The reaction mixture was cooled to 0 °C and then portions of water (65 mL), 3M potassium hydroxide (195 mL) and water (65 mL) were sequentially added slowly by syringe pump. The reaction mixture was stirred under reflux for 2.5 h. Celite was added to the reaction mixture and the product solution was decanted off. The celite was then washed with Et₂O and the combined organic layers were dried (MgSO₄), filtered and the solvent removed under reduced pressure to afford the *endo*-norbornene alcohol **2** as a pale yellow oil (8.97 g, 92 % yield). **¹H NMR** (400 MHz, CDCl₃, δ): 6.13 (dd, *J* = 5.8, 3.1 Hz, 1H, *H*-C=C-*H*), 5.95 (dd, *J* = 5.7, 2.9 Hz, 1H, *H*-C=C-*H*), 3.39 (dd, *J* = 10.5, 6.5 Hz, 1H, CH₂OH), 3.24 (dd, *J* = 10.4, 8.9 Hz, 1H, CH₂OH), 2.91 (br s, 1H, CH-CH=CH-CH), 2.80 (br s, 1H, CH-CH=CH-CH), 2.28 (m, 1H, CH(CO₂Me)), 1.81 (ddd, *J* = 11.6, 9.3, 3.9 Hz, 1H), 1.42 (m, 2H), 1.25 (d, *J* = 8.2 Hz, 1H), 0.50 (ddd, *J* = 7.1, 4.4, 2.6 Hz, 1H); **¹³C NMR** (100 MHz, CDCl₃, δ): 137.5, 132.2, 66.6, 49.6, 43.6, 42.3, 41.7, 28.8; **FT-IR** (neat, cm⁻¹): $\tilde{\nu}$ = 3353, 3057, 2960, 2938, 2867, 1344, 1146, 1056, 1030, 718. This is consistent with data reported in the literature.^[138]



***Endo*-(bicyclo[2.2.1]hept-5-en-2-yl)methyl methanesulfonate (**3**).**^[75]

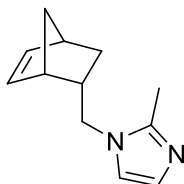
A flame dried 250 mL round-bottomed flask under N₂ was charged with *endo*-5-hydroxymethylbicyclo[2.2.1]hept-2-ene **2** (13.06 g, 105.2 mmol) in dry CH₂Cl₂ (50 mL) and the solution cooled to 0 °C. Methanesulfonyl chloride (8.95 mL, 116 mmol) in dry CH₂Cl₂ (20 mL) was added followed by the drop-wise addition of pyridine (10.2 mL, 126 mmol). The reaction mixture was allowed to warm to room temperature and left to stir for 16 h. The reaction mixture was washed with water (100 mL), 1M HCl (100 mL) and brine (4 x 100 mL). The organic material was dried (MgSO₄), filtered and the solvent removed under reduced pressure to afford the *endo*-mesyl norbornene **3** as a yellow oil (19.98 g, 94 %). **¹H NMR** (400 MHz, CDCl₃, δ): 6.18 (dd, *J* = 5.8, 3.1 Hz, 1H, *H*-C=C-*H*), 5.96 (dd, *J* = 5.7, 2.9 Hz, 1H, *H*-C=C-*H*), 3.97 (dd, *J* = 9.6, 6.6 Hz, 1H, CH₂OMs), 3.78 (t, *J* = 9.6 Hz, 1H, CH₂OMs), 2.97 (s, 3H, S(O₂)CH₃), 2.95 (br s, 1H, CH-CH=CH-CH), 2.83 (br s, 1H, CH-CH=CH-CH), 2.48 (m, 1H, CH-CH(CH₂(OMs))), 1.86 (ddd, *J* = 11.9, 9.3, 3.8 Hz, 1H), 1.47 (d, *J* = 8.4 Hz, 1H), 1.27 (d, *J* = 8.4 Hz, 1H), 0.54 (ddd, *J* = 7.0, 4.4, 2.7 Hz, 1H); **¹³C NMR** (100 MHz, CDCl₃, δ): 138.2,

131.8, 73.4, 49.4, 43.7, 42.2, 38.3, 37.2, 28.7; **FT-IR** (neat, cm^{-1}): $\tilde{\nu}$ = 2970, 2871, 1349, 1333, 1169, 942, 926, 848, 824, 722. This is consistent with data reported in the literature.^[75]



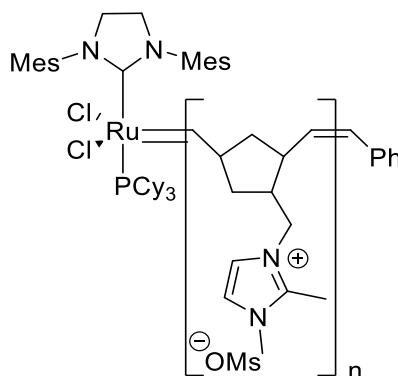
Endo-3-(bicyclo[2.2.1]hept-5-en-2-ylmethyl)-1,2-dimethyl-1H-imidazolium methanesulfonate (4).^[75]

A flame dried 2-neck 100 mL round-bottomed flask under N_2 was charged with *endo*-(bicyclo[2.2.1]hept-5-en-2-yl)methyl methanesulfonate **3** (3.00 g, 14.8 mmol) in dry toluene (2 mL) and 1,2-dimethylimidazole (1.43 g, 14.8 mmol) in dry toluene (2 mL). The reaction mixture was heated to reflux and stirred for 96 h. The solvent was removed under reduced pressure using an external trap. CH_2Cl_2 (10 mL) was added and the reaction mixture was added drop-wise into dry Et_2O (100 mL) under N_2 whilst stirring rapidly. A precipitate formed which was allowed to settle and the solvent was removed via cannula filtration. The product was washed with a further portion of dry Et_2O (100 mL) and the solvent was removed via cannula filtration. The product was dried under reduced pressure to afford the *endo*-norbornene mesylate **4** as a highly hygroscopic beige powder stored under N_2 . **^1H NMR** (400 MHz, CDCl_3 , δ): 7.56 (d, J = 2.1 Hz, 1H, N-CH=CH-N-CH₃), 7.22 (d, J = 2.1 Hz, 1H, N-CH=CH-N-CH₃), 6.30 (dd, J = 5.8, 3.1 Hz, 1H, H-C=C-H), 5.99 (dd, J = 5.8, 2.9 Hz, 1H, H-C=C-H), 3.92 (s, 3H, N-CH₃), 3.80 (t, J = 3.4 Hz, 2H, CH-CH₂-N), 2.87 (br s, 1H, CH-CH=CH-CH), 2.74 (br s, 1H, CH-CH=CH-CH), 2.69 (s, 3H, mesylate CH₃), 2.68 (s, 3H, N=C(CH₃)-N), 2.51 (m, 1H, CH-CH(CH₂N)), 1.92 (ddd, J = 12.0, 9.2, 3.8 Hz, 1H), 1.50 (d, J = 8.4 Hz, 1H), 1.28 (d, J = 8.6 Hz, 1H), 0.62 (ddd, J = 7.0, 4.4, 2.7 Hz, 1H); **^{13}C NMR** (100 MHz, CDCl_3 , δ): 139.6, 131.3, 123.2, 120.8, 52.6, 49.8, 44.2, 42.5, 39.6, 39.2, 35.8, 30.1, 10.4; **FT-IR** (neat, cm^{-1}): $\tilde{\nu}$ = 3104, 2973, 2938, 2874, 1617, 1584, 1538, 1458, 1426, 1209, 1181, 1039, 768, 732. This is consistent with data reported in the literature.^[75]



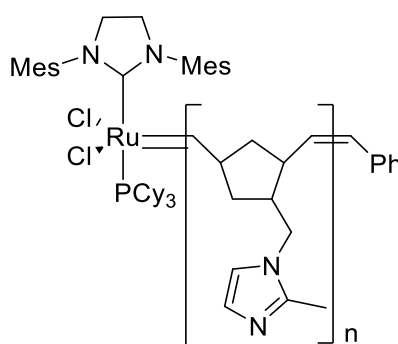
Endo-1-((bicyclo[2.2.1]hept-5-en-2-yl)methyl)-2-methyl-1H-imidazole (5).^[139]

A flame dried 100 mL round-bottomed flask under N₂ was charged with *endo*-(bicyclo[2.2.1]hept-5-en-2-yl)methyl methanesulfonate **3** (5.00 g, 24.7 mmol) and 2-methylimidazole (6.09 g, 74.1 mmol) in dry DMF (13 mL). The reaction mixture was heated to 120 °C and stirred under reflux for 48 h. Et₂O (100 mL) was added and the reaction mixture separated. The resulting aqueous layer was extracted with Et₂O (2 x 100 mL) and the organic layers were combined, washed with water (4 x 100 mL), dried (MgSO₄), filtered and the solvent removed under reduced pressure to afford *endo*-norbornene imidazole **5** as a yellow oil (1.94 g, 42 %). **¹H NMR** (300 MHz, CDCl₃, δ): 6.87 (d, *J* = 1.3 Hz, 1H, N-CH=CH-N-CH₃), 6.79 (d, *J* = 1.3 Hz, 1H, N-CH=CH-N-CH₃), 6.25 (dd, *J* = 5.7, 3.1 Hz, 1H, H-C=C-H), 6.00 (dd, *J* = 5.7, 2.9 Hz, 1H, H-C=C-H), 3.50 (dd, *J* = 13.9, 6.8 Hz, 1H), 3.45 (dd, *J* = 14.1, 9.2 Hz, 1H), 2.82 (br s, 1H, CH-CH=CH-CH), 2.70 (br s, 1H, CH-CH=CH-CH), 2.42 (m, 1H, CH-CH(CH₂N)), 2.33 (s, 3H, N-C(CH₃)-N), 1.86 (ddd, *J* = 11.9, 9.2, 3.9 Hz, 1H), 1.45 (d, *J* = 8.3 Hz, 1H), 1.24 (d, *J* = 8.7 Hz, 1H), 0.60 (ddd, *J* = 7.1, 4.5, 2.6 Hz, 1H); **¹³C NMR** (100 MHz, CDCl₃, δ): 143.8, 138.3, 131.4, 126.2, 118.9, 49.6, 49.4, 43.9, 42.2, 39.7, 29.8, 12.8; **FT-IR** (neat, cm⁻¹): $\tilde{\nu}$ = 3055, 2967, 2939, 2869, 1673, 1525, 1499, 1425, 1343, 1275, 1153, 984, 931, 836, 71/8, 681, 677; **HRMS** (ESI⁺) exact mass calculated for C₁₂H₁₆N₂Na [M+Na]⁺ *m/z* = 211.1211, found *m/z* = 211.1217.



Poly-endo-3-(bicyclo[2.2.1]hept-5-en-2-ylmethyl)-1,2-dimethyl-1H-imidazolium mesylate homo polymer (6).^[75]

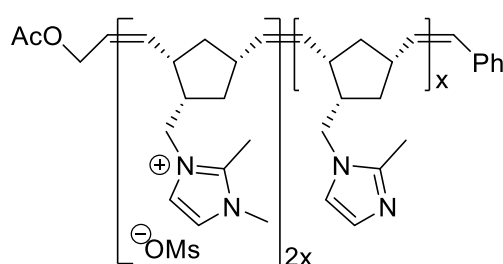
A flame-dried Schlenk flask under N₂ was charged with *endo*-3-((bicyclo[2.2.1]hept-5-en-2-yl)methyl)-1,2-dimethyl-1H-imidazol-3-ium methanesulfonate **4** (200 mg, 0.700 mmol) and 1,3-dinitrobenzene (56.0 mg, 0.500 mmol) NMR standard in dry CH₂Cl₂ (2 mL) and the reaction mixture was stirred. Grubbs catalyst 2nd generation (5.70 mg, 7.00 μmol, 1 mol %) was added and the reaction mixture was heated to 30 °C and stirred for 16 h. The progress of the reaction was monitored by ¹H NMR. The solvent was removed under reduced pressure to afford the imidazolium homo polymer **6** as a brown water soluble solid. ¹H NMR (300 MHz, D₂O, δ): 7.24, 5.34, 5.29, 3.93, 3.80, 3.63, 2.64, 2.39, 2.15, 1.88, 1.73, 1.58, 1.14; ¹³C NMR (100 MHz, CDCl₃, δ): 143.3, 135.5, 129.4, 122.6, 117.1, 38.4, 33.7, 16.6, 9.7; FT-IR (neat, cm⁻¹): ν = 3464, 3125, 2933, 1631, 1589, 1536, 1450, 1421, 1330, 1169, 1039, 926, 771. This is consistent with data reported in the literature.^[75]



Poly-endo-1-((bicyclo[2.2.1]hept-5-en-2-yl)methyl)-2-methyl-1H-imidazole homopolymer (7).^[75]

A flame-dried Schlenk flask under N₂ was charged with 1-((bicyclo[2.2.1]hept-5-en-2-yl)methyl)-2-methyl-1H-imidazole **5** (200 mg, 1.10 mmol) and 1,3-dinitrobenzene (89.0 mg, 500 μmol) NMR standard in dry CH₂Cl₂ (2 mL) and the reaction mixture was stirred. Grubbs

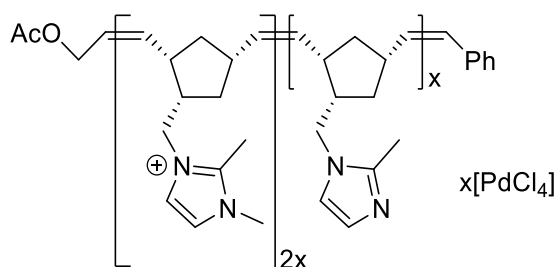
catalyst 2nd generation (8.50 mg, 10.0 μmol , 1 mol %) was added and the reaction mixture was heated to 30 °C and stirred for 16 h. The progress of the reaction was monitored by ¹H NMR. The solvent was removed under reduced pressure to afford the imidazole homo polymer **7** as a brown gel. ¹H NMR (300 MHz, CDCl₃, δ): 6.73 (br, N-CH=CH-N), 5.26 (br, CH₂-N), 3.73 (br), 3.54 (br), 2.93 (br, CHCH₂, polymer backbone), 3.54 (br, CHCH₂, polymer backbone), 2.93 (br, CHCH₂, polymer backbone), 2.68 (br, CHCH₂, polymer backbone), 2.27 (br, N-C(CH₃)-N), 2.02 (br, CHCH₂, polymer backbone), 1.71 (br, CHCH₂, polymer backbone), 1.12 (br, CHCH₂, polymer backbone); ¹³C NMR (100 MHz, CDCl₃, δ): 148.5, 130.8, 128.9, 119.1; FT-IR (neat, cm⁻¹): $\tilde{\nu}$ = 3106, 2939, 2865, 1536, 1499, 1423, 1345, 1275, 1148, 1066, 982, 907, 724, 674.



Poly-endo-3-(bicyclo[2.2.1]hept-5-en-2-ylmethyl)-1,2-dimethyl-1H-imidazolium methanesulfonate-co-endo-1-((bicyclo[2.2.1]hept-5-en-2-yl)methyl)-2-methyl-1H-imidazole (8).^[75]

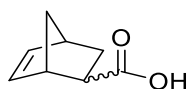
A flame-dried Schlenk flask under N₂ was charged with 3-((bicyclo[2.2.1]hept-5-en-2-yl)methyl)-1,2-dimethyl-1H-imidazol-3-ium methanesulfonate **4** (620 mg, 2.10 mmol) and 1-((bicyclo[2.2.1]hept-5-en-2-yl)methyl)-2-methyl-1H-imidazole **5** (200 mg, 1.00 mmol) in dry CH₂Cl₂ (5 mL) and the reaction mixture was stirred. Grubbs catalyst 2nd generation (26.5 mg, 30.0 μmol , 1 mol %) was added and the reaction mixture was heated to 30 °C and stirred for 72 h. The progress of the reaction was monitored by ¹H NMR. A degassed solution of *cis*-1,4-diacetoxy-2-butene (0.16 mL, 1.00 mmol) in MeOH (0.62 mL) was added and the reaction mixture stirred for 18 h. The reaction mixture was diluted with CH₂Cl₂ (20 mL) and extracted with distilled water (75 mL). The water was removed under reduced pressure to afford a glassy brown solid. ¹H NMR revealed the presence of residual monomer so the polymer was dissolved in distilled water and dialysed (MWCO: 3,500) for 16 h. The water was removed under reduced pressure to afford *endo*-norbornene imidazolium co-polymer **8** as a glassy brown solid (0.153 g, 19 %) ¹H NMR (300 MHz, D₂O, δ): 7.21 (br, Ar-*H*), 6.74 (br, Ar-*H*), 5.21 (br, CH₂-N), 3.91 (br), 3.60 (br, N-CH₃), 2.39 (br, N-CCH₃-N), 2.17 (br), 1.62 (br, CHCH₂, polymer backbone),

0.97 (br, $CHCH_2$, polymer backbone); **FT-IR** (neat, cm^{-1}): $\tilde{\nu} = 3394, 3145, 2940, 2862, 1645, 1589, 1539, 1422, 1180, 1040, 979, 769, 660$.



Palladium loaded poly-endo-3-(bicyclo[2.2.1]hept-5-en-2-ylmethyl)-1,2-dimethyl-1H-imidazolium methanesulfonate-co-endo-1-((bicyclo[2.2.1]hept-5-en-2-yl)methyl)-2-methyl-1H-imidazole (9).

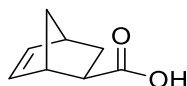
To a round-bottomed flask was added $PdCl_2$ (30.0 mg, 200 μ mol), NaCl (196 mg, 3.40 mmol) and water (5 mL). The flask was heated to 80 $^{\circ}C$ and stirred until the $PdCl_2$ had dissolved. This clear red solution was added to a solution of *endo*-norbornene imidazolium co-polymer **8** (132 mg, 200 μ mol) in water (10 mL) and the reaction mixture was stirred for 16 h at 25 $^{\circ}C$. The product failed to precipitate and was abandoned.



Bicyclo[2.2.1]hept-5-en-2-carboxylic acid (10).

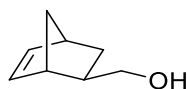
A flame dried 3-neck 250 mL round-bottomed flask under N_2 was charged with bicyclo[2.2.1]hept-5-en-2-carboxylic acid methyl ester **1** (10.7 g, 70.2 mmol) and a solution of sodium ethoxide in EtOH (1.9 M, 25 mL). The reaction mixture was heated to reflux and stirred for 6 days. Potassium hydroxide (23.6 g, 421 mmol) was added and the reaction mixture was heated to reflux and stirred for 48 h. The solvent was removed under reduced pressure to afford a dark brown oil which was extracted with water (150 mL) and washed with ether (3 x 100 mL). The aqueous solution was acidified by drop-wise addition of concentrated hydrochloric acid until a precipitate had formed. The product was extracted with Et_2O (100 mL), dried ($MgSO_4$), filtered and the solvent removed under reduced pressure to afford norbornene carboxylic acid **10** as a brown oil (7.70 g, 79 %). **1H NMR** (400 MHz, $CDCl_3$, δ): 6.19 (dd, $J = 5.7, 3.1$ Hz, 1H, *endo* H-C=C-H), 6.13 (dd, $J = 5.6, 2.9$ Hz, 1H, *exo* H-C=C-H), 6.10 (dd, $J = 5.5, 3.0$ Hz, 1H, *exo* H-C=C-H), (5.98 (dd, $J = 5.7, 2.9$ Hz, 1H, *endo* H-C=C-H), 3.22 (br s, 1H, *endo* CH-CH=CH-CH), 3.08 (br s, 1H, *exo* CH-CH=CH-CH), 2.98 (dt, $J = 9.4, 4.0$ Hz, 1H,

endo CH(CO₂H)), 2.91 (br s, 2H, *endo* & *exo* CH-CH=CH-CH), 2.23 (m, 1H, *exo* CH-CH(COOH)), 1.9 (m, 2H), 1.51 (d, *J* = 8.2 Hz, 1H), 1.39 (m, 4H), 1.28 (d, *J* = 8.3 Hz, 1H); ¹³C NMR (100 MHz, CDCl₃, δ): 182.8, 181.3, 138.1, 137.9, 135.7, 132.4, 49.7, 46.7, 46.4, 45.7, 43.3, 43.2, 42.6, 41.7, 30.3, 29.1; FT-IR (neat, cm⁻¹): $\tilde{\nu}$ = 3046, 2939, 2878, 2361, 2342, 1774, 1730, 1585, 1558, 1446, 1371, 1334, 1271, 1178, 1038, 50, 712. This is consistent with data reported in the literature.^[140]



***Exo*-bicyclo[2.2.1]hept-5-en-2-carboxylic acid (11).**^[141]

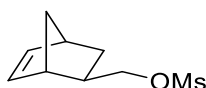
A solution of iodine (10.9 g, 42.9 mmol) and sodium iodide (18.6 g, 124 mmol) in water (72 mL) was prepared. The solution (48 mL) was added drop-wise to a solution of bicyclo[2.2.1]hept-5-en-2-carboxylic acid **10** (7.70 g, 55.7 mmol) and sodium carbonate (16.5 g, 156 mmol) in water (152 mL) until a dark red colour persisted. The solution was decolourised with 10 % sodium thiosulfate (20 mL) and washed with Et₂O (4 x 250 mL). The aqueous layer was acidified (pH 1) with concentrated HCl and then extracted with Et₂O (3x 150 mL). The extract was washed with brine (100 mL), dried (MgSO₄), filtered and the solvent removed under reduced pressure to afford the *exo*-norbornene carboxylic acid **11** as a brown oil (4.50 g, 63 %). ¹H NMR (400 MHz, CDCl₃, δ): 6.14 (dd, *J* = 5.6, 2.9 Hz, 1H, *H*-C=C-*H*), 6.11 (dd, *J* = 5.5, 2.9 Hz, 1H, *H*-C=C-*H*), 3.09 (br s, 1H, CH-CH=CH-CH), 2.92 (br s, 1H, CH-CH=CH-CH), 2.25 (m, 1H, CH-CH(COOH)), 1.94 (dt, *J* = 11.8, 3.7 Hz, 1H), 1.52 (d, *J* = 8.4 Hz, 1H), 1.38 (m, 2H); ¹³C NMR (100 MHz, CDCl₃, δ): 182.8, 138.1, 135.7, 46.7, 46.4, 43.2, 41.7, 30.3; FT-IR (neat, cm⁻¹): $\tilde{\nu}$ = 3065, 2976, 2877, 1699, 1417, 1333, 1242, 1214, 906, 729, 649. This is consistent with data reported in the literature.^[141]



***Exo*-5-bicyclo[2.2.2]hept-2-enylmethanol (12).**^[138]

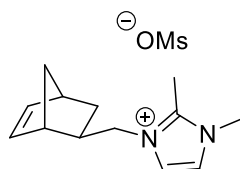
A flame dried, 3-neck 250 mL round-bottomed flask under N₂ was charged with lithium aluminium hydride (2.72 g, 71.7 mmol) in dry THF (24 mL). The mixture was stirred and cooled to 0 °C in an ice bath. *Exo*-bicyclo[2.2.1]hept-5-en-2-carboxylic acid **11** (4.50 g, 33.0 mmol) was dissolved in dry THF (8 mL) and added drop-wise to the reaction mixture. The mixture was allowed to warm to room temperature and stirred for 18 h. The reaction mixture was cooled to 0 °C in an ice bath and then portions of water (27 mL), 3M potassium hydroxide

(81 mL) and water (27 mL) were added slowly by syringe pump. The reaction mixture was stirred under reflux for 1 h. Celite was added to the reaction mixture and the product solution was decanted off. The celite was then washed with Et₂O and the combined organic layers were dried (MgSO₄), filtered and the solvent removed under reduced pressure to afford the *exo*-norbornene alcohol **12** as a yellow oil (3.0 g, 73 % yield). ¹H NMR (400 MHz, CDCl₃, δ): 6.09 (dd, *J* = 5.7, 3.2 Hz, 1H, *H*-C=C-*H*), 6.05 (dd, *J* = 5.6, 2.8 Hz, 1H, *H*-C=C-*H*), 3.68 (dd, *J* = 10.6, 6.5 Hz, 1H, OCH₂), 3.51 (m, 1H, OCH₂), 2.80 (br s, 1H, CH-CH=CH-CH), 2.73 (br s, 1H, CH-CH=CH-CH), 1.72 (br, 1H), 1.59 (m, 1H), 1.25 (m, 3H), 1.09 (m, 1H); ¹³C NMR (100 MHz, CDCl₃, δ): 136.8, 136.5, 67.3, 44.9, 43.2, 41.7, 41.5, 29.5; FT-IR (neat, cm⁻¹): $\tilde{\nu}$ = 3300, 3059, 2957, 2867, 1446, 1332, 1084, 1028, 980, 860, 704, 659. This is consistent with data reported in the literature.^[142]



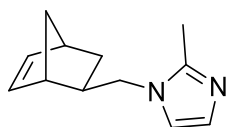
***Exo*-norbornenemethyl methanesulfonate (**13**).**^[75]

A flame dried Schlenk flask under N₂ was charged with *exo*-5-bicyclo[2.2.2]hept-2-enylmethanol **12** (2.70 g, 21.7 mmol) in dry CH₂Cl₂ (11 mL) and the solution cooled to 0 °C. Methanesulfonyl chloride (1.85 mL, 23.9 mmol) in dry CH₂Cl₂ (5 mL) was added followed by the drop-wise addition of pyridine (2.10 mL, 26.1 mmol). The reaction mixture was allowed to warm to room temperature and left to stir for 16 h. The reaction mixture was washed with water (25 mL), 1M HCl (25 mL) and brine (3 x 25 mL). The organic material was dried (MgSO₄), filtered and the solvent removed under reduced pressure to afford the *exo*-mesyl norbornene **13** as a brown oil (4.18 g, 95 %). ¹H NMR (300 MHz, CDCl₃, δ): 6.04 (br s, 2H, *H*-C=C-*H*), 4.22 (dd, *J* = 9.7, 6.5 Hz, 1H, OCH₂), 4.04 (dd, 1H, OCH₂), 2.96 (s, 3H, CH₃), 2.81 (br s, 1H, CH-CH=CH-CH), 2.72 (br s, 1H, CH-CH=CH-CH), 1.76 (m, 1H, CH(CH₂OMs)), 1.28 (m, 3H), 1.12 (dt, *J* = 11.9, 3.9 Hz, 1H); ¹³C NMR (100 MHz, CDCl₃, δ): 137.2, 136.0, 73.9, 44.9, 43.4, 41.6, 38.5, 37.4, 29.4; FT-IR (neat, cm⁻¹): $\tilde{\nu}$ = 3058, 2966, 2872, 1470, 1450, 1416, 1350, 1331, 1170, 972, 942, 869, 826, 709. HRMS (ESI⁺) exact mass calculated for C₉H₁₅O₃S [M+H]⁺ *m/z* = 203.0742, found *m/z* = 203.0745.



Exo-3-((bicyclo[2.2.1]hept-5-en-2-yl)methyl)-1,2-dimethyl-1H-imidazol-3-ium methanesulfonate (14).^[75]

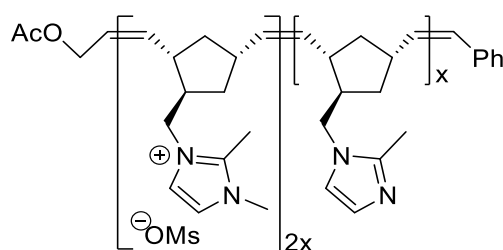
A flame-dried 2-neck 100 mL round-bottomed flask under N₂ was charged with *exo*-norbornenemethyl methanesulfonate **13** (2.6 g, 12.9 mmol) and 1,2-dimethylimidazole (1.24 g, 12.9 mmol) in dry toluene (4 mL). The reaction mixture was heated to reflux and stirred for 96 h. The solvent was removed under reduced pressure using an external trap and the remaining solid was dissolved in dry CH₂Cl₂ (10 mL). The reaction mixture was added drop-wise into a flame-dried Schlenk flask containing Et₂O (100 mL) while stirring rapidly. A precipitate formed which was allowed to settle and the solvent was removed via cannula filtration. The product was washed with a further two portions of Et₂O (2 x 50 mL) and removed via cannula filtration. The remaining solvent was removed under reduced pressure to afford the *exo*-norbornene imidazolium mesylate **14** as a highly hygroscopic fine beige powder stored under N₂. ¹H NMR (300 MHz, CDCl₃, δ): 7.57 (d, *J* = 2.1 Hz, 1H, N-CH=CH-N), 7.32 (d, *J* = 2.0 Hz, 1H, N-CH=CH-N), 6.06 (dd, *J* = 5.7, 2.9 Hz, 1H, H-C=C-H), 5.98 (dd, *J* = 5.7, 3.1 Hz, 1H, H-C=C-H), 4.19 (dd, *J* = 14.3, 7.1 Hz, 1H, OCH₂), 4.04 (dd, *J* = 14.3, 9.1 Hz, 1H, OCH₂), 3.89 (s, 3H, N-CH₃), 2.87 (br s, 1H, CH-CH=CH-CH), 2.67 (s, 3H, mesylate CH₃), 2.62 (s, 3H, N=C(CH₃)-N), 2.49 (br s, 1H, CH-CH=CH-CH), 1.77 (m, 1H, CH(CH₂N)), 1.40 (s, 2H), 1.29 (m, 1H), 1.19 (m, 1H); ¹³C NMR (100 MHz, CDCl₃, δ): 144.0, 137.6, 135.5, 123.1, 121.2, 53.5, 44.9, 43.9, 41.9, 39.6, 39.3, 35.7, 30.8, 10.4; FT-IR (neat, cm⁻¹): $\tilde{\nu}$ = 3108, 2962, 2875, 1614, 1592, 1543, 1463, 1422, 1196, 1126, 1037, 765, 713, 672; HRMS (ESI⁺) exact mass calculated for C₁₃H₂₀N₂ [M+H]⁺ *m/z* = 204.1626, found *m/z* = 204.1621.



Exo-1-((bicyclo[2.2.1]hept-5-en-2-yl)methyl)-2-methyl-1H-imidazole (15).^[139]

A flame-dried 2-neck 100 mL round-bottomed flask under N₂ was charged with *exo*-norbornenemethyl methanesulfonate **13** (1.19 g, 5.90 mmol) and 2-methylimidazole (1.70 g, 20.8 mmol) in dry DMF (4 mL). The reaction mixture was heated to 120 °C and stirred for 48 h. Water (20 mL) was added and the reaction mixture was extracted with CH₂Cl₂ (3 x 50 mL).

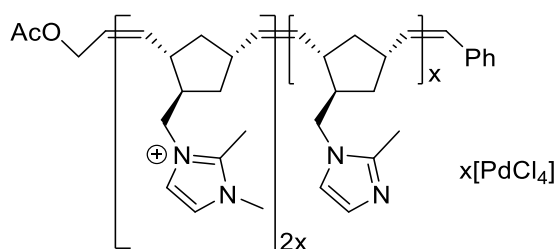
The organic extracts were combined and washed with water (5 x 50 mL), dried (MgSO₄), filtered and the solvent removed under reduced pressure to afford *exo*-norbornene imidazole **15** as a brown oil (0.78 g, 70 %). ¹H NMR (300 MHz, CDCl₃, δ): 6.84 (d, *J* = 1.1 Hz, 1H, N-CH=CH-N-CH₃), 6.77 (d, *J* = 1.3 Hz, 1H, N-CH=CH-N-CH₃), 6.03 (dd, *J* = 5.7, 2.9 Hz, 1H, H-C=C-H), 5.95 (dd, *J* = 5.7, 3.1 Hz, 1H, H-C=C-H), 3.86 (dd, *J* = 14.1, 6.7 Hz, 1H), 3.67 (dd, *J* = 14.1, 9.5 Hz, 1H), 2.82 (br s, 1H, CH-CH=CH-CH), 2.48 (br s, 1H, CH-CH=CH-CH), 2.31 (s, 3H, N-C(CH₃)-N), 1.74 (m, 1H), 1.35 (d, *J* = 7.5 Hz, 1H), 1.25 (m, 2H), 1.13 (ddd, *J* = 11.8, 7.8, 3.8 Hz, 1H); ¹³C NMR (100 MHz, CDCl₃, δ): 144.4, 137.2, 136.0, 127.0, 119.3, 51.1, 44.8, 43.7, 41.8, 40.1, 30.9, 13.2; FT-IR (neat, cm⁻¹): $\tilde{\nu}$ = 3107, 3058, 2963, 2869, 1673, 1499, 1423, 1338, 1275, 985, 707, 677; HRMS (ESI⁺) exact mass calculated for C₁₂H₁₆N₂Na [M+Na]⁺ *m/z* = 211.1211, found *m/z* = 211.1212.



Poly-*Exo*-3-((bicyclo[2.2.1]hept-5-en-2-yl)methyl)-1,2-dimethyl-1H-imidazol-3-ium methanesulfonate-co-*exo*-1-((bicyclo[2.2.1]hept-5-en-2-yl)methyl)-2-methyl-1H-imidazole (16).^[75]

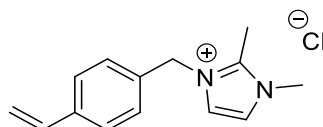
A flame-dried Schlenk flask under N₂ was charged with *exo*-3-((bicyclo[2.2.1]hept-5-en-2-yl)methyl)-1,2-dimethyl-1H-imidazol-3-ium methanesulfonate **14** (600 mg, 2.00 mmol) and *exo*-1-((bicyclo[2.2.1]hept-5-en-2-yl)methyl)-2-methyl-1H-imidazole **15** (190 mg, 1.00 mmol) with 1,3-dinitrobenzene (169 mg, 1.00 mmol) NMR standard in dry CH₂Cl₂ (5 mL) and the reaction mixture was stirred. Grubbs catalyst 2nd generation (25.6 mg, 30.0 μmol, 1 mol %) was added and the reaction mixture was heated to 30 °C and stirred for 72 h. The progress of the reaction was monitored by ¹H NMR. A degassed solution of *cis*-1,4-diacetoxy-2-butene (0.16 mL 1.00 mmol) in MeOH (0.62 mL) was added and the reaction mixture stirred for 18 h. The reaction mixture was diluted with CH₂Cl₂ (20 mL) and extracted with distilled water (75 mL). The water was removed under reduced pressure to afford a glassy brown solid. ¹H NMR revealed the presence of residual monomer so the polymer was dissolved in distilled water and dialysed (MWCO: 3,500) for 16 h. The water was removed under reduced pressure to afford *exo*-norbornene imidazolium co-polymer **16** as a glassy brown solid (0.184 g, 23 %). ¹H NMR (300 MHz, D₂O, δ): 7.27 (br, Ar-*H*), 6.83 (br, Ar-*H*), 5.21 (br, CH₂-N), 3.99 (br), 3.67 (br, N-

CH_3), 2.97 (br), 2.50 (br, N-CCH₃-N), 2.13 (br, CHCH₂, polymer backbone), 1.54 (br, CHCH₂, polymer backbone), 1.08 (br, CHCH₂, polymer backbone); **FT-IR** (neat, cm⁻¹): $\tilde{\nu}$ = 3438, 3135, 2936, 1651, 1589, 1539, 1446, 1422, 1180, 1039, 976, 769.



Palladium loaded poly-*Exo*-3-((bicyclo[2.2.1]hept-5-en-2-yl)methyl)-1,2-dimethyl-1H-imidazol-3-ium methanesulfonate-co-*exo*-1-((bicyclo[2.2.1]hept-5-en-2-yl)methyl)-2-methyl-1H-imidazole (17)

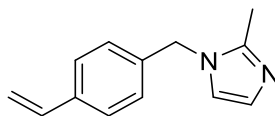
To a round-bottomed flask was added PdCl₂ (39.0 mg, 200 μmol), NaCl (254 mg, 4.30 mmol) and water (6 mL). The flask was heated to 80 °C and stirred until the PdCl₂ had dissolved. This clear red solution was added to a solution of *exo*-norbornene imidazolium co-polymer **16** (171 mg, 2.20 mmol) in water (10 mL) and the reaction mixture was stirred for 16 h at 25 °C. The product failed to precipitate and was abandoned.



1,2-Dimethyl-3-(4-vinylbenzyl)-1H-imidazol-3-ium chloride (18).^[143]

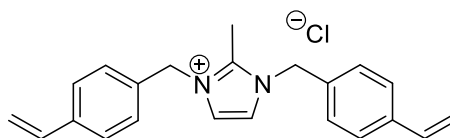
A flame dried 3-neck round bottomed flask under N₂ was charged with 1,2-dimethylimidazole (5.81 g, 60.5 mmol) in dry chloroform (50 mL). 4-Vinylbenzyl chloride (11.1 mL, 78.6 mmol) was added and the reaction mixture was heated to 50 °C and stirred for 18 h. The solvent was removed under reduced pressure and the resulting residue was washed with ethyl acetate (4 x 50 mL). The residual solvent was removed under reduced pressure to afford the imidazolium chloride monomer **18** as a fine white powder (15.0 g, 100 %). **¹H NMR** (400 MHz, CDCl₃, δ): 7.72 (d, J = 2.1 Hz, 1H, N-CH=CH-N-CH₃), 7.69 (d, J = 2.1 Hz, 1H, N-CH=CH-N-CH₃), 7.36 (d, 2H, J = 8.2 Hz, Ar-H ortho to vinyl), 7.27 (d, 2H, J = 8.2 Hz, Ar-H meta to vinyl), 6.64 (dd, J = 17.6, 10.9 Hz, 1H, H_aC=CH_bH_c), 5.72 (d, J = 17.5 Hz, 1H, H_aC=CH_bH_c), 5.53 (s, 2H, Ar-CH₂-N), 5.26 (d, J = 10.9 Hz, 1H, H_aC=CH_bH_c), 3.94 (s, 3H, N-CH₃), 2.75 (s, 3H, N-C(CH₃)-N); **¹³C NMR** (100 MHz, CDCl₃, δ): 144.3, 138.5, 135.8, 132.4, 128.6, 127.2, 123.0, 122.0,

115.4, 52.2, 35.9, 11.0; **Mp**: 186-188 °C; **FT-IR** (neat, cm^{-1}): $\tilde{\nu}$ = 3049, 3006, 2943, 1592, 1514, 1409, 1251, 1174, 826, 663. This is consistent with data reported in the literature.^[143]



1-(4-vinylbenzyl)-2-methylimidazole (19).^[139]

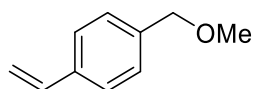
A flame dried Schlenk flask under N_2 was charged with sodium hydride (0.73 g, 30 mmol) in dry DMF (20 mL). The slurry was stirred and cooled to 0 °C. 2-Methylimidazole (3.0 g, 36.5 mmol) was added portion-wise resulting in the liberation of gas and an exotherm. Once the exotherm subsided the reaction was heated to 75 °C for 30 min then to 95 °C for 15 min. The reaction mixture was cooled in ice and 4-vinylbenzyl chloride (4.3 mL, 30 mmol) was added drop-wise. The reaction mixture was heated to 75 °C for 30 min. The reaction mixture was poured on to water (250 mL) and the product extracted with ethyl acetate (2 x 100 mL). The combined extracts were washed with water (180 mL) and brine (50 mL), then extracted with 6 N HCl (2 x 25 mL). The aqueous was washed with Et_2O (20 mL) and basified through addition of solid NaOH. The product was extracted with Et_2O (50 mL), dried (MgSO_4), filtered and the solvent removed under reduced pressure to afford the 2-methyl imidazole styrene **19** as a pale yellow oil (5.55g, 92 %). **^1H NMR** (400 MHz, CDCl_3 , δ): 7.34 (d, J = 8.2 Hz, 2H, Ar-H ortho to vinyl), 6.97 (d, J = 8.0 Hz, 2H, Ar-H meta to vinyl), 6.91 (m, 1H, N-CH=CH-N), 6.80 (m, 1H, N-CH=CH-N), 6.65 (dd, J = 17.6, 10.9 Hz, 1H, $\text{H}_a\text{C}=\text{CH}_b\text{H}_c$), 5.71 (d, J = 17.7 Hz, 1H, $\text{H}_a\text{C}=\text{CH}_b\text{H}_c$), 5.23 (d, J = 10.8 Hz, 1H, $\text{H}_a\text{C}=\text{CH}_b\text{H}_c$), 4.99 (s, 2H, CH_2), 2.29 (s, 3H, CH_3); **^{13}C NMR** (100 MHz, CDCl_3 , δ): 145.0, 137.4, 136.1, 135.8, 127.3, 126.9, 126.8, 120.0, 114.5, 49.5, 13.1; **FT-IR** (neat, cm^{-1}): $\tilde{\nu}$ = 3353, 3006, 2930, 2361, 1631, 1513, 1499, 1423, 1408, 1280, 1130, 988, 912, 827, 732, 670. This is consistent with data reported in the literature.^[144]



2-methyl-1,3-bis(4-vinylbenzyl)-1H-imidazol-3-ium chloride (20).^[143]

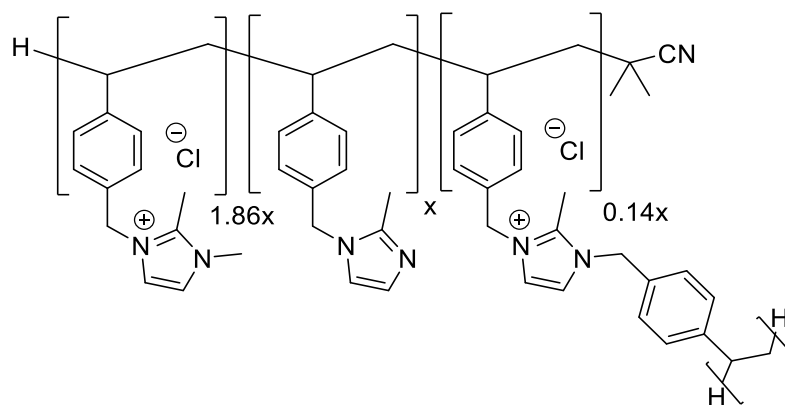
A flame dried 3-neck round-bottomed flask under N_2 was charged with 1-(4-vinylbenzyl)-2-methylimidazole **19** (5.16 g, 26.0 mmol) in dry CHCl_3 (50 mL). 4-Vinylbenzyl chloride (4.8 mL, 34 mmol) was added and the reaction mixture heated to 50 °C and stirred for 18 h. The solvent was removed under reduced pressure and the resulting yellow solid was washed with

ethyl acetate (6 x 80 mL). The product was dried under reduced pressure to afford cross-linker **20** as a fine white powder (8.96 g, 98 %). **¹H NMR** (400 MHz, CDCl₃, δ): 7.56 (m, 2H, N-CH=CH-N), 7.38 (d, *J* = 8.2 Hz, 4H, Ar-H ortho to vinyl), 7.26 (d, *J* = 8.4 Hz, 4H, Ar-H meta to vinyl), 6.66 (dd, *J* = 17.6, 10.9 Hz, 2H, H_aC=CH_bH_c), 5.74 (d, *J* = 17.5 Hz, 2H, H_aC=CH_bH_c), 5.51 (s, 4H, CH₂), 5.28 (d, *J* = 10.9 Hz, 2H, H_aC=CH_bH_c), 2.78 (s, 3H, CH₃); **¹³C NMR** (100 MHz, CDCl₃, δ): 144.2, 138.4, 135.8, 132.4, 128.6, 127.1, 122.1, 115.3; **mp** = 116.6 – 117.3 °C (decomposition); **FT-IR** (neat, cm⁻¹): $\tilde{\nu}$ = 3382, 3116, 3068, 2977, 1630, 1583, 1526, 1514, 1410, 1172, 989, 912, 829, 784, 716; **HRMS** (ESI⁺) exact mass calculated for C₂₂H₂₃N₂ [M]⁺ *m/z* = 315.1861, found *m/z* = 315.1849.



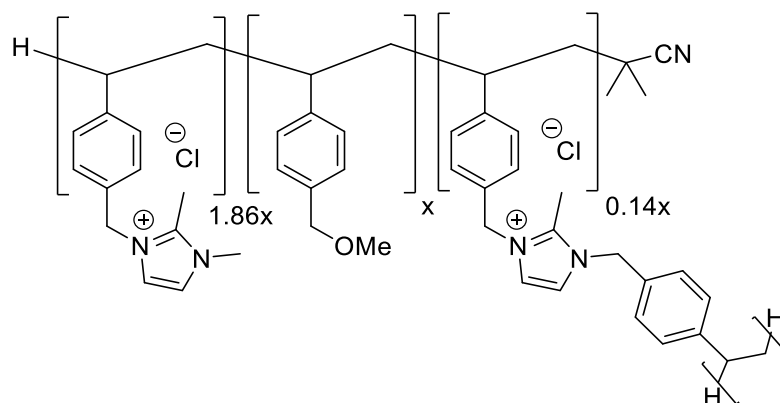
4-Vinylbenzyl methyl ether (**21**).^[145]

A 250 mL round-bottomed flask was charged with 4-vinylbenzyl chloride (9.2 mL, 6.6 mmol,) in MeOH (100 mL). Sodium methoxide (7.1 g, 13.1 mmol) was added and the reaction mixture heated to reflux and stirred for 24 h. The reaction mixture was filtered and the solvent removed under reduced pressure. The crude product was diluted with Et₂O (100 mL) and washed with water (5 x 120 mL). The organic layer was dried (Na₂SO₄), filtered and the solvent removed under reduced pressure. The crude product was purified by column chromatography using a silica column eluting with ethyl acetate: petrol (5:95) and the fractions examined by TLC (same eluent, visualised by UV). The methyl ether **21** was obtained as a colourless oil (3.3 g, 34 %). **¹H NMR** (400 MHz, CDCl₃, δ): 7.40 (d, *J* = 8.2 Hz, 2H, Ar-H ortho to vinyl), 7.30 (d, *J* = 8.0 Hz, 2H, Ar-H meta to vinyl), 6.72 (dd, *J* = 17.6, 10.9 Hz, 1H, H_aC=CH_bH_c), 5.76 (d, *J* = 17.5 Hz, 1H, H_aC=CH_bH_c), 5.25 (d, *J* = 10.9 Hz, 1H, H_aC=CH_bH_c), 4.45 (s, 2H, CH₂), 3.39 (s, 3H, CH₃); **¹³C NMR** (100 MHz, CDCl₃, δ): 136.6, 128.0, 127.2, 126.4, 126.3, 113.9, 74.4, 58.1; **FT-IR** (neat, cm⁻¹): $\tilde{\nu}$ = 2923, 2825, 1630, 1512, 1406, 1380, 1097, 990, 907, 824, 718. This is consistent with data reported in the literature.^[145]



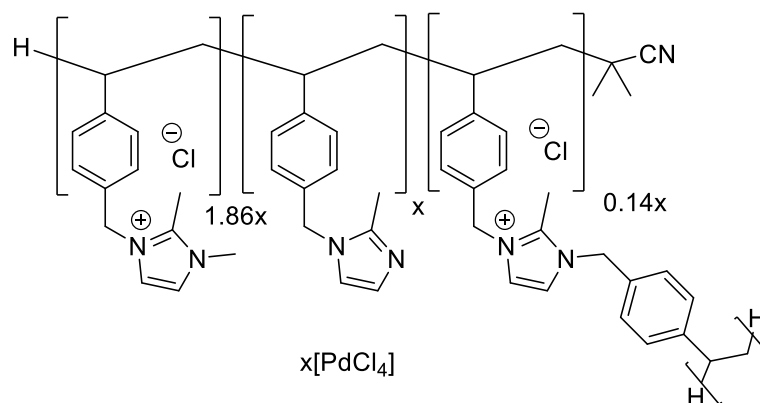
Cross-linked imidazole polymer (**22**).^[146]

To a flame-dried Schlenk flask under N_2 was added AIBN (0.266 g, 1.62 mmol, 5 mol %) followed by 1,2-dimethyl-3-(4-vinylbenzyl)imidazolium chloride **18** (5.00 g, 20.1 mmol), 1-(4-vinylbenzyl)-2-methylimidazole **20** (2.14 g, 10.8 mmol) and cross linker **21** (0.538 g, 1.53 mmol) in dry MeOH (100 mL). The reagents were degassed with 4 freeze/pump/thaw cycles using liquid nitrogen. Upon reaching ambient temperature the reaction mixture was heated to 70 °C for 96 h. The reaction mixture was cooled to room temperature and AIBN (0.266 g, 1.62 mmol, 5 mol %) was added. The reaction mixture was again degassed (3 cycles) and heated to 70 °C for a further 24 h. The solvent was removed under reduced pressure using an external trap and gentle heating to afford the imidazole polymer **22** as an off-white solid (7.60 g, 99 %). 1H NMR (300 MHz, D_2O , δ): 7.19 (br, Ar-H), 7.01 (br, Ar-H), 6.50 (br, N-CH-CH-N), 5.11 (br, Ar-CH₂-N), 3.58 (br, N-CH₃), 2.36 (br, ⁺N-CCH₃-N), 2.02 (br, N-CCH₃-N), 1.41 (br, CHCH₂, polymer backbone), 0.89 (br, CHCH₂, polymer backbone); FT-IR (neat, cm^{-1}): $\tilde{\nu}$ = 3373, 3136, 3054, 2924, 1632, 1588, 1531, 1513, 1454, 1422, 772, 746, 730, 666; CHN Anal. Calc. for $C_{42.12}H_{48.84}N_6Cl_2$ (710.2) C, 71.23; H, 6.93; N, 11.87 %. Found: C, 65.27; H, 6.71; N, 11.46 %.



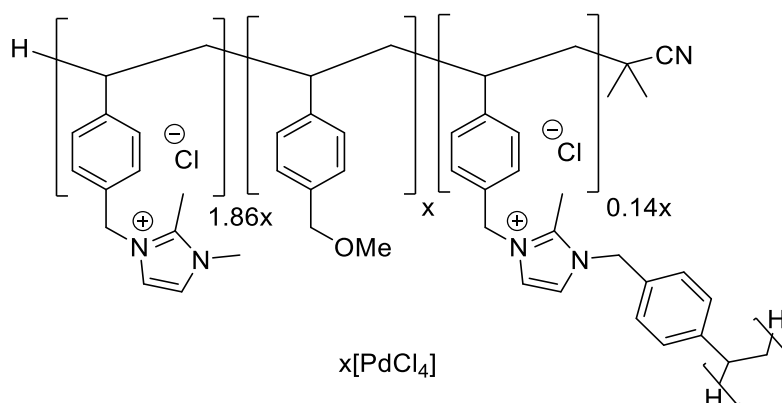
Cross-linked methyl ether polymer (**23**).^[146]

To a flame-dried Schlenk flask under N_2 was added AIBN (0.266 g, 1.62 mmol, 5 mol %) followed by 1,2-dimethyl-3-(4-vinylbenzyl)imidazolium chloride **18** (5.00 g, 20.1 mmol), 4-vinylbenzyl methyl ether **19** (1.60 g, 10.8 mmol) and cross linker **21** (0.538 g, 1.53 mmol) in dry MeOH (100 mL). The reagents were degassed with 4 freeze/pump/thaw cycles using liquid nitrogen. Upon reaching ambient temperature the reaction mixture was heated to 70 °C for 96 h. The reaction mixture was cooled to room temperature and AIBN (0.266 g, 1.62 mmol, 5 mol %) was added. The reaction mixture was again degassed (3 cycles) and heated to 70 °C for a further 24 h. The solvent was removed under reduced pressure using an external trap and gentle heating to afford the methyl ether polymer **23** as an off-white solid (7.03 g, 98 %). 1H NMR (300 MHz, D_2O , δ): 7.22 (br, Ar-*H*), 7.00 (br, Ar-*H*), 6.48 (br, N-*CH-CH*-N), 5.13 (br, Ar-*CH*₂-N), 4.24 (br, Ar-*CH*₂-O), 3.61 (br, N-*CH*₃), 3.19 (br, O-*CH*₃), 2.37 (br, ⁺N-*CCH*₃-N), 1.44 (br, *CHCH*₂, polymer backbone), 0.85 (br, *CHCH*₂, polymer backbone); FT-IR (neat, cm^{-1}): $\tilde{\nu}$ = 3376, 3131, 3055, 2925, 2853, 1709, 1631, 1588, 1536, 1513, 1454, 1421, 1088, 818, 774, 753, 729, 665; CHN Anal. Calc. for $C_{39.12}H_{46.84}N_4OCl_2$ (660.2) C, 71.17; H, 7.15; N, 8.49 %. Found: C, 65.32; H, 7.45; N, 8.50 %.



Palladium loaded cross-linked imidazole polymer (**24**).^[147]

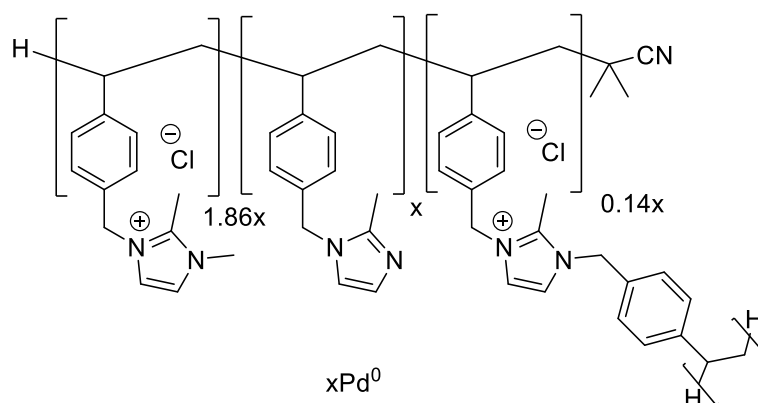
To a round-bottomed flask was added PdCl₂ (494 mg, 2.80 mmol), NaCl (3.26 g, 56.0 mmol) and water (72 mL). The flask was heated to 80 °C and stirred until the PdCl₂ had dissolved. This clear red solution was added to a solution of cross-linked imidazole polymer **22** (2.0 g, 2.8 mmol) in water (20 mL). An orange precipitate appeared immediately and the suspension was stirred for 16 h at 25 °C. The reaction mixture was filtered and washed with water (100 mL), EtOH (100 mL) and Et₂O (100 mL) and the solvent removed under reduced pressure to afford PdCl₄@Imid-PIILP **24** as an orange powder (2.20 g, 88 %). **FT-IR** (neat, cm⁻¹): $\tilde{\nu}$ = 3473, 3128, 3023, 2924, 2853, 1614, 1587, 1536, 1512, 1450, 1422, 1165, 819, 740, 730, 628; **CHN** Anal. Calc. for C_{42.12}H_{48.84}N₆PdCl₄ (887.5) C, 57.00; H, 5.55; N, 9.47 %. Found: C, 36.88; H, 3.52; N, 6.35 %. CHN analysis suggests the encapsulation of solvent within the polymer.



Palladium loaded cross-linked methyl ether polymer (**25**).^[147]

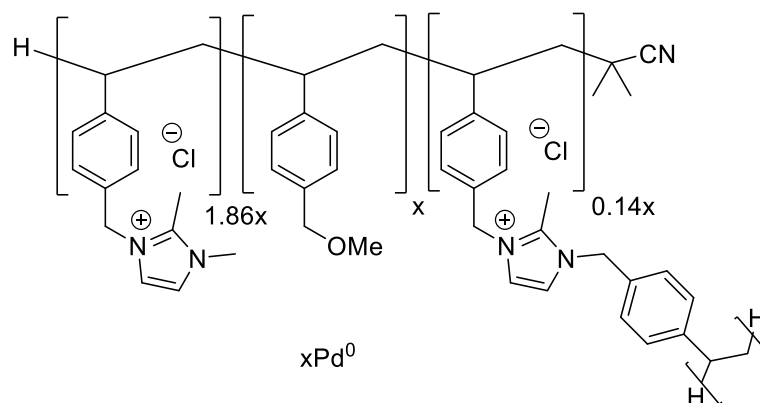
To a round-bottomed flask was added PdCl₂ (532 mg, 3.00 mmol), NaCl (3.50 g, 60.0 mmol) and water (76 mL). The flask was heated to 80 °C and stirred until the PdCl₂ had dissolved. This clear red solution was added to a solution of cross-linked methyl ether polymer **23** (2.00 g, 3.00 mmol) in water (20 mL). An orange precipitate appeared immediately and the suspension was stirred for 16 h at 25 °C. The reaction mixture was filtered and washed with

water (100 mL), EtOH (100 mL) and Et₂O (100 mL) and the solvent removed under reduced pressure to afford PdCl₄@OMe-PIILP **25** as a pink powder (1.89 g, 75 %). **FT-IR** (neat, cm⁻¹): $\tilde{\nu} = 3485, 3125, 3026, 2925, 2852, 1710, 1614, 1587, 1534, 1513, 1451, 1422, 1384, 1238, 1182, 1086, 819, 747, 730$; **CHN** Anal. Calc. for C_{39.12}H_{46.84}N₄OPdCl₄ (837.5) C, 56.10; H, 5.64; N, 6.69 %. Found: C, 51.91; H, 5.33; N, 6.36 %. CHN analysis suggests the encapsulation of solvent within the polymer.



Cross-linked imidazole polymer loaded palladium nanoparticles (**26**).

A stainless steel autoclave was charged with PdCl₄@Imid-PIILP **24** (500 mg) in EtOH (30 mL) and heated to 40 °C under a pressure of 70 psi of hydrogen and stirred for 21 h. The reactor was allowed to cool to room temperature and the resulting black suspension transferred to a flame dried Schlenk flask. The volume was reduced under reduced pressure and Et₂O (50 mL) was added to precipitate the product. The product was filtered and washed with Et₂O (100 mL) then dried under reduced pressure to afford Pd(0)@Imid-PIILP **26** (401 mg, 80 %). **FT-IR** (neat, cm⁻¹): $\tilde{\nu} = 3385, 3127, 2925, 1614, 1588, 1536, 1513, 1451, 1422, 1164, 820, 772, 744, 730, 666$; **CHN** Anal. Calc. for C_{42.12}H_{48.84}N₆PdCl₂ (816.6) C, 61.94; H, 6.03; N, 10.29 %. Found: C, 39.09; H, 4.21; N, 6.61 %. CHN analysis suggests the encapsulation of solvent within the polymer.



Cross-linked methyl ether polymer loaded palladium nanoparticles (**27**).

A stainless steel autoclave was charged with PdCl₄@OMe-PIILP **25** (500 mg) in EtOH (30 mL) and heated to 40 °C under a pressure of 70 psi of hydrogen and stirred for 21 h. The reactor was allowed to cool to room temperature and the resulting black suspension transferred to a flame dried Schlenk flask. The volume was reduced under reduced pressure and Et₂O (50 mL) was added to precipitate the product. The product was filtered and washed with Et₂O (100 mL) then dried under reduced pressure to afford Pd(0)@OMe-PIILP **27** (390 mg, 78 %). **FT-IR** (neat, cm⁻¹): $\tilde{\nu}$ = 3390, 3127, 2924, 2852, 1614, 1457, 1535, 1513, 1451, 1422, 1239, 1183, 1085, 818, 747, 729, 664; **CHN** Anal. Calc. for C_{39.12}H_{46.84}N₄OPdCl₂ (766.6) C, 61.29; H, 6.16; N, 7.31 %. Found: C, 53.76; H, 5.66; N, 6.56 %. CHN analysis suggests the encapsulation of solvent within the polymer.

General procedure for the Suzuki-Miyaura reaction.^[147]

A flame-dried Schlenk flask under N₂ was charged with aryl halide (1 mmol), phenylboronic acid (1.1 mmol), potassium carbonate (1.2 mmol) and catalyst (0.001 mmol, 0.1 mol %). The reaction was initiated by the addition of EtOH (1.2 mL), and H₂O (1.2 mL) and the reaction mixture was heated to 30 °C and stirred for the appropriate length of time. Decane (1 mmol) was added to act as a standard and the reaction mixture was diluted with Et₂O (10 mL), washed with H₂O (5 mL) and the organic extracted filtered through a plug of silica, washing with Et₂O (3 mL) and the solvent removed under reduced pressure. The resulting residue was analysed by GC and ¹H NMR spectroscopy.

General procedure for catalyst mercury poisoning.

A flame-dried Schlenk flask under N₂ was charged with phenylboronic acid (1.1 mmol), potassium carbonate (1.2 mmol) and catalyst (0.001 mmol, 0.1 mol %), EtOH (1.2 mL) and H₂O (1.2 mL). Mercury (0.2 mmol) was added to the mixture and stirred for the appropriate

length of time. Following poisoning the reaction was initiated by the addition of 4-bromotoluene (1 mmol), and the reaction mixture was heated to 30 °C and stirred for 6 h. Decane (1 mmol) was added to act as a standard and the reaction mixture was diluted with Et₂O (10 mL), washed with H₂O (5 mL) and the organic extracted filtered through a plug of silica, washing with Et₂O (3 mL) and the solvent removed under reduced pressure. The resulting residue was analysed by GC and ¹H NMR spectroscopy.

Characterisation of biaryl Suzuki-Miyaura cross-coupling products.

All % conversions were determined by ¹H NMR and by the reduction of the aryl halide starting material in the GC. GC method: 90 °C hold 5 min, ramp for 5 min, rate 4, 120 °C hold 20 min, ramp for 10 min, rate 7, 180 °C hold 15 min. The ¹H NMR data for each cross-coupling product is listed along with the retention time and response factor for each associated aryl halide starting materials.

2-Methylbiphenyl.^[148] ¹H NMR (400 MHz, CDCl₃, δ): 7.42 (t, *J* = 7.7 Hz, 2H), 7.39- 7.30 (m, 3H), 7.22-7.27 (m, 4H), 2.29 (s, 3H). GC RF for 2-bromotoluene = 0.660, Ret. Time: 9.055 min.

3-Methylbiphenyl.^[149] ¹H NMR (300 MHz, CDCl₃, δ): 7.63 (d, *J* = 7.3 Hz, 2H) 7.40 (m, 6H), 7.20 (m, 1H), 2.45 (s, 3H). GC RF for 3-bromotoluene = 0.679, Ret. Time: 9.130 min.

4-Methylbiphenyl.^[148] ¹H NMR (300 MHz, CDCl₃, δ): 7.66 (d, *J* = 6.7 Hz, 2H), 7.59 (d, *J* = 8.3 Hz 2H), 7.51 (t, *J* = 7.9, 2H), 7.43-7.36 (m, 1H), 7.33 (d, *J* = 7.9 Hz, 2H), 2.47 (s, 3H). GC RF for 4-bromotoluene = 0.680, Ret. Time: 9.573 min.

1-Phenyl-3,5-dimethylbenzene.^[150] ¹H NMR (400 MHz, CDCl₃, δ): 7.60 (d, *J* = 7.2 Hz, 3H), 7.44 (t, *J* = 7.6 Hz, 3H), 7.34 (t, *J* = 7.2 Hz, 1H), 6.92 (t, *J* = 7.2 Hz, 1H), 2.29 (s, 6H). GC RF for 1-bromo-3,5-dimethylbenzene = 0.760, Ret. Time: 12.315 min.

4-Tert-butylbiphenyl.^[151] ¹H NMR (400 MHz, CDCl₃, δ): 7.69 – 7.65 (m, 2H), 7.64 – 7.60 (m, 2H), 7.56 – 7.54 (m, 2H), 7.49 (ddd, *J* = 8.1, 7.1, 0.6 Hz, 2H), 7.40 (d, *J* = 7.4 Hz, 1H), 1.45 (s, 9H). GC RF for 1-bromo-4-*tert*-butylbenzene = 0.931, Ret. Time: 21.522 min.

2-Acetylbiphenyl.^[152] ¹H NMR (400 MHz, CDCl₃, δ): 7.56 - 7.49 (m, 2H), 7.43-7.38 (m, 5H), 7.35 - 7.33 (m, 2H), 2.00 (s, 3H). GC RF for 2-bromoacetophenone = 0.625, Ret. Time: 26.043 min.

3-Acetylbiphenyl.^[153] ¹H NMR (400 MHz, CDCl₃, δ): 8.20 (t, *J* = 1.5 Hz, 1H), 7.95 (dt, *J* = 7.5, 1.5 Hz, 1H), 7.81 (ddd, *J* = 7.5, 2.0, 1.0 Hz, 1H), 7.66 – 7.62 (m, 2H), 7.56 (t, *J* = 7.5 Hz, 1H), 7.53 – 7.45 (m, 2H), 7.43 – 7.37 (m, 1H), 2.68 (s, 3H). GC RF for 3-bromoacetophenone = 0.608, Ret. Time: 29.314 min.

4-Acetylbiphenyl.^[154] ¹H NMR (400 MHz, CDCl₃, δ): 8.03 (d, *J* = 8.4 Hz, 2H, 4-CH₃COC₆H₄), 7.69 (d, *J* = 8.0 Hz, 2H, 4-CH₃COC₆H₄), 7.63 (d, *J* = 7.6 Hz, 2H, H_{phenyl}), 7.47 (t, *J* = 7.6 Hz, 2H, H_{phenyl}), 7.40 (t, *J* = 8.0 Hz, 1H, H_{phenyl}), 2.64 (s, 3H, CH₃). GC RF for 4-bromoacetophenone = 0.654, Ret. Time: 34.382 min.

2-Methoxybiphenyl.^[154] ¹H NMR (400 MHz, CDCl₃, δ): 7.54-7.52 (m, 2H, H_{phenyl}), 7.40 (t, *J* = 8.8 Hz, 2H, H_{phenyl}), 7.34-7.29 (m, 3H, 2-OCH₃C₆H₄ and H_{phenyl}), 7.04-6.97 (m, 2H, 2-OCH₃C₆H₄), 3.80 (s, 3H, OCH₃). GC RF for 2-bromoanisole = 0.570, Ret. Time: 17.524 min.

3-Methoxybiphenyl.^[148] ¹H NMR (300 MHz, CDCl₃, δ): 7.63 (d, *J* = 7.6 Hz, 2H), 7.48 (t, *J* = 7.9 Hz, 2H), 7.40 (m, 2H), 7.25-7.15 (m, 2H), 6.94 (dd, *J* = 8.2, 2.5 Hz, 1H), 3.90 (s, 3H). GC RF for 3-bromoanisole = 0.582, Ret. Time: 15.703 min.

4-Methoxybiphenyl.^[154] ¹H NMR (300 MHz, CDCl₃, δ): 7.56- 7.52 (m, 4H, 4-OCH₃C₆H₄ and H_{phenyl}), 7.41 (t, *J* = 7.6 Hz, 2H, H_{phenyl}), 7.30 (t, *J* = 7.2 Hz, 1H, H_{phenyl}), 6.98 (d, *J* = 8.8 Hz, 2H, 4-OCH₃C₆H₄), 3.85 (s, 3H, OCH₃). GC RF for 4-bromoanisole = 0.545, Ret. Time: 17.318 min.

3-Formylbiphenyl.^[155] ¹H NMR (400 MHz, CDCl₃, δ): 10.09 (s, 1H, CHO), 8.10 (s, 1H, ArH), 7.86 (d, *J* = 7.2 Hz, 2H, ArH), 7.62 (d, *J* = 6.0 Hz, 3H, ArH), 7.49–7.41 (m, 3H, ArH), 7.40 (s, 1H, ArH). GC RF for 3-bromobenzaldehyde = 0.518, Ret. Time: 20.593 min.

4-Formylbiphenyl.^[154] ¹H NMR (400 MHz, CDCl₃, δ): 10.06 (s, 1H, CHO), 7.96 (d, *J* = 8.0 Hz, 2H, 4-CHOC₆H₄), 7.76 (d, *J* = 8.4 Hz, 2H, 4-CHOC₆H₄), 7.65 (d, *J* = 8.4 Hz, 2H, H_{phenyl}), 7.49 (t, *J* = 7.6 Hz, 2H, H_{phenyl}), 7.42 (t, *J* = 7.2 Hz, 1H, H_{phenyl}). GC RF for 4-bromobenzaldehyde = 0.548, Ret. Time: 22.812 min.

2-Phenylbenzotrile.^[156] ¹H NMR (400 MHz, CDCl₃, δ): 7.76 (dd, *J* = 8.0, 0.8 Hz, 1H), 7.65 (dd, *J* = 7.6, 1.2 Hz, 1H), 7.62-7.41 (m, 7H). GC RF for 2-bromobenzotrile = 0.630, Ret. Time: 26.353 min.

3-Phenylbenzotrile.^[156] ¹H NMR (400 MHz, CDCl₃, δ): 7.85 (s, 1H), 7.81 (d, *J* = 7.6 Hz, 1H), 7.62 (d, *J* = 7.6 Hz, 1H), 7.57-7.46 (m, 5H), 7.41 (t, *J* = 7.2 Hz, 1H). GC RF for 3-bromobenzotrile = 0.601, Ret. Time: 22.304 min.

4-Phenylbenzotrile.^[154] ¹H NMR (400 MHz, CDCl₃, δ): 7.73-7.67 (m, 4H, 4-CNC₆H₄), 7.59 (d, *J* = 7.6 Hz, 2H, H_{phenyl}), 7.48 (t, *J* = 7.2 Hz, 2H, H_{phenyl}), 7.42 (t, *J* = 8.4 Hz, 1H, H_{phenyl}). GC RF for 4-bromobenzotrile = 0.580, Ret. Time: 26.854 min.

3-Nitrobiphenyl.^[150] ¹H NMR (400 MHz, CDCl₃, δ): 8.45 (s, 1H), 8.19 (d, *J* = 8.4 Hz, 1H), 7.91 (t, *J* = 8.0 Hz, 1H), 7.58-7.63 (m, 3H), 7.50 (t, *J* = 7.2 Hz, 2H), 7.43 (t, *J* = 7.6 Hz, 1H). GC RF for 3-bromonitrobenzene = 0.494, Ret. Time: 31.454 min.

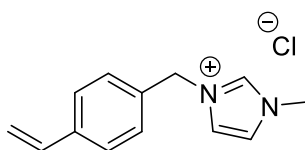
4-Nitrobiphenyl.^[157] ¹H NMR (300 MHz, CDCl₃, δ): 8.31 (d, *J* = 7.1 Hz, 2H), 7.75 (m, 2H), 7.64 (d, *J* = 7.1 Hz, 2H), 7.49 (m, 3H). GC RF for 4-bromonitrobenzene = 0.533, Ret. Time: 36.665 min.

Diethyl 1,1'-Biphenyl-2-ylphosphonate. ¹H NMR (400 MHz, CDCl₃, δ): 7.98 (ddd, *J* = 14.3, 7.7, 1.3 Hz, 1H, C₆H₄P), 7.46 (tt, 7.5, 1.4 Hz, 1H, C₆H₄P), 7.38-7.28 (m, 5H, C₆H₅, C₆H₄P), 7.24 (ddd, *J* = 7.2, 5.6, 1.1 Hz, 1H, C₆H₅), 3.90-3.71 (m, 4H, OCH₂CH₃), 1.05 (t, *J* = 7.1 Hz, 6H, OCH₂CH₃). GC RF for diethyl (2-bromophenyl)phosphonate = 1.482, Ret. Time: 51.057 min.

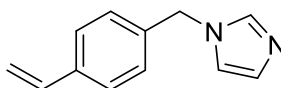
2-Phenylpyridine.^[148] ¹H NMR (400 MHz, CDCl₃, δ): 8.72 (td, *J* = 4.9, 1.5 Hz, 1H), 8.02 (dd, *J* = 7.2, 1.5 Hz, 2H), 7.78-7.72 (m, 2H), 7.49-7.43 (m, 3H), 7.26-7.20 (m, 1H). GC RF for 2-bromopyridine = 0.407, Ret. Time: 10.924 min.

2-Phenylpyrimidine.^[158] ¹H NMR (400 MHz, CDCl₃, δ): 9.25 (s, 1H), 9.01 (s, 2H), 7.64-7.60 (m, 2H), 7.58-7.54 (m, 2H), 7.53-7.49 (m, 1H). GC RF for 5-bromopyrimidine = 0.309, Ret. Time: 7.733 min.

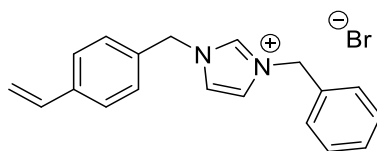
5.3 Experimental Procedures Chapter 3

**1-Methyl-3-(4-vinylbenzyl)-1H-imidazol-3-ium chloride (28).**^[159]

A flame-dried Schlenk flask under N₂ was charged with 1-methylimidazole (2.6 mL, 30 mmol) in CHCl₃ (27 mL). 4-Vinylbenzyl chloride (5.5 mL, 39 mmol) was added and the reaction mixture was stirred for 18 h at 50 °C. The solvent was removed under reduced pressure and the resulting residue was washed with ethyl acetate (4 x 50 mL). The residual solvent was removed under reduced pressure to afford the imidazolium salt **28** as a viscous orange oil (6.71 g, 95 %). ¹H NMR (400 MHz, CDCl₃, δ): 10.9 (s, 1H, N-CH-N), 7.39 (dd, *J* = 14.8, 8.2 Hz, 4H, Ar-H), 7.36 (m, 1H, N-CH=CH-N-CH₃), 7.26 (m, 1H, N-CH=CH-N-CH₃), 6.65 (dd, *J* = 17.6, 10.9 Hz, 1H, H_aC=CH_bH_c), 5.73 (d, *J* = 17.5 Hz, 1H, H_aC=CH_bH_c), 5.54 (s, 2H, Ar-CH₂-N), 5.27 (d, *J* = 10.9 Hz, 1H, H_aC=CH_bH_c), 4.04 (s, 3H, Me); ¹³C NMR (100 MHz, CDCl₃, δ): 138.6, 137.1, 135.8, 132.7, 129.3, 128.9, 127.1, 126.6, 123.8, 122.0, 115.4, 52.9, 36.6; FT-IR (neat, cm⁻¹): $\tilde{\nu}$ = 3134, 3038, 2949, 2850, 1629, 1560, 1513, 1409, 1160, 994, 913, 830, 778, 622. This is consistent with data reported in the literature.^[159]

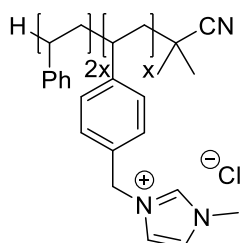
**1-(4-Vinylbenzyl)-1H-imidazole (29).**

A flame-dried Schlenk flask under N₂ was charged with imidazole (13.38 g, 196.6 mmol) in chloroform (40 mL). 4-Vinylbenzyl chloride (5.6 mL, 39 mmol) was added and the reaction mixture was heated to 50 °C and stirred for 18 h. The reaction mixture was washed with water (4 x 100 mL) and brine (100 mL). The solution was dried over MgSO₄, filtered and the solvent removed under reduced pressure to afford the imidazole **29** as a yellow solid (6.14 g, 85%). ¹H NMR (400 MHz, CDCl₃, δ): 7.54 (s, 1H, N-CH-N), 7.37 (d, *J* = 8.2 Hz, 2H, Ar-H ortho to vinyl), 7.10 (d, *J* = 8.2 Hz, 2H, Ar-H meta to vinyl), 7.08 (m, 1H, CH₂-N-CH=CH-N), 6.88 (m, 1H, CH₂-N-CH=CH-N), 6.68 (dd, *J* = 17.6, 10.9 Hz, 1H, H_aC=CH_bH_c), 5.74 (d, *J* = 17.5 Hz, 1H, H_aC=CH_bH_c), 5.25 (d, *J* = 11.0 Hz, 1H, H_aC=CH_bH_c), 5.09 (s, 2H, Ar-CH₂-N); ¹³C NMR (100 MHz, CDCl₃, δ): 137.7, 137.5, 136.1, 135.6, 129.9, 127.6, 126.8, 119.3, 114.7, 50.6; FT-IR (neat, cm⁻¹): $\tilde{\nu}$ = 3108, 3004, 2960, 2933, 1628, 1510, 1437, 1285, 1225, 1104, 1072, 994, 911, 822, 667, 622. This is consistent with data reported in the literature.^[149]



3-Benzyl-1-(4-vinylbenzyl)-1H-imidazol-3-ium bromide (**30**).^[146]

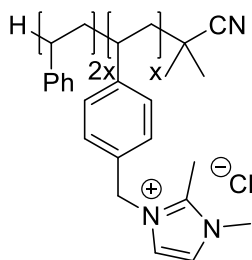
1-(4-Vinylbenzyl)-1H-imidazole **29** (5.94 g, 32.2 mmol) was dissolved in MeCN (30 mL) and stirred. Benzyl bromide (11.5 mL, 96.7 mmol) was added and the reaction mixture was stirred for 18 h. The reaction mixture was added drop-wise in to Et₂O (400 mL) while stirring rapidly upon which a white precipitate formed. The solvent was decanted off and the product was dissolved in MeCN (30 mL). The solvent was removed under reduced pressure to give the benzylated imidazole **30** as a white foam (11.33 g, 99%). **¹H NMR** (400 MHz, CDCl₃, δ): 10.81 (s, 1H, N-CH-N), 7.39 (m, 9H, Ar-H, N-CH=CH-N), 7.22 (m, 2H, Ar-H meta to vinyl), 6.64 (dd, *J* = 17.6, 10.9 Hz, 1H, *H_aC=CH_bH_c*), 5.72 (d, *J* = 17.5 Hz, 1H, *H_aC=CH_bH_c*), 5.52 (s, 4H, Ar-CH₂-N), 5.27 (d, *J* = 10.9 Hz, 1H, *H_aC=CH_bH_c*); **¹³C NMR** (100 MHz, CDCl₃, δ): 138.9, 137.2, 135.8, 132.8, 132.1, 129.7, 129.6, 129.4, 129.1, 127.3, 121.9, 115.6, 53.6, 53.3; **FT-IR** (neat, cm⁻¹): $\tilde{\nu}$ = 3424, 3122, 3051, 2967, 2847, 1556, 1149, 914, 716. **HRMS** (ESI⁺) exact mass calculated for C₁₉H₂₀N₂ [M+H]⁺ *m/z* = 276.1626, found *m/z* = 276.1627.



Poly-1-Methyl-3-(4-vinylbenzyl)-1H-imidazol-3-ium chloride-co-styrene (**31**).^[146]

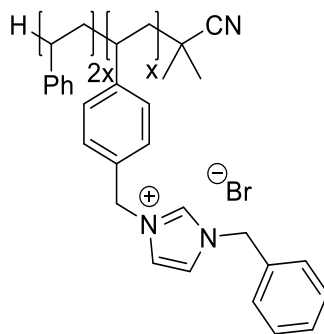
A flame-dried Schlenk flask under N₂ was charged with AIBN (0.71 g, 4.3 mmol, 5 mol %) followed by 1-methyl-3-(4-vinylbenzyl)-1H-imidazol-3-ium chloride monomer **28** (6.71 g, 28.6 mmol) in dry MeOH (100 mL) and styrene (6.6 mL, 57 mmol). The reagents were degassed with 5 freeze/pump/thaw cycles using liquid nitrogen. Upon reaching ambient temperature the reaction mixture was heated to 70 °C and allowed to stir for 40 h. The amount of solvent was reduced under reduced pressure to around half the original volume and then added drop-wise into Et₂O (600 mL) while stirring rapidly to induce precipitation. The product was isolated by filtration, washed with Et₂O (3 x 50 mL) and finally dried under reduced pressure to afford the styrene 3H-imidazolium chloride polymer **31** as a white solid (7.51 g, 59 %). **¹H NMR** (400 MHz, CDCl₃, δ): 9.51 (br, N-CH-N), 7.75 (br, Ar-H), 7.06 (br, Ar-H), 6.49 (br, Ar-H), 5.36 (br,

Ar-CH₂-N), 3.87 (br, N-CH₃), 1.67 (br, CHCH₂, polymer backbone), 1.42 (br, CHCH₂, polymer backbone). The composition of **31** can be determined by comparing the integration of the Ar-CH₂-N protons which derive from **28** with the sum of the integration of the Ar protons which derive from both **28** and styrene. The monomer composition was determined to be 2: 1 styrene: **28** (identical to the feed ratio). **FT-IR** (neat, cm⁻¹): $\tilde{\nu}$ = 3343, 3142, 3056, 3025, 2924, 2849, 1601, 1572, 1493, 1452, 1160, 1031, 760, 700, 619; **CHN** Anal. Calc. for C₂₉H₃₁ClN₂ (443.0) C, 78.62; H, 7.05; N, 6.32 %. Found: C, 74.65; H, 6.76; N, 6.29 %.



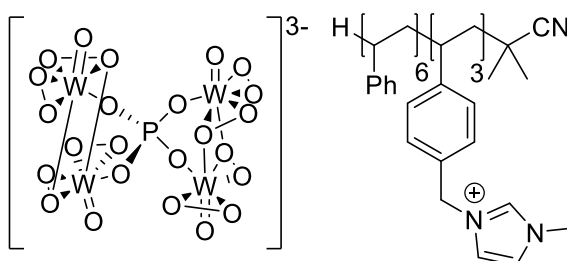
Poly-1,2-Dimethyl-3-(4-vinylbenzyl)-1H-imidazol-3-ium chloride-co-styrene (32).^[146]

A flame-dried Schlenk flask under N₂ was charged with AIBN (0.68 g, 4.1 mmol, 5 mol %) followed by 1,2-dimethyl-3-(4-vinylbenzyl)-1H-imidazol-3-ium chloride monomer **18** (6.82 g, 27.4 mmol) in dry MeOH (100 mL) and styrene (6.3 mL, 55 mmol). The reagents were degassed with 5 freeze/pump/thaw cycles using liquid nitrogen. Upon reaching ambient temperature the reaction mixture was heated to 70 °C and allowed to stir for 40 h. The amount of solvent was reduced under reduced pressure to around half the original volume and then added drop-wise into Et₂O (600 mL) while stirring rapidly to induce precipitation. The product was isolated by filtration, washed with Et₂O (3 x 50 mL) and finally dried under reduced pressure to afford the styrene 1,2-dimethyl-3-(4-vinylbenzyl)imidazolium chloride polymer **32** as a white solid (9.86 g, 79 %). **¹H NMR** (400 MHz, CDCl₃, δ): 7.75 (br, Ar-H), 7.06 (br, Ar-H), 6.48 (br, Ar-H), 5.37 (br, Ar-CH₂-N), 3.79 (br, N-CH₃), 2.56 (br, N-CHCH₃-N), 1.48 (br, CHCH₂, polymer backbone). The composition of **32** can be determined by comparing the integration of the Ar-CH₂-N protons which derive from **18** with the sum of the integration of the Ar protons which derive from both **18** and styrene. The monomer composition was determined to be 2: 1 styrene: **18** (identical to the feed ratio). **FT-IR** (neat, cm⁻¹): $\tilde{\nu}$ = 3290, 3026, 2923, 2850, 1587, 1536, 1513, 1493, 1452, 1034, 761, 701; **CHN** Anal. Calc. for C₃₀H₃₃ClN₂ (457.1) C, 78.83; H, 7.28; N, 6.13 %. Found: C, 73.52; H, 6.83; N, 6.57 %.



Poly-3-Benzyl-1-(4-vinylbenzyl)-1H-imidazol-3-ium bromide-co-styrene (33).^[146]

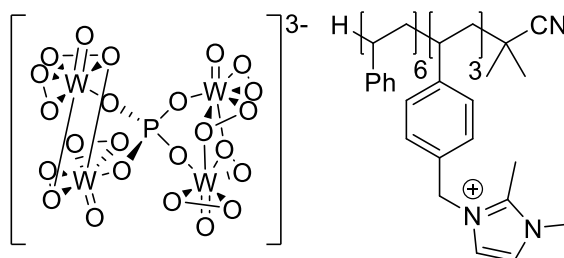
A flame-dried Schlenk flask under N_2 was charged with AIBN (0.81 g, 4.9 mmol, 5 mol %) followed by 3-benzyl-1-(4-vinylbenzyl)-1H-imidazol-3-ium bromide monomer **30** (11.61 g, 32.8 mmol) in MeOH (100 mL) and styrene (6.8 mL, 66 mmol). The reagents were degassed with 5 freeze/pump/thaw cycles using liquid nitrogen. Upon reaching ambient temperature the reaction mixture was heated to 70 °C and allowed to stir for 40 h. The amount of solvent was reduced under reduced pressure to around half the original volume and then added drop-wise into Et₂O (600 mL) while stirring rapidly to induce precipitation. The product was isolated by filtration, washed with Et₂O (3 x 50 mL) and finally dried under reduced pressure to afford the benzylated styrene polymer **33** as a white solid (14.0 g, 76 %). ¹H NMR (400 MHz, CDCl₃, δ): 9.67 (br, N-CH-N), 7.89 (br, Ar-H), 7.45 (br, Ar-H), 7.38 (br, Ar-H), 7.06 (br, Ar-H), 6.48 (br, Ar-H), 5.49 (br, Ar-CH₂-N), 5.38 (br, Ar-CH₂-N), 1.47 (br, CHCH₂, polymer backbone). The composition of **33** can be determined by comparing the integration of the Ar-CH₂-N protons which derive from **30** with the integration of the Ar protons which derive from both **30** and styrene. The monomer composition was determined to be 2: 1 styrene: **30** (identical to the feed ratio). FT-IR (neat, cm⁻¹): $\tilde{\nu}$ = 3406, 3057, 3025, 2925, 2850, 1601, 1558, 1493, 1452, 1149, 759, 700; CHN Anal. Calc. for C₃₅H₃₅BrN₂ (563.6) C, 74.59; H, 6.26; N, 4.97 %. Found: C, 71.69; H, 6.72; N, 5.03 %.



Polymer supported peroxophosphotungstate (34).^[46]

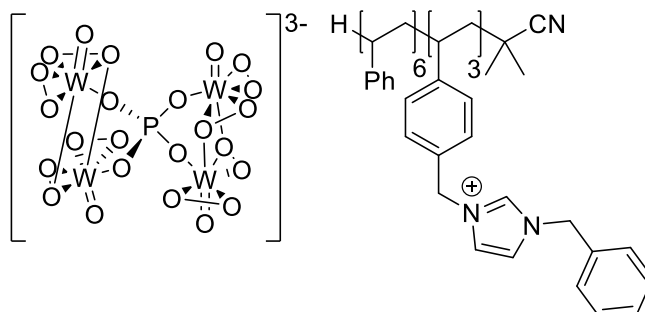
Aqueous hydrogen peroxide solution (35% w/w, 13.4 mL, 155 mmol) was added to a solution of phosphotungstic acid (2.24 g, 800 μmol) in water (1 mL) and the mixture was stirred at room temperature for 30 min. After this time, a solution of polymer **31** (1.00 g, 2.30 mmol) in EtOH

(30 mL) was added and the reaction mixture was stirred for a further 30 min. The reaction mixture was added drop-wise into Et₂O (500 mL) while stirring rapidly to induce precipitation. The product was isolated by filtration, washed with Et₂O (3 x 50 mL) and finally dried under reduced pressure to afford PIILP **34** as an off white crystalline solid (0.80 g, 25 %). **FT-IR** (neat, cm⁻¹): $\tilde{\nu}$ = 3411, 3149, 3026, 2925, 1633, 1602, 1562, 1493, 1452, 1425, 1159, 1080, 1029, 956, 869, 836, 756, 700; **CHN** Anal. Calc. for C₈₇H₉₃N₆O₂₄PW₄ (2373.0) C, 44.03; H, 3.95; N, 3.54 %. Found: C, 41.04; H, 3.99; N, 3.14 %.



Polymer supported peroxophosphotungstate (**35**).^[46]

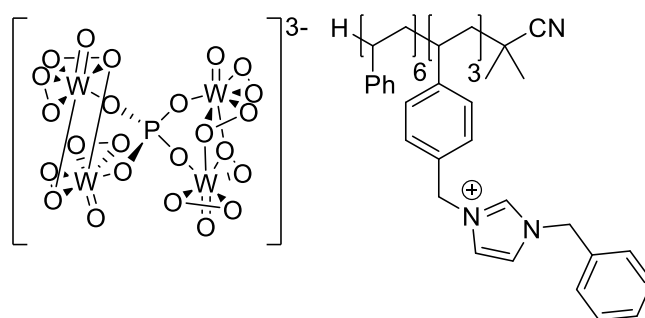
Aqueous hydrogen peroxide solution (35% w/w, 12.9 mL, 151 mmol) was added to a solution of phosphotungstic acid (2.17 g, 800 μ mol) in water (1 mL) and the mixture was stirred at room temperature for 30 min. After this time, a solution of polymer **32** (1.00 g, 2.30 mmol) in EtOH (30 mL) was added and the reaction mixture was stirred for a further 30 min. The reaction mixture was added drop-wise into Et₂O (500 mL) while stirring rapidly to induce precipitation. The product was isolated by filtration, washed with Et₂O (3 x 50 mL) and finally dried under reduced pressure to afford PIILP **35** as an off white crystalline solid (1.50 g, 47 %). **FT-IR** (neat, cm⁻¹): $\tilde{\nu}$ = 3408, 3140, 3026, 2926, 1614, 1493, 1452, 1422, 1078, 949, 820, 759, 701; **CHN** Anal. Calc. for C₉₀H₉₉N₆O₂₄PW₄ (2415.1) C, 44.76; H, 4.13; N, 3.48 %. Found: C, 41.29; H, 4.05; N, 3.38 %.



Polymer supported peroxophosphotungstate (**36**).^[46]

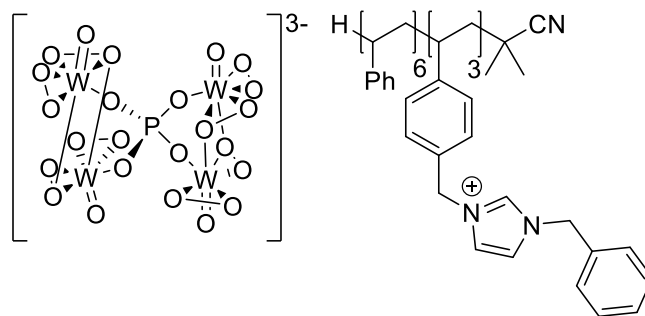
Aqueous hydrogen peroxide solution (35% w/w, 10.2 mL, 118 mmol) was added to a solution of phosphotungstic acid (1.70 g, 600 μ mol) in water (1 mL) and the mixture was stirred at room

temperature for 30 min. After this time, a solution of polymer **33** (1.00 g, 1.80 mmol) in EtOH (50 mL) was added and the reaction mixture was stirred for a further 30 min. The reaction mixture was added drop-wise into Et₂O (500 mL) while stirring rapidly to induce precipitation. The product was isolated by filtration, washed with Et₂O (3 x 50 mL) and finally dried under reduced pressure to afford PIILP **36** as an off white crystalline solid (1.00 g, 37 %). **FT-IR** (neat, cm⁻¹): $\tilde{\nu}$ = 3140, 3061, 3026, 2925, 1712, 1640, 1602, 1558, 1494, 1453, 1148, 1029, 943, 887, 814, 756, 700; **CHN** Anal. Calc. for C₁₀₅H₁₀₅N₆O₂₄PW₄ (2601.3) C, 48.48; H, 4.07; N, 3.23 %. Found: C, 47.45; H, 4.25; N, 3.01 %.



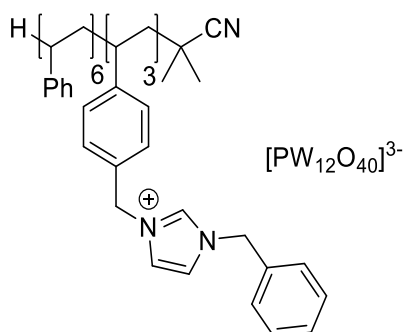
Polymer supported peroxophosphotungstate at high dilution (**37**).^[46]

Aqueous hydrogen peroxide solution (35% w/w, 3.1 mL, 35 mmol) was added to a solution of phosphotungstic acid (0.51 g, 200 μ mol) in water (0.3 mL) and the mixture was stirred at room temperature for 30 min. After this time, a solution of polymer **33** (300 mg, 500 μ mol) in EtOH (150 mL) was added and the reaction mixture was stirred for a further 30 min. The reaction mixture was added drop-wise into Et₂O (500 mL) while stirring rapidly to induce precipitation. The product was isolated by filtration, washed with Et₂O (3 x 50 mL) and finally dried under reduced pressure to afford PIILP **37** as an off white crystalline solid (0.30 g, 37 %). **FT-IR** (neat, cm⁻¹): $\tilde{\nu}$ = 3134, 3061, 3026, 2923, 2851, 1634, 1602, 1558, 1494, 1452, 1147, 1029, 953, 815, 753, 699; **CHN** Anal. Calc. for C₁₀₅H₁₀₅N₆O₂₄PW₄ (2601.3) C, 48.48; H, 4.07; N, 3.23 %. Found: C, 46.18; H, 4.83; N, 3.00 %.



Polymer supported peroxophosphotungstate at increased concentration (**38**).^[46]

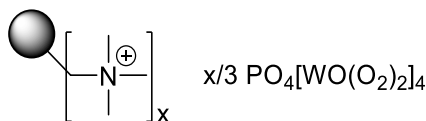
Aqueous hydrogen peroxide solution (35% w/w, 3.1 mL, 35 mmol) was added to a solution of phosphotungstic acid (0.51 g, 0.20 mmol) in water (0.3 mL) and the mixture was stirred at room temperature for 30 min. After this time, a solution of polymer **33** (0.30 g, 0.50 mmol) in EtOH (7.5 mL) was added and the reaction mixture was stirred for a further 30 min. The reaction mixture was added drop-wise into Et₂O (500 mL) while stirring rapidly to induce precipitation. The product was isolated by filtration, washed with Et₂O (3 x 50 mL) and finally dried under reduced pressure to afford PIILP **38** as an off white crystalline solid (0.50 g, 62 %). **FT-IR** (neat, cm⁻¹): $\tilde{\nu}$ = 3140, 3060, 3026, 2922, 1602, 1558, 1494, 1452, 1147, 1079, 946, 876, 812, 698; **CHN** Anal. Calc. for C₁₀₅H₁₀₅N₆O₂₄PW₄ (2601.3) C, 48.48; H, 4.07; N, 3.23 %. Found: C, 28.87; H, 3.08; N, 1.63 %. The CHN analysis suggests incomplete loading of the polymer had occurred.



Polymer supported phosphotungstic acid (**39**).^[46]

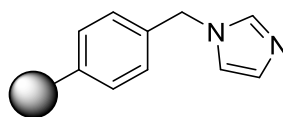
A solution of phosphotungstic acid (1.0 g, 0.40 mmol) in water (6.8 mL) was added to a solution of polymer **33** (0.60 g, 1.1 mmol) in EtOH (30 mL) and the reaction mixture was stirred for 30 min. The reaction mixture was added drop-wise into Et₂O (500 mL) while stirring rapidly to induce precipitation. The product was isolated by filtration, washed with Et₂O (3 x 50 mL) and finally dried under reduced pressure to afford PIILP **39** as an off white crystalline solid (1.3 g, 81 %). **FT-IR** (neat, cm⁻¹): $\tilde{\nu}$ = 3141, 3025, 2923, 1601, 1557, 1493, 1452, 1144, 1078, 974,

894, 799, 698; **CHN** Anal. Calc. for $C_{105}H_{105}N_6O_{40}PW_{12}$ (4328.0) C, 29.14; H, 2.45; N, 1.94 %. Found: C, 30.21; H, 2.70; N, 1.79 %.



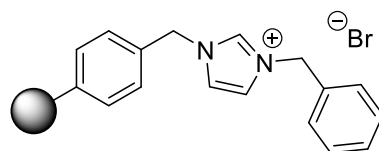
Peroxophosphotungstate loaded Amberlite (40).^[46]

Aqueous hydrogen peroxide solution (35% w/w, 11.9 mL, 139 mmol) was added to a solution of phosphotungstic acid (2.00 g, 700 μ mol) dissolved in water (1.2 mL) and the resulting mixture was a solution stirred at room temperature for 30 min. After this time, the solution was passed through a narrow sinter funnel containing Amberlite IRA 900 chloride form (2.00 g). The Amberlite was then washed with water (50 mL) and Et₂O (50 mL) and the solvent was removed under reduced pressure to afford the functionalised Amberlite as white beads. **FT-IR** (neat, cm^{-1}): $\tilde{\nu}$ = 3401, 3030, 2928, 2362, 2343, 1636, 1614, 1476, 924, 885, 715; **CHN** Found: C, 44.91; H, 7.66; N, 3.81 %. For unfunctionalised Amberlite: C, 59.66; H, 9.82; N, 5.29 %.



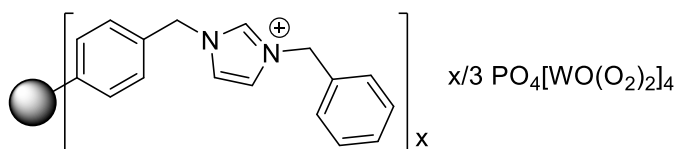
Imidazole loaded Merrifield resin (41).^[159]

A flame-dried Schlenk flask under N₂ was charged with Merrifield resin (2.0 g, 2.0 mmol) (1% divinylbenzene crosslinked, 1.0- 1.3 mmol g⁻¹ Cl, 200- 400 mesh) and imidazole (1.36 g, 20.0 mmol) in dry CHCl₃ (30 mL) and the reaction mixture was heated to 50 °C and stirred for 72 h. The reaction mixture was filtered and washed with CHCl₃ (50 mL), water (50 mL), EtOH (50 mL) and Et₂O (50 mL). The residual solvent was removed under reduced pressure to afford the imidazole loaded Merrifield resin **41** as a white solid (1.75 g, 82 %). **FT-IR** (neat, cm^{-1}): $\tilde{\nu}$ = 3059, 3026, 2922, 2851, 1601, 1493, 1452, 1074, 1028, 755, 697; **CHN** Anal. Calc. N, 2.72 %. Found: C, 86.97; H, 8.54; N, 1.80 %. This nitrogen content corresponds to 0.64 mmol g⁻¹ imidazole loading. For unfunctionalised Merrifield resin: C, 88.20; H, 7.04; N, 0.00 %



Benzylated imidazolium loaded Merrifield resin (**42**).^[146]

A flame-dried Schlenk flask under N₂ was charged with imidazole loaded Merrifield resin **41** (1.65 g) and benzyl bromide (2.38 mL, 20.0 mmol) in dry MeCN (20 mL) and the reaction mixture was allowed to stir for 72 h. The reaction mixture was filtered and washed with MeCN (50 mL) and Et₂O (100 mL). The solvent was removed under reduced pressure to afford the benzylated imidazolium Merrifield resin **42** as a white solid (1.15 g). **FT-IR** (neat, cm⁻¹): $\tilde{\nu}$ = 3059, 3025, 2922, 2850, 1601, 1493, 1452, 1151, 1028, 756, 697; **CHN** Anal. Calc. based on measured loading of imidazole in **41** N, 2.33 %. Found: C, 80.68; H, 7.97; N, 1.43 %. This nitrogen content corresponds to 0.5 mmol g⁻¹ imidazolium loading.



Functionalised Merrifield resin loaded peroxophosphotungstate (**43**).^[46]

Aqueous hydrogen peroxide solution (35% w/w, 4.5 mL, 52 mmol) was added to a solution of phosphotungstic acid (0.75 g, 0.30 mmol) in water (0.5 mL) and the mixture was stirred at room temperature for 30 min. After this time, the solution was added to a suspension of benzylated imidazolium loaded Merrifield resin **42** (0.9 g) in EtOH (47 mL) and the reaction mixture was stirred for a further 30 min. The reaction mixture was added drop-wise into Et₂O (500 mL) while stirring rapidly. The product was isolated by filtration, washed with Et₂O (3 x 50 mL) and finally dried under reduced pressure to afford PIILP **43** as a white crystalline solid (1.2 g, 73 %). **FT-IR** (neat, cm⁻¹): $\tilde{\nu}$ = 3059, 3026, 2922, 2850, 1716, 1602, 1558, 1493, 1452, 1148, 1029, 960, 814, 755, 697; **CHN** Anal. Calc. for N₆O₂₄PW₄N, 1.86 %. Found: C, 63.46; H, 6.16; N, 0.97 %.

General procedure for the catalytic sulfoxidation in batch.^[116]

A flame-dried Schlenk flask under N₂ was charged with sulfide (1.0 mmol), PIILP catalyst (0.005 mmol, 0.5 mol %) and solvent (3 mL) and stirred. The reaction was initiated by the addition of aqueous hydrogen peroxide (35% w/w, 0.21 mL, 2.5 mmol) and allowed to stir at room temperature for 15 min. The reaction mixture was diluted with CH₂Cl₂ (25 mL), washed

with H₂O (50 mL) and the organic extract dried over MgSO₄ and the solvent removed under reduced pressure. The resulting residue was analysed by either ¹H or ¹³C{¹H} NMR spectroscopy to quantify the composition of starting material and products; for each substrate tested an internal standard of 1,3-dinitrobenzene was initially employed to ensure mass balance.

General procedure for the catalytic sulfoxidation recycle studies.^[116]

A PTFE centrifuge tube containing a magnetic stirrer bar was placed in a flame-dried Schlenk flask under N₂. The tube was charged with PIILP catalyst (0.01 mmol, 0.5 mol %), sulfide (2.0 mmol) and solvent (6 mL) and stirred for 2 min. The reaction was initiated by the addition of aqueous hydrogen peroxide (35% w/w, 0.43 mL, 5.0 mmol) and allowed to stir at room temperature for 5 min. After this time the solution was centrifuged (5 min, 14,000 rpm), decanted and the remaining PIILP catalyst washed with the reaction solvent (6 mL), re-centrifuged (5 min, 14,000 rpm) and the solvent was decanted. The reaction solution was diluted with CH₂Cl₂ (25 mL), washed with H₂O (50 mL) and the organic extract dried over MgSO₄ and the solvent removed under reduced pressure. The resulting residue was analysed by ¹H NMR spectroscopy to quantify the composition of starting material and products. The residue in the centrifuge tube was then re-suspended in solvent and reused.

General procedure for the catalytic sulfoxidation tandem recycle studies.

The general procedure for the catalytic sulfoxidation recycle studies was followed with 4-nitrothioanisole (2.0 mmol) and upon re-suspension of the catalyst in the reaction solvent, thioanisole (2.0 mmol) was added and the procedure repeated. Again following re-suspension of the catalyst in the reaction solvent, ethyl phenyl sulfide (2.0 mmol) was added and the procedure repeated for a final time.

General procedure for the catalytic sulfoxidation kinetic studies.^[116]

A flame-dried Schlenk flask under N₂ was charged with sulfide (4.0 mmol), PIILP catalyst (0.02 mmol, 0.5 mol %) and solvent (12 mL) and stirred. The reaction was initiated by the addition of aqueous hydrogen peroxide (35% w/w, 0.86 mL, 10.0 mmol) and the resulting mixture stirred at room temperature for 24 h during which time 0.2 mL aliquots were removed using a wide bore syringe needle and diluted with CH₂Cl₂ (5 mL), washed with H₂O (10 mL) and the organic extract dried over MgSO₄ and the solvent removed under reduced pressure. The resulting residue was analysed by ¹H NMR spectroscopy.

General procedure for segmented and continuous flow catalytic sulfoxidations.^[116]

Two reservoirs were charged with sulfide (5.0 mmol) dissolved in the appropriate solvent (25 mL, 0.2 M) and hydrogen peroxide (1.29 mL, 35%) in the appropriate solvent (25 mL, 0.6 M). A Uniqsis FlowSyn reactor was used to pump 1 mL of each reagent at total flow rates that varied between 0.293 mL min⁻¹ and 8.8 mL min⁻¹ through a T-piece mixer to combine the two streams; in the case of segmented flow an additional reservoir of carrier solvent was also employed. The reaction stream was then flowed through a OMNIFIT® glass column reactor cartridge (10 mm id × 100 mm) packed with 0.1 g of [PO₄{WO- (O₂)₂}₄]@PIILP and 2.0 g of SiO₂ (Geduran® Si 60) and mounted in a FlowSyn column heater. The exiting stream was passed through a back pressure regulator (BPR) and 2 mL fractions were collected into separate vials followed by a 2 mL post-collect. Each sample was diluted with CH₂Cl₂ (10 mL), washed with water (ca. 15 mL), the organic extract dried over MgSO₄, the solvent removed under reduced pressure and the resulting residue analysed by ¹H NMR spectroscopy to quantify the composition of starting material and products.

Characterisation of sulfides, sulfoxides and sulfones.

¹H and ¹³C signals used for calculation of conversion / selectivity for each substrate:

Methyl phenyl sulfide. ¹H NMR (300 MHz, CDCl₃, δ): 2.38 (s, 3H, Me).

Methyl phenyl sulfoxide. ¹H NMR (300 MHz, CDCl₃, δ): 2.64 (s, 3H, Me).

Methyl phenyl sulfone. ¹H NMR (300 MHz, CDCl₃, δ): 2.97 (s, 3H, Me).

Values agree with literature values.^[160]

Methyl 4-nitrophenyl sulfide. ¹H NMR (300 MHz, CDCl₃, δ): 2.48 (s, 3H, Me).

Methyl 4-nitrophenyl sulfoxide. ¹H NMR (300 MHz, CDCl₃, δ): 2.74 (s, 3H, Me).

Methyl 4-nitrophenyl sulfone. ¹H NMR (400 MHz, CDCl₃, δ): 3.07 (s, 3H, Me).

Values agree with literature values.^[161]

Dibenzothiophene. ¹H NMR (300 MHz, CDCl₃, δ): 8.04- 7.98 (m, 2H), 7.75- 7.69 (m, 2H).

Dibenzothiophene sulfoxide. ¹H NMR (300 MHz, CDCl₃, δ): 7.87- 7.84 (m, 2H), 7.67-7.63 (m, 2H).

Dibenzothiophene sulfone. ¹H NMR (300 MHz, CDCl₃, δ): 7.60- 7.54 (m, 2H), 7.49- 7.43 (m, 2H).

Values agree with literature values.^[160]

Ethyl phenyl sulfide. ¹H NMR (300 MHz, CDCl₃, δ): 2.84 (q, *J* = 7.4 Hz, 2H, CH₂).

Ethyl phenyl sulfoxide. ¹H NMR (300 MHz, CDCl₃, δ): 2.80 (q, 1H, *J* = 7.4 Hz, CH₂), 2.70 (q, 1H, *J* = 7.4 Hz, CH₂).

Ethyl phenyl sulfone. ¹H NMR (300 MHz, CDCl₃, δ): 3.03 (q, 2H, *J* = 7.44 Hz, CH₂).

Values agree with literature values.^[160]

Allyl phenyl sulfide. ¹³C NMR (500 MHz, CDCl₃, δ): 35.96 (CH₂).

Allyl phenyl sulfoxide. ¹³C NMR (500 MHz, CDCl₃, δ): 147.38 (C-SO-CH₂), 59.74 (CH₂).

Allyl phenyl sulfone. ¹³C NMR (500 MHz, CDCl₃, δ): 59.74 (CH₂).

Values agree with literature values.^[160]

***n*-Decyl methyl sulfide.** ¹H NMR (300 MHz, CDCl₃, δ): 2.02 (s, 3H, Me).

***n*-Decyl methyl sulfoxide.** ¹H NMR (300 MHz, CDCl₃, δ): 2.49 (s, 3H, Me).

***n*-Decyl methyl sulfone.** ¹H NMR (300 MHz, CDCl₃, δ): 2.83 (s, 3H, Me).

Values agree with literature values.^[162]

Benzyl phenyl sulfide. ¹H NMR (300 MHz, CDCl₃, δ): 3.98 (s, 2H, CH₂).

Benzyl phenyl sulfoxide. ¹H NMR (300 MHz, CDCl₃, δ): 3.95 (d, *J* = 12.6 Hz, 1H), 3.88 (, *J* = 12.6 Hz, 1H).

Benzyl phenyl sulfone. ¹H NMR (300 MHz, CDCl₃, δ): 4.18 (s, 2H, CH₂).

Values agree with literature values.^[163]

Homoallyl phenyl sulfide. ¹H NMR (300 MHz, CDCl₃, δ): 2.89- 2.84 (m, 2H, S-CH₂).

Homoallyl phenyl sulfoxide. ¹H NMR (300 MHz, CDCl₃, δ): 2.82- 2.70 (m, 2H, S-CH₂).

Homoallyl phenyl sulfone. ¹H NMR (400 MHz, CDCl₃, δ): 3.10- 3.04 (m, 2H, S-CH₂).

Values agree with literature values.^[164]

5.4 Experimental Procedures Chapter 4

General procedure for the catalytic sulfoxidation of model oil.

A flame-dried Schlenk flask under N₂ was charged with dibenzothiophene (61.4 mg, 0.33 mmol, 1000 ppm sulfur), PIILP catalyst (8.7 mg, 1.0 mol %) and octane (10 mL) and stirred at the required temperature. MeOH (4 mL) was added and the reaction was initiated by the addition of aqueous hydrogen peroxide (35% w/w, 0.086 mL, 1.0 mmol) and the resulting mixture stirred for 30 min. The layers were separated and the octane dried under reduced pressure. The MeOH layer was passed through a plug of sodium metabisulfite and the solvent removed under reduced pressure. 1,3-Dinitrobenzene (28.0 mg, 0.16 mmol) was added to both samples as a standard and then analysed by ¹H NMR spectroscopy to quantify the composition of starting material and products in both samples.

General procedure for the catalytic sulfoxidation of model oil kinetic study.^[116]

A flame-dried Schlenk flask under N₂ was charged with dibenzothiophene (122.8 mg, 0.66 mmol, 1000 ppm sulfur), PIILP catalyst (17.4 mg, 1.0 mol %) and octane (20 mL) and heated to 60 °C and stirred. MeOH (8 mL) was added and the reaction was initiated by the addition of aqueous hydrogen peroxide (35% w/w, 0.172 mL, 2.0 mmol) and the resulting mixture stirred for 140 min during which time 0.2 mL aliquots of the octane layer were removed. The octane was removed under reduced pressure and 1,3-dinitrobenzene (5.6 mg, 0.03 mmol) was added as a standard and then analysed by ¹H NMR spectroscopy.

General procedure for the catalytic sulfoxidation of model oil recycle study.^[116]

A PTFE centrifuge tube containing a magnetic stirrer bar was charged with PIILP catalyst (4.4 mg, 1.0 mol %), dibenzothiophene (30.7 mg, 0.17 mmol, 1000 ppm sulfur) and octane (5 mL) and heated to 60 °C and stirred. MeOH (2 mL) was added and the reaction was initiated by the addition of aqueous hydrogen peroxide (35% w/w, 0.043 mL, 0.5 mmol) and the resulting mixture stirred for 60 min. After this time the mixture was centrifuged (5 min, 14,000 rpm), decanted and the remaining PIILP catalyst washed with MeOH (2 mL), re-centrifuged (5 min, 14,000 rpm) and the solvent was decanted. The layers are separated and the octane dried under reduced pressure. 1,3-Dinitrobenzene (14.0 mg, 0.08 mmol) is added as a standard and then analysed by ¹H NMR spectroscopy to quantify the composition of starting material in the sample.

General procedure for the catalytic sulfoxidation of crude oil.

A PTFE centrifuge tube containing a magnetic stirrer bar was charged with PIILP catalyst (4.4 mg, 1.0 mol %), crude oil (5 mL) and heated to 60 °C and stirred vigorously. MeOH (2 mL) was added and the reaction was initiated by the addition of aqueous hydrogen peroxide (35% w/w, 0.043 mL, 0.5 mmol) and the resulting mixture stirred for 2 h. After this time the mixture was centrifuged (5 min, 14,000 rpm), decanted and the remaining PIILP catalyst washed with MeOH (2 mL), re-centrifuged (5 min, 14,000 rpm) and the solvent was decanted. The layers are separated and the crude oil dried under reduced pressure. The crude oil was analysed by elemental analysis to quantify the percentage of sulfur remaining in the sample.

REFERENCES

- [1] F. Fringuelli, O. Piermatti, F. Pizzo, L. Vaccaro, *Science of Synthesis* **2010**, 47, 707.
- [2] S. Doherty, in *Catalysis in Ionic Liquids, Vol. 1* (Ed.: J. J. Spivey), Royal Society of Chemistry, Cambridge, **2014**, pp. 44-308.
- [3] D. Zhao, M. Wu, Y. Kou, E. Min, *Catal. Today* **2002**, 74, 157-189.
- [4] H. Olivier-Bourbigou, L. Magna, D. Morvan, *Appl. Catal., A* **2010**, 373, 1-56.
- [5] M. Smiglak, J. D. Holbrey, S. T. Griffin, W. M. Reichert, R. P. Swatloski, A. R. Katritzky, H. Yang, D. Zhang, K. Kirichenko, R. D. Rogers, *Green Chem.* **2007**, 9, 90-98.
- [6] N. D. Khupse, A. Kumar, *Indian J. Chem.* **2010**, 49, 635-648.
- [7] (a)M. C. Buzzeo, R. G. Evans, R. G. Compton, *ChemPhysChem* **2004**, 5, 1106-1120; (b)R. Giernoth, in *In situ NMR Methods in Catalysis* (Eds.: J. Bargon, L. T. Kuhn), Springer Berlin Heidelberg, Berlin, Heidelberg, **2007**, pp. 1-23; (c)Y. Gu, G. Li, *Adv. Synth. Catal.* **2009**, 351, 817-847; (d)J. D. P. Migowski, *Chem. Eur. J.* **2007**, 13, 32-39; (e)R. P. Swatloski, S. K. Spear, J. D. Holbrey, R. D. Rogers, *J. Am. Chem. Soc.* **2002**, 124, 4974-4975; (f)F. van Rantwijk, R. A. Sheldon, *Chem. Rev.* **2007**, 107, 2757-2785; (g)Q. Zhang, S. Zhang, Y. Deng, *Green Chem.* **2011**, 13, 2619-2637.
- [8] M. J. Earle, S. P. Katdare, K. R. Seddon, *Org. Lett.* **2004**, 6, 707-710.
- [9] S. Sugden, H. Wilkins, *Journal of the Chemical Society (Resumed)* **1929**, 1291-1298.
- [10] J. A. Boon, J. A. Levisky, J. L. Pflug, J. S. Wilkes, *J. Org. Chem.* **1986**, 51, 480-483.
- [11] Y. Xiao, S. V. Malhotra, *J. Organomet. Chem.* **2005**, 690, 3609-3613.
- [12] Y. Xiao, S. V. Malhotra, *J. Mol. Catal. A: Chem.* **2005**, 230, 129-133.
- [13] Y. Chauvin, B. Gilbert, I. Guibard, *J. Chem. Soc., Chem. Commun.* **1990**, 1715-1716.
- [14] R. T. Carlin, J. S. Wilkes, *J. Mol. Catal.* **1990**, 63, 125-129.
- [15] J. S. Wilkes, M. J. Zaworotko, *J. Chem. Soc., Chem. Commun.* **1992**, 965-967.
- [16] Q. Yao, E. P. Kinney, Z. Yang, *J. Org. Chem.* **2003**, 68, 7528-7531.
- [17] (a)E. Peris, J. A. Loch, J. Mata, R. H. Crabtree, *Chem. Commun.* **2001**, 201-202; (b)B. Karimi, D. Enders, *Org. Lett.* **2006**, 8, 1237-1240.
- [18] P. Nehra, B. Khungar, K. Pericherla, S. C. Sivasubramanian, A. Kumar, *Green Chem.* **2014**, 16, 4266-4271.
- [19] R. Singh, M. Sharma, R. Mamgain, D. S. Rawat, *J. Braz. Chem. Soc.* **2008**, 19, 357-379.
- [20] F. Bellina, C. Chiappe, *Molecules* **2010**, 15, 2211-2245.
- [21] D. E. Kaufmann, M. Nouroozian, H. Henze, *Synlett* **1996**, 1091-1092.

-
- [22] W. A. Herrmann, V. P. W. Böhm, *J. Organomet. Chem.* **1999**, *572*, 141-145.
- [23] G. Zhang, H. Zhou, J. Hu, M. Liu, Y. Kuang, *Green Chem.* **2009**, *11*, 1428-1432.
- [24] S. P. Stanforth, *Tetrahedron* **1998**, *54*, 263-303.
- [25] N. Miyaura, T. Yanagi, A. Suzuki, *Synth. Commun.* **1981**, *11*, 513-519.
- [26] C. J. Mathews, P. J. Smith, T. Welton, *Chem. Commun.* **2000**, 1249-1250.
- [27] J. P. Hallett, T. Welton, *Chem. Rev.* **2011**, *111*, 3508-3576.
- [28] X. Yang, Z. Fei, T. J. Geldbach, A. D. Phillips, C. G. Hartinger, Y. Li, P. J. Dyson, *Organometallics* **2008**, *27*, 3971-3977.
- [29] S. V. Ley, C. Ramarao, M. D. Smith, *Chem. Commun.* **2001**, 2278-2279.
- [30] C. E. Song, E. J. Roh, *Chem. Commun.* **2000**, 837-838.
- [31] J. Muzart, *Adv. Synth. Catal.* **2006**, *348*, 275-295.
- [32] B. S. Chhikara, R. Chandra, V. Tandon, *J. Catal.* **2005**, *230*, 436-439.
- [33] M. Rong, C. Liu, J. Han, H. Wang, *Catal. Commun.* **2009**, *10*, 362-364.
- [34] C. Venkat Reddy, J. G. Verkade, *J. Mol. Catal. A: Chem.* **2007**, *272*, 233-240.
- [35] Y. Chao, H. Li, W. Zhu, G. Zhu, Y. Yan, *Pet. Sci. Technol.* **2010**, *28*, 1242-1249.
- [36] D. Betz, P. Altmann, M. Cokoja, W. A. Herrmann, F. E. Kühn, *Coord. Chem. Rev.* **2011**, *255*, 1518-1540.
- [37] P. S. Campbell, A. Podgoršek, T. Gutel, C. C. Santini, A. A. H. Pádua, M. F. Costa Gomes, F. Bayard, B. Fenet, Y. Chauvin, *The Journal of Physical Chemistry B* **2010**, *114*, 8156-8165.
- [38] C. P. Mehnert, R. A. Cook, N. C. Dispenziere, M. Afeworki, *J. Am. Chem. Soc.* **2002**, *124*, 12932-12933.
- [39] M.-J. Jin, A. Taher, H.-J. Kang, M. Choi, R. Ryoo, *Green Chem.* **2009**, *11*, 309-313.
- [40] H. Hagiwara, H. Sasaki, N. Tsubokawa, T. Hoshi, T. Suzuki, T. Tsuda, S. Kuwabata, *Synlett* **2010**, 1990-1996.
- [41] A. Taher, J.-B. Kim, J.-Y. Jung, W.-S. Ahn, M.-J. Jin, *Synlett* **2009**, 2477-2482.
- [42] F. Giacalone, M. Gruttadauria, *ChemCatChem* **2016**, *8*, 664-684.
- [43] B. Urbán, D. Srankó, G. Sáfrán, L. Üрге, F. Darvas, J. Bakos, R. Skoda-Földes, *J. Mol. Catal. A: Chem.* **2014**, *395*, 364-372.
- [44] S. Soll, P. Zhang, Q. Zhao, Y. Wang, J. Yuan, *Polymer Chemistry* **2013**, *4*, 5048-5051.
- [45] N. Jiao, Z. Li, Y. Wang, J. Liu, C. Xia, *RSC Advances* **2015**, *5*, 26913-26922.
- [46] S. Doherty, J. G. Knight, J. R. Ellison, D. Weekes, R. W. Harrington, C. Hardacre, H. Manyar, *Green Chem.* **2012**, *14*, 925-929.
- [47] R. J. Young, P. A. Lovell, *Introduction to Polymers*, 3rd ed., CRC Press, Florida, **2011**.

-
- [48] K. Matyjaszewski, *Macromolecules* **2012**, *45*, 4015-4039.
- [49] K. Matyjaszewski, J. Xia, *Chem. Rev.* **2001**, *101*, 2921-2990.
- [50] D. J. Keddie, *Chem. Soc. Rev.* **2014**, *43*, 496-505.
- [51] G. Delaittre, J. Rieger, B. Charleux, *Macromolecules* **2011**, *44*, 462-470.
- [52] P. G. Odell, R. P. N. Veregin, L. M. Michalak, M. K. Georges, *Macromolecules* **1997**, *30*, 2232-2237.
- [53] M. Kato, M. Kamigaito, M. Sawamoto, T. Higashimura, *Macromolecules* **1995**, *28*, 1721-1723.
- [54] J.-S. Wang, K. Matyjaszewski, *J. Am. Chem. Soc.* **1995**, *117*, 5614-5615.
- [55] C. W. Bielawski, R. H. Grubbs, *Prog. Polym. Sci.* **2007**, *32*, 1-29.
- [56] S. W. Benson, F. R. Cruickshank, D. M. Golden, G. R. Haugen, H. E. O'Neal, A. S. Rodgers, R. Shaw, R. Walsh, *Chem. Rev.* **1969**, *69*, 279-324.
- [57] N. Calderon, *Acc. Chem. Res.* **1972**, *5*, 127-132.
- [58] S. Sutthasupa, M. Shiotsuki, F. Sanda, *Polym. J.* **2010**, *42*, 905-915.
- [59] C. Torborg, M. Beller, *Adv. Synth. Catal.* **2009**, *351*, 3027-3043.
- [60] M. Pérez-Lorenzo, *J. Phys. Chem. Lett.* **2012**, *3*, 167-174.
- [61] (a)S.-i. Ikeda, *Acc. Chem. Res.* **2000**, *33*, 511-519; (b)J. Montgomery, *Acc. Chem. Res.* **2000**, *33*, 467-473.
- [62] (a)M. Carril, R. SanMartin, E. Dominguez, *Chem. Soc. Rev.* **2008**, *37*, 639-647; (b)S. R. Chemler, P. H. Fuller, *Chem. Soc. Rev.* **2007**, *36*, 1153-1160; (c)C.-J. Li, *Acc. Chem. Res.* **2002**, *35*, 533-538; (d)B. H. Lipshutz, Y. Yamamoto, *Chem. Rev.* **2008**, *108*, 2793-2795; (e)D. Ma, Q. Cai, *Acc. Chem. Res.* **2008**, *41*, 1450-1460; (f)F. Monnier, M. Taillefer, *Angew. Chem. Int. Ed.* **2008**, *47*, 3096-3099; (g)H. Plenio, *Angew. Chem. Int. Ed.* **2008**, *47*, 6954-6956.
- [63] (a)S. L. Buchwald, C. Bolm, *Angew. Chem. Int. Ed.* **2009**, *48*, 5586-5587; (b)A. Correa, O. Garcia Mancheno, C. Bolm, *Chem. Soc. Rev.* **2008**, *37*, 1108-1117; (c)W. M. Czaplik, M. Mayer, J. Cvengroš, A. J. von Wangelin, *ChemSusChem* **2009**, *2*, 396-417; (d)A. Fürstner, *Angew. Chem. Int. Ed.* **2009**, *48*, 1364-1367; (e)B. D. Sherry, A. Fürstner, *Acc. Chem. Res.* **2008**, *41*, 1500-1511.
- [64] V. Farina, *Adv. Synth. Catal.* **2004**, *346*, 1553-1582.
- [65] A. Fihri, M. Bouhrara, B. Nekoueishahraki, J.-M. Basset, V. Polshettiwar, *Chem. Soc. Rev.* **2011**, *40*, 5181-5203.
- [66] V. Polshettiwar, A. Decottignies, C. Len, A. Fihri, *ChemSusChem* **2010**, *3*, 502-522.
- [67] W. Ostwald, *Z. Phys. Chem.* **1901**, *37*, 385.

-
- [68] C. Pan, K. Pelzer, K. Philippot, B. Chaudret, F. Dassenoy, P. Lecante, M.-J. Casanove, *J. Am. Chem. Soc.* **2001**, *123*, 7584-7593.
- [69] J. Schulz, A. Roucoux, H. Patin, *Chem. Commun.* **1999**, 535-536.
- [70] M. T. Reetz, G. Lohmer, *Chem. Commun.* **1996**, 1921-1922.
- [71] J. D. Aiken, R. G. Finke, *J. Am. Chem. Soc.* **1999**, *121*, 8803-8810.
- [72] (a)E. J. W. Verwey, J. T. G. Overbeek, *Theory of the Stability of Lyophobic Colloids*, Dover Publications Mineola, New York, **1999**; (b)P. Migowski, D. Zanchet, G. Machado, M. A. Gelesky, S. R. Teixeira, J. Dupont, *PCCP* **2010**, *12*, 6826-6833.
- [73] B. Karimi, M. Khorasani, *ACS Catalysis* **2013**, *3*, 1657-1664.
- [74] D. Zhao, Z. Fei, W. H. Ang, P. J. Dyson, *Small* **2006**, *2*, 879-883.
- [75] I. Biondi, G. Laurenczy, P. J. Dyson, *Inorg. Chem.* **2011**, *50*, 8038-8045.
- [76] M. M. Dell'Anna, M. Mali, P. Mastrorilli, A. Rizzuti, C. Ponzoni, C. Leonelli, *J. Mol. Catal. A: Chem.* **2013**, *366*, 186-194.
- [77] M. I. Burguete, E. García-Verdugo, I. Garcia-Villar, F. Gelat, P. Licence, S. V. Luis, V. Sans, *J. Catal.* **2010**, *269*, 150-160.
- [78] T. Gutel, C. C. Santini, K. Philippot, A. Padua, K. Pelzer, B. Chaudret, Y. Chauvin, J.-M. Basset, *J. Mater. Chem.* **2009**, *19*, 3624-3631.
- [79] L. Magna, Y. Chauvin, G. P. Niccolai, J.-M. Basset, *Organometallics* **2003**, *22*, 4418-4425.
- [80] (a)A. V. Gaikwad, A. Holuigue, M. B. Thathagar, J. E. ten Elshof, G. Rothenberg, *Chem. Eur. J.* **2007**, *13*, 6908-6913; (b)M. B. Thathagar, J. E. ten Elshof, G. Rothenberg, *Angew. Chem. Int. Ed.* **2006**, *45*, 2886-2890.
- [81] (a)A. H. M. de Vries, J. M. C. A. Mulders, J. H. M. Mommers, H. J. W. Henderickx, J. G. de Vries, *Org. Lett.* **2003**, *5*, 3285-3288; (b)J. G. de Vries, *Dalton Trans.* **2006**, 421-429.
- [82] A. F. Shmidt, L. V. Mametova, *Kinet. Catal.* **1996**, *37*, 406.
- [83] Y. Nishihara, Y. Inoue, Y. Nakayama, T. Shiono, K. Takagi, *Macromolecules* **2006**, *39*, 7458-7460.
- [84] Y. M. A. Yamada, Y. Uozumi, *Tetrahedron* **2007**, *63*, 8492-8498.
- [85] W. M. Lemke, R. B. Kaner, P. L. Diaconescu, *Inorg. Chem. Front.* **2015**, *2*, 35-41.
- [86] J. Dupont, J. D. Scholten, *Chem. Soc. Rev.* **2010**, *39*, 1780-1804.
- [87] Q. Zhou, S. Wei, W. Han, *J. Org. Chem.* **2014**, *79*, 1454-1460.
- [88] W. Han, C. Liu, Z. Jin, *Adv. Synth. Catal.* **2008**, *350*, 501-508.
- [89] I. Maluenda, O. Navarro, *Molecules* **2015**, *20*, 7528.

-
- [90] (a)N. E. Leadbeater, M. Marco, *J. Org. Chem.* **2003**, *68*, 888-892; (b)C. R. LeBlond, A. T. Andrews, Y. Sun, J. R. Sowa, *Org. Lett.* **2001**, *3*, 1555-1557.
- [91] T. Chen, F. Mao, Z. Qi, Y. Li, R. Chen, Y. Wang, J. Huang, *RSC Advances* **2016**, *6*, 16899-16903.
- [92] R. Fareghi-Alamdari, M. G. Haqiqi, N. Zekri, *New J. Chem.* **2016**, *40*, 1287-1296.
- [93] Y. Li, X. M. Hong, D. M. Collard, M. A. El-Sayed, *Org. Lett.* **2000**, *2*, 2385-2388.
- [94] F. Liu, Z. Fu, Y. Liu, C. Lu, Y. Wu, F. Xie, Z. Ye, X. Zhou, D. Yin, *Ind. Eng. Chem. Res.* **2010**, *49*, 2533-2536.
- [95] P. Kowalski, K. Mitka, K. Ossowska, Z. Kolarska, *Tetrahedron* **2005**, *61*, 1933-1953.
- [96] A. Bayat, M. Shakourian-Fard, M. M. Hashemi, *Catal. Commun.* **2014**, *52*, 16-21.
- [97] A. Rostami, B. Tahmasbi, F. Abedi, Z. Shokri, *J. Mol. Catal. A: Chem.* **2013**, *378*, 200-205.
- [98] A. A. Lindén, M. Johansson, N. Hermanns, J.-E. Bäckvall, *J. Org. Chem.* **2006**, *71*, 3849-3853.
- [99] (a)M. Amini, H. Naslhajian, S. M. F. Farnia, M. Hołyńska, *Eur. J. Inorg. Chem.* **2015**, *2015*, 3873-3878; (b)R. D. Chakravarthy, K. Suresh, V. Ramkumar, D. K. Chand, *Inorg. Chim. Acta* **2011**, *376*, 57-63.
- [100] Q. Zeng, W. Weng, X. Xue, *Inorg. Chim. Acta* **2012**, *388*, 11-15.
- [101] P. Pitchen, E. Dunach, M. N. Deshmukh, H. B. Kagan, *J. Am. Chem. Soc.* **1984**, *106*, 8188-8193.
- [102] T. Soundiressane, S. Selvakumar, S. Ménage, O. Hamelin, M. Fontecave, A. P. Singh, *J. Mol. Catal. A: Chem.* **2007**, *270*, 132-143.
- [103] (a)M. Ciclosi, C. Dinoi, L. Gonsalvi, M. Peruzzini, E. Manoury, R. Poli, *Organometallics* **2008**, *27*, 2281-2286; (b)K. Kamata, T. Hirano, N. Mizuno, *Chem. Commun.* **2009**, 3958-3960; (c)X. Xue, W. Zhao, B. Ma, Y. Ding, *Catal. Commun.* **2012**, *29*, 73-76.
- [104] C. Jahier, S. S. Mal, R. Al-Oweini, U. Kortz, S. Nlate, *Polyhedron* **2013**, *57*, 57-63.
- [105] C. Venturello, R. D'Aloisio, J. C. J. Bart, M. Ricci, *J. Mol. Catal.* **1985**, *32*, 107-110.
- [106] S. D. Jackson, J. S. J. Hargreaves, *Metal oxide catalysis, Vol. 1*, Wiley-VCH, Weinheim, **2008**.
- [107] A. B. Bourlinos, K. Raman, R. Herrera, Q. Zhang, L. A. Archer, E. P. Giannelis, *J. Am. Chem. Soc.* **2004**, *126*, 15358-15359.
- [108] P. G. Rickert, M. R. Antonio, M. A. Firestone, K.-A. Kubatko, T. Szreder, J. F. Wishart, M. L. Dietz, *Dalton Trans.* **2007**, 529-531.

-
- [109] (a)T. L. Greaves, C. J. Drummond, *Chem. Rev.* **2008**, *108*, 206-237; (b)X. Wu, X. Tong, Q. Wu, H. Ding, W. Yan, *J. Mater. Chem., A* **2014**, *2*, 5780-5784; (c)F. Yan, S. Yu, X. Zhang, L. Qiu, F. Chu, J. You, J. Lu, *Chem. Mater.* **2009**, *21*, 1480-1484.
- [110] H. Li, Y. Qiao, L. Hua, Z. Hou, B. Feng, Z. Pan, Y. Hu, X. Wang, X. Zhao, Y. Yu, *ChemCatChem* **2010**, *2*, 1165-1170.
- [111] W. Li, J. Fang, M. Lv, C. Chen, X. Chi, Y. Yang, Y. Zhang, *J. Mater. Chem.* **2011**, *21*, 11340-11346.
- [112] D. C. Duncan, R. C. Chambers, E. Hecht, C. L. Hill, *J. Am. Chem. Soc.* **1995**, *117*, 681-691.
- [113] (a)A. J. Bailey, W. P. Griffith, B. C. Parkin, *J. Chem. Soc., Dalton Trans.* **1995**, 1833-1837; (b)N. J. Campbell, A. C. Dengel, C. J. Edwards, W. P. Griffith, *J. Chem. Soc., Dalton Trans.* **1989**, 1203-1208; (c)A. C. Dengel, W. P. Griffith, B. C. Parkin, *J. Chem. Soc., Dalton Trans.* **1993**, 2683-2688; (d)E. Radkov, R. H. Beer, *Polyhedron* **1995**, *14*, 2139-2143; (e)C. Rocchiccioli-Deltcheff, M. Fournier, R. Franck, R. Thouvenot, *Inorg. Chem.* **1983**, *22*, 207-216.
- [114] X. Shi, X. Han, W. Ma, J. Wei, J. Li, Q. Zhang, Z. Chen, *J. Mol. Catal. A: Chem.* **2011**, *341*, 57-62.
- [115] P. Zhao, M. Zhang, Y. Wu, J. Wang, *Ind. Eng. Chem. Res.* **2012**, *51*, 6641-6647.
- [116] S. Doherty, J. G. Knight, M. A. Carroll, J. R. Ellison, S. J. Hobson, S. Stevens, C. Hardacre, P. Goodrich, *Green Chem.* **2015**, *17*, 1559-1571.
- [117] S. P. Das, J. J. Boruah, N. Sharma, N. S. Islam, *J. Mol. Catal. A: Chem.* **2012**, *356*, 36-45.
- [118] P. P. Lange, Goo, P. Podmore, T. Underwood, N. Sciammetta, *Chem. Commun.* **2011**, *47*, 3628-3630.
- [119] J. M. Ottino, S. Wiggins, *Phil. Trans. R. Soc. Lond. A.* **2004**, *362*, 923-935.
- [120] F. A. Morrison, *An Introduction to Fluid Mechanics, Vol. 1*, Cambridge University Press, New York, **2013**.
- [121] P. N. Dwivedi, S. N. Upadhyay, *Ind. Eng. Chem. Process Des. Dev.* **1977**, *16*, 157-165.
- [122] M. J. Rhodes, *Introduction to Particle Technology*, Wiley, Chichester, **2008**.
- [123] W. Zhu, H. Li, X. Jiang, Y. Yan, J. Lu, J. Xia, *Energy Fuels* **2007**, *21*, 2514-2516.
- [124] S. G. Chatila, *Evaluation of crude oils. In Petroleum Refining Crude Oil. Petroleum Products. Process flowsheets, Vol. 1*, Editions Technip, Paris, **1995**.
- [125] G. Heinrich, S. Kasztelaan, *Hydrotreating In Petroleum Refining Conversion Processes, Vol. 3*, Editions Technip, Paris, **2001**.

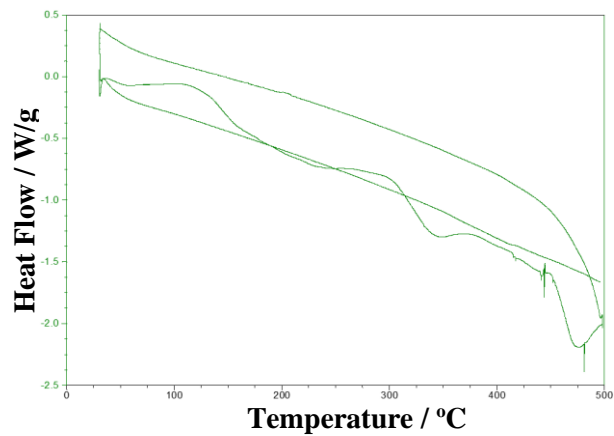
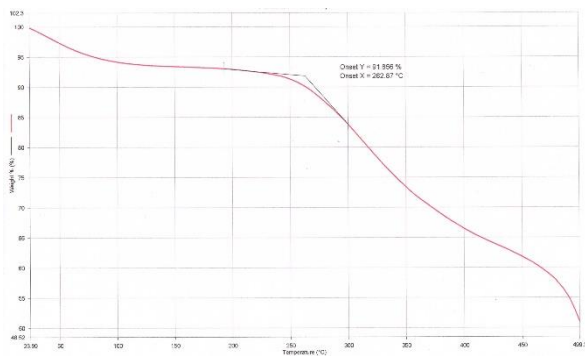
-
- [126] R. Javadli, A. Klerk, *Appl. Petrochem. Res.* **2012**, *1*, 3-19.
- [127] F. P. Hochgesang, in *Thiophene and its derivatives*, Interscience, New York, **1952**, p. 86.
- [128] A. Corma, C. Martínez, G. Ketley, G. Blair, *Appl. Catal., A* **2001**, *208*, 135-152.
- [129] C. Huang, B. Chen, J. Zhang, Z. Liu, Y. Li, *Energy Fuels* **2004**, *18*, 1862-1864.
- [130] L. Yang, J. Li, X. Yuan, J. Shen, Y. Qi, *J. Mol. Catal. A* **2007**, *262*, 114-118.
- [131] J. H. Chang, Y. J. Kim, B. H. Lee, K.-S. Cho, H. W. Ryu, Y. K. Chang, H. N. Chang, *Biotechnol. Prog.* **2001**, *17*, 876-880.
- [132] H. Li, X. Jiang, W. Zhu, J. Lu, H. Shu, Y. Yan, *Ind. Eng. Chem. Res.* **2009**, *48*, 9034-9039.
- [133] H. Li, L. He, J. Lu, W. Zhu, X. Jiang, Y. Wang, Y. Yan, *Energy Fuels* **2009**, *23*, 1354-1357.
- [134] L. He, H. Li, W. Zhu, J. Guo, X. Jiang, J. Lu, Y. Yan, *Ind. Eng. Chem. Res.* **2008**, *47*, 6890-6895.
- [135] W. Zhang, K. Xu, Q. Zhang, D. Liu, S. Wu, F. Verpoort, X.-M. Song, *Ind. Eng. Chem. Res.* **2010**, *49*, 11760-11763.
- [136] A. P. Closson, A. T. Levorse, M. G. Monteleone, (Ed.: I. F. F. Inc.), USA, **2010**, p. 5.
- [137] B. Mathieu, L. Ghosez, *Tetrahedron* **2002**, *58*, 8219-8226.
- [138] T. G. Driver, A. K. Franz, K. A. Woerpel, *J. Am. Chem. Soc.* **2002**, *124*, 6524-6525.
- [139] L. A. Reiter, in *Pfizer Inc., Vol. US4560690 A*, USA, **1985**.
- [140] A. J. M. Janssen, A. J. H. Klunder, B. Zwanenburg, *Tetrahedron* **1991**, *47*, 5513-5538.
- [141] M. Eda, T. Takemoto, S. Ono, T. Okada, K. Kosaka, M. Gohda, S. Matzno, N. Nakamura, C. Fukaya, *J. Med. Chem.* **1994**, *37*, 1983-1990.
- [142] B. S. Lee, S. Mahajan, B. Clapham, K. D. Janda, *J. Org. Chem.* **2004**, *69*, 3319-3329.
- [143] W. Chen, Y. Zhang, L. Zhu, J. Lan, R. Xie, J. You, *J. Am. Chem. Soc.* **2007**, *129*, 13879-13886.
- [144] F. Gu, H. Dong, Y. Li, Z. Si, F. Yan, *Macromolecules* **2014**, *47*, 208-216.
- [145] L.-J. Zhao, C. K.-W. Kwong, M. Shi, P. H. Toy, *Tetrahedron* **2005**, *61*, 12026-12032.
- [146] S. Doherty, J. G. Knight, J. R. Ellison, P. Goodrich, L. Hall, C. Hardacre, M. J. Muldoon, S. Park, A. Ribeiro, C. A. N. de Castro, M. J. Lourenco, P. Davey, *Green Chem.* **2014**, *16*, 1470-1479.
- [147] C. Pavia, E. Ballerini, L. A. Bivona, F. Giacalone, C. Aprile, L. Vaccaro, M. Gruttadauria, *Adv. Synth. Catal.* **2013**, *355*, 2007-2018.
- [148] F. Vallée, J. J. Mousseau, A. B. Charette, *J. Am. Chem. Soc.* **2010**, *132*, 1514-1516.

-
- [149] M. D. Green, J.-H. Choi, K. I. Winey, T. E. Long, *Macromolecules* **2012**, *45*, 4749-4757.
- [150] K. Cheng, S. Hu, B. Zhao, X.-M. Zhang, C. Qi, *J. Org. Chem.* **2013**, *78*, 5022-5025.
- [151] E. Salanouve, G. Bouzemame, S. Blanchard, E. Derat, M. Desage-El Murr, L. Fensterbank, *Chem. Eur. J.* **2014**, *20*, 4754-4761.
- [152] Z. Liu, H. Tan, L. Wang, T. Fu, Y. Xia, Y. Zhang, J. Wang, *Angew. Chem. Int. Ed.* **2015**, *54*, 3056-3060.
- [153] L. Ackermann, C. J. Gschrei, A. Althammer, M. Riederer, *Chem. Commun.* **2006**, 1419-1421.
- [154] C. Liu, X. Rao, Y. Zhang, X. Li, J. Qiu, Z. Jin, *Eur. J. Org. Chem.* **2013**, *2013*, 4345-4350.
- [155] H. Yan, P. Chellan, T. Li, J. Mao, K. Chibale, G. S. Smith, *Tetrahedron Lett.* **2013**, *54*, 154-157.
- [156] Z. Shu, Y. Ye, Y. Deng, Y. Zhang, J. Wang, *Angew. Chem. Int. Ed.* **2013**, *52*, 10573-10576.
- [157] A. Derible, C. Diebold, J. Dentzer, R. Gadiou, J.-M. Becht, C. Le Drian, *Eur. J. Org. Chem.* **2014**, *2014*, 7699-7706.
- [158] M. Gholinejad, F. Hamed, P. Biji, *Dalton Trans.* **2015**, *44*, 14293-14303.
- [159] J.-H. Kim, J.-W. Kim, M. Shokouhimehr, Y.-S. Lee, *J. Org. Chem.* **2005**, *70*, 6714-6720.
- [160] X. Gu, X. Li, Y. Chai, Q. Yang, P. Li, Y. Yao, *Green Chem.* **2013**, *15*, 357-361.
- [161] (a)P. Gogoi, M. Kalita, T. Bhattacharjee, P. Barman, *Tetrahedron Lett.* **2014**, *55*, 1028-1030; (b)G. Yuan, J. Zheng, X. Gao, X. Li, L. Huang, H. Chen, H. Jiang, *Chem. Commun.* **2012**, *48*, 7513-7515.
- [162] M. A. M. Capozzi, C. Cardellicchio, F. Naso, P. Tortorella, *J. Org. Chem.* **2000**, *65*, 2843-2846.
- [163] A. Yoshimura, C. T. Banek, M. S. Yusubov, V. N. Nemykin, V. V. Zhdankin, *J. Org. Chem.* **2011**, *76*, 3812-3819.
- [164] (a)S. Mannathan, C.-H. Cheng, *Chem. Eur. J.* **2012**, *18*, 11771-11777; (b)J. Skarżewski, E. Wojaczyńska, I. Turowska-Tyrk, *Tetrahedron: Asymmetry* **2002**, *13*, 369-375.

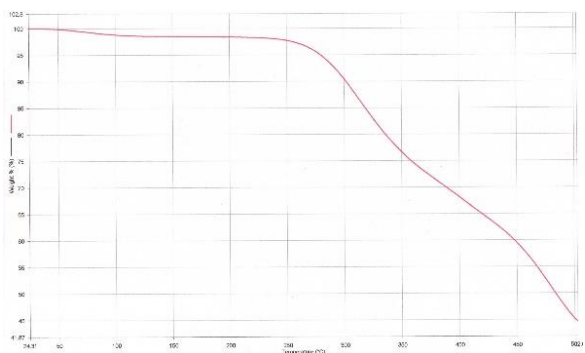
APPENDICES

Appendix 1 TGA/DSC traces of polymers & PIILP materials.

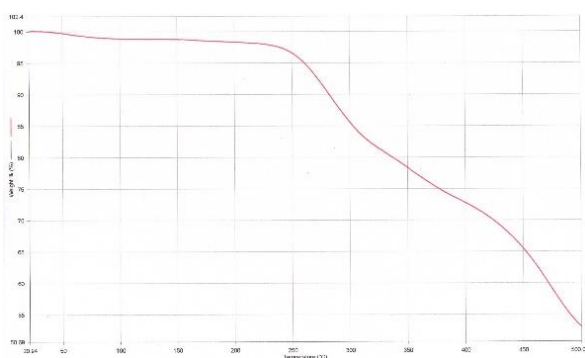
OMe polymer 23:



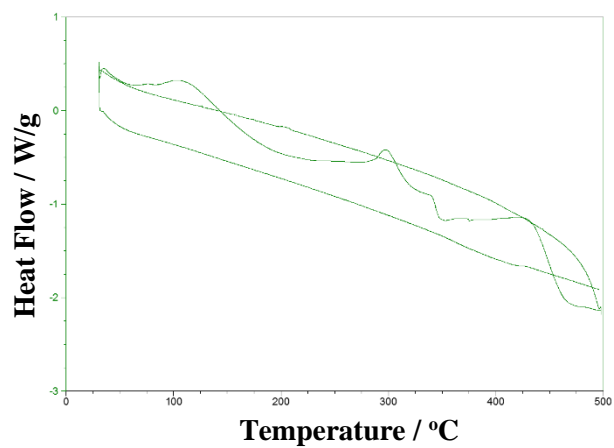
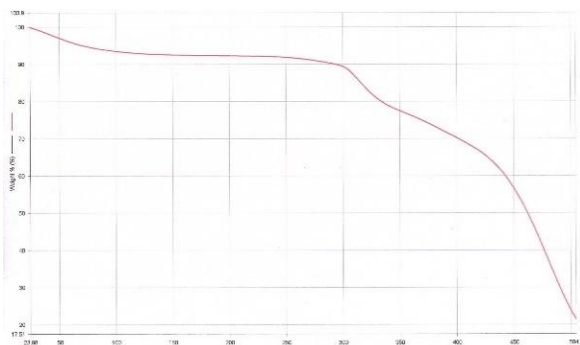
Pd⁰@Imid-PIILP 26:



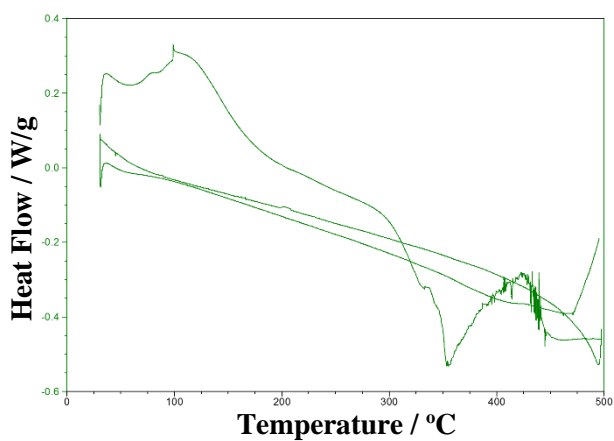
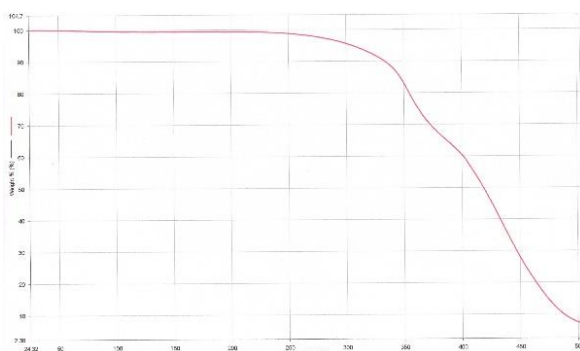
Pd⁰@OMe-PIILP 27:



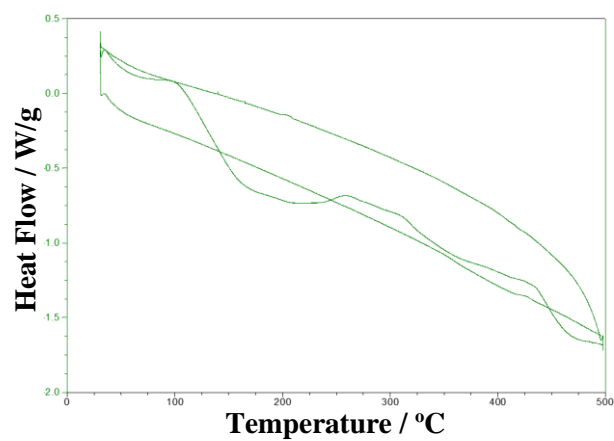
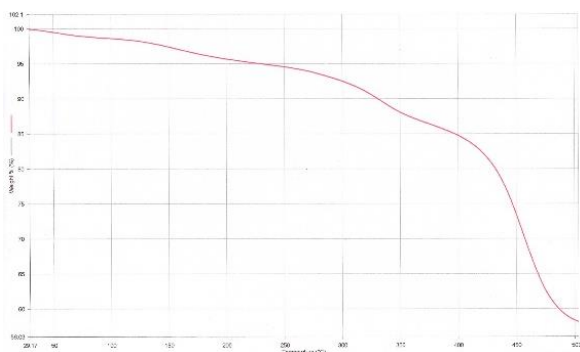
Polymer 31:



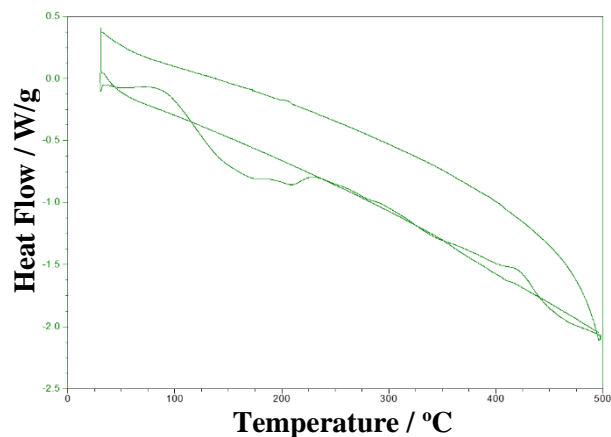
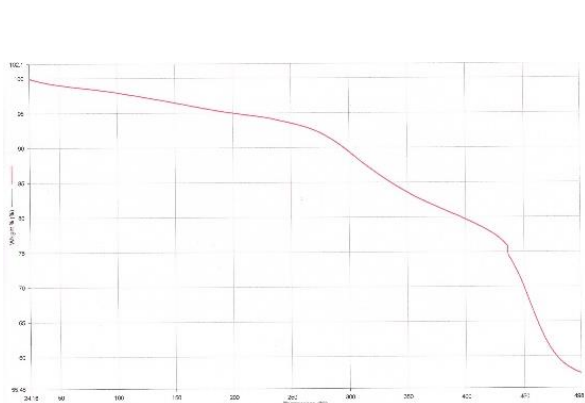
Polymer 33:



POM@PIILP 34:



POM@PIILP 36:



Appendix 2 Determination of polymer composition from CHN analysis.

Polymer 31:

Empirical formula $C_{29}H_{31}ClN_2$ (443.0)

Found: C, 74.65; H, 6.76; N, 6.29 %.

This corresponds to $C_{28}H_{30}N_2$.

Subtract the empirical formula for the imidazolium repeat unit ($C_{13}H_{15}N_2$).

This leaves $C_{15}H_{15}$ which corresponds to the remaining styrene units,

Therefore $15/8 = 1:1.9$ imidazolium: styrene respectively.

Polymer 32:

Empirical formula $C_{30}H_{33}ClN_2$ (457.1)

Found: C, 73.52; H, 6.83; N, 6.57 %.

This corresponds to $C_{26}H_{29}N_2$

Subtract the empirical formula for the imidazolium, repeat unit ($C_{14}H_{17}N_2$).

This leaves $C_{12}H_{12}$ which corresponds to the remaining styrene units,

Therefore $12/8 = 1:1.5$ imidazolium: styrene respectively.

Polymer **33**:

Empirical formula $C_{35}H_{35}BrN_2$ (563.6)

Found: C, 71.69; H, 6.72; N, 5.03 %.

This corresponds to $C_{33}H_{37}N_2$

Subtract the empirical formula for the imidazolium, repeat unit ($C_{19}H_{19}N_2$).

This leaves $C_{14}H_{18}$ which corresponds to the remaining styrene units,

Therefore $14/8 = 1: 1.8$ imidazolium: styrene respectively.

Appendix 3 Determination of POM loading for POM@PIILP materials.

POM@PIILP **35**:

CHN Anal. Calc. for $C_{90}H_{99}N_6O_{24}PW_4$ (2415.119) C, 44.76; H, 4.13; N, 3.48 %.
Found: C, 41.29; H, 4.05; N, 3.38 %.

Therefore: 1 g of PIILP contains 0.0338 g N = 2.413×10^{-3} moles N

(Polymer alone has 4.690×10^{-3} moles N per g from CHN analysis)

Therefore, 1g polymer: (4.690×10^{-3} moles N) and (4.690×10^{-3} moles Cl)

So if 1g of PIILP has 2.413×10^{-3} moles N then 1.94 g of PIILP contains 4.690×10^{-3} moles N which corresponds to 1g of polymer

0.94 g extra mass is from $-3Cl^- + POM = (3 \times (-35.453)) + 1150.31 = 1043.951$

$0.94/1043.951 = 0.900$ mmol of POM = 1.036 g POM

Therefore 1 g of PIILP contains $(1/1.94) \times 1.036 = 0.534$ g POM = 0.464 mmol POM

This corresponds to $(0.464 \text{ mmol} \times 4) = 1.856$ mmol W

= 0.34 g W = **34 %**

POM@PIILP 36:

CHN Anal. Calc. for $C_{105}H_{105}N_6O_{24}PW_4$ (2601.338) C, 48.48; H, 4.07; N, 3.23 %.
Found: C, 47.45; H, 4.25; N, 3.01 %.

Therefore: 1 g of PIILP contains 0.0301 g N = 2.148×10^{-3} moles N

(Polymer alone has 3.590×10^{-3} moles N per g from CHN analysis)

Therefore, 1g polymer: (3.590×10^{-3} moles N) and (3.590×10^{-3} moles Br⁻)

So if 1g of PIILP has 2.148×10^{-3} moles N then 1.67 g of PIILP contains 3.590×10^{-3} moles N which corresponds to 1g of polymer

0.67 g extra mass is from $-3Br^- + POM = (3 \times (-79.904)) + 1150.31 = 910.598$

$0.67/910.598 = 0.736$ mmol of POM = 0.846 g POM

Therefore 1 g of PIILP contains $(1/1.67) \times 0.846 = 0.507$ g POM = 0.441 mmol POM

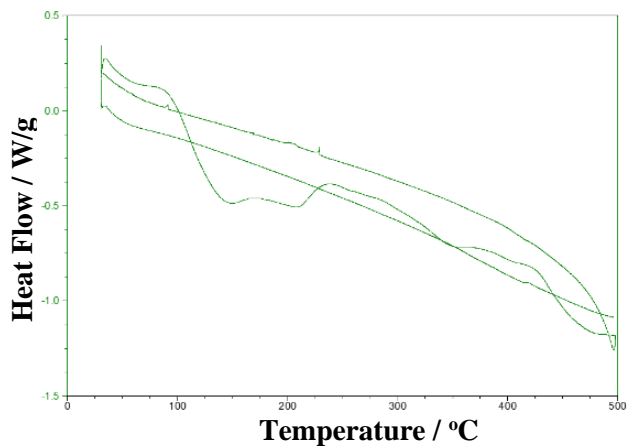
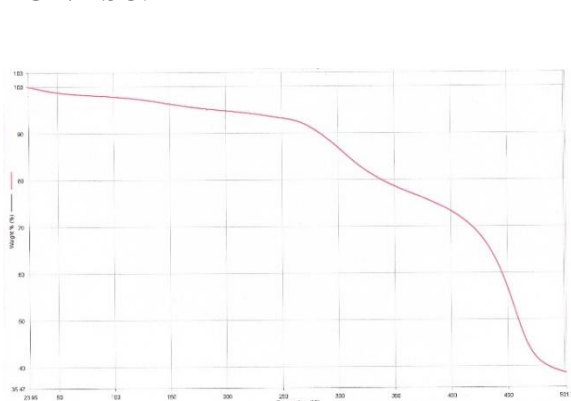
This corresponds to $(0.441 \text{ mmol} \times 4) = 1.764$ mmol W

= 0.32 g W = **32 %**

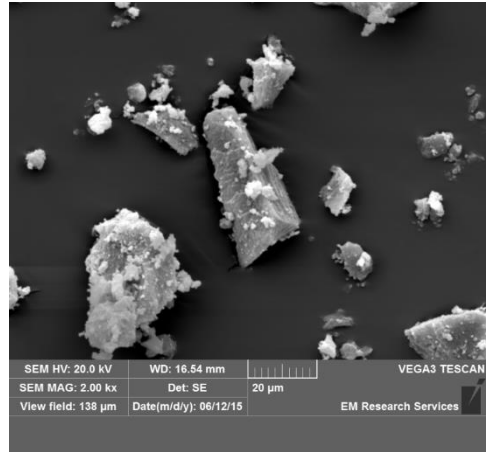
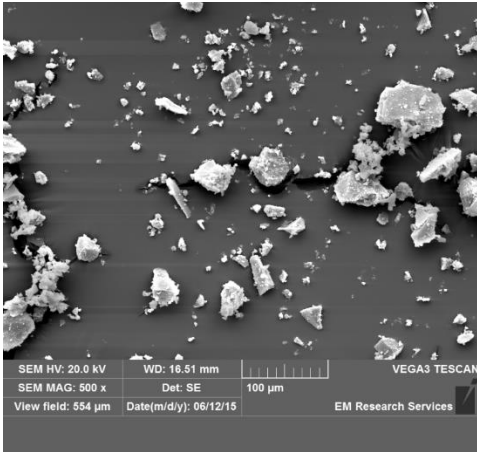
Appendix 4 Characterisation data for varied dilution POM@PIILP materials.

POM@PIILP 42 (x10 dilution):

TGA/DSC:

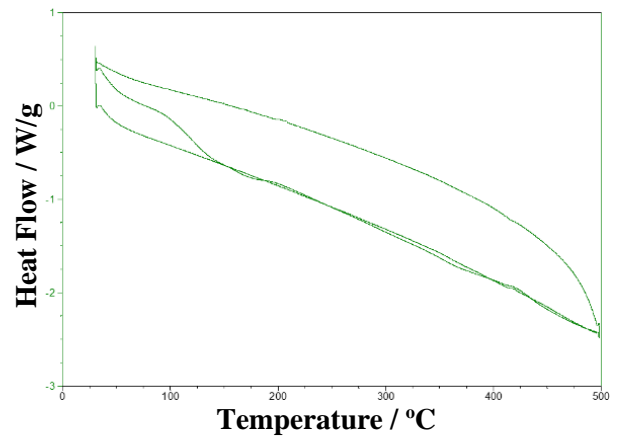
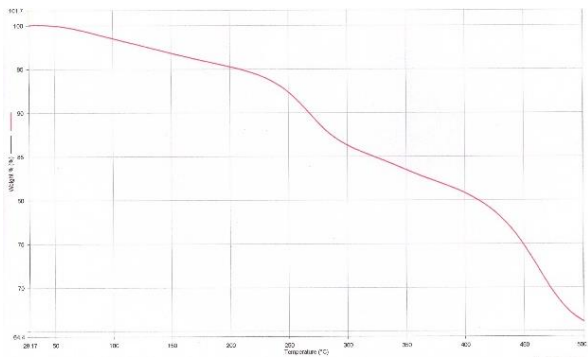


SEM:

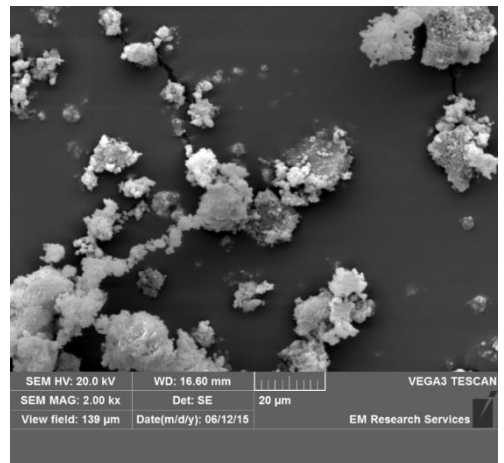
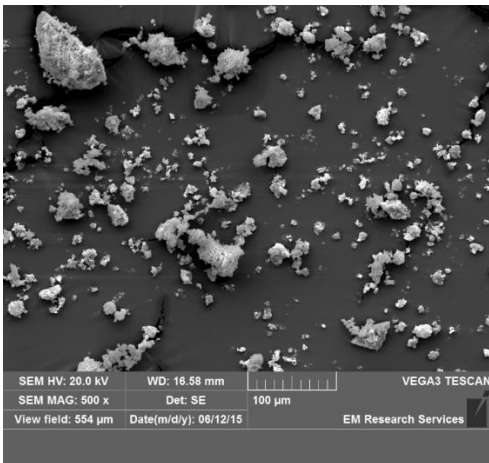


POM@PIILP 43 (x2 concentration):

TGA/DSC:



SEM:

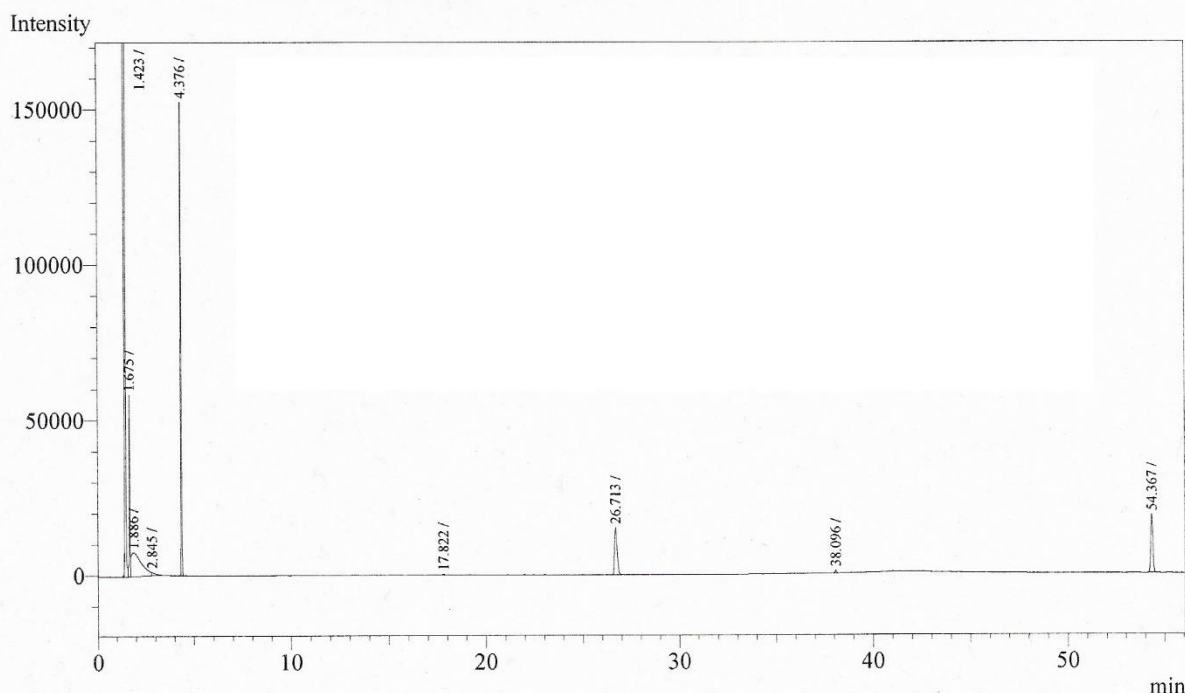


Appendix 5 Representative characterisation data from Chapter 5.

Representative GC of 4-phenylbenzotrile showing reduction in 4-bromobenzotrile at a retention time of 26.713:

Analysis Date & Time : 1/21/2015 5:09:51 PM
 User Name : Admin
 Vial# : 6
 Sample Name : ARC332-1
 Sample ID : ARC332-1
 Sample Type : Unknown
 Injection Volume : 1.00
 ISTD Amount :

Data Name : C:\GCsolution\Data\Ashley\ARC332-1.gcd
 Method Name : C:\GCsolution\Data\Doherty\JackSM01.gcm



Peak#	Ret.Time	Area	Height	Conc.	Unit	Mark	ID#	Cmpd Name
1	1.423	194938496	100754248	0.000		V		
2	1.675	118597	57660	0.000		V		
3	1.886	291362	7710	0.000		V		
4	2.845	13061	1141	0.000		V		
5	4.376	387227	152030	0.000				
6	17.822	1585	311	0.000				
7	26.713	139078	15304	0.000				
8	38.096	3906	950	0.000				
9	54.367	144936	18871	0.000				
Total		196038248	101008225					

Representative GPC of polymer 33:

Cirrus GPC Sample Injection Report

Generated by: Administrator 18 May 2015 14:12
Workbook: C:\Cirrus Workbooks\dafgroupgpc\dafgroupgpc.plw

Sample Details

Sample Name: ARC-RK007 #1
Acquired: 18/05/2015 13:18:08 By Analyst: Administrator
Batch Name: 18_05_2015
Filename: C:\Cirrus Workbooks\dafgroupgpc\18_05_2015-0002.cgrm
Concentration: 1.00 mg/ml K of Sample: 14.1000
Injection Volume: 50.0 ul Alpha of Sample: 0.7000
LIMS ID: Bottle ID:

Workbook Details

Eluent: THF Flow Rate: 1.00 ml/min
Column Set: PL Mixed D Column Set Length: 0 mm
Detector: RI Temperature: Ambient

Analysis Using Method: Manual Analysis

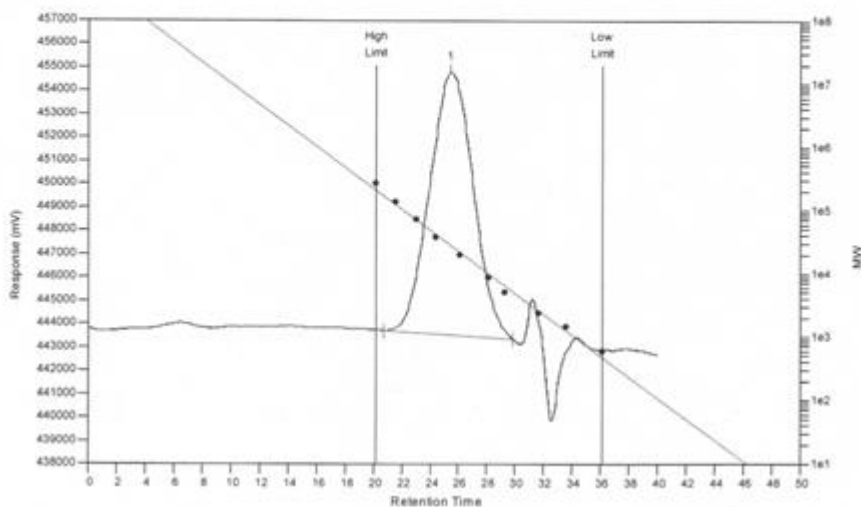
Comments: This method has processing switched on and is set so that you have to select the Peaks for Calibrants & Unknowns

Results File: C:\Cirrus Workbooks\dafgroupgpc\18_05_2015-0002.rst

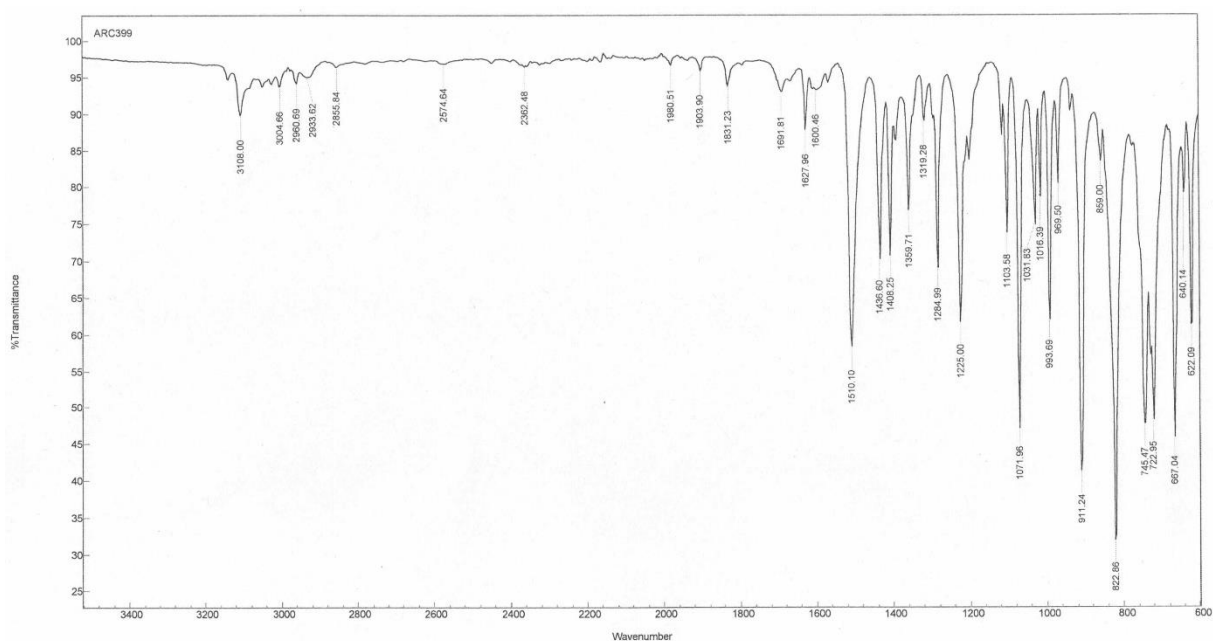
Calibration Used: 12/03/2015 16:01:12

Calibration Type: Narrow Standard Curve Fit Used: 1
Calibration Curve: $y = 8.667926 - 0.165883x^1$

High Limit MW RT: 20.17 mins Low Limit MW RT: 36.17 mins
High Limit MW: 210190 Low Limit MW: 466
K: 14.1000 FRM Name:
Alpha: 0.7000 Flow Marker RT: 0.00 mins
FRCF: 1.0000



Representative FTIR of polymer 1-(4-vinylbenzyl)-1*H*-imidazole **29**:



Representative mass spectrum of 3-benzyl-1-(4-vinylbenzyl)-1*H*-imidazol-3-ium bromide **30**:

Elemental Composition Report

Single Mass Analysis

Tolerance = 10.0 PPM / DBE: min = -5.0, max = 40.0

Element prediction: Off

Number of isotope peaks used for i-FIT = 6

Monoisotopic Mass, Odd and Even Electron Ions

1 formula(e) evaluated with 1 results within limits (all results (up to 1000) for each mass)

Elements Used:

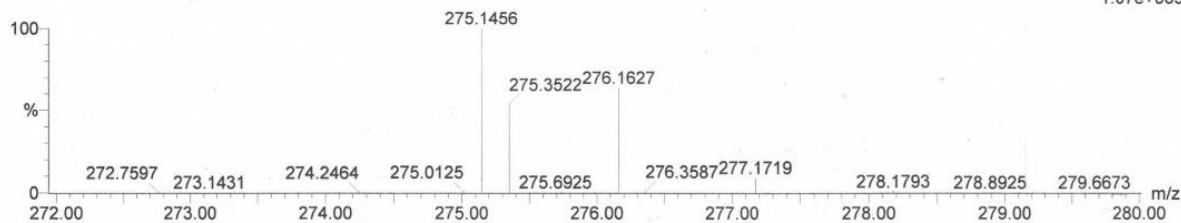
C: 19-19 H: 19-20 N: 2-2 23Na: 0-1

07-Oct-2015

1::2::6

ARC401 245 (1.609)

1: TOF MS ES+
1.07e+005



Minimum:

Maximum:

Mass	Calc. Mass	mDa	PPM	DBE	i-FIT	i-FIT (Norm)	Formula
276.1627	276.1626	0.1	0.4	11.0	610.7	0.0	C19 H20 N2